Design, Synthesis and Conformational Analysis of Hybrid γ-Peptide Foldamers Comprised of Proteinogenic Sidechains and Their Utilization in the Design of Novel Biomaterials

A thesis

Submitted in partial fulfilment of the requirements

Of the degree of

Doctor of Philosophy

By

Sandip V. Jadhav

ID: 20083015

Indian Institute of Science Education and Research, Pune

2013

Dedicated to

Prof. M. S. Wadia

University of Pune

…The great teacher

CERTIFICATE

This is to certify that the work incorporated in the thesis entitled **"Design, Synthesis and Conformational Analysis of Hybrid γ-Peptide Foldamers Comprised of Proteinogenic Sidechains and Their Utilization in the Design of Novel Biomaterials"** submitted by Sandip V. Jadhav carried out by the candidate at the Indian Institute of Science Education of Research (IISER), Pune, under my supervision. The work presented here or any part of it has not been included in any other thesis submitted previously for the award of any degree or diploma from any other University or institution.

30th December, 2013

Dr. Hosahudya N. Gopi
(Research Supervisor)
Associate Professor, IISER, Pune
Pune-411008, India

Declaration

I hereby declare that the thesis entitled **"Design, Synthesis and Conformational Analysis of Hybrid γ-Peptide Foldamers Comprised of Proteinogenic Sidechains and Their Utilization in the Design of Novel Biomaterials"** submitted for the degree of Doctor of Philosophy in Chemistry at Indian Institute of Science Education of Research (IISER), Pune has not been submitted by me to any other University or Institution. This work was carried out at the, Indian Institute of Science Education of Research (IISER), Pune, India under supervision of Dr. Hosahudya N. Gopi.

30th December, 2012

Sandip V. Jadhav
ID: 20083015
Senior Research Fellow
Dept. of Chemistry, IISER-Pune
Pune - 411008

Acknowledgements

Dr. Hosahudya N. Gopi is someone who has a major influence on my life. Being my advisor, I would like to express my special appreciation and thanks to you… sir you have been a tremendous mentor for me. I would also like to thank you for encouraging my research and for allowing me to grow as a research scientist. I cannot forget the freedom which you have given to me to work and explore the research ideas. I could not have imagined better advisor and mentor for my doctoral studies. Your advice on both research as well as on my career have been priceless. Thank you very much sir for making me capable.

I am sincerely thankful to our Director, Prof. K. N. Ganesh, for providing world class facilities during my research stay here at Indian Institute of science education and research, Pune, India. I always remain stunned to see his love and passion for science. Also, I am thankful to each and every chemistry faculty in IISER-Pune for their help.

I would like to thank Dr. H. V. Thulasiram (National Chemical Laboratory, Pune) and Dr. Partha Hazra (IISER, Pune). Being the members of my research advisory committee, I want to thanks both of you for your brilliant comments and suggestions. I have special thanks to entire "Dr. Thulasiram laboratory" from NCL Pune for their uninterrupted support in initial days.

I thank Prof. Dilip D. Dhavale, Chemistry department of Pune University, who will always remain positive role model for me. I also want to thank the most adorable Prof. M. S. Wadia and Dr. H. R. Sonawane for their continuous guidance and suggestions.

Vidhyarthi Sahayyak Samiti (Student Welfare Association) of Pune, is the institution which turned my entire life other way round. I must be indebted throughout my life to such a great institution for allowing me to know meaning of life and their values.

I am really lucky to have wonderful lab mates who have played a very crucial role in my day to day life during my research tenure. My special thanks to Dr. Anupam Bandyopadhyay and Sachitanand Mali with whom I started my doctoral research carrier in 2008. These are the two personalities who always supported me morally and scientifically during my entire research stay at IISER, Pune. I also thanks to my lab mates Mothukuri Ganesh Kumar, Sushil Benke, Rajkumar Misra, Rahi M. Reja, Anindita, Rupal, Ankita and Shivani. I want to thank former member of our lab Sumeet Kumar Singh, Shiva Shankar, Neha Agrawal and Kumar Sourav. I cannot forget the members those who worked for short duration in the lab but really helped me by their own way including Thaksen Jadhav, Prashant Ghadge, Varsha, Rohini, Robins, Ajay

Soni, Mona, Anur and Akash. "Dr. Gopi laboratory" will always remain an unforgettable episode in my entire life.

*I must acknowledge the help from Dr. T. S. Mahesh (NMR), Dr. V. G. Anand (XRD), Dr. Sudipta Basu (Extruder), Dr. Souvik Dutta (SEM) and Dr. Ashish Lele (Rheometry). I want to thank Archana Jogdand for X-ray instrumental support. I am also thankful to my friends Gopal, Shekhar Shinde, Pradip Pachfule, Biplab Jorder, Amar Mohite, Prakash Sultane, Deepak Jain, Nitin Bansode, Vijay Kadam, Maroti Pawar Arun Tanpure, Anupam Sawant, Pramod Sabale, Abhik Mallik and entire Medeleeve block. I also want to thank Mr. Saiyyad and Mr. Pappu for their initial support when I started my research carrier. I have a special thank to the each and every last member of our cricket team **THE ALCHEMIST** for bringing those precious moments in my life.*

It would have not possible for me to complete my doctoral work without the support from my family. I have highest gratitude to my mother and my father. There is no one other than my mother who has greater impact on my life. She taught me many values that define who I am now. I have to thank my two elder sisters Savita and Rohini for making my childhood so beautiful and encouraging me till this moment to pursue my goal. Their love for me is always unconditional. The thesis will of course remain incomplete without mentioning the motivation, blessings and love of my mother-in-law and my father-in-law. I will always be indebted to them for believing in me and allowing their daughter to marry me. I also want to thank my brother-in-law Akshay for his support and encouragement. Most importantly, I would like to thank my dear wife Priyanka. Her support, encouragement, quiet patience and untiring love were definitely laid the foundation upon which the past ten years of my life have been built. Her tolerance of my occasional rude moods is a testament in itself of her unyielding devotion and love. Thank you Priyanka for always being my pillar, my joy and my guiding light.

This last word of acknowledgements I have saved to thank the God, the Almighty, for the wisdom and perseverance that he has been bestowed upon me during this research project, and indeed, throughout my life. Finally, I will be forever grateful to Lord, for the most memorable gift in my life, my son Ayush.

Sandip V. Jadhav

CONTENTS

Chapter 1

Efficient Access to Enantiopure γ^4-Amino Acids

Chapter 2

Design, Synthesis, Conformations and self- Assembly of Hybrid α,γ^4-Peptides

Chapter 3

Remarkable Thermoresponsive Nanofibers from γ-Peptides

Chapter 4

γ-Amino Acid Mutated α-Coiled Coils as Mild Thermal Triggers for Liposome Delivery

ABBREVIATIONS

Ac = Acyl

Ac_2O = Acetic anhydride

AcOEt = Ethyl acetate

ACN = Acetonitrile

AFM = Atomic Force Microscopy

Aib = α-Amino isobutyric acid

Aic = γ-Amino isocaproic acid

Ar = Aryl

Bn = Benzyl

Boc = tert-Butoxycarbonyl

$(Boc)_2O$ = Boc anhydride

Bu = Butyl

Bu^i- = Isobutyl

Bu^t- = Tertiary butyl

Calcd. = Calculated

Cbz = Benzyloxycarbonyl

CD = Circular Dichroism

dg = dehydro gamma

COSY =Correlation spectroscopy

DCC = N, N'-Dicyclohexylcarbodiimide

DCM = Dichloromethane

DiPEA = Diisopropylethyl Amine

DLS = Dynamic Light Scattering

DMF = Dimethylformamide

DMSO = Dimethylsulfoxide

DNA = Deoxyribonucleic acid

EDX = Energy Dispersive X-ray

EDC = Ethyl-N,N-dimethyl-3-aminopropylcarbodiimide

EtOH = Ethanol

EtOAc = Ethyl acetate

Fmoc = 9-Fluorenylmethoxycarbonyl

Fmoc-OSu = N-(9-Fluorenylmethoxycarbonyloxy) succinimide

g = gram

hrs = hours

HBTU = O-Benzotriazole-N,N,N',N'-tetramethyluronium hexafluorophosphate

HCl = Hydrochloric acid

HOBt = Hydroxybenzotriazol

HPLC = High Performance Liquid Chromatography

IBX = 2-Iodoxybenzoicacid

ITC = Isothermal Titration Calorimetry

LAH = Lithium Aluminium Hydride

LMWG = Low Molecular Weight Gelators

MALDI-TOF/TOF = Matrix-Assisted Laser Desorption /Ionization – Time of Flight

MATLAB = Matrix Laboratory

MBHA = Methyl bezhydrylamine

Me = Methyl

MeOH = Methanol

mg = milligram

min = Minutes

μL = Microliter

μM = Micromolar

mL = milliliter

mM = millimolar

mmol = millimoles

m.p. = Melting Point

MS = Mass Spectroscopy

MSA = Methanesulfonic acid

N = Normal

NHS = *N*-hydroxysuccinimide

NMP = N-methyl pyrrolidone

NMR = Nuclear Magnetic Resonance

NOE = Nuclear Overhauser Effect

PC = α-Phosphatidylcholine

PEG = Poly Ethylene Glycol

PG = Protecting Group

PNT = Peptide Nanotubes

ppm = Parts per million

Py = Pyridine

R_f = Retention factor

RMS = Root Mean Square

ROESY = Rotating Frame NOE Spectroscopy

RT = Room Temperature

SEM = Scanning Electron Microscopy

TEM = Transmission Electron Microscopy

TFA = Trifluoroacetic acid

THF = Tetrahydrofuran

TOCSY = TOtal Correlation SpectroscopY

ABSTRACT

Over the last two decades, backbone modified β-peptide foldamers have been extensively investigated towards design of biologically active peptidomimetics. Comparatively, the foldamers containing γ-amino acids with proteinogenic side-chains are less studied may be in part due to the difficulties in accessing enantiopure γ-amino acids and possible chaos in folding of peptides due to the introduction of additional two torsional variables in each building block. In this regard, we sought to investigate the folding properties of hybrid peptides composed of γ^4-amino acids, their structural analogy with the protein secondary structures and their applications in biomaterials.

Detailed investigations reveal that despite their increased backbone flexibility, γ^4-amino acids have showed a higher propensity towards helical organization even in the simple monomeric building block. The conformational analysis of various α, γ^4-hybrid peptides suggests that they adopt stable 12-helical conformations in solution and solid state. The structural analogy with α-peptide helices, β-peptide 12-helix, helical wheel diagram, helical parameters and their hierarchical self-assembly of 12-helices into elongated peptide nanotubes have been investigated. In addition, conformationally biased unusual extended sheet type of structures from the homooligomers 4,4-dialkyl γ-amino acids (Aic) and their spontaneous self-assembly into nanofibers and thermoreversible organogels in various organic solvents is studied. Besides this, we have also investigated the γ^4-amino acid mutated α-coiled coils as mild hyperthermia triggers for controlled release of entrapped molecules from liposomes. Based on these investigations, this thesis is divided into four chapters.

PUBLICATIONS

1. Efficient access to enantiopure γ^4-amino acids with proteinogenic sidechains and structural investigation of γ^4-Asn and γ^4-Ser in hybrid peptide helices.
   Jadhav, S. V.; Misra, R.; Singh, S. K.; Gopi, H. N. *Chem. Eur. J.* **2013**, *19*, 16256.
2. γ-Amino acid mutated α-coiled coils as mild thermal triggers for liposome delivery.
   Jadhav, S. V.; Singh, S. K.; Reja, R. M.; Gopi, H. N. *Chem. Commun.* **2013,** *49*, 11065.
3. Remarkable thermoresponsive nanofibers from γ-peptides.
   Jadhav, S. V.; Gopi, H. N. *Chem. Commun.* **2013**, *49*, 9179.
4. Protein secondary structure mimetics: crystal conformations of α/γ^4-hybrid peptide12-helices with proteinogenic sidechains and their analogy with α- and β-peptide helices.
   Jadhav, S. V.; Bandyopadhyay, A.; Gopi, H. N. *Org. Biomol. Chem.* **2013**, *11*, 509.
5. A facile synthesis and crystallographic analysis of *N*-protected β-amino alcohols and short peptaibols.
   Jadhav, S. V.; Bandyopadhyay, A.; Benke, S. N.; Mali, S. M.; Gopi, H. N. *Org. Biomol. Chem.* **2011**, *9*, 4182.
6. α/γ^4-Hybrid peptide helices: synthesis, crystal conformations and analogy with the α-helix.
   Bandyopadhyay, A.; **Jadhav, S. V.**; Gopi, H. N. *Chem. Commun.* **2012**, *48*, 7170.
7. Copper (II) mediated facile and ultra fast peptide synthesis in methanol.
   Mali, S. M.; **Jadhav, S. V.**; Gopi, H. N. *Chem. Commun.* **2012**, *48*, 7085.
8. Thiazole-carbonyl interactions: a case study using phenylalanine thiazole cyclic tripeptides.
   Mali, S. M.; Schneider, T. E.; Bandyopadhyay, A.; **Jadhav, S. V.**; Werz, D. B.; Gopi, H. N. *Cryst. Growth. Des.* **2012**, *12*, 5643.
9. Synthesis of α, β-unsaturated γ-amino esters with unprecedented high (*E*)-stereoselectivity and their conformational analysis in peptides.
   Mali, S. M.; Bandyopadhyay, A.; **Jadhav, S. V.**; Kumar, M. G.; Gopi, H. N. *Org. Biomol. Chem.* **2011**, *9*, 6566.

10. Tin (II) chloride assisted synthesis of *N*-protected γ-amino β-keto esters through semipinacol rearrangement.
    Bandyopadhyay, A.; Agrawal, N.; Mali, S. M.; **Jadhav, S. V.**; Gopi, H. N. *Org. Biomol. Chem.* **2010**, *9*, 6566.
11. Nanotubes from helical α,γ^4-peptide foldamers.
    Jadhav, S. V.; Misra, R.; Mali, S. M.; Gopi, H. N.
    manuscript under preparation.

Chapter 1

Efficient Access to Enantiopure γ^4-Amino Acids

1.1 Introduction

Proteins are the most abundant natural biopolymers and are responsible for various biochemical processes in living organisms. Nature precisely chooses proteins to carry out many biological functions because of their ability to fold into definite and rigid three dimensional conformations (Figure 1.1). This intriguing folding property of proteins creates "active-sites" which draws the various functional groups together from distal region of their primary structure.

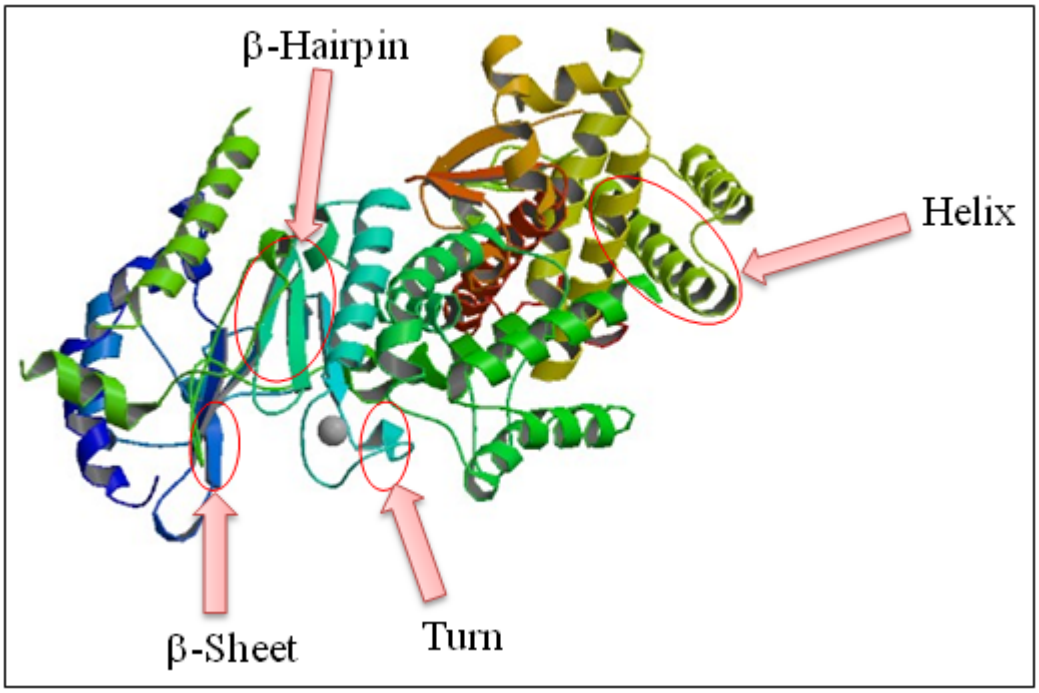

Figure 1.1 Crystal conformation of Human DNA primase. PDB code- 4BPX

Inspection of protein three-dimensional structures suggests their complex tertiary folds and quaternary associations. Disintegration of a protein tertiary structure, hypothetically, leads to a limited number of secondary structural elements, such as β-sheets, helices, and turns, which are assembled using loosely structured loops (Figure 1.1). These protein secondary structures are locally defined, meaning that there can be many different secondary motifs present in one single protein molecule. *De novo* design of existing or novel protein folds demands a thorough understanding of the rules that underlines protein structures and their stability.[1] The *de novo* design of proteins as well as peptide secondary structures has not only expanded our understanding towards the folding and functions of proteins but also provides enormous opportunities in the structure based drug design.[2] Based on the folding principles of protein, it is feasible for the structure based drug design using α-peptides,

however, the main disadvantage of α-peptides is that their proteolytic instability. Considerable attention has been paid over the past several decades on polypeptides composed of α-amino acids, with natural proteins and the use of stereochemically constrained amino acids and templates in the design of folded polypeptides.[3] The success of this endeavor has also been applied to the design of well defined secondary structure mimetics from the oligomers of non-ribosomal amino acids such as β-, γ- and other non-natural amino acid templates.

1.2 Beta-peptide foldamers

The term foldamers was first coined by Prof. Samuel H. Gellman, he states that foldamer is "any polymer with strong tendency to adopt a specific compact conformation".[4] A variety of foldamers that mimic the protein secondary structures have been designed using various organic templates and non-natural amino acids.

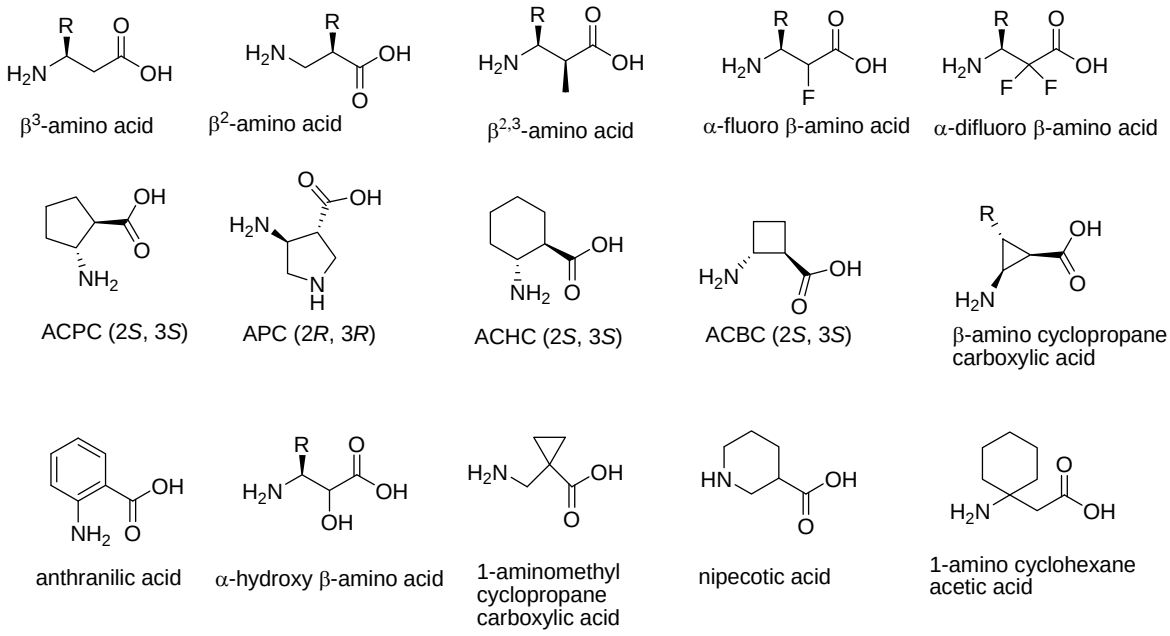

Figure 1.2 Beta-amino acid building blocks for foldamer synthesis.

Over the past two decades, β-peptides composed of β-amino acids have emerged as very versatile candidate in the area of foldamers. In their pioneering work Gellman[5] and Seebach[6] introduced cyclic β-amino acids and chiral acyclic β-amino acids, respectively. Further, Sharma and colleagues extensively investigated the β-peptide oligomers generated from carbo-β-amino acids.[7] Raiser et al. showed the utilization of the cyclic β-amino acids

in the design of β-peptides.[8] In addition Aitken and colleagues [9]and Fulop et al.[10] showed utilization of various cyclic β-amino acids in the design of β-peptide foldamers. Acyclic β-amino acids are homologated species of α-amino acids. β-Peptides from the β-amino acids are particularly interesting in understanding protein structure and stabilization because β-amino acids are close relatives to α-amino acids as they are only one methylene unit away from natural α-amino acids. Double homologation of α-amino acids leads to γ^4-amino acids. Depending on the position of the side chain on backbone, β-amino acids are classified as β^3- and β^2-amino acids (Figure 1.2) whereas γ-amino acids are classified into γ^2-, γ^3- and γ^4-amino acids (Figure 1.5). In addition, β-peptides have been proved to have proteolytic and metabolic stability and the prospects of intracellular delivery.[11] These properties of β-peptides endorse them as very attractive candidates from biomedical and drug design perspective.[12] Oligomers of cyclic and acyclic β- peptides form unique, stable secondary structures.The main secondary structures displayed by the β-peptides are again classified as helices, sheets and turns. Helices are mostly studied secondary structures found in proteins. Ironically, β-peptide produced a variety of helical secondary structures which are not seen in the alpha-peptides (Figure 1.3). The helices produced by the β-peptides are recognized as C14-, C12-, C10- and C8-helices.[13] The helices from β-peptides have different polarities with respect to their C and N-termini. The C8- and C12-helices have a hydrogen bond direction (C ←N), which is the same as that observed in α-peptides, whereas in the C10- and C14- structures the hydrogen bonding directions (N←C) are reversed. Similar to α-peptides, β-peptides also produced parallel and antiparallel sheets however, with change in the polarity and net dipole.[14a]

Balaram and colleagues demonstrated the systematic incorporation of β-amino acids and higher homologues amino acids into α-peptide helices, β-sheets and β-hairpin supersecondary structures.[14] The advantage of hybrid peptides with heterogeneous backbone (peptides with α and other β- and γ-amino acids) is that a variety of hydrogen bonded helical structures can be generated by varying the amino acid sequence patterns. Extensive investigations revealed that β-, γ-, mixed α/β- and α/γ-hybrid peptides adopt various ordered helical conformations including 14-, 12-, 10/12-, 9- and 8-helices. In contrast to the 14-helical conformations of cyclic β-amino acids with six membered ring constraint (trans-2-aminocyclohexane carboxylic acid) [15] and acyclic β-amino acids (β^3-

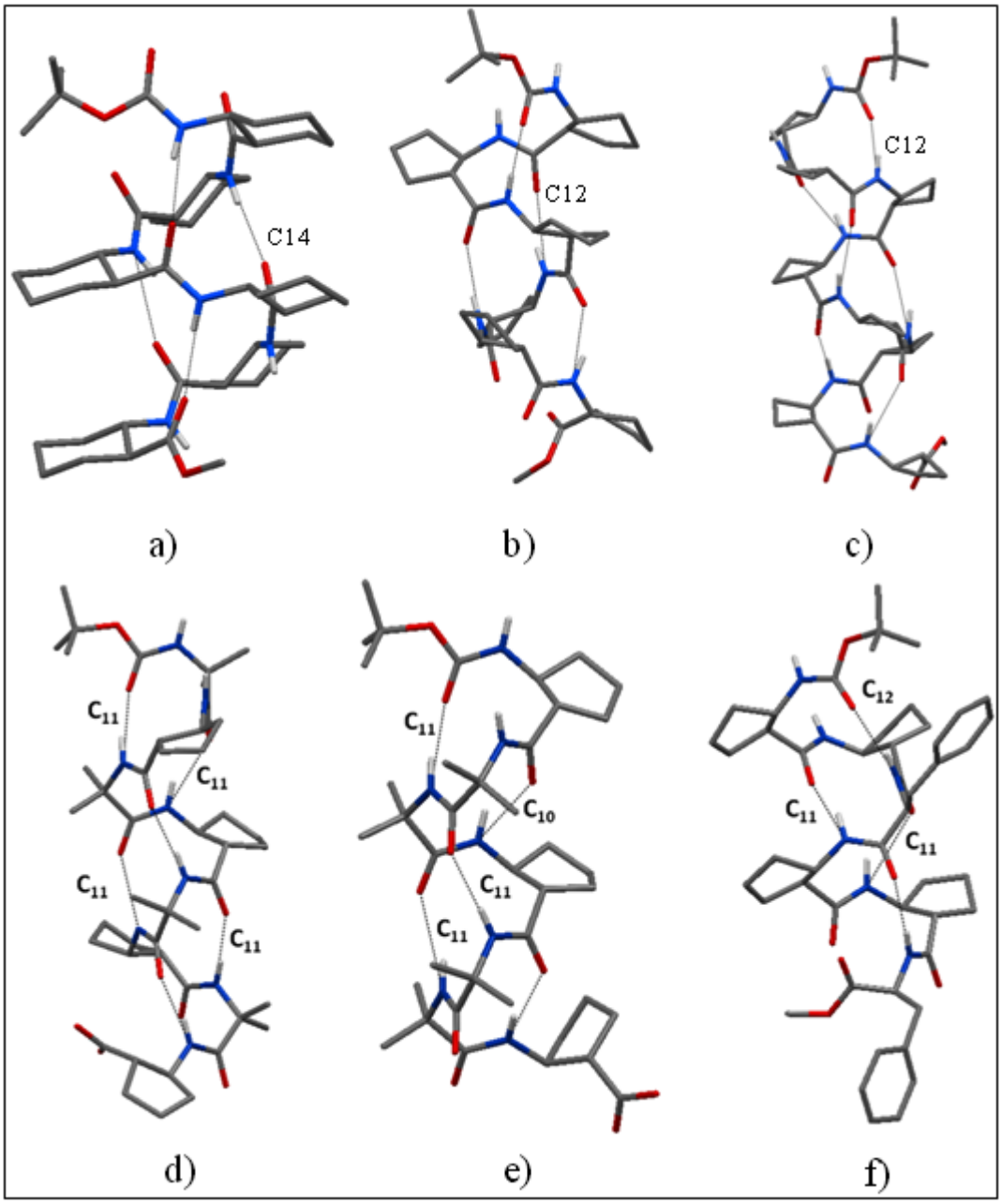

Figure 1.3 Helical crystal structure conformation oligomers of a) *trans*-ACHA (14-helix), b) *trans*-ACPC (12-helix), c) cyclobutane β-amino acid (12-helix) and examples of experimentally characterized hybrid peptides d) αβ Boc-Aib-ACPC-Aib-ACPC-Aib-ACPC-Aib-ACPC-OBn, d) ααβ with 10/11/11 helix, Boc-ACPC-Aib-Aib-ACPC-Aib-Aib-ACPC-OBn, f) ββα 12/11/11 helix, Boc-ACPC-ACPC-Phe-ACPC-ACPC-Phe-OBn,

and β^2-amino acids), [6b] the homooligomers of cyclic β-amino acids with four (trans-2-aminocyclobutane carboxylic acid)[9], five (trans-2-aminocyclopentane carboxylic acid and its derivatives)[16]membered ring constraint and bicycle[3.3.1] heptane skeleton[17]displayed the 12-helical conformations. These cyclic ring constraints of the amino acids preorganize

the β-peptide backbone to adopt stable helical conformations. In addition, Gellman et al and others have demonstrated the inhibitions of various protein-protein interactions using 12-helical scaffolds.[12] Further, Lee *et al.* showed the exceptional self-assembly behaviour of the 12-helical peptides.[18]

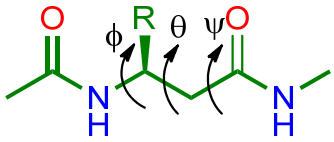

Figure 1.4 Torsional variables in β-amino acids.

Introduction of additional backbone atom in the β-amino acid residues leads to additional torsional freedom θ (C^{β}-C^{α}) along with ϕ (N-C^{β}) and ψ (C^{α}-CO) as in the case of α-amino acid residues (Figure 1.4). This additional torsional variable (θ) in β-amino acids is expected to increase the torsional freedom that possibly leads to the less ordered secondary structures in β-peptides comprised of acyclic β-residues compared to that of α-peptides. However, it is quite surprising to notice that formation of stable higher ordered structures in β-peptides even after introducing additional torsional variable in β-residues.

1.3 γ-Peptide foldamers

In contrast to the β-peptides and heterooligomers containing β-amino amino acids, the progress in field of γ-peptides (oligomers of double homologated α- amino acids) is lagging behind. In addition, very little is known about the heterooligomers containing α- and γ-amino acids. This is probably due to the difficulty of obtaining stereochemically pure γ-amino acids. However, in their preliminary investigations Seebach and colleagues[19] and Hanessian et al.[20] recognized the 14-helical conformations of the oligomers of γ^4-amino acids. In addition, Hofmann and colleagues predicted the wide range of helical organizations from the oligomers of γ^4-amino acids using *ab initio* theoretical calculations.[21] Further, in their pioneering work Balaram and colleagues reported the various ordered helical conformations from the homo and heterooligomers of gabapentin (3, 3-dialkyl-γ-amino acid), a anticonvulsant drugs for the neuropathic pain as well as for the treatment of epilepsy.[22] In contrast to the γ-peptides with backbone homologated γ-amino acids, the homooligomers of gabapentin displayed C9 and C7 helical conformations. In addition, the α,γ-hybrid peptides composed of gabapentin showed

either C12 or combinations of C12 and C10 H-bonding patterns in the helical peptides. Sharma and colleagues reported the left-handed helical conformations of γ-peptides composed of carbo-γ-amino acids (γ-Caas) along γ-aminobutyric acid (GABA) in solution.[23] Further, Smith and colleagues showed extended sheet structures with bifurcated H-bonds from the $\gamma^{2,3}$-cyclopropane side-chain amino acids.[24] In contrast, $\gamma^{2,3}$-trans-dioxolane-constrained homooligomers adopted C7 helical conformations in solution suggesting the importance of the cyclic ring size and relative peptide conformations.[25] Recently, Gellman and colleagues reported the C14 helical conformations in single crystals from the homooligomers of cyclic γ-amino acids.[26] Besides these cyclic and acyclic γ-amino acids, there are also reports on the utilization of the γ-amino acids containing back bone heteroatoms such as O (Oxygen) and N (Nitrogen). Yang and colleagues reported conformational properties of both α-aminoxy peptides and β-aminoxy peptides.[27] They observed that C8 helical conformations in α-aminoxy peptides and C9 helices and turns in the case of β-aminoxy peptides. Further, Le Grel et al. showed insertion of NH moiety in the backbone of β^3-amino acids between the amine and β-carbon, which leads to the azaamino acids.[28] Similar to the amino oxypeptides, the structures of azapeptides are stabilized by short range turn like H-bonds. Guichard and colleagues replaced the α-carbon with NH group in γ^4-amino acids and constructed urea peptides.[29] The structural investigation of the urea peptides showed that they adopted 14-helical conformations. Very recently, γ-amino acids with thiazole backbone are also explored to build stable foldamers.[30] The structures of γ-amino acids utilized for foldamer synthesis are shown in Figure 1.5.

In comparison with β- and other γ-peptides with various types of γ-amino acids, very little is known in the γ- and hybrid γ-peptides composed of γ-amino acids with proteinogenic side-chains. It is very well recognized that amino acid side-chains play a significant role in structure, function and hierarchical assembly of proteins. Furthermore, Seebach who pioneered in the β- and γ-peptide foldamers himself stated that "*The structural diversity of γ-amino acids and γ-peptides have not been elucidated nearly as well as that of β-peptides: it is expected to be richer*".[31] With this background we sought to investigate the facile, mild, racemization free and scalable protocol for the synthesis of γ-amino acids building block with proteinogenic side-chains. Here, in the chapter 1, we are reporting the synthesis of various unprotected γ-amino acids through single pot reduction of benzyl esters of N-

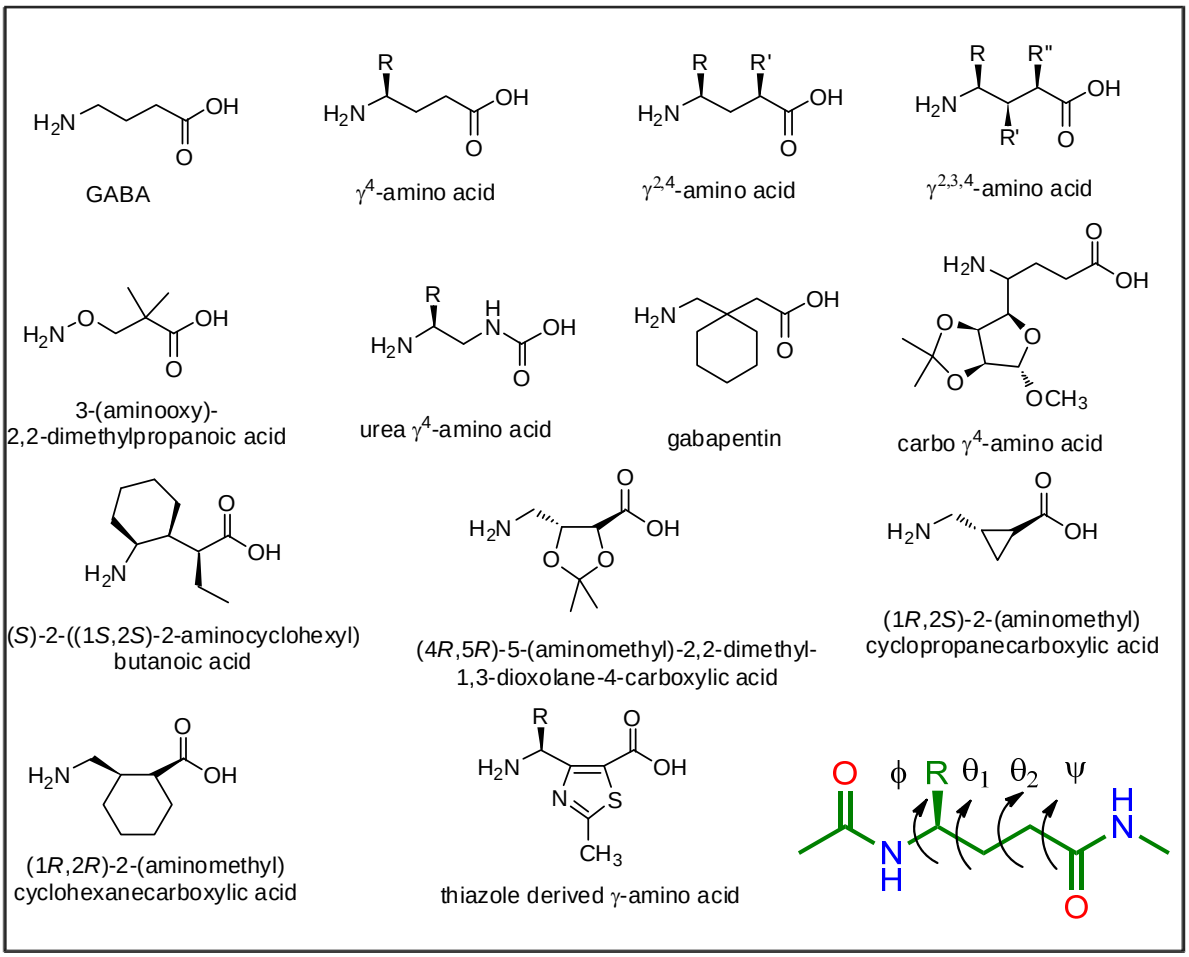

Figure 1.5 γ-Amino acid building blocks for foldamer synthesis. Torsional variables of γ-amino acid are also depicted.

Cbz-protected E-vinylogous amino acids, racemization studies of γ-amino acids, single crystal conformations of various unprotected γ-amino acids and N-protected γ-amino acids. The crystal conformation of unprotected γ-amino acids displayed the general tendency to adopt *gauche* conformation along the θ1 (C^{γ}-C^{β}).

1.4 Results and Discussions

1.4.1 Strategy for synthesis of γ^4-amino acids

Synthesis of β^3-amino acids with proteinogenic side-chains was essentially achieved by Arndt-Eistert homologation using activated α-amino acid with freshly generated diazomethane (Scheme 1.1a).[6b] In principle, this homologation protocol can be applied to

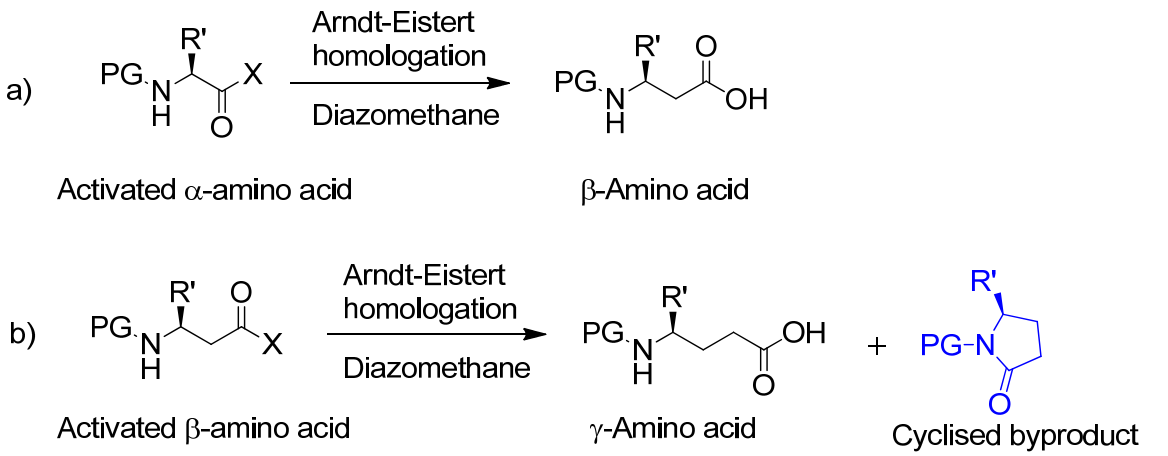

Scheme 1.1 a) Synthesis of β-amino acids by Arndt-Eistert homologation. b) Formation of cyclic by-product during γ-amino acid synthesis by Arndt-Eistert homologation of activated β-amino acid.

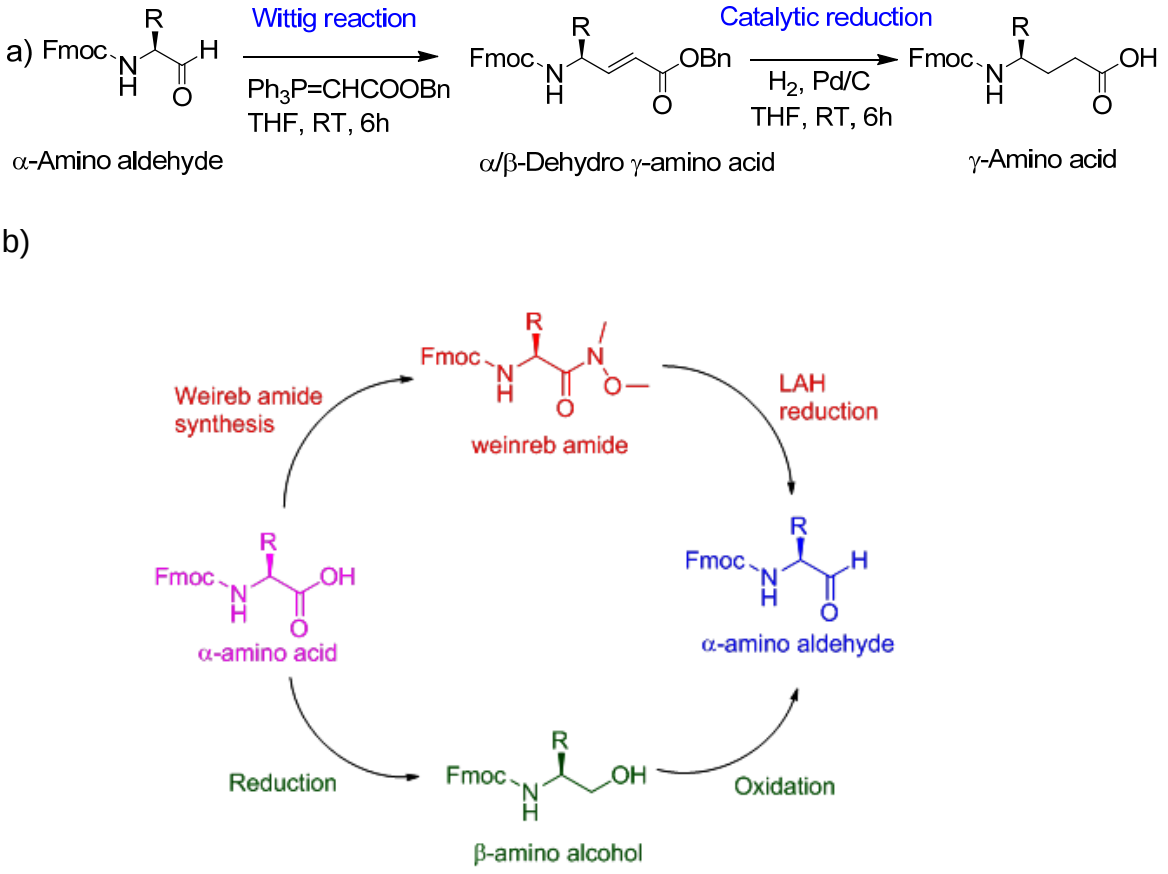

Scheme 1.2 a) Proposed scheme for synthesis of γ-amino acids. b) Two possible ways to synthesise α-amino aldehyde from α-amino acids.

the synthesis of γ^4-amino acids starting from β-amino acid and subsequent Arndt-Eistert homologation of to γ-amino acids (Scheme 1.1b). The major drawback of this protocol is that the partial cyclization of the ketene obtained after the Wolff rearrangement of β-amino acid diazoketones, as reported by Seebach et al.[6b] As a part of our continuous search for robust and scalable protocol that can be compatible for both Fmoc- and Boc-protecting groups for synthesis of γ-amino acids, we realized that benzyl esters of N-Fmoc-protected α, β-unsaturated γ-amino acids can be utilized as starting materials for the synthesis of solid phase compatible N-Fmoc-γ^4-amino acids after catalytic hydrogenation for the concomitant reduction of double bonds as well as benzyl ester deprotection in a single step (Scheme 1.2a). The purpose to choose Fmoc-protection for the N-terminal is that one can readily use these Fmoc-γ-amino acids on solid phase after the synthesis. We recently reported the synthesis ofα, β-unsaturated γ-amino acids with excellent *E*-selectivity using Wittig reaction starting from amino aldehydes.[32] The α-amino aldehydes is in turn can be synthesized from their

corresponding α-amino acids (Scheme 1.2b). Synthesis of α-amino aldehydes from the direct reduction of Weinreb amides of corresponding amino acids in the presence of lithium aluminium hydride is also known.[33] We noticed that premature cleavage of Fmoc-group during the LAH reduction that leads to the lower yields of Fmoc-amino aldehydes. In addition, Weinreb amine is also an expensive reagent. With these drawbacks we look for another mild protocol for the synthesis of α- amino aldehydes. It has been known that α- amino aldehydes can be synthesized from the oxidation of β-amino alcohols obtained from the reduction of corresponding α-amino acids. We sought to adopt β-amino alcohol route for the synthesis of amino aldehydes.

1.4.2 Synthesis of β-amino alcohols

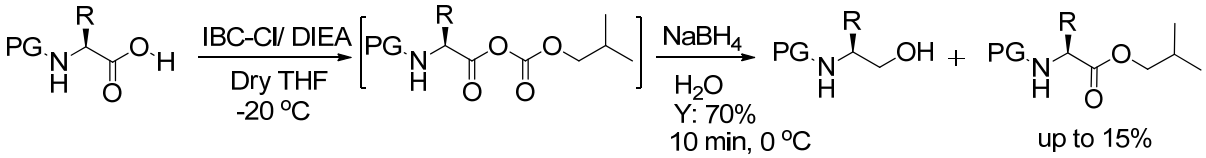

Scheme 1.3 Mixed anhydride method for synthesis of β-amino alcohol.

As N-Fmoc protected β-amino alcohols are the starting materials for the synthesis of functionalized γ-amino acids, we followed the most widely used mixed anhydride protocol

for the synthesis as shown in Scheme 1.3; however, in our hands yields were lower than the expected, and we found up to 15% of the isobutyl ester as a by-product. [34] In our continuing search for mild, low-cost and high-yielding methods for the synthesis of N-protected β-amino alcohols, we envisioned that N-hydroxysuccinimide esters would be ideal precursor because of their easy accessibility, shelf-stability and cost-effectiveness. N-Hydroxysuccinimide (HOSu) has been widely used as an additive in carbodiimide-mediated peptide couplings to reduce racemization.[35] Recently, the use of N-hydroxysuccinimide esters in the synthesis of N-protected homoserines starting from aspartic and glutamic acids has been demonstrated.[36] Further, the combination of carbodiimide and HOSu has been used in the immobilization of proteins, peptides, antibodies on sensor surfaces.[37] Because of their shelf-stability and slow reactivity, N-hydroxysuccinimide esters have also been used in the single-step synthesis of dipeptide acids.[38] A schematic representation of the synthesis of N-protected β-amino alcohols using N-hydroxysuccinimide is shown in Scheme 1.4. We synthesized a variety of N-hydroxysuccinimide esters of Fmoc-amino acids using DCC as a coupling agent in

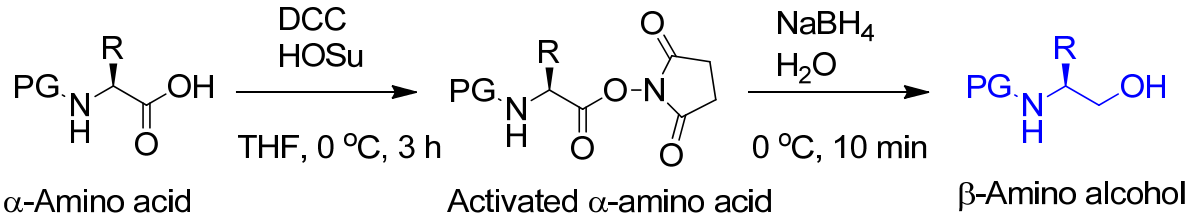

Scheme 1.4 Schematic representation of synthesis of N-protected β-amino alcohols using N-hydroxysuccinimide esters.

quantitative yield. In a typical reaction procedure, the succinimide esters were dissolved in distilled THF and then treated with a solution of $NaBH_4$ in ice-cold water. The course of the reaction was monitored By TLC. Intriguingly, it was found that within 5 min the active ester was completely converted to alcohol; however, we continued the reaction for another 5 min. A list of Fmoc-protected β-amino alcohols synthesized using this method is given in Table 1.1. Except Fmoc-Ile-OH (entry 5), all Fmoc-β-amino alcohols were isolated in yields above 80%. For comparison, we synthesized the same Fmoc- β-amino alcohols using mixed anhydride method ('IBC-Cl'), and yields are given in Table 1.1. A clear

Table 1.1: Comparison of Fmoc-protected β-amino alcohol obtained from HOSu and IBC-Cl method.

Entry	Fmoc-AAol	% yield		mp ^{o}C		$[\alpha]_D^{25}$ (c =1, MeOH)	
		HOSu	IBC-Cl	HOSu	IBC-Cl	HOSu	IBC-Cl
1	Fmoc-Alaol	90	70	150- 153	150-153	-2.0	-1.5
2	Fmoc-D-Alaol	85	NS	148-151	---	+2.0	---
3	Fmoc-Valol	90	76	121-122	124-127	-13.0	-13.6
4	Fmoc-Leuol	81	68	133-135	135-136	-20.1	-17.0
5	Fmoc-Ileol	65	50	114-116	108-110	-11.7	-13.0
6	Fmoc-Thr(OBu^{t})ol	85	55	oil	oil	+6.1	+6.4
7	Fmoc-Asp(OBu^{t})ol	92	47	93-96	95-96	-7.4	-7.0
8	Fmoc-Lys(Boc)ol	75	64	136-138	114	-6.9	-6.0
9	Fmoc-Asn(Trt)ol	90	65	155-159	132-134	-12.3	-10.3
10	Fmoc-Gln(Trt)ol	85	72	74-77	73-77	-5.8	-6.7

Table 1.2: Boc-protected β-amino alcohols and di-, tri-, and pentapeptide alcohols synthesized using the N-hydroxysuccinimide method

Entry	Alcohol	% Yield	$[\alpha]_D^{25}$ (c = 1, MeOH)
11	Boc-Alaol	80	-8.5
12	Boc-Valol	70	-17.6
13	Boc-Leuol	85	-23.2
14	Boc-Prool	78	-45.7
15	Boc-Trpol	75	-22.2
16	Boc-Ala-Valol	86	-22.2
17	Boc-Val-Valol	82	-34.7
18	Boc-Val-Leuol	82	-35.9
19	Boc-Ala-Leu-Valol	76	-34.5
20	Boc-Aib-Ala-Leuol	79	-13.6
21	Boc-Val-Leu-Ala-Val-Leuol	65	ND

improvement of the yields can be observed for the N-hydroxysuccinimide method relative to the mixed anhydride method in the case of side-chain-protected amino acids (entries 6–10). The optical rotation and the melting points of Fmoc-β-amino alcohols derived from the N-hydroxysuccinimide esters are in agreement with the mixed anhydride method (Table 1.1). Given these encouraging results, we extended the same methodology to the synthesis of Boc- β-amino alcohols. The *N*-hydroxysuccinimide esters of Boc-amino acids were prepared from the coupling reaction of Boc-amino acids and HOSu using DCC as a coupling agent (Scheme 1.4). A list of Boc-β-amino alcohols is given in Table 1.2 (entries 11–15). The yields and optical rotations of Boc-β-amino alcohols from the succinimide

method are in agreement with the mixed anhydride method (data not shown). Except for 15, all Boc-β-amino alcohols were isolated as oils.

1.4.3 Racemisation study of alcohols with Chiral HPLC

To investigate the racemization during the synthesis of β-amino alcohols, we synthesized Fmoc-β-amino alcohols from D-, L- and DL-alanine. These amino alcohols were subjected to chiral HPLC separation using a chiralpack AD column. The HPLC profiles of Fmoc-protected D-, L- and DL-Alaol is shown in Figure 1.6. Single peaks were obtained for Fmoc-L-Alaol and Fmoc-D-Alaol at t_R 6.24 min and 7.66 min, respectively. For the DL mixture two peaks with t_R at 6.26 and 7.70 min were observed, corresponding to the individual enantiomers. These results indicate that no racemization occurred during the syntheses of the β-amino alcohols.

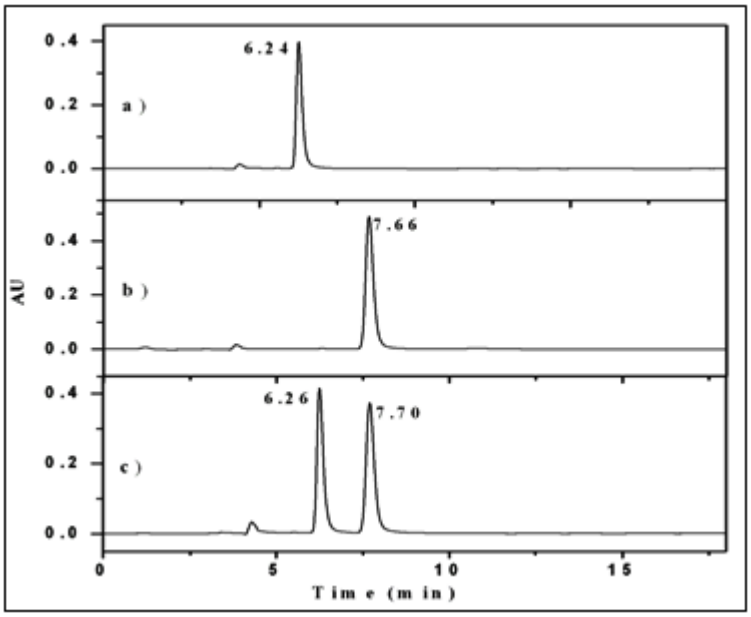

Figure 1.6 Chiral HPLC of Fmoc-protected L-, D- and DL-Alaol. HPLC was performed on a chiralpack AD column using 90% isopropanol in *n*-hexane as the solvent system in the isocratic mode with a flow rate of 1 mL min^{-1}. HPLC profiles for: a) Fmoc-L-Alaol; b) Fmoc-D-Alaol; c) Fmoc-DL-Alaol.

1.4.4 Peptide alcohol/ Peptaibol

Due to their biological importance, a variety of methods have been reported in the literature for the synthesis of peptide alcohols, including the nucleophilic substitution of free amino alcohols in N-protected amino acid benzotriazoles,[39] O–N acyl transfer of peptide esters[40] and the coupling reaction of N-protected amino acids and free amino

alcohols using standard coupling reaction conditions.[41]We further explored whether N-hydroxysuccinimide method can be extended to the synthesis of peptide alcohols. To extend this methodology to peptide alcohols, we synthesized the following methyl esters of Boc-protected dipeptides using a DCC and HOBt protocol – Boc-Ala- Val-OMe, Boc-Val-Val-OMe and Boc-Val-Leu-OMe. The pure dipeptide acids were obtained after the saponification of methyl esters using 1N NaOH.

1.4.5 Synthesis of di-, tri- and penta-peptide alcohol

The dipeptide acids were converted to *N*-hydroxysuccinimide active esters using DCC and HOSu in ice-cold THF. The separated DCU was filtered, and the filtrate containing Boc-dipeptide active ester was reduced *in situ* using $NaBH_4$ in water. As anticipated, all peptide alcohols were isolated in pure form without column purification in high yields (Table 2, entries 16, 17 and 18). The results from both ^{1}H-NMR and HPLC reveal single enantiomers as the products, indicating that the synthesis is free from racemization. We further extended this methodology to the synthesis of Boc-protected tripeptide alcohols, Boc-Ala-Leu-Valol (entry **19**), Boc-Aib- Ala-Leuol (entry **20**) and a pentapeptide alcohol, Boc-Val-Leu-Ala-Val-Leuol (entry **21**). Most peptaibols are Aib (α,α-dimethyl glycine)-rich peptides,[42] so we included Aib in peptaibol **20** to mimic the C-terminal sequences of peptaibols. The tri- and pentapeptide acids were obtained after the saponification of the C-terminal methyl esters. These peptide acids were converted to active esters as described for the dipeptide acids and subjected to *in situ* reduction. The tripeptide alcohols (**19** and **20**) were isolated in pure form without column purification in good yields, while the peptaibol (**21**) was purified by reverse-phase HPLC using a C18 column. Out of all the peptides, we were able to obtain single crystals for Boc-Ala-Valol (**16**) and Boc-Aib-Ala-Leuol (**20**). The conformation of these peptide alcohols is described in Figure 1.7.

1.5 Crystal structures of β-amino alcohol and dipeptide alcohols

Crystals of Fmoc-Valol were obtained after slow evaporation of ethyl acetate, and the crystal structure is shown in Figure 1.7A.The molecule adopted an extended-sheet type of assembly by the intermolecular H-bonding of NH and OH groups with the urethane carbonyl of the neighbouring molecule. Crystals of the dipeptide alcohol **16** obtained in methanol solution yield the structure shown in Figure 1.7B. Two molecules appear in the

asymmetric unit, with significant variation in the torsional values. The dipeptide alcohol adopted an irregular structure in the crystal packing. Notably, an energetically unfavourable *cis*-Boc–urethane bond is observed in the molecule B (Figure 1.7B).

1.5.1 Crystal structures of tripeptide alcohol

Colourless crystals of peptaibol **20** were obtained after slow evaporation of $CHCl_3$, and the X-ray diffraction analysis is described below. Interestingly, a well-folded structure of the

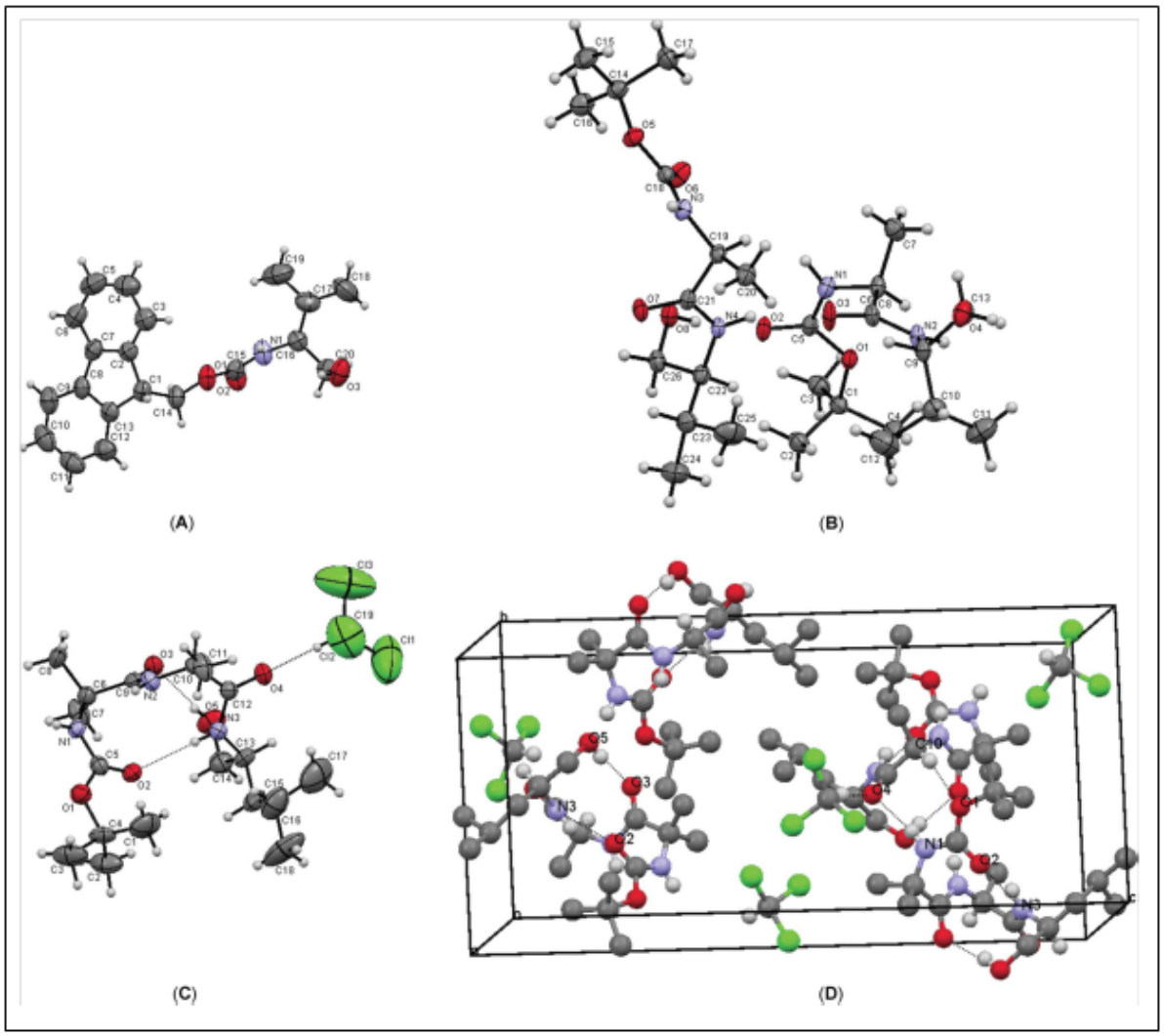

Figure 1.7 A) Crystal structures of Fmoc-Valol (3), Boc-Ala-Valol (16) and Boc-Aib-Ala-Leuol (20). The H-atoms are not labeled for clarity. A: The crystal structure of Fmoc-Valol. B: ORTEP diagram showing the two molecules of 16 (A and B) in the asymmetric unit. C: ORTEP diagram showing the conformation of the tripeptide alcohol in crystals. Two intramolecular H bonds are shown by dotted lines. The interaction of solvent molecule($CHCl_3$) with peptide through a CH---O hydrogen bond is also shown. D: The unit cell showing four molecules of tripeptide alcohol and four molecules of $CHCl_3$ in the asymmetric unit. All side-chain H-atoms are omitted for clarity

tripeptide alcohol is observed in the crystals, as shown in the ORTEP diagram (Figure 1.7C). The crystallographic asymmetric unit contains four molecules of tripeptide alcohol and four solvent $CHCl_3$ molecules. Intriguingly, two peptaibols are connected by intermolecular hydrogen bonding, while the other two are independent (Figure 1.7D). Two intramolecular hydrogen bonds correspond to Boc C=O---NH Leuol(3), and Aib(1) C=O---OH Leu(3)ol observed in the crystal structure (Figure 1.7C). As a consequence of the two intramolecular C10 hydrogen bonds, two types of β-bends are observed. The relevant torsional angles and hydrogen bond parameters are tabulated in Tables 1.3 and 1.4,

Table 1.3: Torsion angles in (°) tripeptide alcohol **20**

Peptide	Residue	ϕ	ψ	ω	$\chi 1$	$\chi 2$	$\chi 3$
20	Aib1	-60	-30	179	---	---	---
	Ala2	-61	-25	172	175	---	---
	Leu-ol3	-110	58	---	-55	-179	-53

Table 1.4: Intra- and intermolecular H-bonding in crystals of the tripeptide **20**

No	Donar (D)	Aceptor (A)	Type	A-H (Å)	D-A (Å)	D-H---A (angle)
1	N1	O4	Intermolecular (NH---O=C)	2.142	2.994	171
2	N3	O2	Intramolecular (NH---O=C)	2.203	2.974	149
3	O5	O3	Intramolecular (O-H---O=C)	2.188	2.914	148
4	C10	O1	Intermolecular (C-H---O)	2.548	3.505	165
5	C19[a]	O4	Intermolecular (C-H---O=C)	2.126	3.102	171

respectively. A ten-membered H-bond between the urethane carbonyl and the Leu NH (1→4) leading to the formation of a type III β-turn with torsional angles ϕ_1 = -60°, ψ_1 = -30°, ϕ_2 = -61° and ψ_2 = -25.27°.Interestingly, the type III β-turn was further stabilized by another C10 H-bond between the Ala2 carbonyl and the terminal OH (Figure 1.7C). The solvent $CHCl_3$ interacted with the peptaibol through a CH---O hydrogen bond having an H---O distance of 2.126 A° and a C–H---O angle of 171°. However, interaction between the $CHCl_3$ molecules is not observed in the structure (the Cl---Cl distance is 3.9A°). It appears that the solvent is stabilizing the crystal packing by filling the vacant space. The two folded conformers of the tripeptide alcohol are held together by two intermolecular hydrogen bonds between Aib(1) NH and Ala(2) CO and between the Boc-urethane oxygen O1 and Ala2 CαH in the crystals (Figure 1.7D). Overall, we observed an irregular structure in the dipeptide alcohol and a well-defined type III β-turn in the tripeptide alcohol. The type III β-turn in the tripeptide alcohol may be induced by the presence of the conformationally restricted dialkyl amino acid residue (Aib) at the N-terminus of the tripeptide. Toniolo et al. and others have also shown the formation of type III and III' β-turns by di- and tripeptides containing dialkyl amino acids.[43]

1.6 Synthesis and crystal structures of γ^4-amino acids

β-Amino alcohols obtained from HOSu method were subsequently oxidised to α-amino aldehydes using oxidizing reagent IBX. The N-protected amino aldehydes were subjected to the Wittig reaction. Using the earlier reported method in our laboratory we synthesised the various pure Fmoc-protected-*E*-vinylogous benzyl esters (Scheme 1.5).[32] The pure Fmoc-protected-*E*-vinylogous benzyl esters were subjected to the catalytic hydrogenation for the

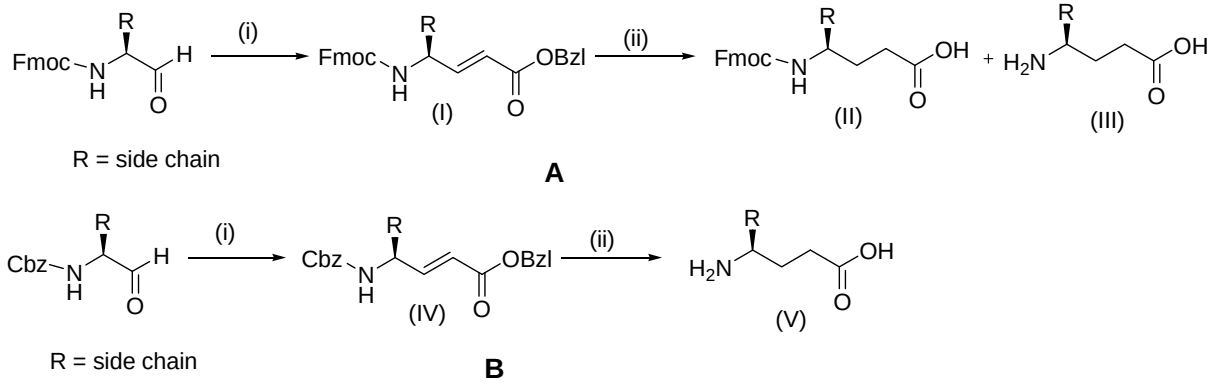

Scheme 1.5 a) Synthesis of A) Fmoc-protected γ^4-amino acids and B) freeγ^4-amino acids ; i) Ph_3P=CH-COOBzl, THF; ii) Pd/C, H_2, 10% CH_3COOH in THF.

concomitant reduction of double bonds as well as benzyl ester deprotection. During the process catalytic hydrogenation, we isolated the by-product 9-methyl-9H-fluorene which suggests the Fmoc- group deprotection during the process and leads to the decreased yield of final N-Fmoc protected γ^4-amino acids.[44] The lower yields and unexpected byproduct motivated us to search for a suitable protecting group strategy for the synthesis of γ^4-amino acids. In the process, we realized that amino protecting group Cbz (benzyloxy carbonyl) and benzyl ester can be removed at once using catalytic hydrogenation under neutral or mild acidic conditions with concomitant reduction of the double bond. For this purpose various N-Cbz-protected *E*-α, β-unsaturated amino acid benzyl esters were synthesized using Wittig reaction. The schematic representation of the synthesis of γ^4-amino acids starting from N- Cbz-amino aldehydes is shown in Scheme 1.5. All N-Cbz-protected *E*-α, β-unsaturated amino acid benzyl esters (Ia-m, Table 1.5) were subjected to the catalytic hydrogenation in 10% acetic acid in THF. The solvent conditions were optimized based on the solubility of the free amino acids in acidic solution. As anticipated the hydrogenolysis of both Cbz- and benzyl ester along with the double bond reduction were achieved in a single Step (Figure 1.8) and the γ^4-amino acids (IIa-m) were isolated as acetate salts in moderate to good yields (60- 90%). No cyclised products of γ-residues were observed in the process of catalytic hydrogenation from the *E*-vinylogous amino acids. Except, γ^4Ala (IIa), (D)γ^4Val(IIc), γ^4Ser(OBu^t) (IIf) and γ^4Trp (IIj), we were able to obtain the single crystals for all other nine γ^4-amino acids listed in Table 5 (IIb, IId, IIe IIg-i and IIk-m). The crystal conformations of γ^4-amino acids are shown in the Figure 1.9. The torsional values were measured by introducing additional variables θ_1 (N-C^{γ}-C^{β}-C^{α}) and θ_2 (C^{γ}-C^{β}-C^{α}-C=O). It has been observed that γ-residues adopt *gauche* conformation along θ_1 and θ_2 in helical peptides.[45] Here, crystal structure analysis of γ-residues revealed that except γ^4-Asp, all free γ^4-amino acids adopted *gauche* conformation along θ_1 and *anti* conformation along θ_2, which underlines the propensity of γ^4-residues towards helical organization (Table 1.6). Further, all free γ^4-amino acids were protected with the Fmoc- group using Fmoc-OSu/Na_2CO_3 and isolated in a moderate to good yields. Depending on synthetic requirement, these free γ^4-amino acids can be further protected with various protecting groups (Figure 1.10)

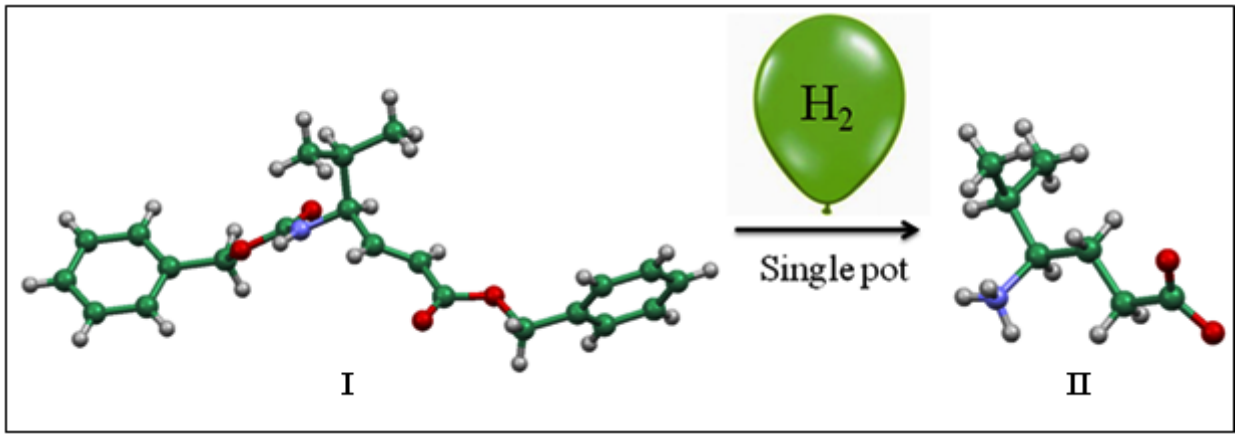

Figure 1.8 Single pot conversion of Cbz-*dg*Val-OBzl to γ^4-Val

Table 1. 5: γ^4-Amino acids from Cbz-protected E-vinylogous amino benzyl esters

No.	(I)	(II)	% Yield
a	Cbz-dgAla-OBzl	H-γAla-OH	82
b	Cbz-dgVal-OBzl	H-γVal-OH	76
c	Cbz-(D)dgVal-OBzl	H- (D)γVal-OH	70
d	Cbz-dgLeu-OBzl	H-γLeu-OH	86
e	Cbz-dgIle-OBzl	H-γIle-OH	65
f	Cbz-dgSer(OtBu)-OBzl	H-γSer(OtBu)-OH	75
g	Cbz-dgThr(OtBu)-OBzl	H-γThr(OtBu)-OH	80
h	Cbz-dgAsp(OtBu)-OBzl	H-γAsp(OtBu)-OH	90
i	Cbz-dgGlu(OtBu)-OBzl	H-γGlu(OtBu)-OH	81
j	Cbz-dgTrp-OBzl	H-γTrp-OH	80
k	Cbz-dgTyr-OBzl	H-γTyr-OH	85
l	Cbz-dgAib-OBzl	H-γAib-OH	60
m	Cbz-dgPhe-OBzl	H-γPhe-OH	75

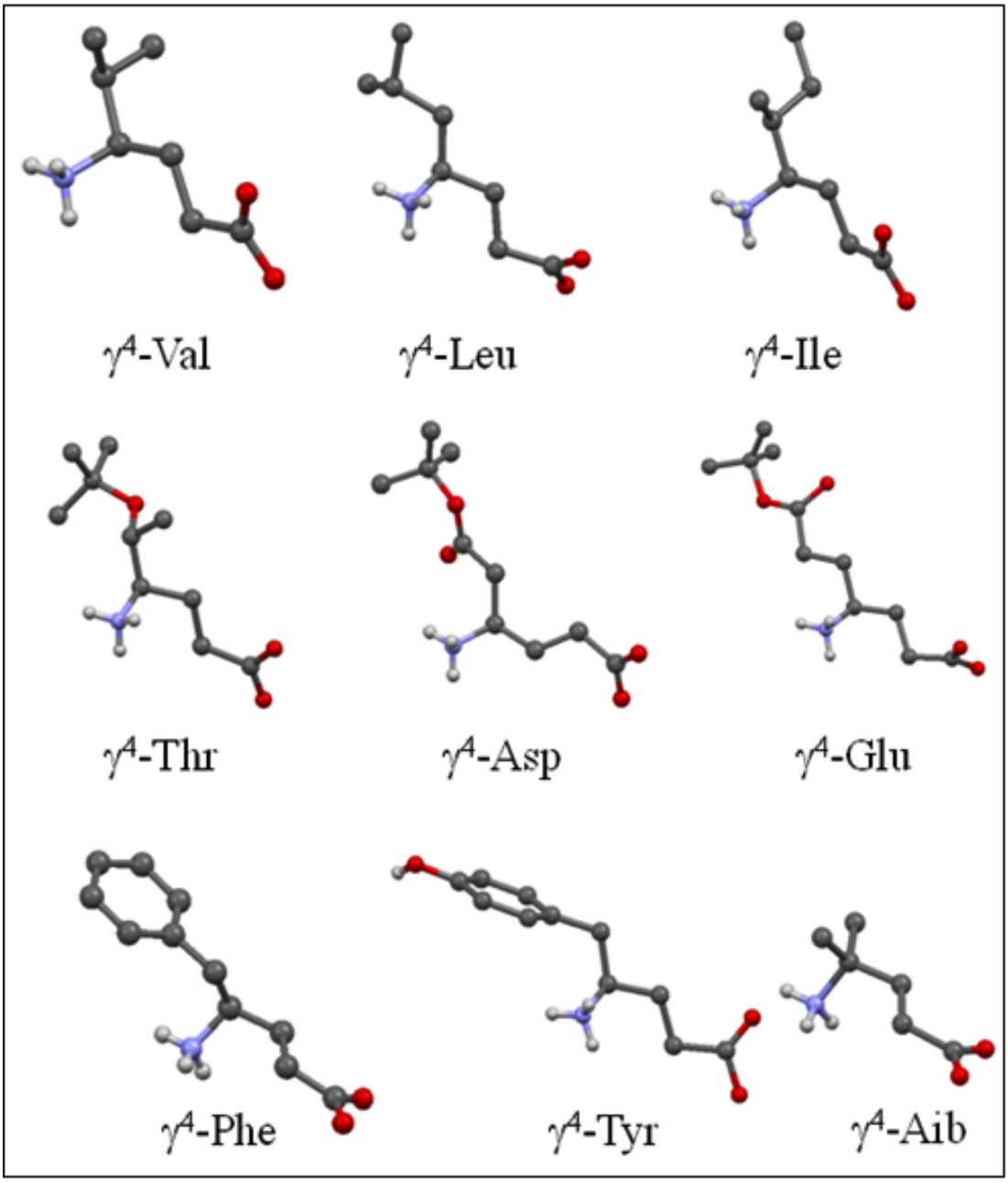

Figure 1.9 Crystal structures of γ^4-amino acids.

Table 1.6: Additional torsion angles for γ^4-amino acids

γ^4 amino acid	θ_1	θ_2	θ_1'	θ_2'
Val	64.58	-176.60	---	---
Leu	56.20	174.94	---	---
Ile	66.59	-168.75	---	---
Thr	67.29	-160.17	---	---
Asp	-176.57	-168.79	-73.59	---
Glu	53.49	177.11	-64.96	-170.91
Tyr	63.04	173.33	---	---
Aib	-64.12	171.20	---	---
Phe	-63.0	-170.0	---	---

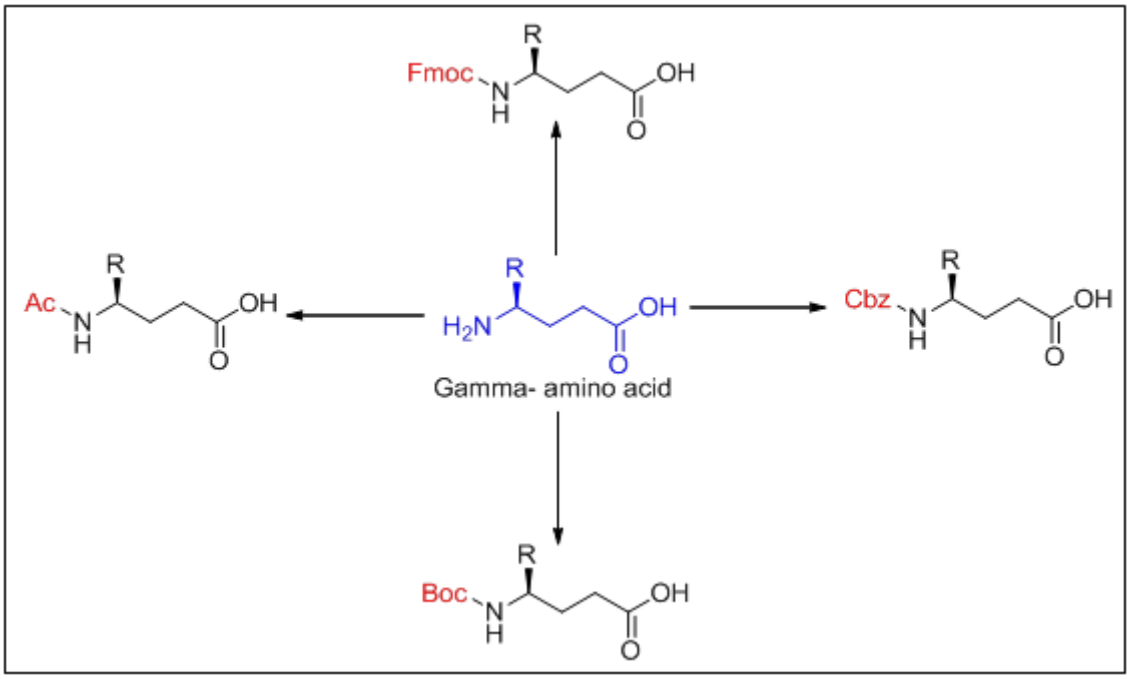

Figure 1.10 N-terminal protections of γ^4-amino acids with different protecting groups

1.7 Racemization studies of γ^4-amino acids

Further, to understand the racemization during the synthesis of γ^4-amino acids, we coupled Fmoc-γ^4Ala obtained after the Fmoc-protection of γ^4-Ala, with (-), (+) and (±) α-methyl benzylamine using standard DCC/HOBt coupling conditions. All three amide derivatives were isolated and subjected to the chiral HPLC using CHIRALPAK®IA analytical column. The HPLC profiles of all three amide derivatives are shown Figure 1.11. The

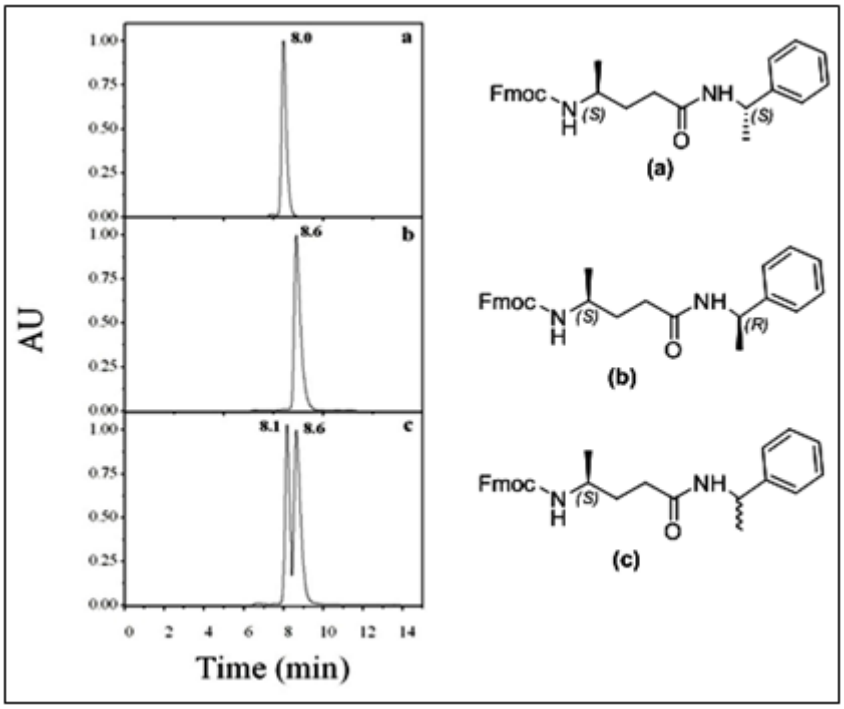

Figure 1.11 Chiral HPLC for (-), (+) and (±) α-methyl benzylamine derivatives of Fmoc- γ^4-alanine**:** Chiral HPLC of was performed on chiralpack IA column using 70 % isopropanol in *n*-hexane as a solvent system in isocratic mode with flow rate of 0.5 mL/min:

a) HPLC profile of (9H-fluoren-9-yl)methyl (S)-5-oxo-5-((*S*)-1-phenylethylamino)pentan-2-ylcarbamate
b) HPLC profile of (9H-fluoren-9-yl)methyl (S)-5-oxo-5-((*R*)-1-phenylethylamino)pentan-2-ylcarbamate
c) HPLC profile of (9H-fluoren-9-yl)methyl (S)-5-oxo-5-(±)-1-phenylethylamino)pentan-2-ylcarbamate.

Fmoc-γ^4-Ala derivative with (-) α-methyl benzylamine (A) eluted with the t_R 8.0 min, while the amide with (+) α -methyl benzylamine (B) eluted at t_R 8.6 min. The Fmoc-γ^4-Ala derivative with (±)α -methyl benzylamine (C) gave two peaks at t_R 8.1 and 8.6 min

corresponding to the (A) and (B), respectively. The results indicate that the procedure that we adapted for the synthesis of γ^4-amino acids is free from the racemization.

1.8 Conclusions

In conclusion, we have developed the mild and efficient synthesis of various N- and C-terminal unprotected stereochemically pure γ^4-amino acids from the benzyl esters of N-Cbz-*E*-vinylogous γ-amino acids, through multiple hydrogenolysis and the double bond reduction in one pot catalytic hydrogenation. In the process, we have also developed a new, mild racemisation free protocol for the synthesis of β-amino alcohols and peptaibols. For the synthesis of alcohols we showed that HOSu method is superior than IBC-Cl method as it requires no dry condition, gives higher yields and works at 0 ^{o}C. In addition, this method was found to be compatible with Fmoc, Boc, and other side-chain protecting groups. The α-amino aldehyde obtained from oxidation of β-amino alcohols was directly subjected to the Witting reaction. Using Witting reaction benzyl esters of N-Cbz-*E*-vinylogous γ-amino acids were synthesized and subjected for catalytic hydrogenation. All γ^4-amino acids with various proteinogenic sidechains were isolated from moderate to good yields. Further, we proved that the method we adopted for the synthesis of γ-amino acids is free from racemisation. The crystal conformations of various γ^4-residues reveal that they adopt helix favouring *gauche* conformations along the N-C-C-C bond (θ_1) and *anti* conformation along the C-C-C-C (θ_2) bond. With this mild and facile protocol in hand we synthesized and studied conformations of various α,γ-hybrid peptides in the Chapter 2.

1.9 Experimental section

1.9.1General procedure for the synthesis of Fmoc- or Boc- protected β-amino alcohol from *N*-hydroxysuccinimide esters:

To a solution of Fmoc- or Boc-protected amino acid (2 mmol) and N-hydroxysuccinimide (0.345 g, 3 mmol) at 0 ^{o}C in THF (5 mL), was added DCC (0.413 g, 2 mmol), and reaction was stirred at this temperature for 1 h. precipitated DCU was filtered and washed with THF (3 X 2 mL), combined organic layer was cooled to ice temperature and the solution of sodium borohydride (0.152 g, 4 mmol) in water (1 mL) was added in one portion which leads to the vigorous evolution of gas. After 5 min, 5 mL of 0.5 N HCl was added to

quench unreacted $NaBH_4$. Reaction mixture was extracted in EtOAc (3 X 10 mL), and combined organic layer was washed with 5% Na_2CO_3 (3 X 10 mL),brine (3 X 10 mL),dried over Na_2SO_4, and concentrated in *vacuo*. After work up procedure, Boc protected beta amino alcohols were obtained as pure product over 80-90% yield. Fmoc protected Products were purified over silica gel column chromatography to get pure beta amino alcohol over 70-90% yield.

1.9.2 General procedure for the synthesis of *N*-protected β-amino alcohol using mixed anhydride method:

Isobutyl chloroformate (0.26 mL, 2 mmol) was added dropwise to the solution of N-protected amino acid (2 mmol) and DiPEA(0.35 mL,2 mmol) at -15 to -20 ^oC in THF (5 mL), After 5 min. precipitate of DiPEA hydrochloride salt was filtered and washed with THF (2 X 3 mL). Combined organic layer was cooled in salt-ice temperature and the solution of sodium borohydride (0.152 g, 4 mmol) in water (1 mL) was added in one portion which leads to strong evolution of gas. After 5 min, 5 mL of 0.5 N HCl was added to quench unreacted $NaBH_4$. The reaction mixture was extracted in EtOAc (3 X 10 mL), washed with 5% Na_2CO_3 (3 X 10 mL), brine (3 X 10 mL), dried over Na_2SO_4 and concentrated in *vacuo*.

1.9.3 Peptide synthesis

Dipeptide and tripeptide were synthesized by conventional solution-phase methods by using a fragment-condensation strategy. The *tert*-butyloxycarbonyl group was used for N-terminus protection, and the C-terminus was protected as a methyl ester. Deprotections were performed with trifluoroacetic acid and saponification for the N- and C-termini, respectively. Couplings were mediated by dicyclohexylcarbodiimide (DCC)/1-hydroxybenzotriazole (HOBt). The tripeptide Boc-Aib-Ala-Leu-OMe was prepared by [2+1] condensation involving an N-terminus dipeptide acid Boc-Aib-Ala-OH and H-Leu-OMe using DCC/N-Hydroxysuccinimide (HOSu). Another Tripeptide Boc-Ala-Leu-Val-OMe was prepared by [2+1] condensation involving N-terminus dipeptide acid Boc-Ala-Leu-OH and H-Val-OMe, by using DCC/N-Hydroxysuccinimide (HOSu).

1.9.4 General procedure for the synthesis of Boc protected dipeptide alcohol and tripeptide alcohol (Peptaibol)

The previous procedure was utilized to synthesize Boc protected dipeptides, tripeptides and pentapeptide alcohols. Products were obtained over 70-90% yield in pure form after work up procedure which are then further subjected to the IBX oxidation.

1.9.5 Crystal structures of alcohols

Crystal structure of Fmoc-Val-ol (3).

CCDC No.: 794215

$C_{20}H_{23}N_1O_3$; A colourless crystal with approximate dimensions 0.85 x 0.50 x 0.25 mm gave a Monoclinic with space group *P2(1);a* = 4.942(4), *b* =11.622(11), *c* = 15.783(14) Å, $\alpha = 90^o$ $\beta = 93.573(14)^o$ $\gamma = 90^o$; *V* = 904.7(14)Å^3; *T* = 296 (2) K; *Z* = 2; ρ_{calcd} =1.195 Mgm^{-3}; $2\theta max$ = 56.56°; $MoK\alpha\lambda$= 0.71073 Å. Fine-focus sealed tube source with graphite monochromator. *R* = 0.0410 (for 2760 reflections with $I>2\sigma(I)$); *wR* = 0.0508 which was refined against $|F^2|$ and *S* = 1.456, for 220 parameters and 4239 unique reflections. The structure was obtained by direct methods using SHELXS-97.[29] All non-hydrogen atoms were refined isotropically. The hydrogen atoms were fixed geometrically in the idealized position and refined in the final cycle of refinement as riding over the atoms to which they are bonded. μ = 0.08 mm^{-1}; Minimum/maximum residual electron density –0.161/0.107 eÅ^{-3}.

Crystal structure of Boc-Ala-Val-ol (16)

CCDC No.: 805264

$C_{13}H_{26}N_2O_4$; A colourless crystal with approximate dimensions 0.70 x 0.60 x 0.15 mm gave an orthorhombic space group *Pbca; a* = 9.704(3), *b* =13.077(3), *c* = 25.661(7) Å, $\alpha = \beta = \gamma = 90^o$; *V* = 3256.3(15)Å^3; *T* = 296 (2) K; *Z* = 8; ρ_{calcd} =1.119 Mgm^{-3}; $2\theta max$ = 44.04°; $MoK\alpha\lambda$= 0.71073 Å. Fine-focus sealed tube source with graphite monochromator. *R* = 0.0677 (for 2585 reflections with $I>2\sigma(I)$); *wR* = 0.1646 which was refined against $|F^2|$ and *S* = 1.068, for 358 parameters and 3995 unique reflections. The structure was obtained by direct methods using SHELXS-97.[29] All non-hydrogen atoms were refined isotropically. The hydrogen atoms were fixed geometrically in the idealized position and

refined in the final cycle of refinement as riding over the atoms to which they are bonded, μ = 0.082 mm^{-1}; Minimum/maximum residual electron density –0.24/0.287 $eÅ^{-3}$.

Crystal structure of Boc-Aib-Ala-Leuol (20)

CCDC No.: 794216

A colourless crystal with approximate dimensions 1.2 \ 0.55 \ 0.15 mm had the following characteristics: formula $C_{18}H_{35}N_3O_5.CHCl_3$; crystal class orthorhombic; space group *P*212121; a = 10.578(4); b = 11.206(4); c = 23.306(8) A° ; $\alpha = \beta = \gamma = 90°$; V = 2762.7(17)$A^{°3}$; T = 296(2) K; Z = 4; r_{calc} = 1.185 Mgm^{-3}; $2\theta max$ = 56.56°; Mo-Kα λ = 0.71073 A° . A fine-focus sealed tube source with a graphite monochromator was used. Treatment of H atoms was mixed-type. R = 0.0673 (for 1573 reflection $I > 2\sigma(I)$), wR = 0.1608, which was refined against $|F^2|$ and S = 0.715 for 280 parameters and 6526 unique reflections. The structure was obtained by direct methods using SHELXS-97. All nonhydrogen atoms were refined anisotropically. The hydrogen atoms were fixed geometrically in the idealized position and refined in the final cycle of refinement as riding over the atoms to which they are bonded; μ = 0.361 mm^{-1}; minimum/maximum residual electron density -0.233/0.444 $eA^{°-3}$.

1.9.6 Synthesis of N-Cbz-protected amino aldehyde using IBX

The N-Cbz-protected β-amino alcohol (8 mmol) was refluxed with IBX (5.6 g, 20 mmol) in EtOAc (30 mL) for 2-4 hr. After completion of reaction (monitored by TLC), the IBX was filtered through celite. Filtrate was evaporated to dryness under *vacuum* which gives N-Cbz-protected β-amino aldehyde in a quantitative yield which immediately subjected to the Wittig reaction.

1.9.7 Synthesis of N-Cbz-protected *E*-vinylogous amino ester

To the solution of *N*-Cbz-protected β-amino aldehyde (6 mmol) in dist. THF (25 mL) was added Wittig ylide (2.454g, 6 mmol). The reaction mixture was stirred at room temperature for 4-8 hrs. After completion, the reaction mixture was evaporated to dryness. Pure Wittig product was obtained over 70-80% yield after silica gel (100-200 mesh) column purification using ethyl acetate/petroleum ether (60-80 °C) solvent system.

1.9.8 Synthesis of (γ^4) amino acid from Cbz-protected *E*-vinylogous amino ester

The suspension of activated Pd/C (20% by weight) and the Cbz-protected *E*-vinylogous amino ester (5 mmol) in THF (30 mL) [or in acetic acid (30 mL) or 10% acetic acid in methanol/THF] was stirred overnight at room temperature in the presence of Hydrogen gas (H_2 balloon). After completion, the Pd/C was filtered through a bed of celite and the filtrate was evaporated to dryness under *vacuum* to get gummy γ^4-amino acids. The pure γ^4-amino acids were isolated after the reprecipitation from cold ethyl ether. Overall yield was 60-90%.

1.9.9 Synthesis of (9H-fluoren-9-yl)methyl (S)-5-oxo-5-((S)-1-phenylethylamino)pentan-2-ylcarbamate and (9H-fluoren-9-yl)methyl (S)-5-oxo-5-((R)-1-phenylethylamino)pentan-2-ylcarbamate

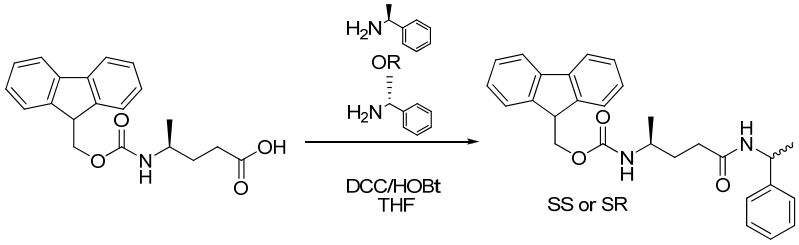

To the solution of Fmoc-γ^4Ala-OH (0.339 g, 1 mmol) and (*R*)-(+)-α-methyl benzylamine or (*S*)-(-)-α-methyl benzylamine or (±) -α-methyl benzylamine (0.191 mL, 1.5 mmol) in THF (3 mL) was added HOBt (135 mg, 1 mmol) followed by DCC (0.206 g, 1 mmol) at 0 ^oC and the reaction mixture was stirred for about 4 hrs under N_2 atmosphere. Precipitated DCU was filtered through celite. The filtrate was concentrated under *vacuum* and diluted with water (50 mL). The reaction mixture was extracted with EtOAc (3 X 50 mL), and the combined organic layer was washed with 5% HCl (3 X 10 mL), brine (3 X 10 mL), dried over Na_2SO_4, and concentrated under *vacuum*. The crude amide derivatives were isolated over 85% yield after column purification and directly used for HPLC analysis

1.10 Crystal structure report of γ^4-amino acids

X-ray quality crystals were grown by solvent slow evaporation as mentioned in table 7.

Table 1.7 Crystallization conditions (Slow evaporation of a methanol/water)

γ^4-amino acid	crystallization condition (solvent mixture)
Val	Solvent Evaporation (MeOH/H_2O)
Leu	Solvent Evaporation (MeOH/H_2O)
Ile	Solvent Evaporation (MeOH/H_2O)
Thr	Solvent Evaporation (MeOH/H_2O)
Asp	Solvent Evaporation (MeOH/H_2O)
Glu	Solvent Evaporation (MeOH/H_2O)
Tyr	Solvent Evaporation (MeOH/H_2O)
Aib	Solvent Evaporation (MeOH/H_2O)
Phe	Solvent Evaporation (MeOH/H_2O)

1.10.1 General procedure for crystallization of γ^4-amino acids

All crystallization attempts were conducted at room temperature. All γ^4-amino acids were precipitated from diethyl ether and dried well under vacuum before keeping for crystallization. Glass sample vials (2 mL) were washed with acetone and dried under a nitrogen gas stream before use. PARAFILM "M" was used to close the vial. HPLC-grade solvents were used for crystallization. γ^4-Amino acid (10-20 mg) was dissolved in methanol (1.0 mL). The solution was transferred through a syringe filter into a glass vial. A few drops of water (0.5 mL) were added with gentle shaking of vial to get clear solution. The vial was closed with a PARAFILM, and then pricked gently with clean and sharp needle to introduce 4 to 5 pores on PARAFILM so as to let the solvent mixture evaporate slowly. High-quality crystals were obtained within few days, before sample was completely dry.

Data Collection

A colorless crystal with difractable dimensions was selected under oil under ambient conditions and attached on nylon CryoLoops with Paraton-N (Hampton Research). The crystal was mounted in a stream of cold nitrogen at 100(2) K and centered in the X-ray beam by using a video camera.

The crystal evaluation and data collection were performed on a Bruker KAPPA APEX II CCD Duo diffractometer (operated at 1500 W power: 50 kV, 30 mA) with Mo Kα (λ = 0.71073 Å) radiation and the diffractometer to crystal distance of 6.0 cm.

The initial cell constants were obtained from three series of ω scans at different starting angles. Each series consisted of 12 frames collected ω with the exposure time of 10-20 seconds per frame. Obtained reflections were successfully indexed by an automated indexing routine built in the SMART program.

The data were collected by using the full sphere data collection routine to survey the reciprocal space to the extent of a full sphere to a resolution of 0.75 Å, with an exposure time 10-20 sec per frame. The data integration and reduction were processed with SAINT[46] software. A multi-scan absorption correction was applied to the collected reflections.

Structure Solution and Refinement

The systematic absences in the diffraction data were yielded chemically reasonable and computationally stable results of refinement.[47]

A successful solution by the direct methods provided most non-hydrogen atoms from the *E*-map. The remaining non-hydrogen atoms were located in an alternating series of least-squares cycles and difference Fourier maps. All non-hydrogen atoms were refined with anisotropic displacement coefficients. All hydrogen atoms were included in the structure factor calculation at idealized positions and were allowed to ride on the neighbouring atoms with relative isotropic displacement coefficients.

Crystal data and structure refinement for γ^4-val

CCDC No.: 855464

Empirical formula:C_7 H_{15} N_1 O_2 ; Formula weight :145.20; Temperature:100(2) K ;

Wavelength:0.71073 Å ; Crystal system: Monoclinic ; Space group: P21; Unit cell dimensions: a = 7.910(4)Å, b = 6.385(4)Å , c = 8.214(5)Å, α = 90°, β = 99.231(12) (3)° , γ= 90°; Volume:409.5(4)Å^3 ; Z:2 ; Density (calculated): 1.178Mg/m^3 ; Absorption coefficient (μ):0.085mm^{-1}; F (000):160; Crystal size:0.50 x 0.40 x 0.05 mm^3 ; Theta range for data collection: 2.51 to 28.28° ; Index ranges :-10<=h<=9, -8<=k<=5, -10<=l<=10 ; Reflections collected: 4000 ; Independent reflections: 1584 [R(int) = 0.0610] ; Completeness to theta (28.28°) : 95.6 % ; Absorption correction: Empirical with SADABS; Max. and min. Transmission: 0.996 and 0.960; Refinement method: Full-matrix least-squares on F^2 ; Data / restraints / parameters: 1584 / 1 / 94 ; Goodness-of-fit on F^2 : 0.897; Final R indices [I>2sigma(I)]: R1 = 0.0591, wR2 = 0.1348; R indices (all data): R1 = 0.1111, wR2 = 0.1637 ; Absolute structure parameter : -1(3); Largest diff. peak and hole :0.201 and -0.267 e.Å^{-3}.

Crystal data and structure refinement for γ^4-Leu

CCDC No.: 855479

Empirical formula: C_8 H_{17} N_1 O_2, (O) ; Formula weight :175.23; Temperature:100(2) K ;Wavelength :0.71073 Å ; Crystal system :Monoclinic ; Space group:C2 ; Unit cell dimensions: a = 9.781(13)Å , b = 7.585(9)Å , c = 14.142(16)Å, α = 90°, β = 95.03(2) (3)° , γ = 90°; Volume:1045(2)Å^3 ; Z :4 ; Density (calculated):1.114Mg/m^3 ; Absorption coefficient (μ) :0.084mm^{-1} ; F (000):348; Crystal size :0.70 x 0.20 x 0.10 mm^3 ; Theta range for data collection :1.45 to 28.28° ; Index ranges:-6<=h<=12, -10<=k<=10, -18<=l<=18 ; Reflections collected:6041 ; Independent reflections :2151 [R(int) = 0.1850] ; Completeness to theta = 28.28° :98.1 % ; Absorption correction: Empirical with SADABS ; Max. and min. Transmission: 0.992 and 0.980; Refinement method :Full-matrix least-squares on F^2 ; Data / restraints / parameters:2151 / 1 / 112; Goodness-of-fit on F^2 :0.895; Final R indices [I>2sigma(I)] :R1 = 0.0761, wR2 = 0.1826; R indices (all data):R1 = 0.1943, wR2 = 0.2402 ; Absolute structure parameter :2(4); Largest diff. peak and hole :0.328 and -0.343 e.Å^{-3}.

Crystal data and structure refinement for γ^4-Ile

CCDC No.: 855480

Empirical formula: C_8 H_{17} N_1 O_2 ; Formula weight:159.23; Temperature :100(2) K ;

Wavelength :0.71073 Å ; Crystal system: Monoclinic ; Space group:P21; Unit cell dimensions: a = 7.942(5)Å, b = 6.086(4)Å, c = 9.985(6)Å , α = 90° , β = 105.458(12) (3)°, γ = 90°; Volume : 465.2(5)Å^3 ; Z:2 ; Density (calculated):1.137Mg/m^3 ; Absorption coefficient (μ) :0.080mm^{-1} ; F (000):176; Crystal size :0.30 x 0.20 x 0.10 mm^3 ; Theta range for data collection:2.12 to 27.80° ; Index ranges :-10<=h<=10, -7<=k<=7, -12<=l<=13; Reflections collected:7256 ; Independent reflections:2040 [R(int) = 0.0689]; Completeness to theta = 27.80° :98.3 % ; Absorption correction: Empirical with SADABS ; Max. and min. Transmission: 0.992 and 0.981; Refinement method :Full-matrix least-squares on F^2 ; Data / restraints / parameters :2040 / 1 / 104 ; Goodness-of-fit on F^2 :0.864; Final R indices [I>2sigma(I)]:R1 = 0.0569, wR2 = 0.1376; R indices (all data):R1 = 0.0969, wR2 = 0.1662 ; Absolute structure parameter : 1(2); Largest diff. peak and hole :0.294 and -0.212 e.Å^{-3}.

Crystal data and structure refinement for γ^4-Thr

CCDC No.: 855481

Empirical formula:C_{10} H_{21} N_1 O_3 ; Formula weight:203.28; Temperature :100(2) K ; Wavelength:0.71073 Å ; Crystal system :Monoclinic ; Space group:P21; Unit cell dimensions: a = 7.780(6)Å, b = 6.275(5)Å , c = 12.396(10)Å, α = 90°, β = 103.480(15) (3)°, γ = 90°. Volume :588.5(8)Å^3 ; Z :2 ; Density (calculated):1.147Mg/m^3 ; Absorption coefficient (μ):0.083mm^{-1} ; F (000):224; Crystal size :0.80 x 0.30 x 0.20 mm^3 ; Theta range for data collection :1.69 to 28.36° ; Index ranges:-10<=h<=5, -8<=k<=7, -16<=l<=16; Reflections collected :5670 ; Independent reflections:2099 [R(int) = 0.0427] ; Completeness to theta = 28.36°:99.4 % ; Absorption correction :Empirical with SADABS ; Max. and min. Transmission :0.984and 0.971; Refinement method: Full-matrix least-squares on F^2 ; Data / restraints / parameters:2099 / 1 / 132; Goodness-of-fit on F^2 :0.669; Final R indices [I>2sigma(I)] :R1 = 0.0477, wR2 = 0.1137;R indices (all data):R1 = 0.0722, wR2 = 0.1401 ; Absolute structure parameter :-0.6(16); Largest diff. peak and hole: 0.187 and -0.248 e.Å^{-3}.

Crystal data and structure refinement for γ^4-Asp

CCDC No.: 955482

Empirical formula:C_{10} H_{17} N_1 O_4 ; Formula weight :217.26; Temperature:100(2) K ; Wavelength :0.71073 Å ; Crystal system: Monoclinic; Space group :P21; Unit cell

dimensions: a = 6.039(7)Å, b = 5.657(7)Å, c = 17.257(19)Å α = 90°, β = 91.628(18) (3)°, γ = 90°; Volume :589.3(12)Å^3 ; Z:2 ; Density (calculated) :1.213Mg/m^3 ; Absorption coefficient (μ) :0.093mm^{-1} ; F (000) :232; Crystal size:0.80 x 0.30 x 0.20 mm^3 ; Theta range for data collection: 1.18to 28.28° ; Index ranges :-8<=h<=8, -7<=k<=7, 22<=l<=23; Reflections collected :8874 ; Independent reflections :2781 [R(int) = 0.1321] ; Completeness to theta = 28.28°:100 % ; Absorption correction: Empirical with SADABS ; Max. and min. Transmission : 0.982and 0.967; Refinement method :Full-matrix least-squares on F^2 ; Data / restraints / parameters :2781 / 1 / 141; Goodness-of-fit on F^2 :0.969; Final R indices [I>2sigma(I)] :R1 = 0.0936, wR2 = 0.2170; R indices (all data): R1 = 0.2121, wR2 = 0.2983 ; Absolute structure parameter: -1(4); Largest diff. peak and hole:0.581 and -0.360 e.Å^{-3}.

Crystal data and structure refinement for γ^4-Glu

CCDC No.: 955483

Empirical formula:C_{11} H_{21} N_1 O_4, (O); Formula weight :247.29; Temperature :100(2) K ; Wavelength :0.71073 Å ; Crystal system: Monoclinic ; Space group:C2 ; Unit cell dimensions : a = 9.167(3)Å , b = 7.548(3)Å, c = 19.916(7)Å, α = 90°, β = 96.500(7) (3)°, γ = 90°. Volume :1369.1(8)Å^3 ; Z :4 ; Density (calculated):1.2Mg/m^3 ; Absorption coefficient (μ) :0.094mm^{-1} ; F (000):504; Crystal size:0.40 x 0.10 x 0.10 mm^3 ; Theta range for data collection: 1.03to 28.33° ; Index ranges: -12<=h<=12, -10<=k<=10, -26<=l<=26; Reflections collected: 12388 ; Independent reflections : 3372 [R(int) = 0.0874] ; Completeness to theta = 28.33° : 100 % ; Absorption correction : Empirical with SADABS; Max. and min. Transmission :0.991and 0.989 ; Refinement method : Full-matrix least squares on F^2 ; Data / restraints / parameters: 3372 / 1 / 158; Goodness-of-fit on F^2 :1.033; Final R indices [I>2sigma(I)] :R1 = 0.1006, wR2 = 0.2653; R indices (all data) : R1 = 0.1563, wR2 = 0.3139 ; Absolute structure parameter: -1(3); Largest diff. peak and hole: 1.210and 0.624 e.Å^{-3}.

Crystal data and structure refinement for γ^4-Tyr

CCDC No.: 955484

Empirical formula: C_{11} H_{15} N_1 O_3, 2(C), (O); Formula weight: 249.26; Temperature : 100(2) K ; Wavelength: 0.71073 Å ; Crystal system: Monoclinic ; Space group :P21; Unit cell dimensions : a = 7.7580(9)Å, b = 8.5078(10)Å, c = 9.4843(11)Å, α = 90°, β =

105.481(2) (3)°, γ = 90°; Volume : 603.29(12)Å^3 ; Z : 2 ; Density (calculated) :1.372Mg/m^3 ; Absorption coefficient (μ) :0.102mm^{-1} ; F (000): 264; Crystal size : 0.60 x 0.55 x 0.60 mm^3 ; Theta range for data collection :2.23to 28.28° ; Index ranges :-10<=h<=10, -11<=k<=11, 12<=l<=12; Reflections collected : 6041 ; Independent reflections: 2897 [R(int) = 0.0213] ; Completeness to theta = 28.28° :100 % ; Absorption correction : Empirical with SADABS ; Max. and min. Transmission : 0.941and 0.941; Refinement method: Full-matrix least-squares on F^2 ; Data / restraints / parameters : 2897 / 1 / 165; Goodness-of-fit on F^2 :1.202; Final R indices [I>2sigma(I)] : R1 = 0.0353, wR2 = 0.1267; R indices (all data) :R1 = 0.0361, wR2 = 0.1327 ; Absolute structure parameter :-1.2(9); Largest diff. peak and hole : 0.494and -0.442 e.Å^{-3}.

Crystal data and structure refinement for γ^4-Aib

CCDC No.: 955485

Empirical formula:C_6 H_{13} N_1 O_2; Formula weight :131.17; Temperature:100(2) K ; Wavelength :0.71073 Å ; Crystal system: Orthorhombic; Space group :P 21 21 21; Unit cell dimensions : a = 6.420(4)Å, b = 7.967(4)Å, c = 13.983(7)Å, α = 90°, β = 90°, γ = 90°. Volume: 715.2(7)Å^3 ; Z:4 ; Density (calculated) :1.218Mg/m^3 ; Absorption coefficient (μ) :0.090mm^{-1} ; F (000): 288; Crystal size : 0.70 x 0.60 x 0.60 mm^3 ; Theta range for data collection : 2.91to 28.70° ; Index ranges: -5<=h<=8, -10<=k<=9, -18<=l<=16; Reflections collected: 4266 ; Independent reflections: 1784 [R(int) = 0.0299] ; Completeness to theta = 28.70° :100 % ; Absorption correction: Empirical with SADABS ; Max. and min. Transmission :0.947and 0.939; Refinement method : Full-matrix least-squares on F^2; Data / restraints / parameters: 1784 / 0 / 85; Goodness-of-fit on F^2 : 0.835; Final R indices [I>2sigma(I)] : R1 = 0.0340, wR2 = 0.1006; R indices (all data) : R1 = 0.0377, wR2 = 0.1050 ; Absolute structure parameter : -1.4(10); Largest diff. peak and hole : 0.357and -0.233 e.Å^{-3}.

Crystal data and structure refinement for γ^4-Phe

CCDC No.: 901427

Crystals ofγ^4-Phe were grown by slow evaporation from a solution of aqueous methanol. A single crystal, rectangular in shape (0.50 × 0.40 × 0.20 mm3) was mounted on a loop. The X-ray data were collected at 100(2) K temperature on a Bruker AXS SMART APEX CCD

diffractometer using Mo-K α radiation (λ = 0.71073 Å), ω-scans (2θ = 54.88°), for a total number of 8120 independent reflections. Space group P21; a = 7.757(5), b = 6.483(4), c = 9.907(7) Å; α = γ = 90.00°, β = 92.808(12) (3)°.V = 497.6(6) $Å^3$, monoclinic P; Z = 2 for chemical formula $C_{11}H_{15}N_1O_2$; ρcalcd = 1.290 Mg m^{-3}; μ = 0.088 mm^{-1}; F (000) = 208. The structure was obtained by direct methods using SHELXS-97. All non-hydrogen atoms were refined anisotropically. The hydrogen atoms were fixed geometrically in the idealized position and refined in the final cycle of refinement as riding over the atoms to which they are bonded. The final R value was 0.0704 (wR2 = 0.1626) for 2196 observed reflections ($F^0 \geq 4\sigma$ ($|F^0|$)) and 128 variables; S = 0.947. The largest deference peak and hole were 0.424 and−0.314 e $Å^{-3}$, respectively.

Crystal data and structure refinement for Cbz-dgVal-OBzl

CCDC No.: 855463

Empirical formula: C_{22} H_{25} N_1 O_4; Formula weight : 367.43; Temperature : 100(2) K ; Wavelength : 0.71073 Å ; Crystal system : Orthorhombic; Space group : P 21 21 21; Unit cell dimensions : a = 5.268(4) Å, b = 14.117(10) Å, c = 25.722(18) Å, α = 90°, β = 90°, γ = 90°; Volume:1913(2) $Å^3$; Z :4 ; Density (calculated) :1.276 Mg/m^3 ; Absorption coefficient (μ) :0.087 mm^{-1} ; F (000) :784; Crystal size: 0.35x 0.30 x 0.10 mm^3 ; Theta range for data collection : 1.58to 28.28° ; Index ranges: -7<=h<=7, -18<=k<=18, -34<=l<=34; Reflections collected: 32750; Independent reflections: 4732 [R(int) = 0.1263] ; Completeness to theta = 28.28° :100 % ; Absorption correction :Empirical with SADABS ; Max. and min. Transmission : 0.991and 0.970; Refinement method : Full-matrix least-squares on F^2 ; Data / restraints / parameters : 4732 / 0 / 247; Goodness-of-fit on F^2 :0.883 ; Final R indices [I>2sigma(I)]: R1 = 0.0590, wR2 = 0.1300; R indices (all data): R1 = 0.1300, wR2 = 0.1687 ; Absolute structure parameter : 0.0(18); Largest diff. peak and hole: 0.306and -0.262 e.$Å^{-3}$.

1.11 Spectroscopic Data for compounds

1.11.1 Spectroscopic Data for *N*-protected β-amino alcohols obtained from the *N*-hydroxysuccinimide method

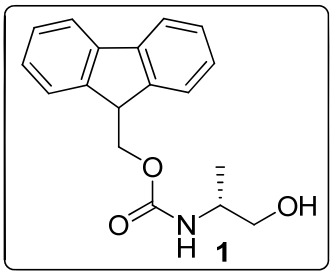

1

(R)-(9H-fluoren-9-yl)methyl 1-hydroxypropan-2-ylcarbamate (1) : white solid (0.505 g, 85%), mp 148-151 ^{o}C; **^{1}H NMR** (400 MHz, $CDCl_3$) δ 7.77 (d, J = 7.36 Hz, 2H), 7.58 (d, J = 7.32 Hz, 2H), 7.40 (t, J = 7.50 Hz, 2H), 7.31 (td, J = 0.85 Hz, J = 7.60 Hz, 2H), 4.94 (bs, 1H), 4.42 (d, J = 6.44 Hz, 2H), 4.22 (t, J = 6.44 Hz, 1H), 3.82 (bs, 1H), 3.64-3.52 (m, 2H), 3.83 (bs, 1H), 3.68-3.51 (m, 2H), 2.40 (bs, 1H), 1.18 (d, J = 6.43 Hz, 3H); **^{13}C NMR** (100 MHz, $CDCl_3$) δ 156.56, 143.85, 141.29, 127.67, 127.02, 124.99, 119.94, 66.78, 48.91, 47.21, 33.87, 25.72, 17.23; **MALDI TOF/TOF**- *m/z* calcd. for $C_{18}H_{19}NO_3$ $[M+K]^+$ 336.1002, obsrvd. 335.9430, **$[\alpha]_D^{25}$** = +2 (c = 1, MeOH).

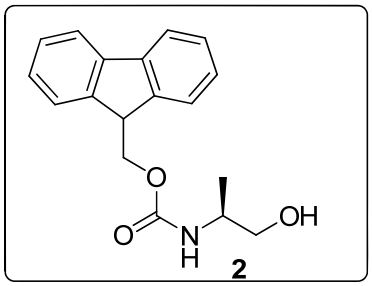

2

(S)-(9H-fluoren-9-yl)methyl 1-hydroxypropan-2-ylcarbamate (2) : white solid (0.534g, 90%); mp 150-153^{o}C; **^{1}H NMR** (400 MHz, $CDCl_3$) δ 7.77 (d, J =7.36 Hz, 2H), 7.60 (d, J = 7.32 Hz, 2H), 7.47 (t, J = 7.52 Hz, 2H), 7.32 (td, J = 0.9 Hz, J = 7.62 Hz, 2H), 4.86 (bs, 1H), 4.43 (d, J = 6.44 Hz, 2H), 4.22 (t, 6.44 Hz, 1H), 3.83 (bs, 1H), 1.18 (d, J = 6.44 Hz, 3H); **^{13}C NMR** (100 MHz, $CDCl_3$) δ 156.60, 143.86, 141.32, 127.69, 127.04, 125.01, 119.97, 66.92, 66.62, 48.94, 47.23, 17.34; **MALDI TOF/TOF**- *m/z* calcd. for $C_{18}H_{19}NO_3$ $[M+K]^+$ 336.1002, obsrvd. 335.9779, **$[\alpha]_D^{25}$** = -2.0 (c = 1, MeOH).

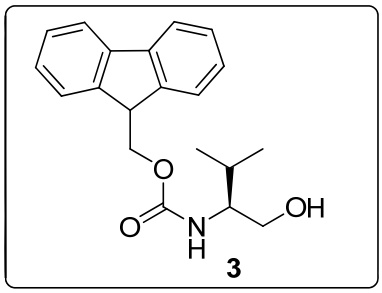

3

(S)-(9H-fluoren-9-yl)methyl 1-hydroxy-3-methylbutan-2-ylcarbamate (3) : white solid (0.520 g, 80%), mp 121-122 ^{o}C, **^{1}H NMR** (400 MHz, $CDCl_3$) δ 7.75 (d, J = 7.33 Hz, 2H), 7.59 (d, J = 7.30 Hz, 2H), 7.45 (t, J = 7.51 Hz, 2H), 7.32 (td, J = 0.9 Hz, J=7.62 Hz, 2H), 4.90 (bs, 1H), 4.45 (d, J = 6.44 Hz, 2H), 4.21 (t, J = 6.44 Hz, 1H), 3.66 (m, 2H), 3.46 (m, 1H), 2.04 (bs, 1H), 1.83 (m, 1H), 0.94 (m, 6H); **^{13}C NMR** (100 MHz, $CDCl_3$) δ 157.05, 143.86, 141.32, 127.65, 127.02, 124.97, 119.94, 66.54, 63.72, 58.53, 47.29, 29.15, 19.47, 18.61; **MALDI TOF/TOF**- *m/z* calcd. for $C_{20}H_{23}NO_3$ $[M+Na]^+$ 348.1576, obsrvd. 348.0117, **$[\alpha]_D^{25}$** = -13.0 (c = 1, MeOH).

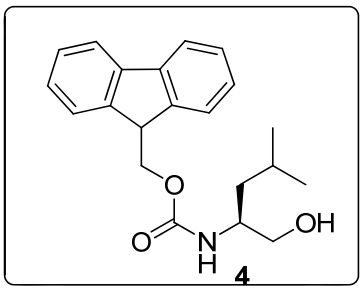

4

(S)-(9H-fluoren-9-yl)methyl 1-hydroxy-4-methylpentan-2-ylcarbamate (4): white solid (0.549 g, 81%), mp 133-135^{o}C, **^{1}H NMR** (400 MHz, $CDCl_3$) δ 7.77 (d, J = 7.76 Hz, 2H), 7.59 (d, J = 7.32 Hz, 2H), 7.40 (t, J = 7.32 Hz, 2H), 7.32 (t, J = 7.32 Hz, 2H), 4.78 (bs, 1H), 4.45 (d, J = 6.88 Hz, 2H), 4.21 (t, J = 6.88 Hz, 1H), 3.85 (m, 1H), 3.65 (m, 1H), 3.58 (m, 1H), 1.63 (m, 3H), 1.32 (m,1H), 0.92 (dd, J = 2.28 Hz, J = 6.2 Hz, 6H) **; ^{13}C NMR** (100 MHz, $CDCl_3$) δ 156.76, 143.85, 141.33, 127.67, 127.03, 125.0, 119.95, 66.47, 66.05, 51.30, 47.30, 40.34, 24.72, 23.04, 22.10; **MALDI TOF/TOF**- *m/z* calcd. for $C_{21}H_{25}NO_3$ $[M+K]^+$ 378.1472, obsrvd. 377.9655, **$[\alpha]_D^{25}$** = -20.1 (c = 1, MeOH).

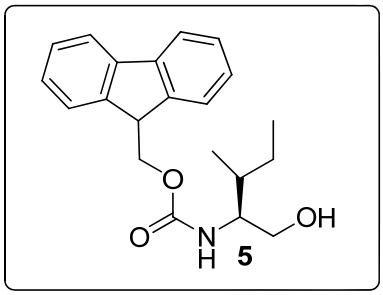

5

(9H-fluoren-9-yl)methyl (2S,3R)-1-hydroxy-3-methylpentan-2-ylcarbamate (5): white solid (0.423 g, 65%), mp 114-116 ^{o}C; **^{1}H NMR** (400 MHz, $CDCl_3$) δ 7.77 (d, J = 7.8 Hz, 2H), 7.60 (d, J = 7.32 Hz, 2H), 7.41 (t, J = 7.36Hz,2H), 7.32 (dt, J = 1.36 Hz, J=7.32 Hz, 2H), 4.88 (bd, J = 8.24 Hz,1H) , 4.44 (d, J = 6.4 Hz, 2H), 4.22 (t, J = 6.4 Hz, 1H), 4.12 (bs,1H), 3.68 (m,2H), 3.54 (m, 1H), 1.93 (m, 1H), 1.13 (m,2H), 0.92 (m,6H); **^{13}C NMR** (100 MHz, $CDCl_3$) δ 157.00, 143.85, 141.32, 127.65, 127.02, 124.98, 119.94, 66.51, 63.49, 57.36, 47.31, 35.83, 25.40, 15.48, 11.35; **MALDI TOF/TOF**- *m/z* calcd. for $C_{21}H_{25}NO_3$ $[M+K]^+$ 378.1472, obsrvd. 377.9658, **$[\alpha]_D^{25}$** = -11.7 (c = 1, MeOH).

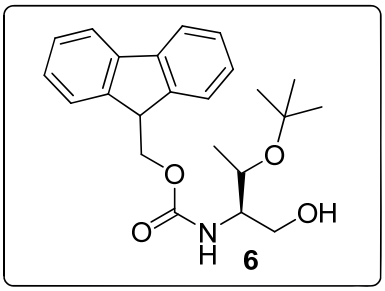

6

(9H-fluoren-9-yl) methyl (2R, 3S)-3-tert-butoxy-1-hydroxybutan-2-ylcarbamate (6): colorless oil (0.651 g, 85%); **^{1}H NMR** (400 MHz, $CDCl_3$) δ 7.76 (d, J = 7.76 Hz, 2H), 7.61 (d, J = 7.6 Hz, 2H), 7.40 (t, J = 7.32 Hz, 2H), 7.32 (t, J = 7.32 Hz, 2H), 5.28 (bd, J = 7.76 Hz,1H) , 4.41 (m,2H), 4.23 (t, J = 6.88 Hz, 1H), 3.96 (m, 1H), 3.66 (m, 3H), 2.86 (bs,1H), 1.21 (s,9H), 1.16 (d, J = 5.96 Hz, 3H) ; **^{13}C NMR** (100 MHz, $CDCl_3$) δ 157.28, 144.16, 141.56, 127.94, 127.30, 125.34, 120.23, 74.59, 67.45, 67.06, 63.96, 57.39, 47.53, 28.91, 20.36 ; **MALDI TOF/TOF**- *m/z* calcd. for $C_{23}H_{29}NO_4$ $[M+Na]^+$ 406.1994, obsrvd. 406.0422; **$[\alpha]_D^{25}$** = +6.1 (c = 1, MeOH).

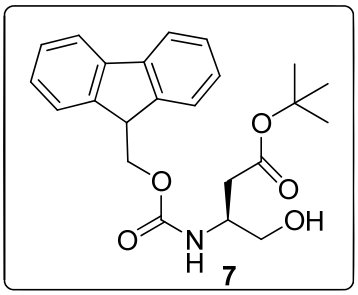

7

(S)-*tert*-butyl 3-(((9H-fluoren-9-yl)methoxy)carbonylamino)-4-hydroxybutanoate (7): white solid (0.730 g, 92 %), mp 93-96 ^{o}C; **^{1}H NMR** (400 MHz, $CDCl_3$) δ 7.77 (d, J = 7.8 Hz, 2H), 7.59 (d, J = 7.32 Hz, 2H), 7.40 (t, J = 7.32 Hz, 2H), 7.31 (t, J =7.32 Hz, 2H), 5.54 (bs, 1H) , 4.40 (d, J =6.92,2H), 4.22 (t, J = 6.92 Hz, 1H), 4.03 (m,1H), 3.74 (m,2H), 2.57-2.52 (m,2H), 1.46 (s,9H); **^{13}C NMR** (100 MHz, $CDCl_3$) δ 171.10, 156.30, 143.79, 141.28, 127.69, 127.03, 125.02, 119.96, 82.00, 67.95, 66.84, 64.53, 49.92, 47.15, 37.26, 28.00; **MALDI TOF/TOF**- *m/z* calcd. for $C_{23}H_{27}NO_5$ $[M+K]^+$ 436.1526, obsrvd. 435.9662; **[α]$_D^{25}$** = -7.4 (c = 1, MeOH).

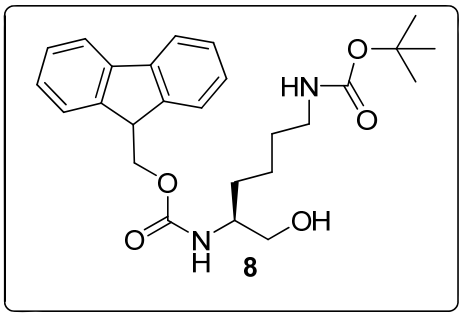

8

(S)-(9H-fluoren-9-yl)methyl6-((tert-butoxycarbonyl)amino)-1-hydroxyhexan-2-ylcarbamate (8): white solid (0.681 g, 75%), mp 136-138 ^{o}C; **^{1}H NMR** (400 MHz, $CDCl_3$) δ 7.75 (d, J = 7.77 Hz, 2H), 7.60 (d, J = 7.31 Hz, 2H), 7.41 (t, J = 7.32 Hz, 2H), 7.32 (t, J = 7.32 Hz, 2H), 5.10 (bs, 1H), 4.60 (bs, 1H), 4.40 (d, J = 6.90 Hz,2H), 4.21 (t, J = 6.90 Hz, 1H), 3.62 (bs,3H), 3.18-3.07 (m, 2H), 2.56 (bs, 1H), 1.67 (m,2H), 1.47 (m,2H), 1.43 (s,9H), 1.36 (m, 2H); **^{13}C NMR** (100 MHz, $CDCl_3$) δ 156.78, 156.53, 144.00, 141.42, 127.77, 127.15, 125.16, 120.05, 80.00, 66.69, 64.78, 53.03, 47.38, 39.61, 30.43, 30.09, 28.50, 22.60; **MALDI TOF/TOF**- *m/z* calcd. for $C_{26}H_{34}N_2O_5$ $[M+Na]^+$ 477.2399, obsrvd. 477.2375 and *m/z* calcd. for $C_{21}H_{26}N_2O_3$ $[M\text{-}Boc+H]^+$ 355.2022, obsrvd. 355.1945 , **[α]$_D^{25}$** = -6.9 (c = 1, MeOH).

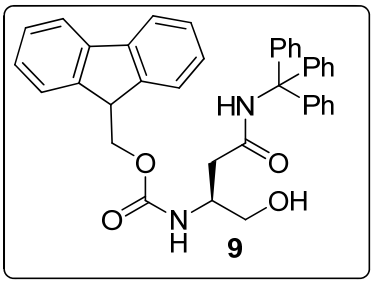

9

(S)-(9H-fluoren-9-yl)methyl 1-hydroxy-4-oxo-4-(tritylamino)butan-2-ylcarbamate (9) : white solid (1.048 g, 90%)[a], mp 155-159 ^{o}C ; **^{1}H NMR** (400 MHz, $CDCl_3$) δ 7.74-7.17 (m, 23H), 7.03 (bs,1H), 5.77 (d, J = 7.28 Hz, 1H), 4.32 (m, 2H), 4.15 (t, J = 6.88 Hz, 1H), 3.91 (m, 1H), 3.64 (m, 2H), 3.43 (bs, 1H), 2.71 (m, 2H); **^{13}C NMR** (100 MHz, $CDCl_3$) δ 171.00, 156.63, 144.07, 141.25, 128.53, 128.02, 127.70, 125.05, 119.96, 80.7, 70.95, 66.88, 49.97, 47.10, 39.50; **MALDI TOF/TOF**- *m/z* calcd. for $C_{38}H_{34}N_2O_4$ $[M+Na]^+$ 605.2416, obsrvd. 605.2652; **$[\alpha]_D^{25}$** = -12.3 (c = 1, MeOH).

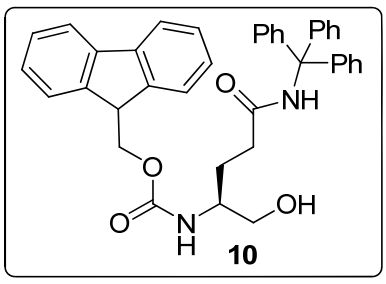

10

(S)-(9H-fluoren-9-yl)methyl 1-hydroxy-5-oxo-5-(tritylamino)pentan-2-ylcarbamate (10) : white solid (1.013 g, 85%), mp 74-77 ^{o}C ; **^{1}H NMR** (400 MHz, $CDCl_3$) δ 7.72 (d, J = 7.36 Hz, 2H), 7.56 (d, J = 7.36 Hz,2H), 7.39-7.16 (m,19H), 6.93 (s, 1H), 5.36 (d, J = 8.72 Hz, 1H), 4.50 (bs,1H), 4.37 (m, 2H), 4.17 (t, J = 6.88 Hz, 1H) , 3.53 (m,1H), 3.39 (m, 2H), 2.28 (m,2H), 1.79 (m, 2H); **^{13}C NMR** (100 MHz, $CDCl_3$) δ 172.40, 156.83, 144.54, 143.94, 141.41, 128.73, 128.06, 127.80, 127.18, 125.19, 120.08, 70.75, 66.59, 64.09, 52.76, 47.36, 33.57, 26.40; **MALDI TOF/TOF**- *m/z* calcd. for $C_{39}H_{36}N_2O_4$ $[M+Na]^+$ 619.2573, obsrvd. 619.2513; **$[\alpha]_D^{25}$** = -5.8 (c = 1, MeOH).

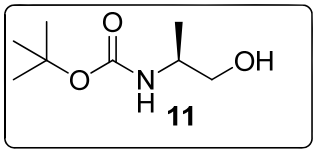

11

(*S*)-*tert*-butyl 1-hydroxypropan-2-ylcarbamate (11) : colorless oil (0.280 g, 80%); **^{1}H NMR** (400 MHz, $CDCl_3$) δ 4.74 (bs,1H), 3.77 (m, 1H), 3.57 (m, 2H), 1.44 (s,9H), 1.15 (d, J = 6.88 Hz, 3H); **^{13}C NMR** (100 MHz, $CDCl_3$) δ 156.45, 79.72, 67.15, 48.57, 28.44, 17.39 ; **LCMS/MS** - *m/z* calcd. for $C_8H_{17}NO_3$ $[M+Na]^+$ 198.1106, obsrvd. 198.1172; **$[\alpha]_D^{25}$** = -8.5 (c = 1, MeOH).

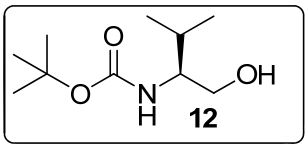

12

(*S*)-*tert*-butyl 1-hydroxy-3-methylbutan-2-ylcarbamate (12): colorless oil (0.312 g, 77 %); **^{1}H NMR** (400 MHz, $CDCl_3$) δ 4.83 (bs, 1H), 3.52 (m, 2H), 3.43 (m,1H), 3.10 (bs, 1H), 1.82 (m.1H), 0.94 (m, 6H); **^{13}C NMR** (100 MHz, $CDCl_3$) δ 156.97, 79.57, 64.05, 58.04, 29.33, 28.34, 19.58, 18.53 ; **LCMS/MS** - *m/z* calcd. for $C_{10}H_{21}NO_3$ $[M+Na]^+$ 226.1419, obsrvd. 226.1481; **$[\alpha]_D^{25}$** = -17.6 (c = 1, MeOH).

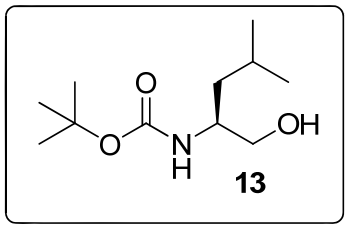

13

***(S)*-*tert*-butyl 1-hydroxy-4-methylpentan-2-ylcarbamate (13) :** colorless oil (0.369 g, 85%); **^{1}H NMR** (400 MHz, $CDCl_3$) δ 4.75 (bs, 1H), 3.71 (m, 1H), 3.55 (m, 2H), 2.98 (bs, 1H), 1.67 (m, 1H), 1.45 (s, 9H), 1.30 (m, 2H), 0.93 (dd, J = 1.4 Hz, J = 6.42 Hz, 6H) ;**^{13}C NMR** (100 MHz, $CDCl_3$) δ 156.64, 79.60, 66.35, 50.97, 40.58, 28.64, 24.86, 23.12, 21.13, 14.24; **LCMS/MS** - *m/z* calcd. for $C_{11}H_{23}NO_3$ $[M+Na]^+$ 240.1576, obsrvd. 240.1544; **$[\alpha]_D^{25}$** = -23.2 (c = 1, MeOH).

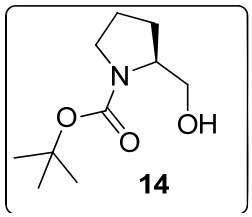

14

***(S)*-*tert*-butyl 2-(hydroxymethyl)pyrrolidine-1-carboxylate (14) :** colorless oil (0.313 g, 78%); **^{1}H NMR** (400 MHz, $CDCl_3$) δ 3.98 (m,1H), 3.59 (m, 2H), 3.92 (m, 2H), 2.04 (m,2H), 1.82 (m,2H), 1.47 (s, 9H)`; **^{13}C NMR** (100 MHz, $CDCl_3$) δ 157.27, 80.35, 67.69,

60.21, 47,63, 30.09, 24.38, 22.03; **LCMS/MS** - *m/z* calcd. for $C_{10}H_{19}NO_3$ $[M+Na]^+$ 224.1263, obsrvd. 224.1223; $[\alpha]_D^{25}$ = -45.7 (c = 1, MeOH).

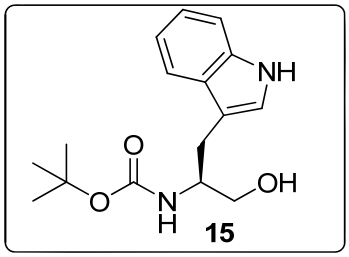

15

***(S)-tert*-butyl 1-hydroxy-3-(1H-indol-3-yl)propan-2-ylcarbamate (15):** white solid (0.414 g, 75%), mp 99-103 ^oC; **^{1}H NMR** (400 MHz, $CDCl_3$) δ 8.30 (bs, 1H), 7.64 (d, J = 7.8 Hz, 1H), 7.34 (d, J = 7.8 Hz, 1H), 7.19 (t, J = 7.32 Hz, 1H), 7.11 (t, J = 7.8 Hz, 1H), 7.00 (d, J = 6.88 Hz, 1H), 4.92 (bs, 1H), 3.97 (m, 1H), 3.60 (m, 2H), 2.97 (d, J = 5.96 Hz, 2H), 2.78 (bs,1H), 1.42 (s, 9H) ; **^{13}C NMR** (100 MHz, $CDCl_3$) δ 156.60, 136.35, 127.73, 122.90, 122.15, 119.46, 118.93, 111.71, 111.31, 79.83, 64.85, 53.22, 28.46, 27.01; **LCMS/MS** - *m/z* calcd. for $C_{16}H_{22}N_2O_3$ $[M+K]^+$ 329.1267, obsrvd. 328.9698; $[\alpha]_D^{25}$ = -22.2 (c = 1, MeOH).

1.11.2 Spectroscopic Data for the Boc-protected peptaibols

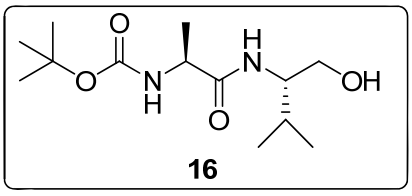

16

***tert*-butyl (*S*)-1-((S)-1-hydroxy-3-methylbutan-2-ylamino)-1-oxopropan-2-ylcarbamate (16):** off-white solid (0.471 g, 86%); **^{1}H NMR** (400 MHz, $CDCl_3$) δ 6.57 (bs, 1H), 5.14 (bs, 1H), 4.13 (m, 1H), 3.70 (m, 2H), 3.50 (m, 1H), 1.89 (m, 1H), 1.44 (s,9H), 1.37 (d, J = 6.88 Hz, 3H), 0.93 (m,6H); **^{13}C NMR** (100 MHz, $CDCl_3$) δ 173.59, 155.99, 80.58, 63.76, 57.34, 50.57, 33.98, 28.36, 25.01, 19.61, 18.67; **MALDI TOF/TOF**- *m/z* calcd. for $C_{13}H_{26}N_2O_4$ $[M+Na]^+$ 297.1790, obsrvd. 297.0301; $[\alpha]_D^{25}$ = -22.2 (c = 1, MeOH).

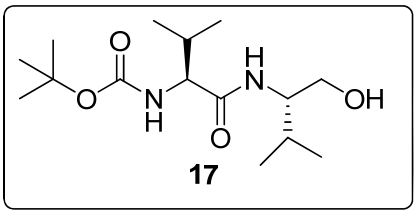

17

***tert*-butyl(*S*)-1-((*S*)-1-hydroxy-3-methylbutan-2-ylamino)-3-methyl-1-oxobutan-2-ylcarbamate (17) :** off-white solid (0.495 g, 82%); **^{1}H NMR** (400 MHz, $CDCl_3$) δ 6.36 (bs, 1H), 5.12 (bs, 1H), 3.84 (m, 1H), 3.67 (m, 3H), 1.89 (m, 2H), 1.44 (s, 9H), 0.96 (m, 12H); **^{13}C NMR** (100 MHz, $CDCl_3$) δ 173.59, 155.99, 80.58, 63.76, 57.34, 50.57, 33.98, 29.01, 28.36, 25.67, 25.01, 19.60, 18.67; **MALDI TOF/TOF**- *m/z* calcd. for $C_{15}H_{30}N_2O_4$ $[M+K]^+$ 341.1843, obsrvd. 341.0229; **$[\alpha]_D^{25}$** = -34.7 (c = 1, MeOH).

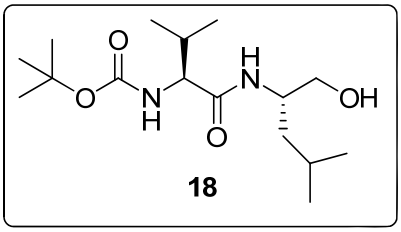

18

***tert*-butyl(*S*)-1-((*S*)-1-hydroxy-4-methylpentan-2-ylamino)-3-methyl-1-oxobutan-2-ylcarbamate (18) :** off-white solid (0.518 g, 82%); **^{1}H NMR** (400 MHz, $CDCl_3$) δ 6.11 (bs,1H), 5.02 (bs,1H), 4.08 (m,1H), 3.84-3.66 (m, 2H), 3.53 (m, 1H), 2.16 (m, 1H), 1.62 (m,2H), 1.45 (s,9H), 1.35 (m, 1H), 0.93 (m, 12H); **^{13}C NMR** (100 MHz, $CDCl_3$) δ 172.27, 156.23, 80.31, 65.93, 60.71, 50.14, 39.99, 30.42, 28.34, 24.87, 23.15, 22.11, 19.43; **MALDI TOF/TOF**- *m/z* calcd. for $C_{16}H_{32}N_2O_4$ $[M+K]^+$ 355.1999, obsrvd. 355.0220; **$[\alpha]_D^{25}$** = -35.9 (c = 1, MeOH).

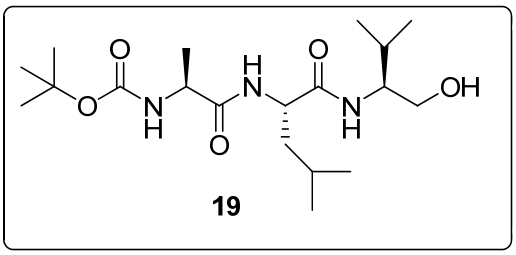

19

***tert*-butyl (*S*)-1-((*S*)-1-((*S*)-1-hydroxy-3-methylbutan-2-ylamino)-4-methyl-1-oxopentan-2-ylamino)-1-oxopropan-2-ylcarbamate (19) :** white solid (0.612 g, 79%); **^{1}H NMR** (400 MHz, $CDCl_3$) δ 6.69 (m,1H), 5.10 (d, J = 5.36 Hz, 1H), 4.36 (m, 1H), 4.22 (d, J = 7.36 Hz, 1H), 4.11 (m, 1H), 3.66 (m, 2H), 3.47 (m, 1H), 3.03 (bs, 1H), 1.71 (m,

4H), 1.45 (s, 9H), 1.36 (d, J = 7.08 Hz, 3H), 1.16-0.89 (m, 12H); **^{13}C NMR** (100 MHz, $CDCl_3$) δ 173.35, 172.43, 156.92, 80.96, 63.86, 57.66, 49.22, 40.51, 34.01, 30.39, 28.93, 25.68, 25.02, 23.12, 19.61, 19.06, 17.85; **MALDI TOF/TOF**- *m/z* calcd. for $C_{19}H_{37}N_3O_5$ $[M+K]^+$ 426.2370, obsrvd. 426.0512; **$[\alpha]_D^{25}$** = -34.59 (c = 1, MeOH).

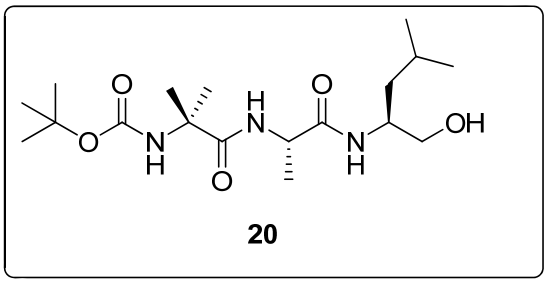

20

***tert*-butyl 1-((*S*)-1-((*S*)-1-hydroxy-4-methylpentan-2-ylamino)-1-oxopropan-2-ylamino)-2-methyl-1-oxopropan-2-ylcarbamate (20) :** white solid (0.567 g, 76%) ; **^{1}H NMR** (400 MHz, $CDCl_3$) δ 7.07 (bs, 1H), 6.57 (bd, J = 5.04 Hz, 1H), 5.10 (bs, 1H), 4.22 (m, 1H), 3.70 (m, 2H), 3.47 (m, 1H), 3.09 (bs,1H), 1.94-1.68 (m, 12H), 1.46 (s, 9H), 0.90 (m, 6H); **^{13}C NMR** (100 MHz, $CDCl_3$) δ 175.10, 172.58, 171.31, 81.37, 65.67, 60.51, 57.01, 50.26, 39.55, 34.01, 30.39, 28.31, 25.02, 22.27, 17.80, 14.27; **MALDI TOF/TOF**- *m/z* calcd. for $C_{18}H_{35}N_3O_5$ $[M+K]^+$ 412.2214, obsrvd. 412.0356; **$[\alpha]_D^{25}$** = -13.6 (c = 1, MeOH).

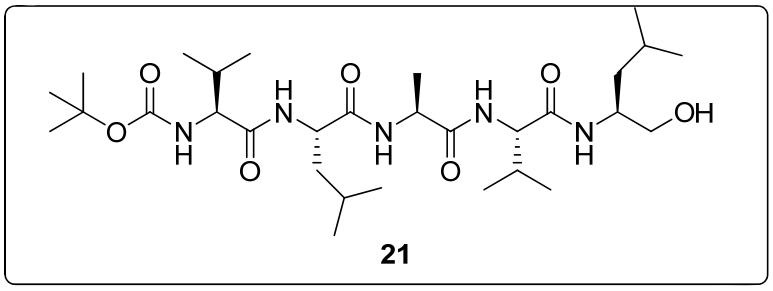

21

***tert*-butyl (3*S*,6*S*,9*S*,12*S*,15*S*)-15-(hydroxymethyl)-6-isobutyl-12-isopropyl-2,9,17-trimethyl-4,7,10,13-tetraoxo-5,8,11,14-tetraazaoctadecan-3-ylcarbamate:** white solid (0.032 g, 65%); **^{1}H NMR** (400 MHz, DMSO d_6) δ 7.97 (d, J = 8 Hz,1H,-NH of Ala_3), 7.79 (d, J = 8.24,1H, -NH of Leu_2), 7.57 (d, J = 8.72 Hz, 1H,-NH of Val_4), 7.46 (d, J = 8.60 Hz, 1H, -NH of Leu_5), 6.71 (d, J = 8.72 Hz,1H,-NH of Val_1), 4.60 (t, J = 5.96 Hz,1H,-OH), 4.25 (m, 2H,α CH of Leu_2 and Ala_3), 3.97 (m, 1H, α CH of Val_4), 3.68 (m, 2H, α CH of Val_1 and β CH of Leu_5), 3.22-3.09 (m, 2H, α CH_2 of Leu_5), 1.85 (m, 2H, β CH of Val_1 and Val_4), 1.52 (m, 2H, γ CH of Leu_2 and δ CH of Leu_5), 1.36 (m, 2H, β CH_2 of

Leu_2),1.31 (s, 9H, ^{t}Boc of Val_1), 1.20 (m, 2H, γ CH_2 of Leu_5), 1.10 (d, J = 6.88 Hz, 3H, β CH_3 of Ala_3), 0.69-0.81(m, 24H, γ CH_3 of Val_1 and Val_4,δ CH_3 of Leu_2,ω CH_3 of Leu_5); **MALDI TOF/TOF**- *m/z* calcd. for $C_{30}H_{57}N_5O_7$ $[M+K]^+$ 638.3895, obsrvd. 638.1087 and *m/z* calcd. for $C_{30}H_{57}N_5O_7$ $[M-{}^tBoc + Na]^+$ 522.3631, obsrvd. 522.1472.

1.11.3 Spectroscopic Data for vinylogous amino acids

(*S, E*)-benzyl 4-(benzyloxycarbonylamino)pent-2-enoate (Ia): colorless oil (1.648 g, 81 %); **[α] $_D^{25}$** = - 17.7 (c = 1, MeOH); **^{1}H NMR** (400 MHz, $CDCl_3$) δ 7.35 (m, 10H), 6.91 (dd, J = 4 Hz, J = 16 Hz, 1H), 5.95 (d, J = 16 Hz, 1H), 5.16 (s, 2H), 5.09 (m, 2H), 4.96 (m, 1H), 4.47 (m, 1H), 1.25 (d, J = 4 Hz, 3H); **^{13}C NMR** (100 MHz, $CDCl_3$) δ 165.8, 155.7, 149.3, 135.0, 127.5, 127.3, 126.8, 118.7, 114.3, 65.4, 48.4, 29.4, 18.4; **MALDI TOF/TOF**- *m/z* calcd. for $C_{20}H_{21}NO_4$ $[M+Na]^+$ 362.1363, obsrvd. 362.1391.

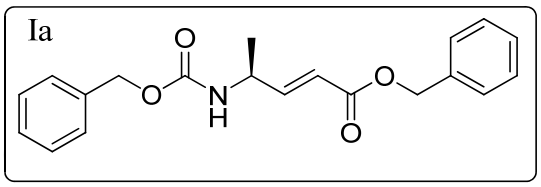

(*S, E*)-benzyl 4-(benzyloxycarbonylamino)-5-methylhex-2-enoate (Ib): colorless oil (1.718 g, 78 %); **[α] $_D^{25}$** = - 4.4 (c = 1, MeOH); **^{1}H NMR** (400 MHz, $CDCl_3$) δ 7.33 (m, 10H), 6.89 (m, 1H), 5.97 (m, 1H), 5.17 (m, 2H), 5.09 (m, 2H), 4.85 (m, 1H), 4.24 (m, 1H), 1.87 (m, 1H), 0.91 (m, 6H) ; **^{13}C NMR** (100 MHz, $CDCl_3$) δ 165.9, 155.8, 147.5, 136.2, 135.8, 128.5, 128.2, 128.1, 121.4, 67.0, 66.3, 57.3, 32.1, 18.8; **MALDI TOF/TOF**- *m/z* calcd. for $C_{22}H_{25}NO_4$ $[M+Na]^+$ 390.1681, obsrvd. 390.1696.

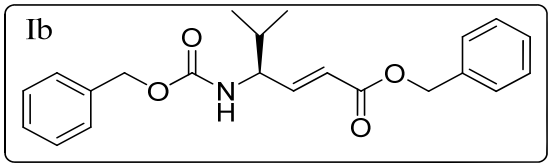

(*R, E*)-benzyl 4-(benzyloxycarbonylamino)-5-methylhex-2-enoate (Ic): colorless oil (1.652 g, 75 %); **[α] $_D^{25}$** = + 4.4 (c = 1, MeOH); **^{1}H NMR** (400 MHz, $CDCl_3$) δ 7.35 (m, 10H), 6.91 (dd, J = 8 Hz, J = 16 Hz, 1H), 5.98 (d, J = 16 Hz, 1H), 5.17 (s, 2), 5.10 (s, 2H), 4.84 (bd, J = 12 Hz, 1H), 4.26 (m, 1H), 1.87, (m, 1H), 0.91 (m, 6H); **^{13}C NMR** (100 MHz, $CDCl_3$) δ 165.9, 155.8, 147.5, 136.2, 135.8, 128.5, 128.2, 128.1, 121.4, 67.0, 66.3, 57.3,

32.1, 18.8, 17.9; **MALDI TOF/TOF**- *m/z* calcd. for $C_{22}H_{25}NO_4$ $[M+Na]^+$ 390.1681, obsrvd. 390.1683.

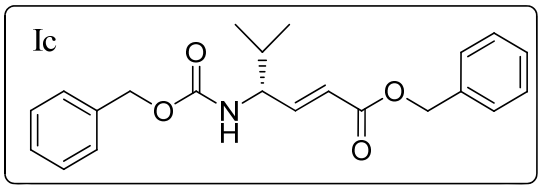

(*S, E*)-benzyl 4-(benzyloxycarbonylamino)-6-methylhept-2-enoate (Id): colorless oil (1.761 g, 77 %); **[α]** $_D^{25}$ = - 15.8 (c = 1, MeOH); **^{1}H NMR** (400 MHz, $CDCl_3$) δ 7.36 (m, 10H), 6.88 (dd, *J* = 8 Hz, *J* = 16 Hz, 1H), 5.98 (d, *J* = 16 Hz, 1H), 5.17 (s, 2H), 5.09 (m, 2H), 4.78 (m, 1H), 4.40 (m, 1H), 1.66 (m, 1H), 0.91 (d, *J* = 8 Hz, 6H); **^{13}C NMR** (100 MHz, $CDCl_3$) δ 166.1, 155.6, 149.0, 135.8, 128.5, 128.2, 120.3, 66.9, 66.3, 50.3, 43.6, 24.6, 22.7; **MALDI TOF/TOF**- *m/z* calcd. for $C_{23}H_{27}NO_4$ $[M+Na]^+$ 404.1838, obsrvd. 404.1886.

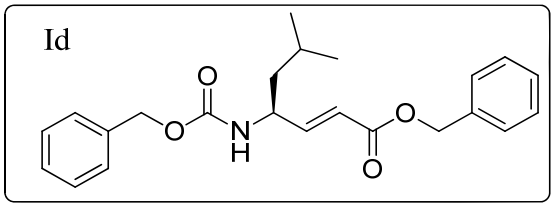

(*4S, 5R, E*)-benzyl 4-(benzyloxycarbonylamino)-5-methylhept-2-enoate (Ie): colorless oil (1.372 g, 60 %); **[α]** $_D^{25}$ = - 2.7 (c = 1, MeOH); **^{1}H NMR** (400 MHz, $CDCl_3$) δ 7.37 (m, 10H), 6.90 (dd, *J* = 4 Hz, *J* = 16 Hz, 1H), 5.98 (d, *J* = 16 Hz, 1H), 5.17 (s, 2H), 5.10 (s, 2H), 4.87 (bd, *J* = 8Hz, 1H), 4.34 (m, 1H), 1.67 (m, 1H), 145-1,15 (m, 2H), 0.90 (m, 6H); **^{13}C NMR** (100 MHz, $CDCl_3$) δ 165.9, 155.8, 147.2, 136.2, 135.8, 128.5, 128.3, 126.9, 121.5, 67.0, 66.3, 65.3, 38.8, 25.2, 15.2, 11.5; **MALDI TOF/TOF**- *m/z* calcd. for $C_{23}H_{27}NO_4$ $[M+Na]^+$ 404.1838, obsrvd. 404.1812.

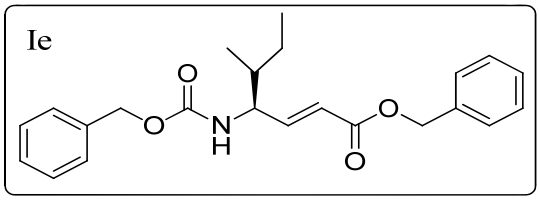

(*R, E*)-benzyl 4-(benzyloxycarbonylamino)-5-tert-butoxypent-2-enoate (If): colorless oil (2.047 g, 83 %); **[α]** $_D^{25}$ = + 4.5 (c = 1, MeOH); **^{1}H NMR** (400 MHz, $CDCl_3$) δ 7.37 (m, 10H), 6.97 (dd, *J* = 8 Hz, *J* = 16 Hz, 1H), 6.02 (d, *J* = 16 Hz, 1H), 5.30 (d, *J* = 8 Hz, 1H),

5.18 (s, 2H), 5.11 (m, 2H), 4.47 (m, 1H), 3.50 (m, 2H), 1.14 (s, 9H); **^{13}C NMR** (100 MHz, $CDCl_3$) δ 166.0, 155.8, 147.0, 136.2, 135.9, 128.5, 128.1, 126.9, 121.7, 73.5, 67.0, 66.3, 62.9, 54.6, 27.3; **MALDI TOF/TOF**- *m/z* calcd. for $C_{24}H_{29}NO_5$ $[M+Na]^+$ 434.1943, obsrvd. 434.1956.

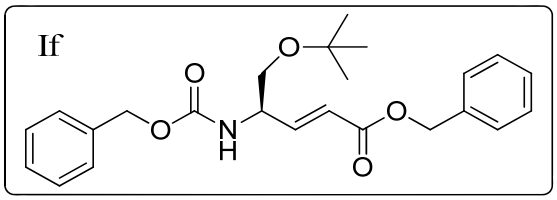

(*4R, 5S, E*)-benzyl 4-(benzyloxycarbonylamino)-5-tert-butoxyhex-2-enoate (Ig): colorless oil (2.143 g, 84 %); **$[\alpha]_D^{25}$** = + 18.1 (c = 1, MeOH); **^{1}H NMR** (400 MHz, $CDCl_3$) δ 7.36 (m, 10H), 6.98 (dd, *J* = 4 Hz, *J* = 16 Hz, 1H), 5.98 (d, *J* = 16 Hz, 1H), 5.25 (d, *J* = 16 Hz, 1H), 5.18 (s, 2H), 5.11 (m, 2H), 4.28 (m, 1H), 3.81 (m, 2H), 1.16 (d, *J* = 4 Hz, 3H), 1.12 (s, 9H); **^{13}C NMR** (100 MHz, $CDCl_3$) δ 165.9, 156.1, 148.0, 136.2, 135.9, 128.5, 128.1, 126.9, 121.0, 74.0, 68.0, 67.0, 66.2, 57.4, 28.5, 20.4; **MALDI TOF/TOF**- *m/z* calcd. for $C_{25}H_{31}NO_5$ $[M+Na]^+$ 448.2100, obsrvd. 448.2162.

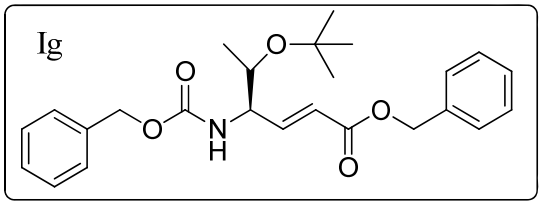

.

(*S, E*)-1-benzyl 6-tert-butyl 4-(benzyloxycarbonylamino)hex-2-enedioate (Ih): colorless oil (2.292 g, 87 %); **$[\alpha]_D^{25}$** = - 5.7 (c = 1, MeOH); **^{1}H NMR** (400 MHz, $CDCl_3$) δ 7.33 (m, 10H), 6.93 (dd, *J* = 4 Hz, *J* = 16 Hz, 1H), 6.00 (d, *J* = 16 Hz, 1H), 5.77 (d, *J* = 8 Hz, 2H), 5.15 (s, 2H), 5.09 (m, 1H), 4.70 (m, 1H), 2.54 (dd, *J* = 4 Hz, *J* = 16 Hz, 2H), 1.38 (s, 9H); **^{13}C NMR** (100 MHz, $CDCl_3$) δ 165.2, 155.1, 146.5, 135.8, 135.2, 128.0, 127.7, 121.00, 120.8, 81.5, 66.6, 66.0, 48.4, 39.0, 27.6; **MALDI TOF/TOF**- *m/z* calcd. for $C_{25}H_{29}NO_6$ $[M+Na]^+$ 462.1893, obsrvd. 462.1822.

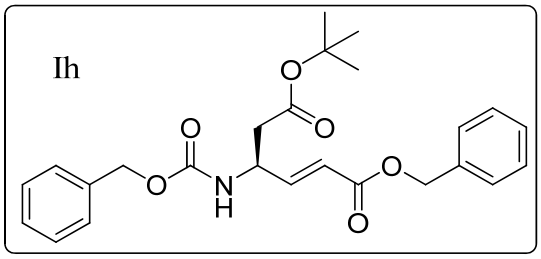

(*S, E*)-1-benzyl 7-tert-butyl 4-(benzyloxycarbonylamino)hept-2-enedioate (Ii): colorless oil (2.284 g, 84 %); **[α]** $_D^{25}$ = - 10.3 (c = 1, MeOH); **^{1}H NMR** (400 MHz, $CDCl_3$) δ 7.36 (m, 10H), 6.87 (dd, J = 4 Hz, J = 16 Hz, 1H), 5.98 (d, J = 16 Hz, 1H), 5.16 (s, 1H), 5.09 (m, 1H), 5.08 (bs, 1H), 4.37 (m, 1H), 2.30 (m, 2H), 1.85 (m, 2H), 1.41 (s,9H); **^{13}C NMR** (100 MHz, $CDCl_3$) δ 172.3, 165.8, 155.6, 147.8, 136.1, 135.7, 128.5, 128.1, 121.1, 80.9, 67.0, 66.4, 51.9, 31.8, 29.0, 28.0; **MALDI TOF/TOF**- *m/z* calcd. for $C_{26}H_{31}NO_6$ $[M+Na]^+$ 476.2049, obsrvd. 476.2066.

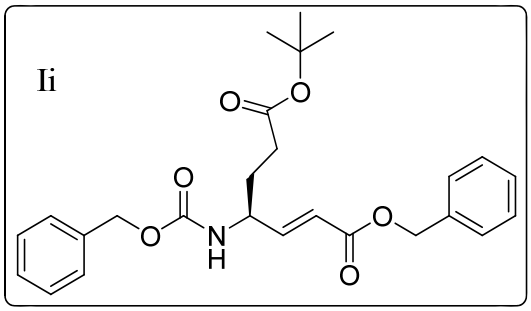

(*S, E*)-benzyl 4-(benzyloxycarbonylamino)-5-(1H-indol-3-yl)pent-2-enoate (Ij): white solid (2.408 g, 88 %), mp 110.5 ^{o}C; **[α]** $_D^{25}$ = + 4.1 (c = 1, MeOH); **^{1}H NMR** (400 MHz, $CDCl_3$) δ 8.26 (bs, 1H), 7.57 (d, J = 8 Hz, 1H), 7.36 – 7.10 (m, 13H), 7.04 (dd, J = 8 Hz, J = 16 Hz, 1H), 6.95 (s, 1H), 5.95 (d, J = 16 Hz, 1H), 5.17 (s, 2H), 5.09 (s, 2H), 5.01 (bs, 1H), 4.79 (m, 1H), 3.07 (m, 2H); **^{13}C NMR** (100 MHz, $CDCl_3$) δ 165.9, 155.8, 147.2, 140.9, 139.6, 136.2, 135.8, 128.5, 128.3, 126.9, 121.5, 113.8, 67.0, 66.3, 56.3, 38.8; **MALDI TOF/TOF**- *m/z* calcd. for $C_{28}H_{26}N_2O_4$ $[M+Na]^+$ 477.1790, obsrvd. 477.1739.

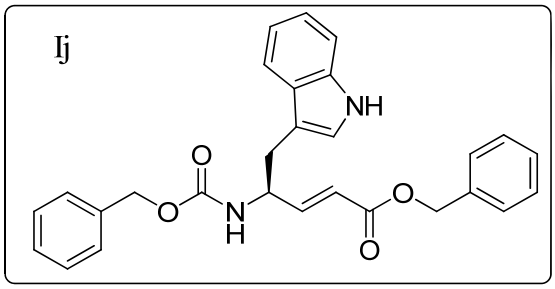

(*S, E*)-benzyl 4-(benzyloxycarbonylamino)-5-(4-hydroxyphenyl)pent-2-enoate (Ik): : white solid (2.380 g, 92 %), mp 98.4 ^{o}C; **[α]** $_D^{25}$ = + 6.7 (c = 1, MeOH); **^{1}H NMR** (400 MHz, $CDCl_3$) δ 7.36 (m, 10H), 6.96 (m, 3H), 6.71 (m, 2H), 5.89 (d, J = 16 Hz, 1H), 5.17 (m, 2H), 5.06 (m, 2H), 4.81 (m, 1H), 4.63 (m, 1H), 2.83 (m, 2H); **^{13}C NMR** (100 MHz, $CDCl_3$) δ 166.0, 154.9, 148.0, 135.7, 130.5, 128.6, 128.2, 128.1, 120.9, 115.6, 67.1, 66.4,

53.0, 39.8; **MALDI TOF/TOF**- *m/z* calcd. for $C_{26}H_{25}NO_5$ $[M+Na]^+$ 454.1630, obsrvd. 454.1684.

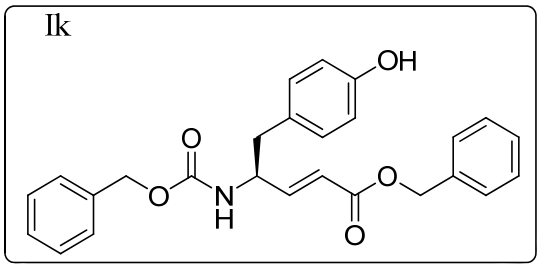

(*E*)-benzyl 4-(benzyloxycarbonylamino)-4-methylpent-2-enoate (Il): colorless oil (1.313 g, 62 %); **^{1}H NMR** (400 MHz, $CDCl_3$) δ 7.37 (m, 10H), 7.05 (d, J = 16 Hz, 1H), 5.90 (d, J = 16 Hz, 1H), 5.17 (s, 2H), 5.05 (s, 2H), 4.92 (bs, 1H), 1.43 (s, 6H); **^{13}C NMR** (100 MHz, $CDCl_3$) δ 166.4, 154.5, 153.4, 136.3, 135.9, 132.0, 128.6, 128.2, 118.6, 114.9, 66.4, 53.2, 27.2, 21.7; **MALDI TOF/TOF**- *m/z* calcd. for $C_{21}H_{23}NO_4$ $[M+Na]^+$ 376.1525, obsrvd. 376.1523.

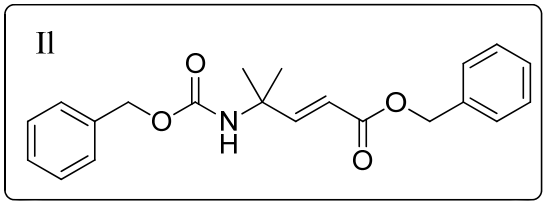

(S, E)-benzyl 4-(benzyloxycarbonylamino)-5-phenylpent-2-enoate (Im): white solid, mp

57.5 ^{o}C; [α] D^{25} = - 5.1(c = 1, MeOH); ^{1}H NMR (400 MHz, $CDCl_3$) δ 7.34 (m, 15H), 6.96 (dd, J = 4 Hz, J = 16 Hz, 1H), 5.91 (d, J = 16 Hz, 1H), 5.15 (s, 2H), 5.04 (s, 2H), 4.66 (m, 1H), 2.87 (m, 2H); ^{13}C NMR (100 MHz, $CDCl_3$) δ 166.09, 155.80, 148.05, 136.03, 129.57, 128.45, 128.30, 127.22, 121.21, 67.15, 66.58, 60.65, 40.78; MALDI TOF/TOF- *m/z* calcd. for $C_{26}H_{25}NO_4$ $[M+Na]^+$ 438.1681, obsrvd. 438.1632.

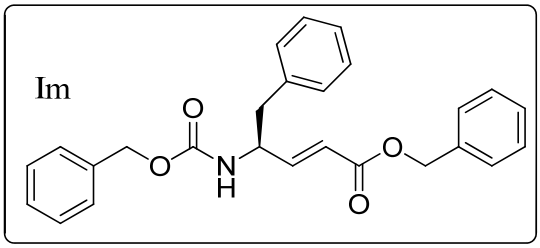

1.11.4 Spectroscopic Data for γ^4 amino acids

(*S*)-4-aminopentanoic acid (IIa): colorless oil (0.479 g, 82 %); **[α]** $_D^{25}$ = - 3.0 (c = 1, H_2O); **^{1}H NMR** (400 MHz, D_2O) δ 3.36 (m, 1H), 2.38 (m, 2H), 1.93-1.81 (m, 2H), 1.28 (d, *J* = 4 Hz, 3H); **^{13}C NMR** (100 MHz, D_2O) δ 177.0, 47.1, 29.7, 28.9, 17.2; **MALDI TOF/TOF**- *m/z* calcd. for $C_5H_{11}NO_2$ $[M+Na]^+$ 140.0687, obsrvd. 140.0666.

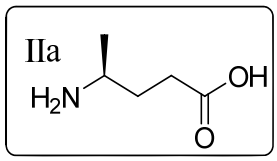

(*R*)-4-amino-5-methylhexanoic acid (IIb): white solid (0.551 g, 76 %), mp 178 ^oC; **[α]** $_D^{25}$ = - 1.8 (c = 1, H_2O); **^{1}H NMR** (400 MHz, D_2O) δ 3.06 (m, 1H), 2.35 (m, 3H), 1.76 (m, 2H), 0.92 (m, 6H); **^{13}C NMR** (100 MHz, D_2O) δ 174.8, 57.3, 33.7, 29.7, 26.0, 17.5, 16.7; **MALDI TOF/TOF**- *m/z* calcd. for $C_7H_{15}NO_2$ $[M+Na]^+$ 168.1000, obsrvd. 168.1035.

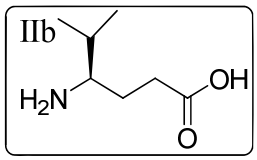

(*S*)-4-amino-5-methylhexanoic acid (IIc): white solid (0.507 g, 76 %), mp 178 ^oC; **[α]** $_D^{25}$ = + 1.8 (c = 1, H_2O); **^{1}H NMR** (400 MHz, D_2O) δ 3.03 (m, 1H), 2.25 (m, 3H), 1.74 (m, 2H), 0.92 (m, 6H); **^{13}C NMR** (100 MHz, D_2O) δ 174.8, 61.1, 32.4, 29.7, 26.0, 17.5, 16.7; **MALDI TOF/TOF**- *m/z* calcd. for $C_7H_{15}NO_2$ $[M+Na]^+$ 168.1000, obsrvd. 168.1021.

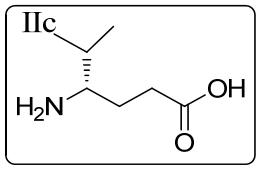

(*R*)-4-amino-6-methylheptanoic acid (IId): white solid (0.684 g, 86 %), mp 154 ^oC; **[α]** $_D^{25}$ = -8.6 (c = 1, H_2O); **^{1}H NMR** (400 MHz, D_2O) δ 3.25 (m, 1H), 2.25 (m, 2H), 1.81 (m, 2H), 1.62 (m, 1H), 1.42 (m, 2H), 0.84 (d, *J* = 4 Hz, 6H) ; **^{13}C NMR** (100 MHz, D_2O) δ 181.6, 50.0, 41.2, 33.3, 29.0, 23.8, 21.8, 21.2; **MALDI TOF/TOF**- *m/z* calcd. for $C_8H_{17}NO_2$ $[M+Na]^+$ 182.1157, obsrvd. 182.0886.

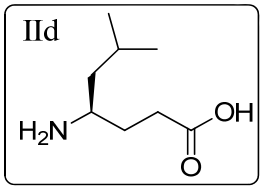

(*4R, 5R*)-4-amino-5-methylheptanoic acid (IIe): white solid (0.517 g, 65 %), mp 154 ^{o}C; **[α]** $_{D}^{25}$ = + 1.0 (c = 1, H_2O); **^{1}H NMR** (400 MHz, D_2O) *δ* 3.15 (m, 1H), 2.26 (m, 2H), 1.85 (m, 1H), 1.69 (m, 2H), 1.39-1.15 (m, 2H), 0.90 (m, 6H) ; **^{13}C NMR** (100 MHz, D_2O) *δ* 181.7, 56.0, 36.5, 33.9, 24.9, 24.5, 13.4, 10.8; **MALDI TOF/TOF**- *m/z* calcd. for $C_8H_{17}NO_2$ $[M+Na]^+$ 182.1157, obsrvd. 182.0959.

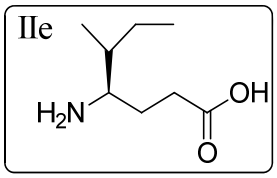

(*R*)-4-amino-5-*tert*-butoxypentanoic acid (IIf): white solid (0.709 g, 75 %), mp 126 ^{o}C; **[α]** $_{D}^{25}$ = - 16.6 (c = 1, H_2O); **^{1}H NMR** (400 MHz, D_2O) *δ* 3.60-3.40 (m, 2H), 3.26 (m, 1H), 2.25 (m, 2H), 1.79 (m, 2H), 1.15 (s, 9H) ; **^{13}C NMR** (100 MHz, D_2O) *δ* 180.8, 75.1, 61.1, 51.8, 33.1, 26.4, 25.6; **MALDI TOF/TOF**- *m/z* calcd. for $C_9H_{19}NO_3$ $[M+Na]^+$ 212.1263, obsrvd. 212.1261.

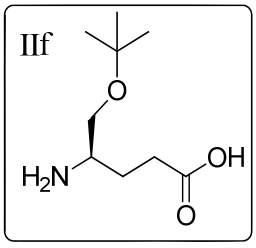

(*4R, 5S*)-4-amino-5-*tert*-butoxyhexanoic acid (IIg): white solid (0.812 g, 80 %), mp 127 ^{o}C; **[α]** $_{D}^{25}$ = - 12.6 (c = 1, H_2O); **^{1}H NMR** (400 MHz, D_2O) *δ* 3.81 (m, 1H), 2.97 (m, 1H), 2.29 (m, 2H), 1.91-1.71 (m, 2H), 1.18 (m, 12H); **^{13}C NMR** (100 MHz, D_2O) *δ* 181.1, 76.3, 67.3, 56.5, 33.5, 27.6, 25.3, 19.1; **MALDI TOF/TOF**- *m/z* calcd. for $C_{10}H_{21}NO_3$ $[M+Na]^+$ 226.1619, obsrvd. 226.1610.

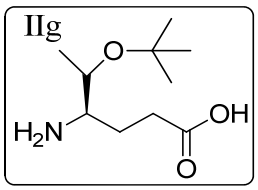

(*R*)-4-amino-6-*tert*-butoxy-6-oxohexanoic acid (IIh): white solid (0.977 g, 90 %), mp 139 ^{o}C; **[α]** $_{D}^{25}$ = - 15.9 (c = 1, H_2O); **^{1}H NMR** (400 MHz, D_2O) δ 3.55 (qn, J = 8 Hz, 1H), 2.65 (m, 2H), 2.26 (t, J = 8 Hz, 2H), 1.85 (m, 2H), 1.40 (s, 9H) ; **^{13}C NMR** (100 MHz, D_2O) δ 181.0, 171.4, 83.8, 48.3, 37.3, 33.3, 28.5, 27.1; **MALDI TOF/TOF**- *m/z* calcd. for $C_{10}H_{19}NO_4[M+Na]^+$ 240.1212, obsrvd. 240.1268.

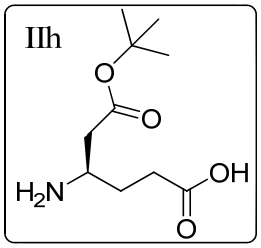

(*R*)-4-amino-7-*tert*-butoxy-7-oxoheptanoic acid (IIi): white solid (0.936 g, 81 %), mp 149 ^{o}C; **[α]** $_{D}^{25}$ = - 3.6 (c = 1, H_2O); **^{1}H NMR** (400 MHz, D_2O) δ 3.22 (qn, J = 8 Hz, 1H), 2.37 (t, J = 8 Hz, 2H), 2.24 (t, J = 8 Hz, 2H), 1.84 (m, 4H), 1.39 (s, 9H); **^{13}C NMR** (100 MHz, D_2O) δ 181.3, 174.3, 82.9, 51.2, 33.3, 31.1, 30.2, 28.3, 27.2; **MALDI TOF/TOF**- *m/z* calcd. for $C_{11}H_{21}NO_4[M+Na]^+$ 254.1368, obsrvd. 254.1322.

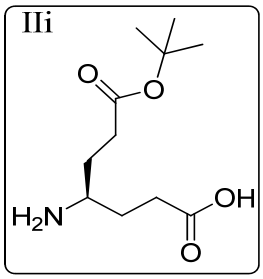

(*R*)-4-amino-5-(1H-indol-3-yl)pentanoic acid (IIj): off white solid (0.928 g, 80 %), mp 186 ^{o}C; **[α]** $_{D}^{25}$ = - 5.6 (c = 1, H_2O); **^{1}H NMR** (400 MHz, D_2O) δ 7.62 (d, J = 8 Hz, 1H), 7.47 (d, J = 8 Hz, 1H), 7.26 (s, 1H), 7.21 (t, J = 8 Hz, 1H), 7.13 (t, J = 8 Hz, 1H), 3.54 (m, 1H), 3.18-2.96 (m, 2H), 2.35 (d, J = 8 Hz, 2H), 1.91 (m, 2H); **^{13}C NMR** (100 MHz, DMSO d_6) δ 174.3, 136.6, 130.0, 127.5, 121.7, 121.6, 119.0, 112.0, 108.9, 61.6, 37.1, 28.6, 27.5; **MALDI TOF/TOF**- *m/z* calcd. for $C_{13}H_{16}N_2O_2[M+Na]^+$ 255.1109, obsrvd. 255.1087.

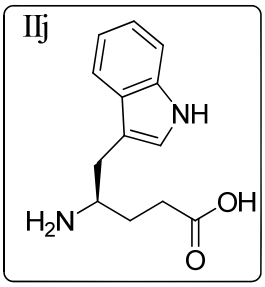

(*R*)-4-amino-5-(4-hydroxyphenyl)pentanoic acid (IIk): white solid (0.888 g, 85 %), mp 194 ^{o}C; **[α] $_{D}^{25}$** = - 6.8 (c = 1, H_2O); **^{1}H NMR** (400 MHz, D_2O) δ 7.12 (d, J = 12 Hz, 2H), 6.83 (d, J = 8 Hz, 2H), 3.40 (qn, J = 8 Hz, 1H), 2.94-2.72 (m, 2H), 2.31 (d, J = 8 Hz, 2H), 1.86 (m, 2H); **^{13}C NMR** (100 MHz, D_2O) δ 176.2, 154.2, 130.4, 126.7, 115.32, 52.3, 36.6, 29.3, 26.4; **MALDI TOF/TOF**- *m/z* calcd. for $C_{11}H_{15}NO_3[M+Na]^+$ 232.0950, obsrvd. 232.0932.

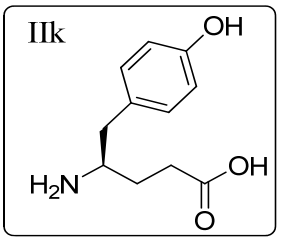

4-amino-4-methylpentanoic acid (IIl): white solid (0.393 g, 60 %), mp 198 ^{o}C; **^{1}H NMR** (400 MHz, D_2O) δ 2.20 (t, J = 8 Hz, 2H), 1.84 (t, J = 8 Hz, 2H), 1.28 (s, 6H); **^{13}C NMR** (100 MHz, D_2O) δ 177.0, 47.1, 29.7, 28.9, 17.2; **MALDI TOF/TOF**- *m/z* calcd. for $C_6H_{13}NO_2[M+K]^+$ 170.0583, obsrvd. 170.0874.

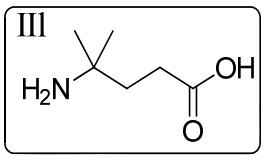

(R)-4-amino-5-phenylpentanoic acid (IIm): white solid (0.687 g, 90 %), mp 135 ^{o}C; [α] D^{25} = - 11.2 (c = 1, H_2O); ^{1}H NMR (400 MHz, D_2O) δ 7.33-7.24 (m, 5H), 3.47 (qn, J = 4 Hz, 1H), 3.00-2.82 (m, 2H), 2.30 (t, J = 8 Hz, 2H), 1.86 (dd, J = 8 Hz, J = 12 Hz, 2H) ; ^{13}C NMR (100 MHz, D_2O) δ 181.04, 135.76, 129.43, 129.12, 127.51, 115.01, 53.12, 38.12, 33.28, 28.50; MALDI TOF/TOF- *m/z* calcd. for $C_{11}H_{15}NO_2$ $[M+Na]^+$ 216.1000, obsrvd. 216.1060.

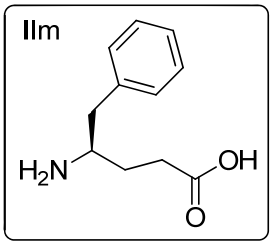

c) (9H-fluoren-9-yl)methyl (S)-5-oxo-5-((S)-1-phenylethylamino)pentan-2-ylcarbamate: white solid (0.300 g, 68 %), mp 180 ^{o}C; **[α]** $_{D}^{25}$ = - 6.3 (c = 1, MeOH); **^{1}H NMR** (400 MHz, DMSO d_6) δ 8.15 (bs, 1H), 7.82 (d, J = 8 Hz, 2H), 7.67 (d, J = 8 Hz, 2H), 7.39 (t, J = 8 Hz, 2H), 7.28 (m, 6H), 7.19 (m, 1H), 7.06 (bs, 1H), 4.93 (m, 1H), 4.28 (d, J = 4 Hz, 2H), 4.19 (t, J = 8 Hz, 1H), 3.52 (m, 1H), 2.14 (t, J = 8 Hz, 2H), 1.65 (t, J = 8 Hz, 2H), 1.35 (d, J = 4 Hz, 3H), 1.08 (d, J = 4 Hz, 3H); **^{13}C NMR** (100 MHz, DMSO d_6) δ 171.0, 155.5, 144.7, 143.8, 140.7, 128.0, 127.4, 126.8, 126.4, 125.8, 125.1, 119.9, 65.0, 48.5, 47.6, 46.8, 33.3, 32.1, 22.2, 20.8; **MALDI TOF/TOF**- *m/z* calcd. for $C_{28}H_{30}N_2O_3$ $[M+Na]^+$ 465.2154, obsrvd. 465.2124.

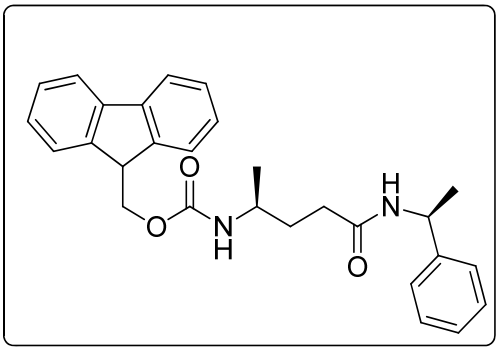

d) (9H-fluoren-9-yl)methyl (S)-5-oxo-5-((R)-1-phenylethylamino)pentan-2-ylcarbamate (IVb): white solid (0.313 g, 71 %), mp 180 ^{o}C; **[α]** $_{D}^{25}$ = + 2.9 (c = 1, MeOH); **^{1}H NMR** (400 MHz, DMSO d_6) δ 8.12 (bs, 1H), 7.79 (d, J = 8 Hz, 2H), 7.64 (d, J = 8 Hz, 2H), 7.36 (t, J = 8 Hz, 2H), 7.26 (m, 6H), 7.17 (m, 1H), 7.06 (bs, 1H), 4.91 (m, 1H), 4.25 (d, J = 4 Hz, 2H), 4.18 (t, J = 8 Hz, 1H), 3.50 (m, 1H), 2.12 (t, J = 8 Hz, 2H), 1.61 (t, J = 8 Hz, 2H), 1.32 (d, J = 4 Hz, 3H), 1.06 (d, J = 4 Hz, 3H); **^{13}C NMR** (100 MHz, DMSO d_6) δ 171.0, 155.5, 144.7, 143.8, 140.7, 128.0, 127.4, 126.9, 126.4, 125.8, 125.1, 119.9, 65.0, 48.5, 47.6, 46.9, 33.3, 32.1, 22.2, 20.8; **MALDI TOF/TOF**- *m/z* calcd. for $C_{28}H_{30}N_2O_3$ $[M+Na]^+$ 465.2154, obsrvd. 465.2147.

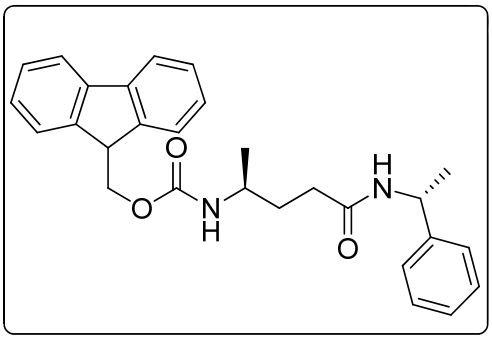

1.12 References

1. a) Dill, K. A. *Biochemistry* **1990**, *29*, 7133. b) Dill, K. A.; MacCallum, J. L. *Science* **2012**, *338*, 1042. b) Baltzer, L.; Nilsson, H.; Nilsson, J. *Chem. Rev.* **2001**, *101*, 3153. c) DeGrado, W. F.; Summa, C. M.; Pavone, V.; Nastri, F.; Lombardi, A. *Annu. Rev. Biochem.* **1999**, *68*, 779.
2. a) Karle, I. L.; Das, C.; Balaram, P. *Proc. Natl. Acad. Sci., USA* **2000**, *97*, 3034. b) De Zotti, M.; Biondi, B.; Park, Y.; Hahm, K. S.; Crisma, M.; Toniolo, C.; Formaggio, F. *Amino Acids* **2012**, *43*, 1761.c) Saragovi, H. U.; Greene, M. I.; Chrusciel, R. A.; Kahn, M. *Bio-Technol.* **1992**, *10*, 773.
3. a) Venkatraman, J.; Shankaramma, S. C.; Balaram, P. *Chem. Rev.* **2001**, *101*, 3131. b) Gehenn, K.; Stege, J.; Reed, J. *Anal. Biochem.* **2006**, *356*, 12. c) Narang, P.; Bhushan, K.; Bose, S.; Jayaram, B. *Phys Chem Chem Phys* **2005**, *7*, 2364. d) Darbre, T.; Reymond, J. L. *Acc. Chem. Res.* **2006**, *39*, 925.
4. Gellman, S. H. *Acc. Chem. Res.* **1998**, *31*, 173.
5. a) Appella, D. H.; Christianson, L. A.; Karle, I. L.; Powell, D. R.; Gellman, S. H. *J. Am. Chem. Soc.,* **1996**, *118*, 13071. b) Appella, D. H.; Christianson, L. A.; Karle, I. L.; Powell, D. R.; Gellman, S. H. *J. Am. Chem. Soc.,* **1999**, *121*, 6206. c) Appella, D. H.; Christianson, L. A.; Klein, D. A.; Richards, M. A.; Powell, D. R.; Gellman, S. H. *J. Am. Chem. Soc.,* **1999**, *121*, 7574.
6. a) Hintermann, T.; Gademann, K.; Jaun, B.; Seebach, D. *Helv. Chim. Acta*, **1998**, *81*, 983. b) Seebach, D.; Beck, A. K.; Bierbaum, D. J. *Chem. Biodiv.,* **2004**, *1*, 1111.
7. a) Sharma, G. V. M.; Reddy, R.; Krishna, P. R.; Ravi Sankar, A.; Narsimulu, K., Kumar, S. K.; Jayaprakash, P.; Jagannadh, B.; Kunwar, A. C. *J. Am. Chem. Soc.*, **2003**, *125*, 13670. b) Sharma, G. V. M.; Chandramouli, N.; Choudhary, M.;

Nagendar, P.; Ramakrishna, K. V. S.; Kunwar, A. C.; Schramm, P.; Hofmann, H. -J. *J. Am. Chem. Soc.*, **2009**, *131*, 17335.

8. a) Guitot, K.; Carboni, S.; Reiser, O.; Piarulli, U. *J. Org. Chem.,* **2009**, *74*, 8433. b) De Pol, S.; Zorn, C.; Klein, C. D.; Zerbe, O.; Reiser, O. *Angew. Chem., Int. Ed. Engl.,* **2004**, *43*, 511. c) Berlicki, L.; Pilsl, L.; Weber, E.; Mandity, I. M.; Cabrele, C.; Martinek, T. A.; Fulop, F.; Reiser, O. *Angew. Chem., Int. Ed. Engl.,* **2012**, *5*, 2208. d) Pilsl, L. K.; Reiser, O. *Amino Acids* **2011**, *41*, 709.
9. Fernandes, C.; Faure, S.; Pereira, E.; Thery, V.; Declerck, V.; Guillot, R.; Aitken, D. J. *Org. Lett.* **2010**, *12*, 3606.
10. a) Martinek, T. A.; Fulop, F. *Chem. Soc. Rev*. 2012, **41**, 687. b) Fulop, F.; Forro, E.; Toth, G. K. *Org. Lett*. **2004**, *6*, 4239. c)
11. Hook, D.F.; Bindschadler, P.; Mahajan, Y. R.; Sebesta, R.; Kast, P.; Seebach, D. *Chem. Biodiv.* **2005**, *2*, 591.
12. (a) Horne, W. S.; Price, J. L.; Gellman, S. H. *Proc. Natl. Acad. Sci. U.S.A.* **2008**, *105*, 9151. (b) English, E. P.; Chumanov, R. S.; Gellman, S. H.; Compton, T. *J. Biol. Chem.* **2006**, *281*, 2661. c) Imamura, Y.; Watanabe, N.; Umezawa, N.; Iwatsubo, T.; Kato, N.; Tomita, T.; Higuchi, t.; *J. Am. Chem. Soc.* **2009**, *131*, 7353.
13. Cheng, R.P.; Gellman, S. H.; DeGrado, W. F. *Chem. Rev.* **2001**, *101*, 3219.
14. a) Karle, I.; Gopi, H. N.; Balaram, P. *Proc. Natl. Acad. Sci. U.S.A.* **2002**, *99*, 5160. b) Sonti, R.; Gopi, H. N.; Muddegowda, U.; Ragothama, S.; Balaram, P. *Chem. Eur. J.* **2013**, *19*, 5955. b)) Vasudev, P. G.; Chatterjee, S.; Shamala, N.; Balaram, P. *Chem. Rev.* **2011**, *111*, 657.
15. Appella, D. H.; Christianson, L. A.; Karle, I. L.; Powell, D. R.; Gellman, S. H. *J. Am. Chem. Soc.* **1996**, *118*, 13071.
16. Choi, S. H.; Guzei, I. A.; Spencer, L. C.; Gellman, S. H. *J. Am. Chem. Soc.* **2010**, *132*, 13879.
17. Mandity, I. M.; Fulop, L.; Vass, E.; Toth, G. K.; Martinek, T. A.; Fulop, F. *Org. Lett*. **2010**, *12*, 5584.
18. Kwon, S.; Jeon, A.; Yoo, S. H.; Chung, I. S.; Lee, H.-S. *Angew. Chem. Int. Ed.* **2010,** *49*, 8232.
19. Hintermann, T.; Gademann, K.; Jaun, Seebach, D. *Helv. Chim. Acta.* **1998**, *81*, 893.
20. Hanessian, S.; Luo, X.; Schaum, R.; Michnick, S. *J. Am. Chem. Soc.* **1998**, *120*, 8569.
21. Baldauf, C.; Gunther, R.; Hofmann, H. -J.; *J. Org. Chem.* **2006**, *71*, 1200.

22. Vasudev, P. G.; Chatterjee, S.; Shamala, N.; Balaram, P. *Acc. Chem. Res*. **2009**, *42*, 1628.
23. Sharma, G. V. M.; Jayaprakash, P.; Narsimulu, K.; Sankar, A. R.; Reddy, K. R.; Kunwar, A. C. *Angew. Chem. Int. Ed.* **2006**, *45*, 2944.
24. Khurram, M.; Qureshi, N.; Smith, M. D. *Chem. Commun*. **2006**, 5006.
25. Kothari, A.; Khurram, M.; Qureshi, N.; Beck, E. M.; Smith, M. D. *Chem. Commun*. **2007**, 2814.
26. Guo, L.; Zhang, W.; Reidenbach, A. G.; Giuliano, M. W.; Guzei, I. A.; Spencer, L. C.; Gellman, S. H. *Angew. Chem. Int. Ed.* **2011**, *50*, 5843.
27. a) Lee, X.; Yang, D. *Chem. Commun*. **2006**, 3367. b) Chen, F.; Zhu, N.-Y.; Yang, D. *J. Am. Chem. Soc.* **2004**, *126*, 15980.
28. Cheguillaume, A.; Salaun, A.; Sinbandhit, S.; Potel, M.; Gall, P.; Baudy-Floch, M.; Le Grel, P. *J. Org. Chem.* **2001**, *66*, 4923.
29. Pendem, N.; Nelli, Y. R.; Douat, C.; Fischer, L.; Laguerre, M.; Ennifar, E.; Kauffman, B.; Guichard, G. *Angew. Chem. Int. Ed.* **2013**, *52*, 4147.
30. Mathieu, L.; Legrand, B.; Deng, C.; Vezenkov, L.; Wenger, E.; Didierjean, C.; Amblard, M.; Averlant-Petit, M. C.; Masurier, N.; Lisowski, V.; Martinez, J.; Maillard, L. T. *Angew. Chem. Int. Ed.* **2013**, *52*, 6006.
31. Seebach, D.; Hook, D. F.; Glattli, A. *Biopolymers (Peptide Science)* **2006**, *84*, 23.
32. Mali, S. M.; Bandyopadhyay, A.; Jadhav, S. V.; Kumar, M. G.; Gopi, H. N. *Org. Biomol. Chem*. **2011**, *9*, 6566.
33. Bandyopadhyay, A.; Agrawal, N.; Mali, S. M.; Jadhav, S. V.; Gopi, H. N. *Org Biomol Chem.* **2010**, *8*, 4855.
34. Falorni, M.; Porcheddu, A.; Taddei, M. *Tetrahedron Lett*. **1999**, *40*, 4395.
35. a) Williams, P. L.; Albericio, F.; Giralt, E. *Chemical approaches to the synthesis of peptides and proteins* **1997**, CRC press. b) Bodanszky, M. *Peptide Chemistry: A practical text book, 2nd Ed*. **1988,** Springer-Ver- lag, Berlin.
36. a) Jackson, R. F. W.; Moore, R. J.; Dexter, C. S. *J. Org. Chem*. **1998**, *63*, 7875. b) Haug, B. E.; Rich, D. H. *Org. Lett*. **2004**, *6*, 4783.
37. a) Grabarek, Z.; Gergely, J. *Anal. Biochem*. **1990**, *185*, 131. b) Staros, J. V.; Wright, R. W.; Swingle, D. M. *Anal. Biochem.* **1986**, *156*, 220. c) Marcel, J.; Fischer, E. *Methods Mol. Biol*. **2010**, *627*, 55.

38. a) Anderson, G. W.; Zimmerman, J. E.; Callahan, F. M. *J. Am. Chem. Soc.* **1964,** *86*, 1839. b) Bodanszky, M.; Bodanszky, A. *The Practice of Peptide Synthesis*, Springer, *Berlin* **1984**, p138.
39. Katritzky, A. R.; Abo-Dya, N. E.; Tala, S. R.; Gyanda, K.; Abdel-Samii, Z. K. *Org. Biomol. Chem*. **2009**, *7*, 4444.
40. Tailhades, J.; Gidel, M. A.; Grossi, B.; Lecaillon, J.; Brunel, L.; Subra, G.; Martinez, J.; Amblard, M. *Angew. Chem. Int. Ed*. **2010**, *49*, 117.
41. a) Zhang, X.; Rodrigues, J.; Evans, L.; Hinkle, B.; Ballantyne, L.; Pena, M. *J. Org. Chem.* **1997**, *62*, 6420. b) Abell, A. D.; Jones, M. A.; Neffe, A. T.; Aitken, S. G. ; Cain, T. P.; Payne, R. J.; McNabb, S. B.; Coxon, J. M.; Stuart, B. G.; Pearson, D.; Lee, H. Y.-Y. ; Morton, J. D. *J. Med. Chem*. **2007**, *50*, 2916. c) Gilbertson, S. R.; Lan, P. *Tetrahedron Lett*. **2002**, *43*, 6961. d) Pastor, I. M.; Vastila, P.; Adolfsson, H. *Chem.–Eur. J*. **2003**, *9*, 4031.
42. a) Shamala, A.N.; Balaram, P. *Chem. Biodivers.* **2008**, *5*, 1238. b) Toniolo, C.; Benedetti, G. *Trends Biochem*. **1991**, *16*, 350.
43. (a) Toniolo, C.; Crisma, M.; Formaggio, F.; Peggion, C. *Biopolymers* **2001**, *60*, 396. (b) Mahalakshmi, R.; Balaram, P. *Methods Mol. Biol.* **2006**, *340*, 71. (c) Gessmann, R.; Bruckner, H.; Petratos, K. *J. Pept. Sci.* **2003**, *9*, 753. (d) Venkataram Prasad, B.V.; Shamala, N.; Nagaraj, R.; Chandrasekaran, R.; Balaram, P. *Biopolymers* **1979**, *18*, 1635. (e) Poli, A. Moretto, M. D.; Crisma, M.; Peggion, C.; Formaggio, F.; Kaptein, B.; Broxterman, Q. B.; Toniolo, C. *Chem.–Eur. J.* **2009**, *15*, 8015.
44. a) Mandal, P. K.; Ren, Z.; Chen, X.; Xiong, C.; McMurray, J. S. *J. Med. Chem.* **2009**, *52*, 6126. b) Loukas, V.; Noula, C.; Kokotos, G. *J. Pept. Sci*. **2003**, *9*, 312.
45. a) Basuroy, K. ; Dinesh, B.; Shamala, N.; Balaram, P. *Angew. Chem. Int. Ed.* **2012**, *51*, 8736. b) Basuroy, K.; Dinesh, B.; Shamala, N.; Balaram, P. *Angew. Chem. Int. Ed.* **2013**, *52*, 3136.
46. *SAINT Plus*, (Version 7.03); Bruker AXS Inc.: Madison, WI, 2004.
47. Sheldrick, G. M. *Acta. Cryst*. **2008** SHELXL. *A64*, 112.

1.13 Appendix I: Representative Characterization data for synthesized compounds.

Characterization for only representative compound is provided.

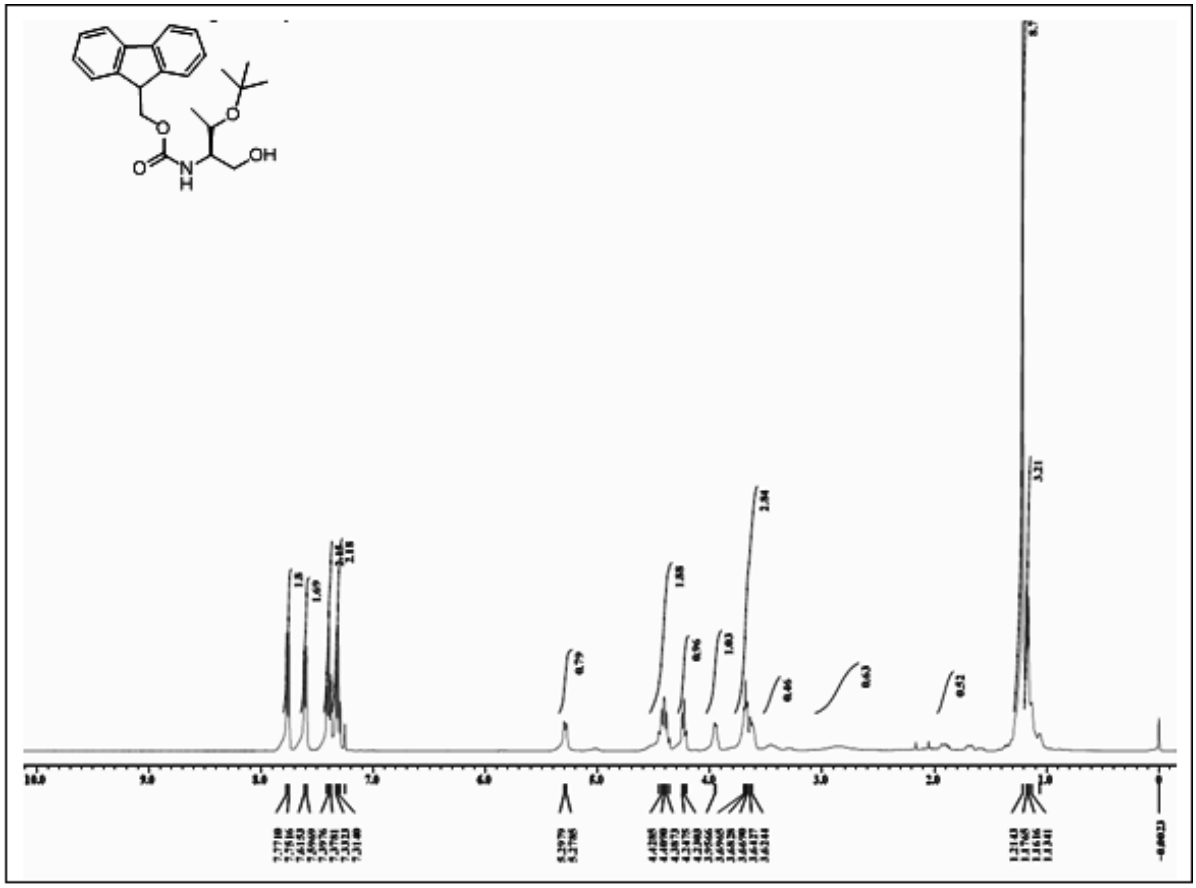

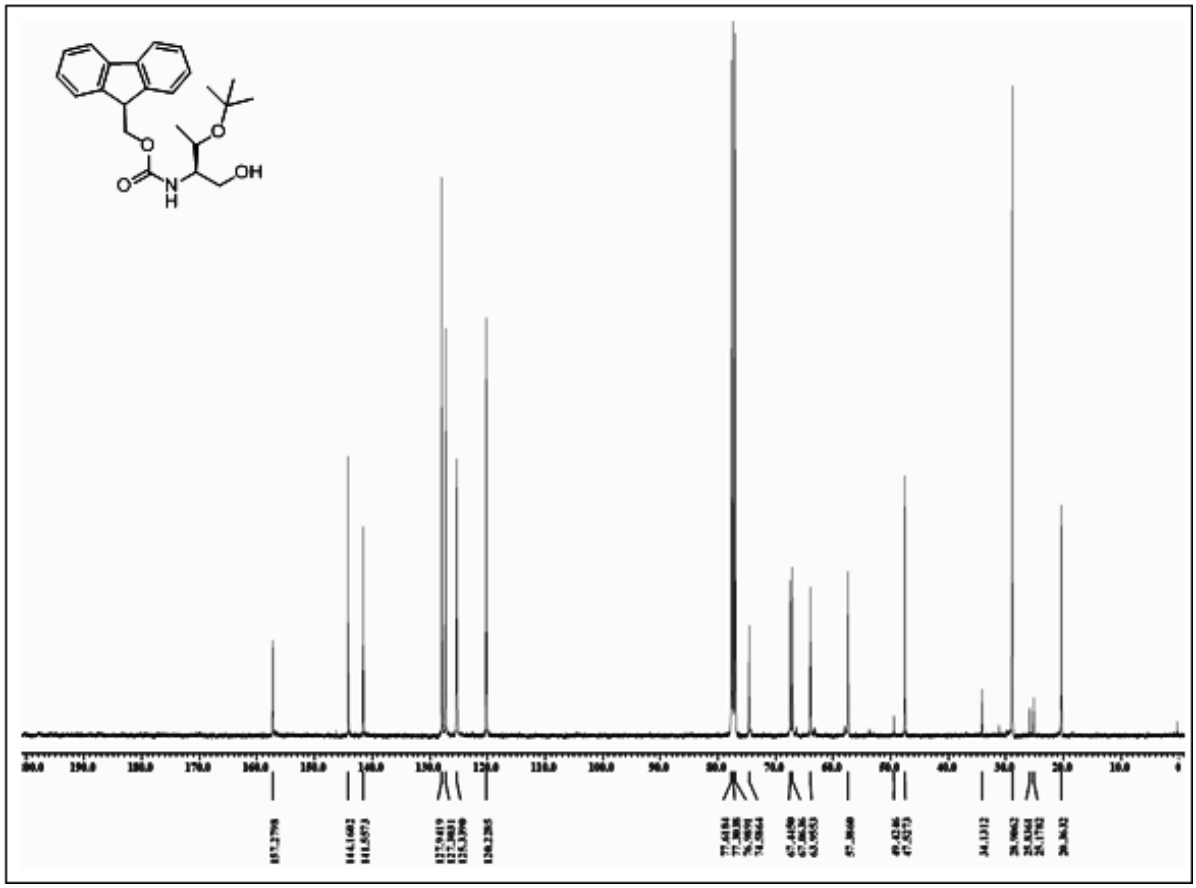

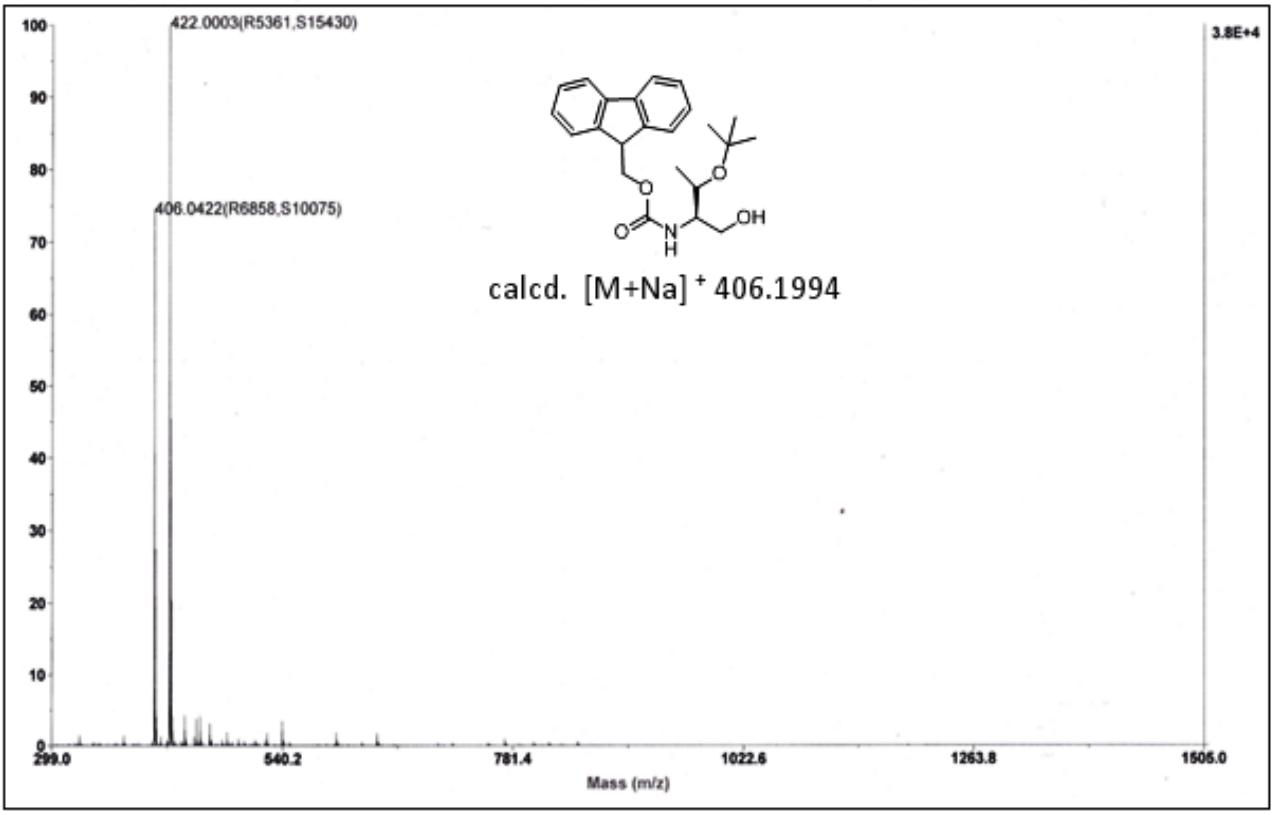

calcd. $[M+Na]^+$ 406.1994

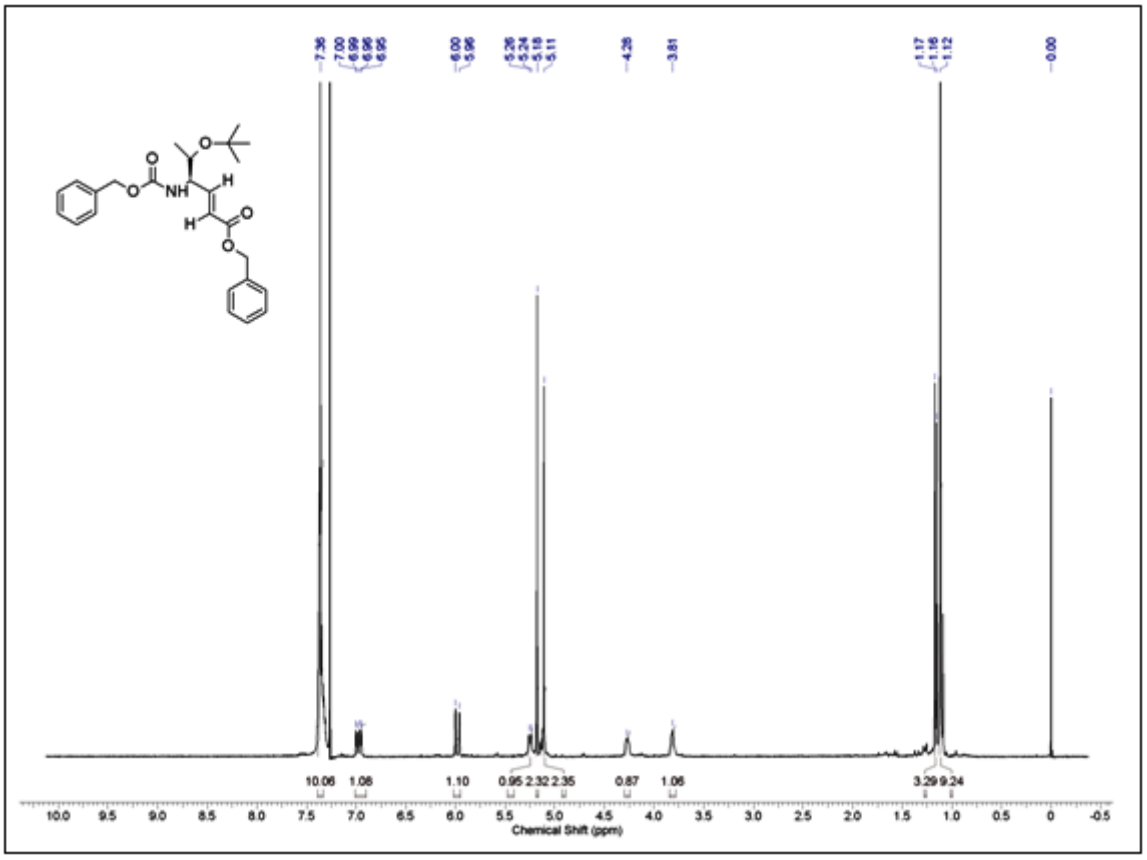
7.36
7.00
6.99
6.96
6.95
6.00
5.98
5.26
5.24
5.18
5.11
4.26
3.81
1.17
1.16
1.12
0.00
10.06
1.06
1.10
0.95
2.32
2.35
0.87
1.06
3.29
9.24
Chemical Shift (ppm)

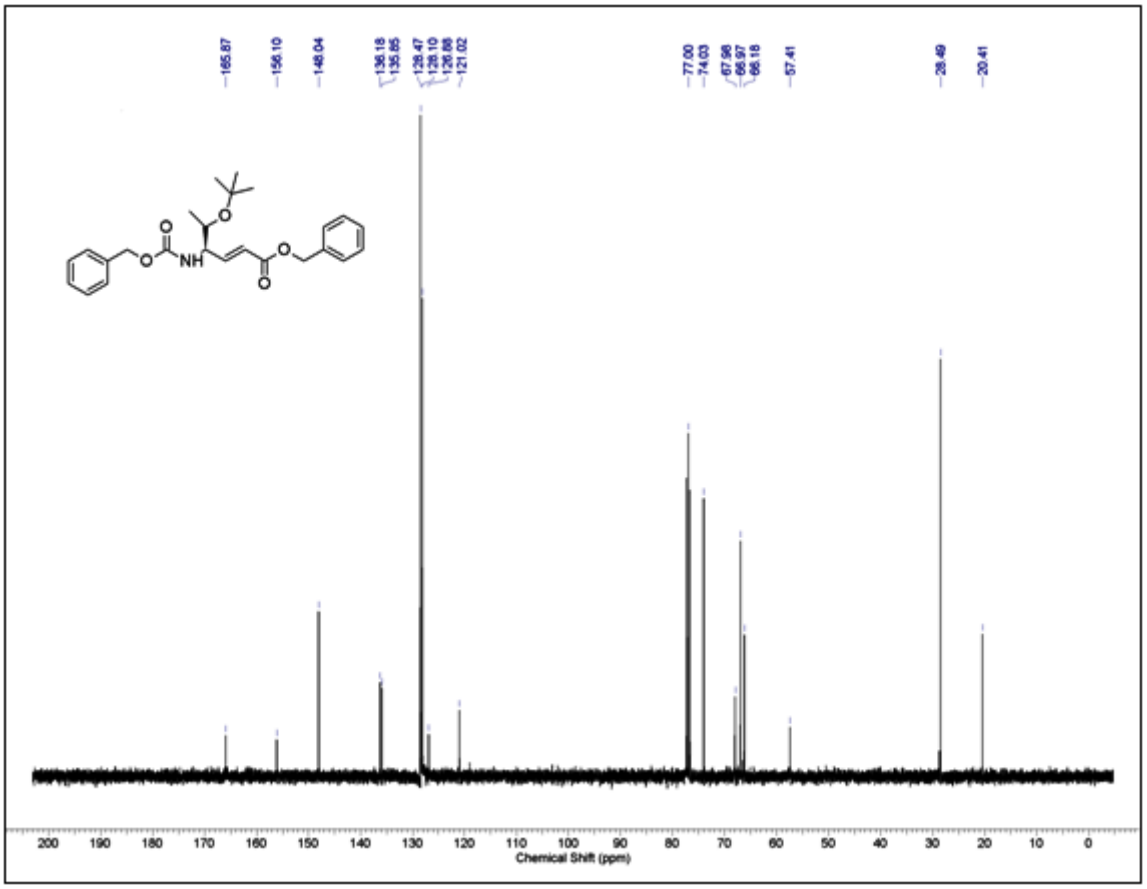
165.87
156.10
148.04
136.18
135.65
128.47
128.10
126.88
121.02
77.00
74.03
67.98
66.97
66.18
57.41
28.49
20.41
Chemical Shift (ppm)

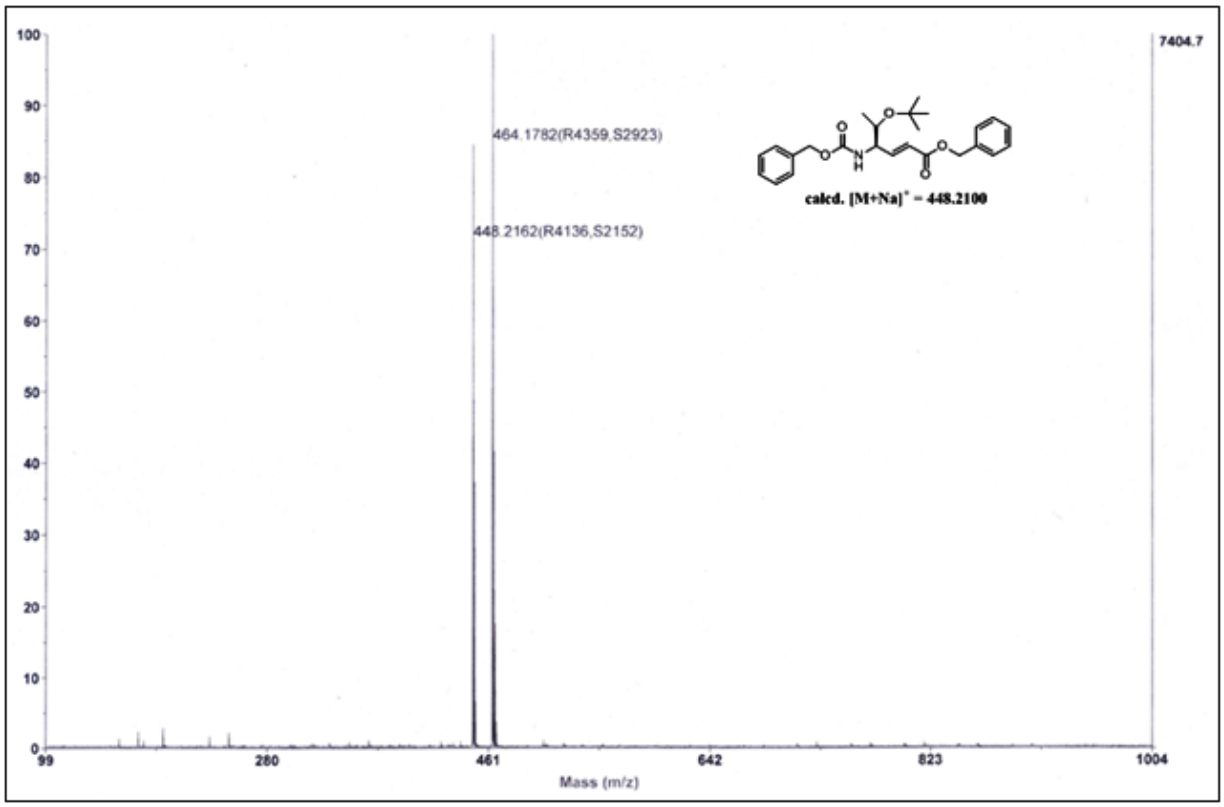
100
90
80
70
60
50
40
30
20
10
0
99
280
461
642
823
1004
Mass (m/z)
464.1782(R4359,S2923)
448.2162(R4136,S2152)
7404.7
calcd. [M+Na]+ = 448.2100

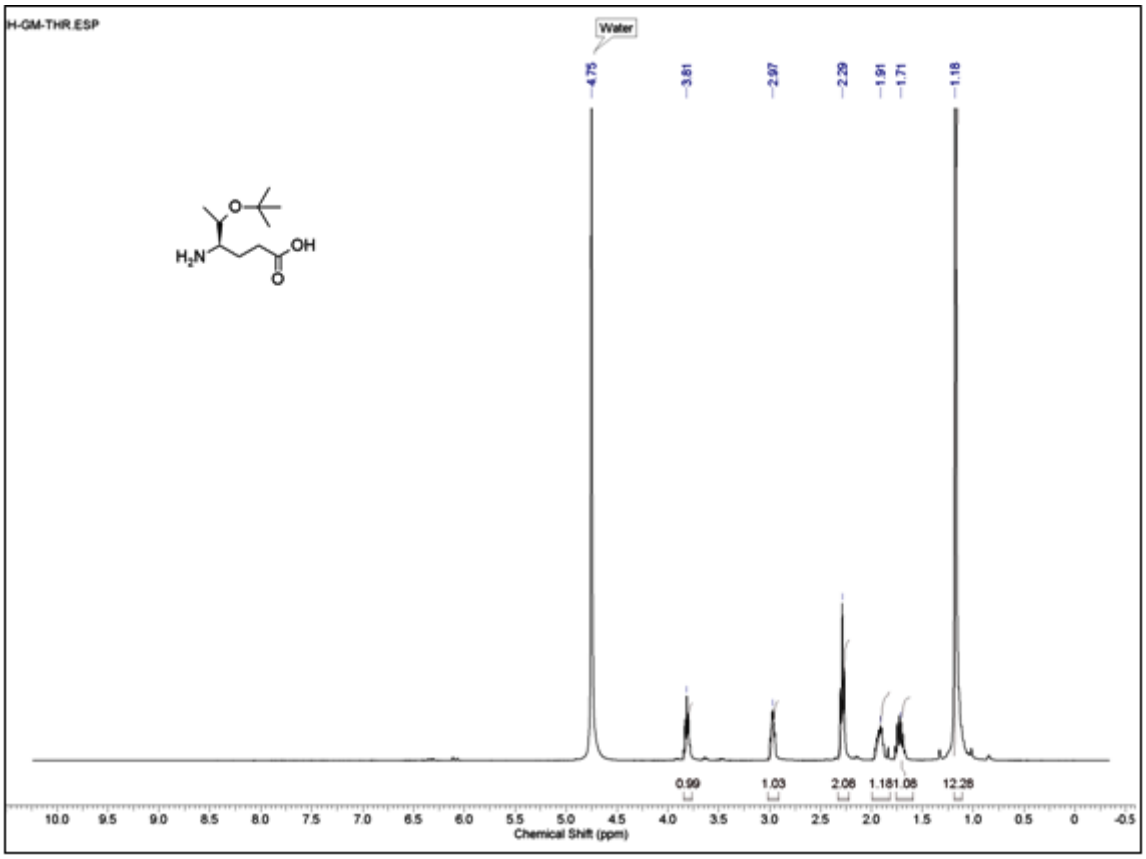
H-GM-THR.ESP
Water
4.75
3.81
2.97
2.29
1.91
1.71
1.18
0.99
1.03
2.06
1.18
1.08
12.28
Chemical Shift (ppm)

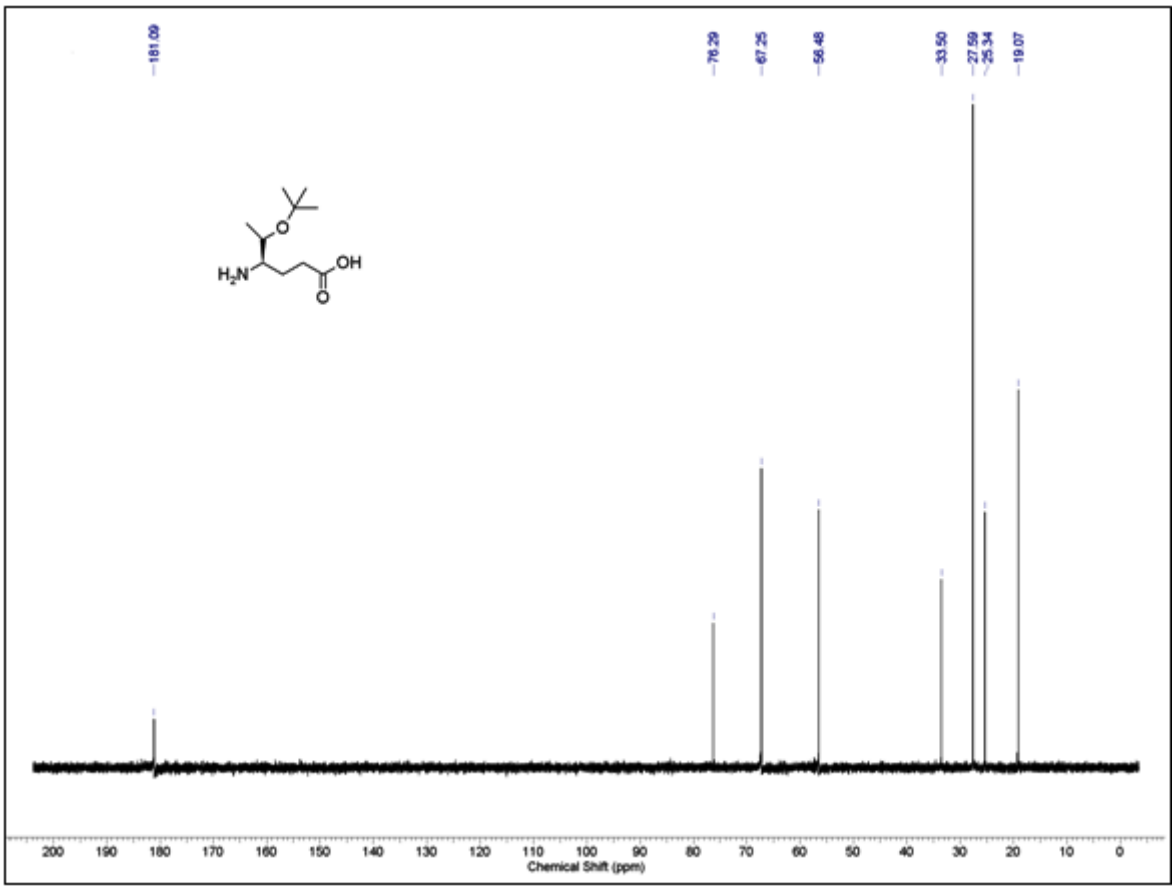
181.09
76.29
67.25
56.48
33.50
27.59
25.34
19.07
Chemical Shift (ppm)

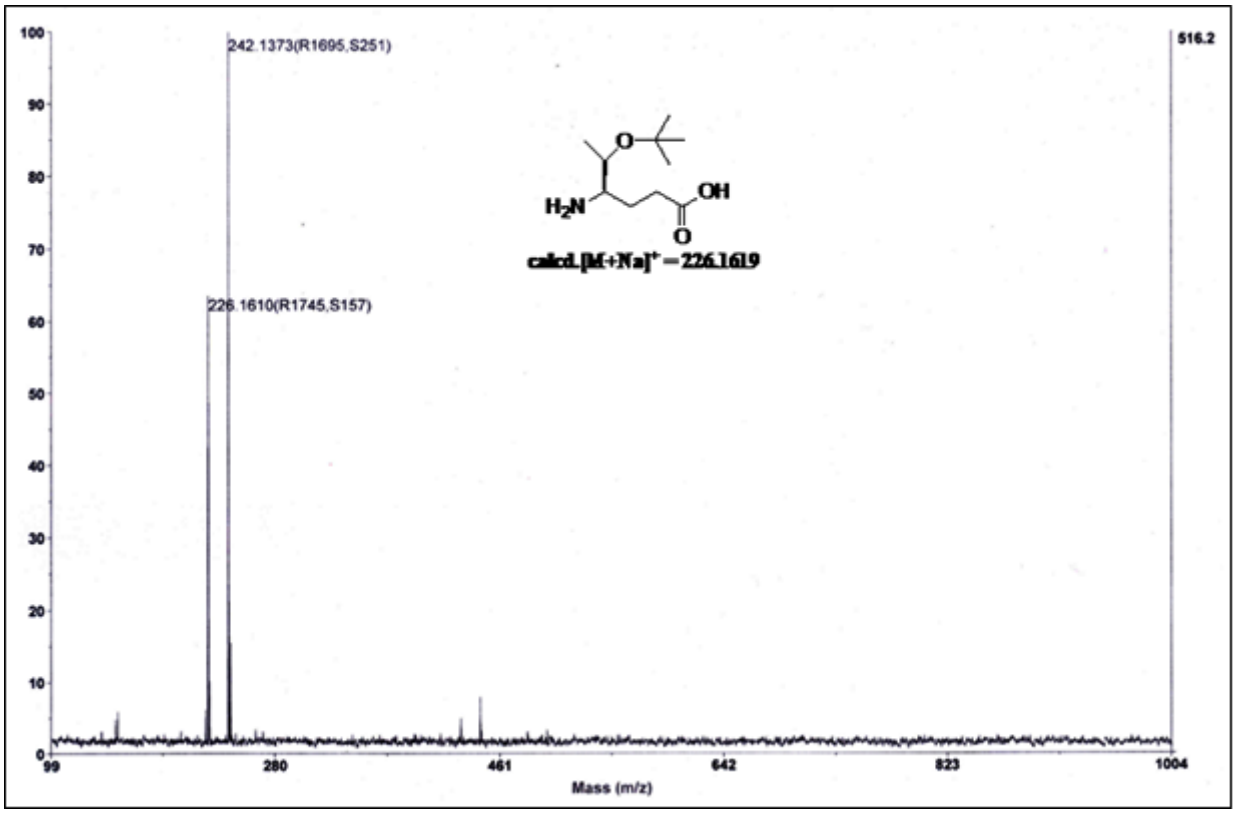
242.1373(R1695,S251)
516.2
226.1610(R1745,S157)
calcd.[M+Na]+ = 226.1619
100
90
80
70
60
50
40
30
20
10
0
99
280
461
642
823
1004
Mass (m/z)

Chapter 2

Design, Synthesis, Conformations and Self-Assembly of Hybrid α,γ^4-Peptides

2.1 Introduction

Helices constitute the major secondary structural components of proteins.[1] Based on the nature of the internal hydrogen bonding pattern, these helical secondary structures can be further classified as C13-helix (or α- helix), C10-helix (3_{10}-helix) and C7-helix (or γ-helix).[2] In all these α-peptide helical structures, the directionality of the hydrogen bond with respect to the chain direction (C←N) is the same. α-Helix is predominantly occurred in nature compared to the other two. The α-helices are stabilized by canonical 13-membered intramolecular H-bonds (1←5) between the residues *i* (*CO*) and *i+4 (NH)*. The helical parameters for α-helix such as residue- per-turn, rise-per-turn and radius of the α-helix were found to be the 3.6, 5.5, and 2.3 Å respectively. The 3_{10}-helix occurs less frequently in proteins, and the helical structure is stabilized by canonical 10-membered intramolecular H-bonds between the residues *i* and *i+3* (1←4). The helical parameters for 3_{10} helix such as residue-per-turn, rise-per-turn and the radius were found to be 3.2, 5.8 and 2.1 Å respectively. The γ-helices are stabilized by 7-membered intramolecular H-bonds between the residues *i* and *i+2* and rarely observed in protein structures. Further, helix associated supersecondary structures such as helical bundles, helix-turn-helix (α,α), helix-β-sheet motifs (α, β-motif), α-helical hairpin motifs, coiled-coils etc. are also observed in the nature. Helices often play a crucial role in mediating protein-protein and protein-nucleic acids (DNA and RNA) interactions.[3] Disrupting these interactions with isolated helical structures is of paramount importance not only to understand the biological consequences of the interactions but also from the perspective of drug design. Several approaches have been developed to mimic the short and stable α-peptide helices including covalent cross-linkage of amino acids side-chains,[4] utilization of C-C covalent bond as intramolecular H-bond surrogate [5] or non-peptidic organic templates.[6] As mentioned in the Chapter 1, the recent exponential growth of β- and γ-peptide foldamers provides an alternative and straightforward approach to mimic protein secondary structures.[7] Homooligomers of β-amino acids and γ-amino acids produced different types of unique helices with respect to the type of amino acids utilised. The helical patterns adopted by the peptides from β-amino acids has briefly described in the previous chapter. Foldamers comprised of γ-residues have also been recently investigated. In addition to the homooligomers of non-natural amino acids, another very attractive area in the foldamer

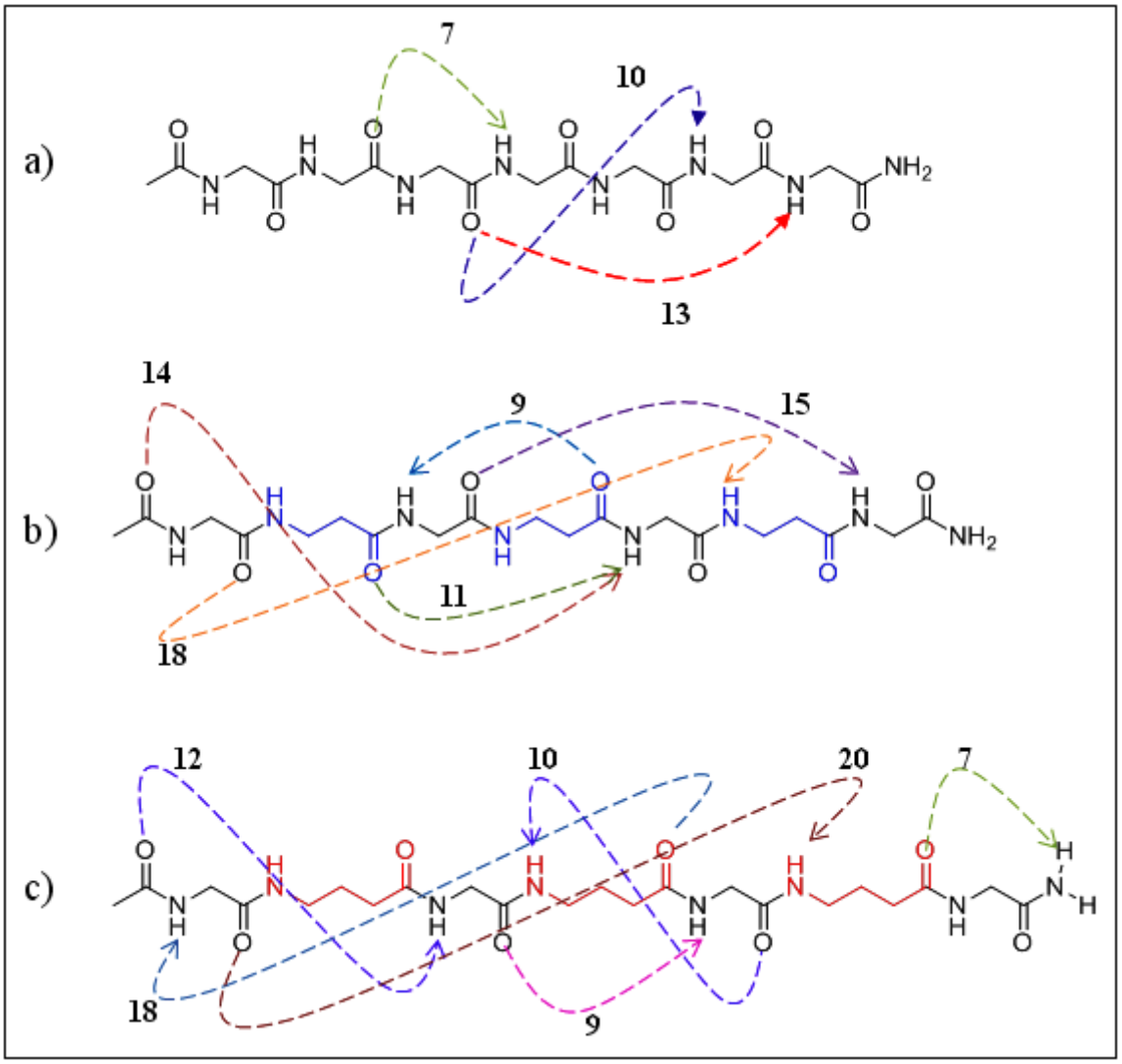

Figure 2.1 Possible H-bond pseudocycles for a) α-peptides, b) α/β-peptides and c) α/γ-peptides. Side chains are not shown for clarity. β and γ-residues are shown in blue and red color, respectively.

research is heterooligomers or hybrid peptides comprised with α and other β- and γ-amino acids. The hypothesis of the hybrid peptide concept in the foldamer design was demonstrated by Balaram and colleagues in the crystal structure of hybrid peptide containing unsubstituted β-and γ-amino acids.[8] The advantage of hybrid peptides with heterogeneous backbone is that conformational diversity in the helical peptides can be achieved based on variation in the stoichiometry and patterns of the residues combination. Subsequently, Reiser and co-workers,[9] and Gellman et al.[10] conducted the structural studies of various α/β hybrid peptides. Further, Sharma and co-workers demonstrated the 'mixed' H-bonding patterns C9/11[7a] and C14/15[7e] in α/β hybrid peptides.[11] Muraleedharan et al. have shown the 11-helical structures from the α/$\beta^{2,3}$hybrid peptides.[7l] Chandrasekhar laboratory synthesized novel helical foldamers from 1:1 α/nucleoside derived β-amino

acid sequences.[7m] The 14/15-helix-like conformation reported by Seebach et al. in the α/β hybrid peptides was further supported by Balaram and colleagues using X-ray structures. Extensive investigations revealed that β-, γ-, mixed α/β- and α/γ-hybrid peptides adopt various ordered helical conformations including 14/15, 14-, 12-, 10/12-, 9/11, 9- and 8-helices.[7e, 12]

Based on analysis of various H-bond pseudocycles obtained from the hybrid sequences, it is also possible to predict types of pseudocycles involved in the hybrid sequences based the directionality of H-bonding the helix (Figure 2.1). The different types of hybrid helices based on 1←4 and 1←5 H-bonds is given in the Table 2.1 and 2.2, respectively.

Table 1.1 Possible H-bonding pseudocycles in hybrid peptides

a) 1←4($CO_i\cdots HN_{i+3}$)

	α	β	γ	δ
α	10	11	12	13
β	11	12	13	14
γ	12	13	14	15
δ	13	14	15	16

b) 1←5 ($CO_i\cdots HN_{i+4}$)

	αα	αβ/βα	αγ/γα	ββ	βγ/ γβ	γγ
α	13	14	15	15	16	17
β	14	15	16	16	17	18
γ	15	16	17	17	18	19

Further, Gellman's group exploited the diversity of hybrid peptides in the biological applications. In one of their studies, they have shown the formation of three and four helix bundle by the systematic α→ β^3 modification at selected position with yeast protein GCN4-p1(33-residue α-peptide) and GCN4-pLI respectively (Figure 2.2).[13] Each β^3-residue bears the side chain of the α-residue. The crystallographic data of these two peptides provided first high-resolution insight for heterogeneous backbone that can adopt helix bundle structure. Further the same group has shown the formation of heterohelical quaternary bundle with Acid-pLL (Figure 2.2). Schepartz laboratory has also explored the quaternary structures from β-peptide bundles recently.[14]

In comparison with the hybrid peptides composed of α- and β-amino acids, hybrid peptides composed of α-and γ- amino acids in general, and α- and γ^4-amino acids with proteinogenic side chain in particular, are less explored. Recently, based on the theoretical calculations Hoffmann and colleagues proposed the most stable 12-helical conformations

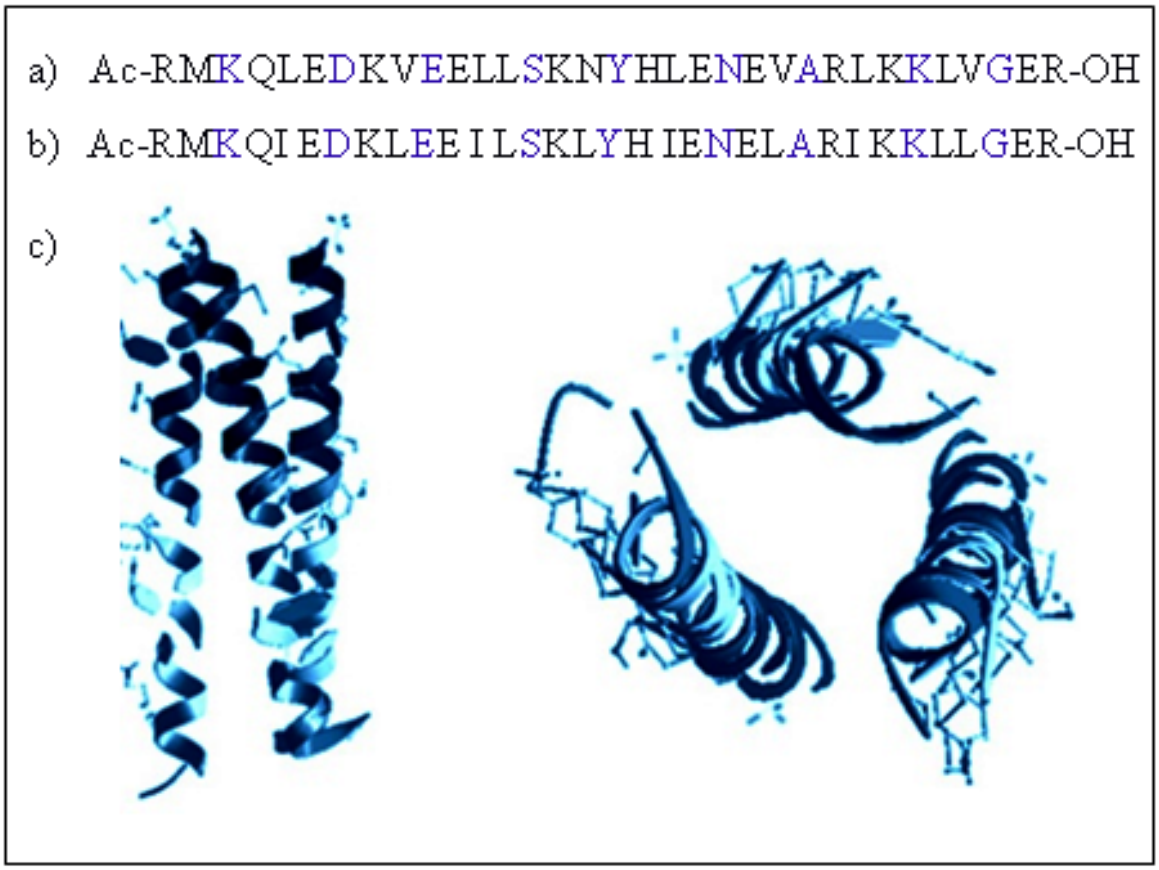

Figure 2.2 Primary sequence of a) GCN4-p1and b) GCN4pLI. $\alpha\rightarrow\beta^3$ substitution is shown in blue color. c) Three helix bundle from the crystal structure of α/β-hybrid peptide (PDB-2OXJ).

(Figure 2.3A) from heterooligomers composed of 1:1 alternating α- and unsubstituted γ-amino acids along with other helical conformations.[15] In addition, Balaram and colleagues[16] experimentally demonstrated the formation of stable right handed 12-helical conformations using α and 3, 3-dialkyl γ-amino acids (Figure 2.3B). In continuation, Sharma, et al. reported the 10/12 mixed helix formation using C-linked carbo γ-amino acids in α/γ-mixed hybrid peptides.[17] Further, Gellman's group[18] showed the formation of 12-helix in hybrid peptides containing cyclic γ-amino acids (Figure 2.3C) and α-amino acids. In addition, we have showed the 12-helical organizations in the short α/γ^4-hybrid peptides obtained through the direct transformation from α/vinylogous hybrid peptides using catalytic hydrogenation.[19] In this study, the geometrical constraints of the double bonds in the hybrid vinylogous peptides which forced them to adopt unusual planar conformations were removed by catalytic hydrogenation. After the geometrical constrains of the double bonds were released, the H-bond strength dominates the conformational flexibility of the saturated γ^4-amino acids to accommodate into the helical conformations.

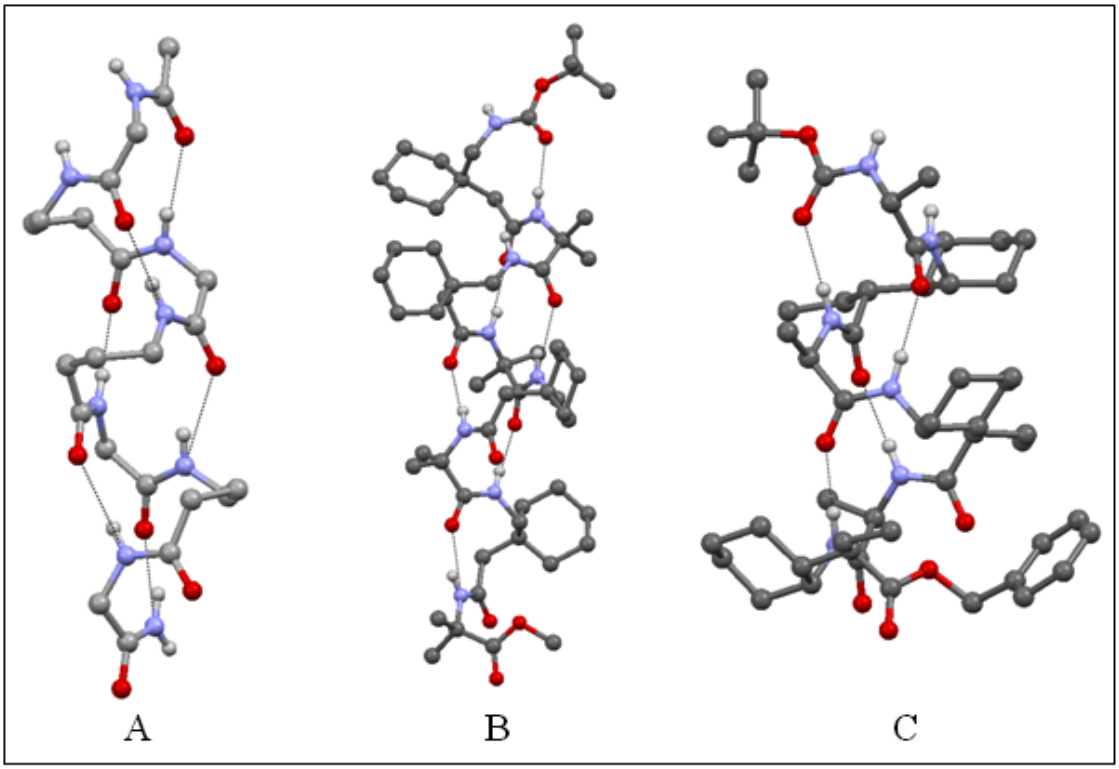

Figure 2.3 12-Helical conformations of 1:1 hybrid α/γ-peptides reported A) theoretically by Hoffman[15]B) in crystals by Balaram [16] and C) in crystals by Gellman[18]

In most of these cases stereochemically constrained amino acids have been used to induce the helical conformation in the peptides.

Thus far very little is known regarding the α,γ-hybrid peptides containing γ^4-amino acids and no information has been available regarding the helical parameters of 12-helices. Though γ^4-amino acids have shown preference towards the helical organization, most of the α,γ-hybrid peptides were derived from the stereochemically constrained either α- or γ-amino acids. In addition, there are no reports regarding usage of γ^4-amino acids with polar side-chains in synthesis and analysis of hybrid peptides. The easy accessibility of γ^4-amino acids from the Chapter 1 provides unique opportunity to seek the answers for many of these questions. In the Chapter 2, we are reporting the design, the solid phase synthesis and single crystal conformations of various α/γ^4-hybrid heptapeptides containing γ-amino acids with hydrophobic as well as polar side-chains. In addition, we have investigated the 12-helical conformations of α,γ^4-hybrid peptide without having any stereochemically constrained amino acids in single crystals. Based on the crystal structure information we calculated the helical parameters of α/γ^4-hybrid peptides, their helical wheel diagram, and

the analogy with 3_{10}-helix, α-helix and β-peptide 12-helices. In addition, we investigated the self-assembling properties of hybrid 12-helices.

2.2 Results and Discussion

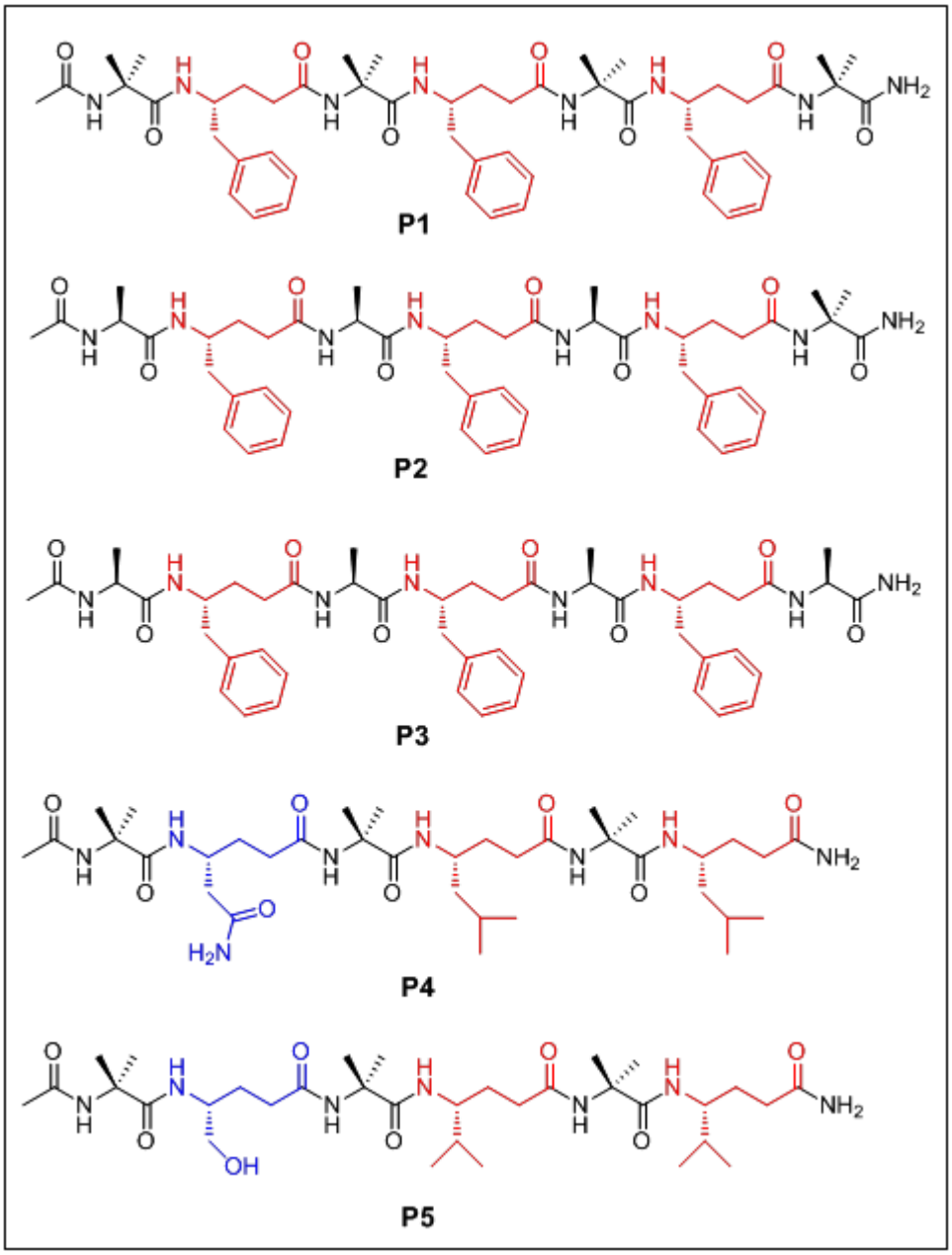

Figure 2.4 Sequence of designed α/γ-peptides. Hydrophobic γ-residues are shown in red and polar γ-residues are shown in blue color.

In order to understand the conformational properties of α,γ-hybrid peptides, various peptides containing γ^4-amino acids comprised of proteinogenic side-chains have been designed. The sequences of these peptides are shown in Figure 2.4. Required γ-amino

acids were synthesized using the one pot protocol described in the Chapter 1 and protected with the solid phase compatible Fmoc-group. All peptides were synthesized on Knorr Amide MBHA resin using standard Fmoc-chemistry protocol. The coupling reactions were mediated by HBTU/HOBt coupling conditions. The stereochemically constrained helix favoring α, α-dialkyl amino acid (Aib)[20] was used as an α-amino acid in 1:1 alternating α/γ^4-hybrid peptide **P1** along with γ^4-Phe. To understand whether α/γ^4-hybrid peptides can fold into helical conformations without any stereochemical constrain; we designed **P2** and **P3**. In the case of **P2**, except the C-terminal Aib, all other Aibs in **P1** are replaced with L-Ala. In **P3** all Aibs are replaced with L-Ala. In case of hexapeptide **P4**, γ-Asn was used at the second position along with γ-Leu residues at positions 4 and 6. Similarly, γ-Ser was incorporated at the second position along with γ-Val residues at the positions 4 and 6. In both the peptides we used Aib as a α-amino acid. All peptides **P1**-**P5** were purified using reverse phase HPLC and the mass of the peptides were confirmed using MALDI-TOF/TOF.

Crystal structures are very important in understanding the helical parameters such as residue-per- turn, rise-per-turn, helical radius and the projection of amino acid side-chains in the newly designed peptides. Keeping this in mind, we attempted to grow the X-ray quality crystals from all these peptides in a various solvent combinations.

2.2.1 Crystal conformations of α/γ^4-hybrid heptapeptides

Single crystals of peptides **P1** and **P2** were obtained from the slow evaporation of aqueous methanol/trifluoroethanol solution. The suitable X-ray quality single crystals of **P3** were obtained after repeated attempts of slow evaporation from aqueous methanol solution. The X-ray structures of all three peptides are shown in Figure 2.5. Instructively, all three peptides adopted right-handed helical conformations with consecutive 12-memberd H-bonds [C=O(i)---H-N(i+3), 12-atom ring H-bonds, down plane of Figure 2.5]. Similar to the native α-amino acid helices, α/γ^4-hybrid helices displayed the backward H-bonding directionality and subsequent macrodipole. The 12-helix conformation in the all α/γ^4-hybrid peptides **P1**-**P3** are stabilized by six consecutive 1←4 [C=O(i)---H-N(i+3)] intramolecular H-bonds. Both C-terminal amide and N-terminal Ac-group are involved in the intramolecular H-bonds. Additionally, the packing mode of individual peptides revealed that each helical peptide is interconnected with the other helical peptides in head-

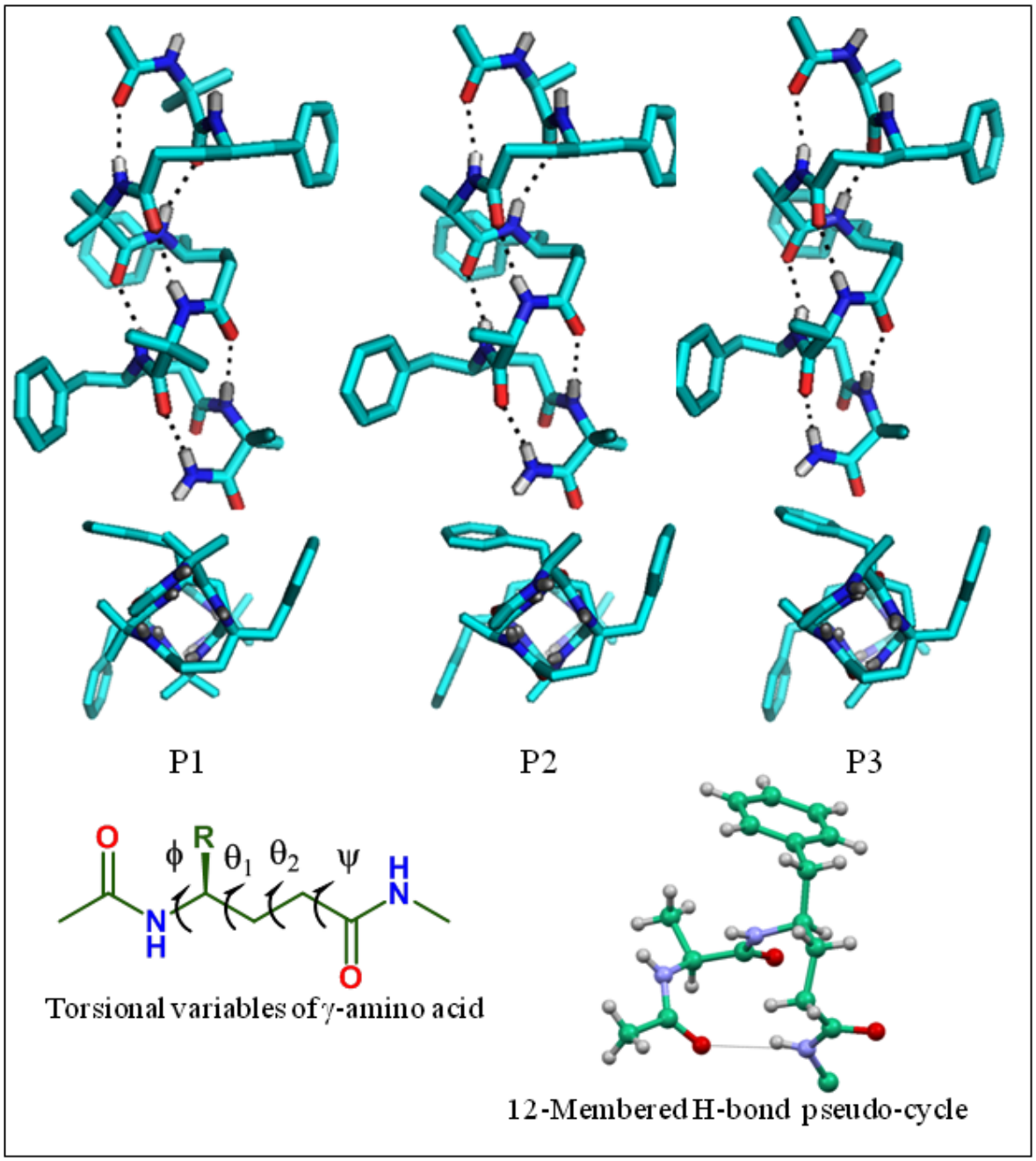

Figure 2.5 12-Helical X-ray crystal structures of hybrid peptides **P1**-**P3**. View along helical axis is shown in down plane along with torsional variables of γ-amino acid and representative 12-membered Hydrogen bonded pseudo-cycle.

to-tail fashion through four intermolecular H-bonds. The inter and intramolecular H-bond parameters of all three peptides are tabulated in Tables 2.1-2.3.

2.2.2 Hydrogen bonding parameters for peptide P1-P3

Table 2.1 Intra and intermolecular Hydrogen bonds of **P1** [dist in Å and bond angle in deg]. Intramolecular H-bonds are 1←4 backward type.

D-H---A	Dist. H---A(Å)	Dist D---A(Å)	∠D-H---A(°)
N(3)-H(3)...O(1)	2.13	2.99	174.2
N(4)-H(4)...O(2	1.97	2.79	158.4
N(5)-H(5)...O(3)	2.09	2.93	167.9
N(6)-H(6)...O(4)	2.04	2.85	157.0
N(7)-H(7)...O(5)	2.13	2.99	175.3
N(8)-H(8)...O(6)	1.99	2.82	162.7
N(1)-H(1)...O(7)$^{\#}$	2.07	2.93	175.2
N(2)-H(1)...O(8)$^{\#}$	2.02	2.82	154.3
N(1)-H(1)*...O(7)	2.06	2.93	175.2
N(2)-H(1)*...O(8)	2.02	2.82	154.3

Symmetry transformations used to generate equivalent atoms:

1+x,y,1+z, * -1+x,y,-1+z

Table 2.2 Intra and intermolecular Hydrogen bonds of P2 [dist in Å and bond angle in deg]. Intramolecular H-bonds are 1←4 backward type.

D-H---A	Dist. H---A(Å)	Dist D---A(Å)	∠D-H---A(°)
N(3)-H(3)...O(1)	2.15	2.99	168.5
N(4)-H(4)...O(2)	2.10	2.91	155.9
N(5)-H(5)...O(3)	2.17	3.00	163.0
N(6)-H(6)...O(4)	1.98	2.81	161.4
N(7)-H(7)...O(5)	2.19	3.05	173.3
N(8)-H(8)...O(6)	1.96	2.80	167.0
N(1)-H(1)...O(7)$^{\#}$	2.05	2.90	167.5
N(2)-H(1)...O(8)$^{\#}$	2.00	2.80	154.0
N(1)-H(1)*...O(7)	2.05	2.90	167.5
N(2)-H(1)*...O(8)	2.00	2.80	154.0

Symmetry transformations used to generate equivalent atoms:

1+x,-1+y,1+z, * -1+x,1+y,-1+z

Table 2.3 Intramolecular and intermolecular Hydrogen bonds for P3 [Å and deg]. Intramolecular H-bonds are 1←4 backward type.

D-H---A	Dist. H---A(Å)	Dist D---A(Å)	∠D-H---A(°)
N(3)-H(3)...O(1)	2.12	2.95	162.6
N(4)-H(4)...O(2)	2.00	2.82	159.8
N(5)-H(5)...O(3)	2.01	2.87	178.1
N(6)-H(6)...O(4)	2.02	2.81	152.5
N(7)-H(7)...O(5)	2.13	2.95	160.3
N(8)-H(8)...O(6)	1.93	2.74	156.7
N(1)-H(1)...O(7)$^{\#}$	1.98	2.84	172.3
N(2)-H(1)...O(8)$^{\#}$	2.07	2.85	150.2
N(1)-H(1)*...O(7)	1.98	2.84	172.3
N(2)-H(1)*...O(8)	2.01	2.86	150.2

Symmetry transformations used to generate equivalent atoms:

x,y,1+z, * x.y,-1+z

Inspection of the crystal structure of **P1** reveals that Aib residues adopted right handed helical conformations by having average ϕ and ψ values –58 ± 3° and –40 ±5°, respectively. The dihedral angles of γ^4-Phe residues were measured by introducing two additional variables θ_1 (N–C_γ–C_β–C_α) and θ_2 (C_γ–C_β–C_α–C) as shown in Figure 2.5 (down plane). In contrast to the free γ^4-amino acid structures mentioned in Chapter 1, the stereochemical analysis of γ^4-Phe residues in all the peptides reveal that, they adopted *gauche*$^+$, *gauche*$^+$ (g^+, g^+, $\theta_1 \approx \theta_2 \approx 60°$) local conformation about the C_β– C_γ and C_α–C_β bonds. The average ϕ and ψ values of γ^4-residues were found to be 125 ± 7 and -118 ± 10°, respectively. The H-bonding pattern between the 1←4 residues and directionality of the H-bond in all α/γ^4 hybrid peptides (**P1-P3**) indicating the backbone expanded version of a 3_{10}-helix.[1, 20b] In contrast to the average ϕ and ψ values of 3_{10}-helix (-49°, -26°), The L-Ala in the peptides **P2** and **P3** displayed the average ϕ and ψ values -68 ± 3° and -33.03 ± 3°, respectively. The torsional angles of hybrid peptides **P1-P3** are tabulated and given in the Tables 2.4-2.6. A plot of ϕ and ψ angles of all

2.2.3 Tortion angles for peptide P1-P3

Table2.4 Torsion angles [deg] of **P1**

residue	ϕ	θ_1	θ_2	Ψ	ω
Aib 1	-57.36	---	---	-44.84	-175.8
γ^4Phe 2	-118.58	**50.17**	**65.79**	-132.87	-168.17
Aib 3	-62.57	---	---	-34.64	-174.56
γ^4Phe 4	-128.58	**52.62**	**59.61**	-116.56	-173.08
Aib 5	-58.22	---	---	-39.10	-171.56
γ^4Phe 6	-128.38	**51.05**	**62.35**	-118.54	-173.19
Aib 7	-55.37	---	---	-38.23	---

Table 2.5 Torsion angles [deg] of **P2**

residue	ϕ	θ_1	θ_2	Ψ	ω
Ala 1	-70.13	---	---	-34.61	179.86
γ^4Phe 2	-126.99	**50.26**	**64.09**	-120.09	-167.98
Ala 3	-73.05	---	---	-29.92	-179.84
γ^4Phe 4	-126.38	**52.92**	**59.86**	-113.02	-172.72
Ala 5	-65.01	---	---	-36.46	-176.51
γ^4Phe 6	-119.02	**49.25**	**65.42**	-123.77	-174.36
Aib 7	-55.32	---	---	-45.29	---

Table 2.6 Torsion angles [deg] for **P3**

residue	ϕ	θ_1	θ_2	Ψ	ω
Ala 1	-73.11	---	---	-30.65	-176.25
γ^4Phe 2	-128.64	**47.65**	**60.82**	-113.74	-170.49
Ala 3	-67.49	---	---	-34.37	-177.51
γ^4Phe 4	-125.45	**49.82**	**61.39**	-123.42	-171.85
Ala 5	-62.53	---	---	-29.26	-176.09
γ^4Phe 6	-130.18	**53.00**	**57.36**	-108.33	-174.62
Ala 7	-65.30	---	---	-35.50	---

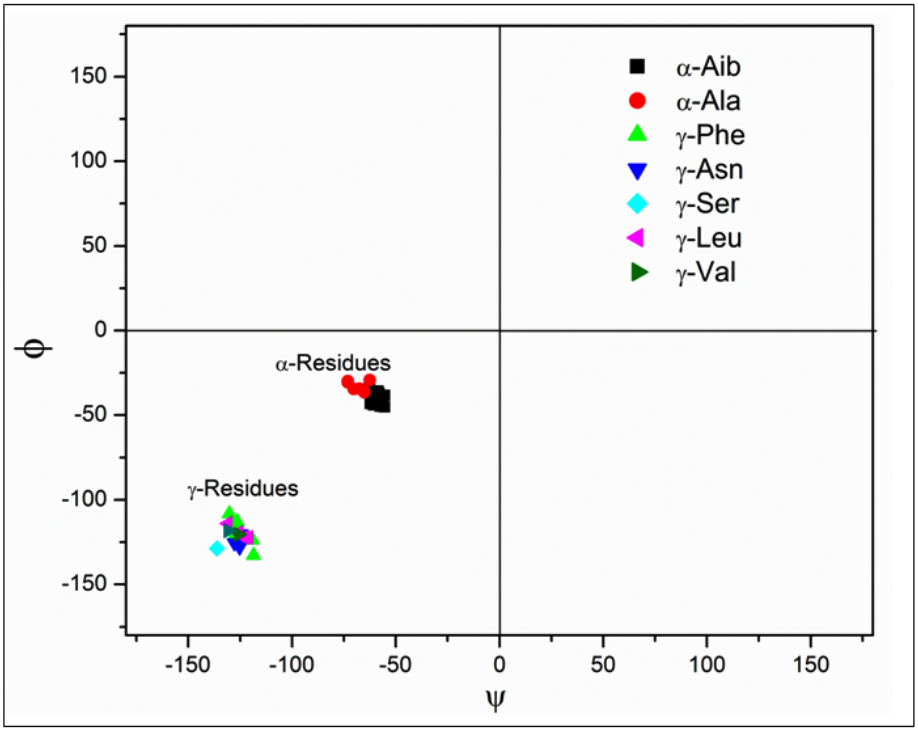

Figure 2.6 A two dimensional Ramachandran type plot depicting ϕ and ψ values in the α/γ^4-hybrid peptides **P1**-**P5**. The torsional variables θ_1 and θ_2 in γ-residues were kept constant as they always take the values close to ≈60° in the hybrid helices.

residues in peptides **P1-P3** are shown in Figure 2.6. Keeping θ_1 and θ_2 as constant, two distinct regions in the left quadrant of the Ramachandran map[21]can be recognised for γ-and α-residues. In comparison between the α-residues in α/γ^4-hybrid peptides and 3_{10}-helix, a clear distinction can be observed particularly in the ϕ values. The L-Ala displayed an average of 10° higher value over the sterically constrained dialkyl amino acids in α/γ^4-hybrid peptide and an average 19° over the α-residues in the 3_{10}-helix. The crystal structure results suggest that a stable 12-helix can be constructed using either the stereochemically constrained Aib or simple unconstrained α-residues in the combination 1:1 alternating γ^4-residues. Further, the top view of the 12-helices indicate the projections of the side chains at four corners of the helical cylinder (Figure 2.5). In comparison to the α, β-and γ-peptides, the distinct orientation of the amino acid side-chains were observed in α/γ^4-hybrid 12-helices. Based on these information, we predicted the helical wheel diagram for α/γ^4-hybrid peptide 12-helices (Figure 2.7). In hindsight, the analysis of the packing modes of all three peptide helices reveals the importance of proteinogenic amino acid side-chains. In contrast to **P1** and **P2**, peptide **P3** with α-alanine residues showed the

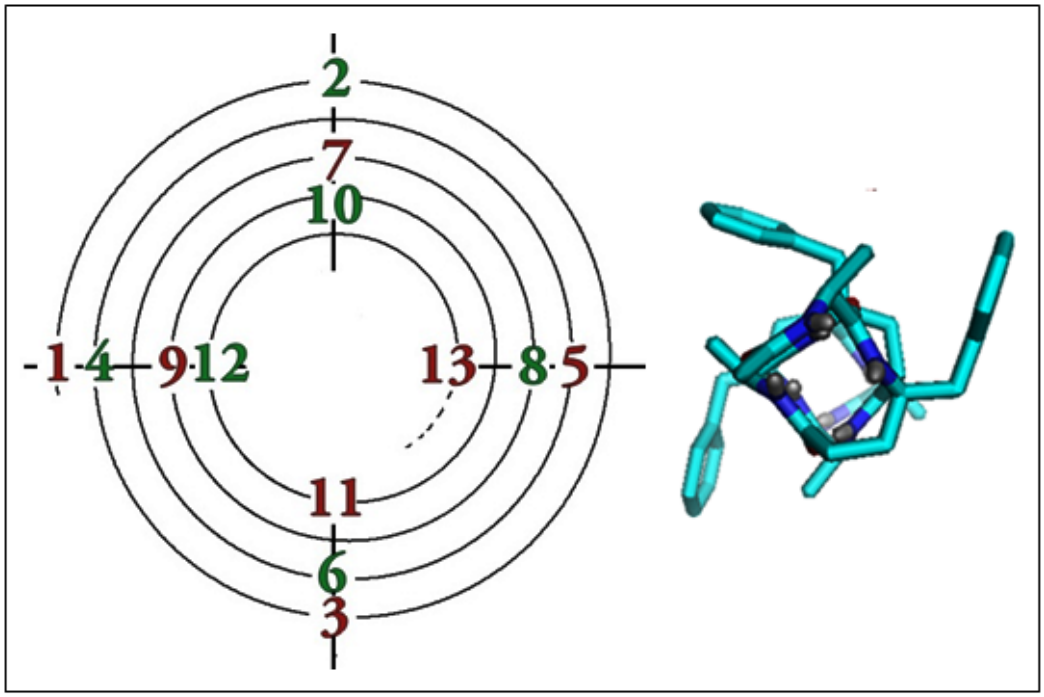

Figure 2.7 The helical wheel diagram depicting side chain projection in α/γ^4-hybrid peptides. α-Amino acids are shown in red while γ^4-amino acids are shown in green. Top view of **P1** is also shown for comparison.

lateral interactions between the two anti-parallel helices. The packing of antiparallel helices are stabilized by the side-chain hydrophobic as well as CH--π interactions. The anti-parallel packing of **P3** is shown in Figure 2.8. These packing interactions may provide the guidance for structure based design from α/γ^4-hybrids to target protein structures. In addition two water molecules are located at C- and N-terminals of the antiparallel helices played crucial role in interconnecting the two helices.

2.2.4 Structural analogy with α-peptide helices, β-peptide 12-helices and helical parameter analysis

The intriguing results from the hybrid peptides **P1**, **P2** and **P3**, encourage us to determine the helical parameters of α/γ^4-hybrid peptide 12- helices. The helical parameters were calculated from the set of four consecutive α-carbons using reported methods.[22] The analysis reveals all characteristic features such as residue-per-turn, rise-per-turn and the radius of α/γ^4-hybrid peptide 12-helix. The average helical parameters obtained from the three crystal structures are tabulated in the Table 2.7. Recently, Gellman et al. reported the

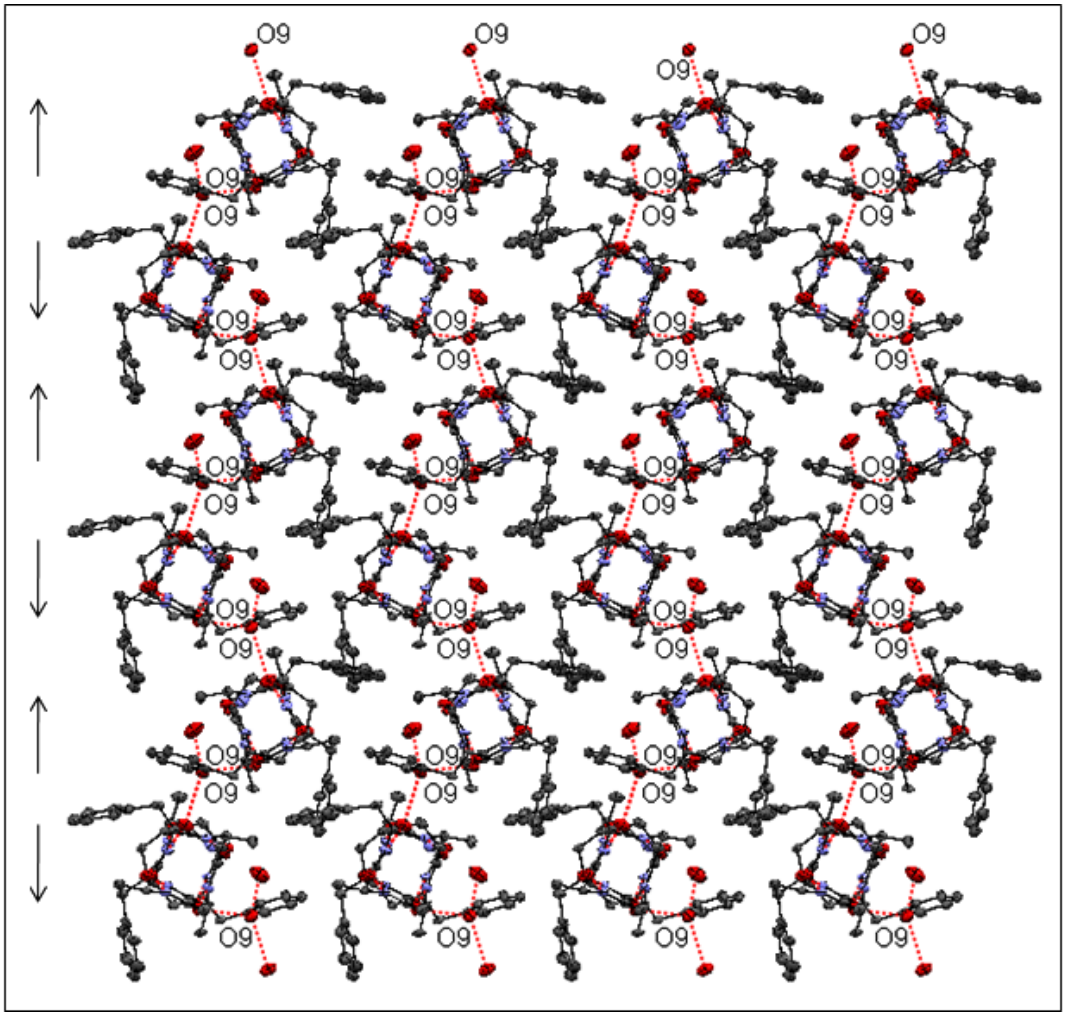

Figure 2.8. A view of crystal packing of peptide **P3** along the crystallographic c-axis. The water molecule O9 participated in molecular packing through H-bonding (dotted red lines) is also shown. Arrows indicates the direction of helix in corresponding row suggesting the antiparallel lateral packing of helices.

helical parameters for the β-peptide 12-helix[23]containing stereochemically constrained cyclic β- amino acids. Interestingly, the helical parameters calculated for the α/γ^4-hybrid peptides are in good agreement with the β-peptide12-helices [residue- per-turn (2.7), rise-per-turn (5.4 Å) and radius (2.1 Å)] generated from the cyclopentane backbone constraints. The overlay of the peptide **P3** on the β-peptide[23] 12-helix is shown in Figure 2.10A. For comparison, the average structural parameters of β-peptide 12-helices and the 3_{10}-helix[1] are tabulated in the Table 2.7. In addition, α/γ^4-hybrid peptide 12-helices displayed very similar CD signature as that of β-peptide 12-helices with CD maxima at 205 nm and a weak minima at 218 nm (Figure 2.9).[20] The negative parameters of 12-helices generated from the cyclobutane ring constraints confirm the left-handed helical conformation of the

Table 2.7 Average helical parameters of backward 1←4 H-bonded helices.

Peptide backbone	**res/turn** *n*	**rise/turn** *p*(Å)	**rise/res** *d*(Å)	**radius** *r*(Å)
α/γ^4-peptide (12-helix)	2.7	5.3	2.0	2.1
β-peptide(trans ACPC)12-helix[a]	2.7	5.4	2.0	2.1
β-peptide(trans ACBC)12-helix[b]	-2.7*	-5.4*	2.0	2.2
3_{10}-helix[c]	3.2	5.8	1.8	2.0

*Negative sign indicates left handed helical turn. [a]Ref. 23, [b]Ref. 24 and [c]Ref. 1

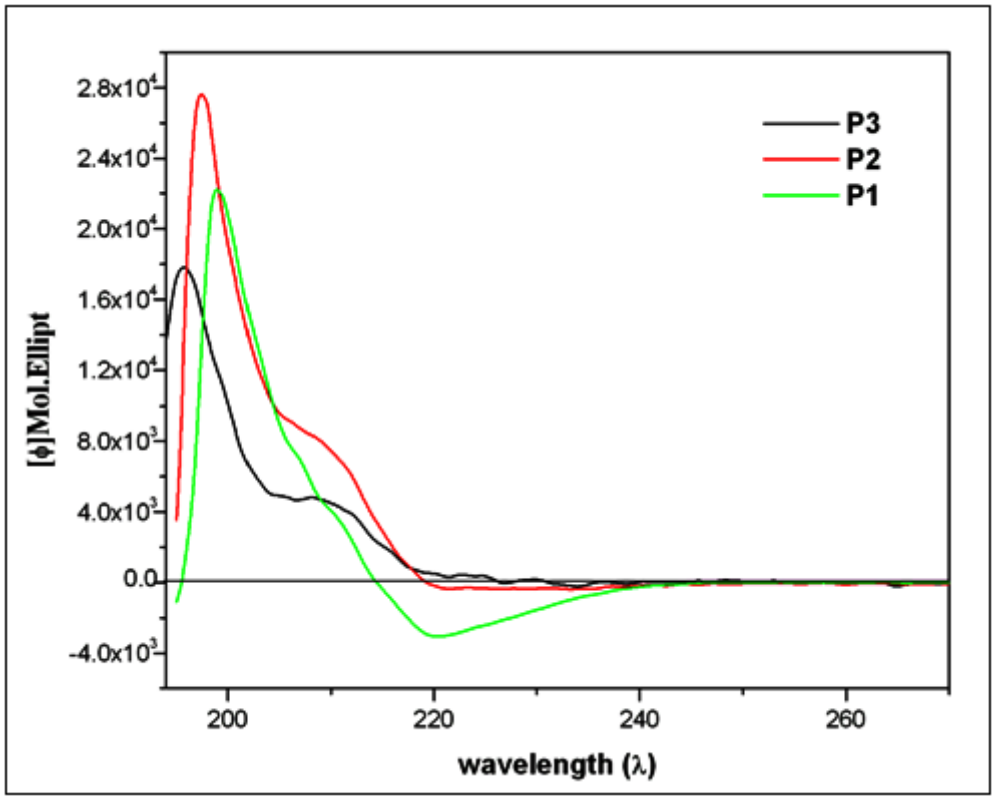

Figure 2.9. Circular dichroism spectra of α/γ^4-heptapeptides **P1**, **P2** and **P3** (0.2 mM) in Methanol at 20 ^oC.

β-peptide.[24] Further, we superimposed the α/γ^4-hybrid peptide **P3** over the α-helix and 3_{10}-helix to understand the backbone correlation and the side-chain orientation as the H-bonding directionality of hybrid peptide 12-helices were very similar to that of α-peptides helices. The superposition of the backbone conformations of **P3** over the α-helix (from the protein Human DNA Polymerase Beta, PBD code -1ZQA, sequence- 94-102)[25] and the 3_{10}-helix[26] are shown in Figure 2.10B-C respectively. Instructively, the backbone conformation of the hybrid heptapeptide **P3** is well correlated with the nine residues of the α-helix, while good correlation of **P3** with heptapeptide 3_{10}-helix was observed. The structures of the β-peptide 12-helix, α-helix and 3_{10}-helix were generated using the co-ordinates reported in the literature.[27] The top view of the superimposed **P3** with the α-helix and 3_{10}-helix signify the projection of the amino acid side-chains (Figure 2.10 down plane). The backbone correlation and the side-chain projections of α/γ^4-hybrid peptide helices with respect to the α-helix suggests that these hybrid peptides can be exploited as mimics of α-peptide helices. Further, with the availability of broad

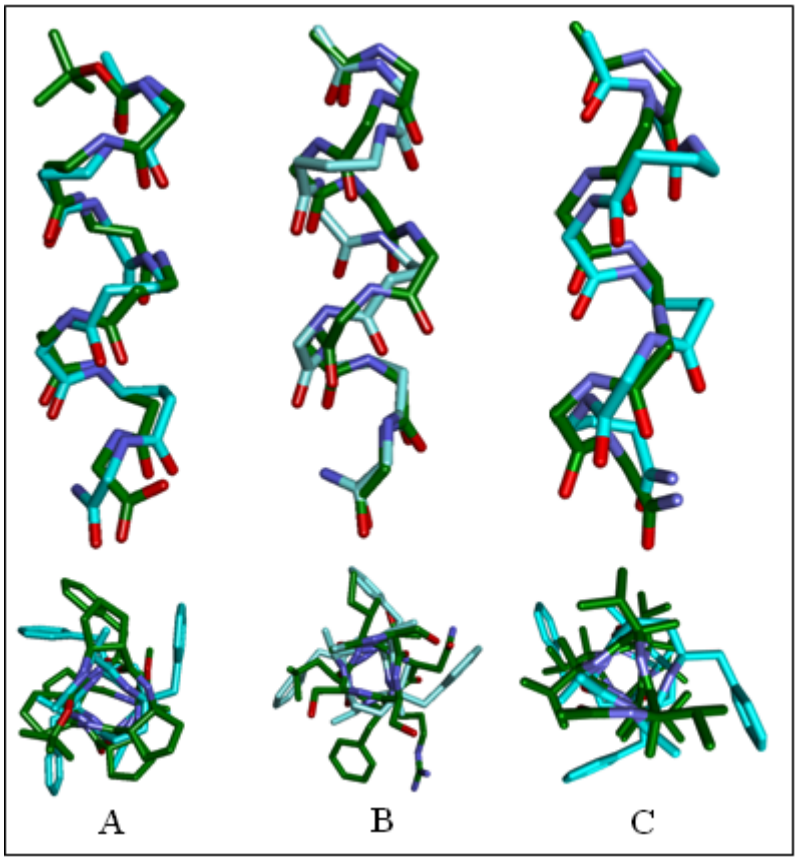

Figure 2.10 Superposition of α/γ^4-hybrid peptide **P3 (**light blue**)** on (a) β-peptide 12-helix, (b) α-helix and (c) 3_{10}-helix. The top view (lower plane) depicting the projection of amino acids side-chains.

side-chain diversity in both α-and γ^4-amino acids, these α/γ^4-hybrid peptides stand unique than the other α/γ-hybrid peptides. The structural analysis of α/γ-hybrid peptides containing backbone homologated γ^4-amino acids with proteinogenic side chains presented here may be useful for the design of functional foldamers similar to the β- and α/β-hybrid peptides.

2.2.5 Crystal structures of hybrid hexapeptides P4 and P5

Peptide **P4** and **P5** are comprised of polar side chain containing γ^4-amino acids γ^4-Asn and γ^4-Ser, respectively. Suitable X-ray quality crystals of **P4** and **P5** were obtained from the slow evaporation of aqueous methanol solution. The X-ray structures of the hybrid peptides **P4** and **P5** is shown in Figure 2.11. As anticipated both the peptides adopted 12-helical conformations in single crystals. Single crystal analysis of **P4** reveals the presence of four molecules in the asymmetric unit. The helical structure is stabilized by four

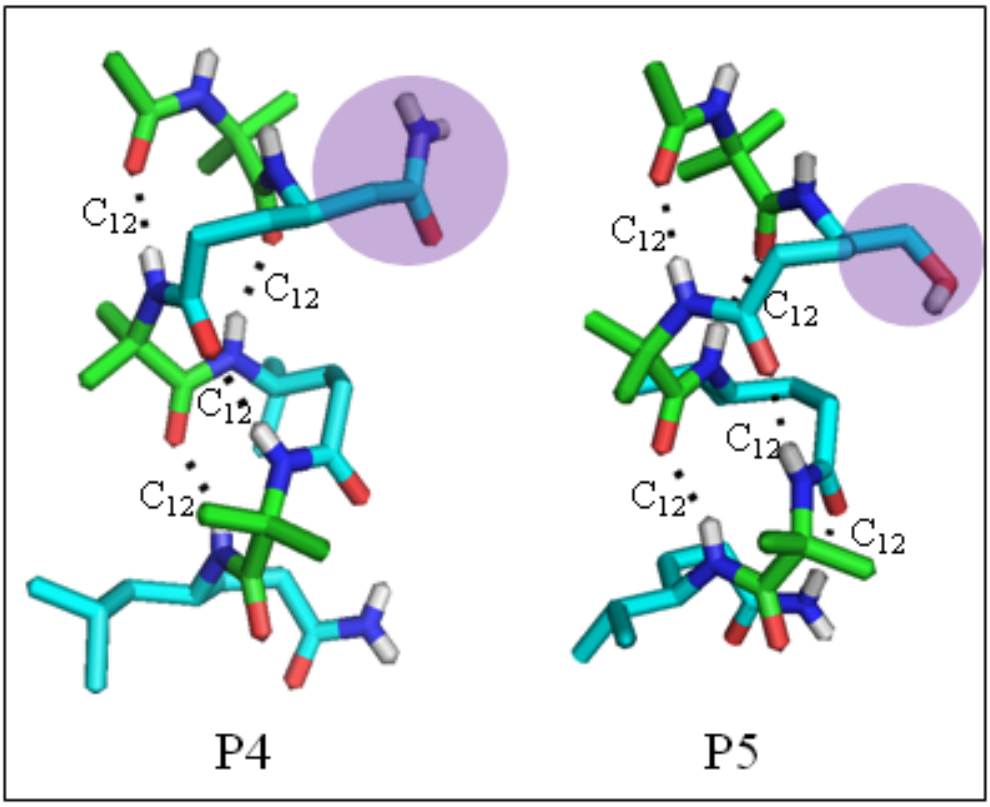

Figure 2.11 12-Helical X-ray crystal structures of α,γ^4-hybrid peptides **P4** and **P5**. γ^4-Residues are shown in cyan and polar side-chain ofγ^4-Asn and γ^4-Ser is highlighted with circle.

intramolecular hydrogen bonds between i and i+3 residues [C=O(i)---H-N(i+3),12-atom ring H-bonds]. The peptides are fully hydrated with twenty water molecules. The top view of the peptide is shown in Figure 2.12 A. Remarkably, the hydrophobic groups projected away from the water molecules and the polar head groups containing amide side-chains are projected inside in the crystal packing. All four peptide molecules in the asymmetric unit are oriented anti-parallel to one another. Interestingly, the side-chain amide groups of γ^4-Asn in all four anti-parallel helices are involved in the interhelical H-bonding (Figure 2.12B). Water molecules are mostly accumulated near the polar side chain of γ^4-Asn of **P4** (Figure 2.12C-D). In contrast to the other α,γ-hybrid peptides, γ^4-Asn side-chain drives helical oligomerization through H-bonding in **P4**. Similar kind of interhelical hydrogen bonds that regulates the strong interactions has been observed in the membrane proteins.[28] The analysis of the torsional variables of γ^4-residues, γ^4-Asn and γ^4-Leu, reveal that both θ_1 and θ_2 adopted *gauche*$^+$, *gauche*$^+$ conformations and nicely accommodated into the helix. Interestingly, the C-terminal amide NH is not participated in the canonical intramolecular H- bonding, however, it involved in strong intermolecular H-bonding with N-terminal amides of other helix and water molecules. Peptide **P5** was synthesized by replacing γ^4-Asn with γ^4-Ser and γ^4-Leu with γ^4-Val. Crystal structure analysis depicts single molecule of **P5** in the asymmetric unit. Analysis of the crystal structure reveal that **P5** also shows a right handed helical conformation and the structure is stabilized by five consecutive intramolecular 12-membered H-bonds between the i and i+3 residues. Both C-terminal amide NH and N-terminal acetyl CO groups are involved in the intramolecular H-bonding. Similar to the γ-residues in **P1-P3**, the torsional variables θ_1 and θ_2 of the γ-residues, γ^4-Ser and γ^4-Val, adopted *gauche*$^+$, *gauche*$^+$ conformations and accommodated into the helix. The polar N-terminal NHs and C-terminal carbonyl groups involved in the intermolecular H-bonds with other helical peptides in a head-to-tail fashion mediated by a single water molecule. On substitution of γ^4-Asn with γ^4-Ser, helical oligomerisation through the side-chain amide H- bonding interactions were not observed. However, γ^4-Ser side chain hydroxyl group is directly involved in the intermolecular H-bonding with C-terminal backbone amide group of the other helical peptide. The anti-parallel sidewise interactions of **P5** are shown in the Figure 2.13.

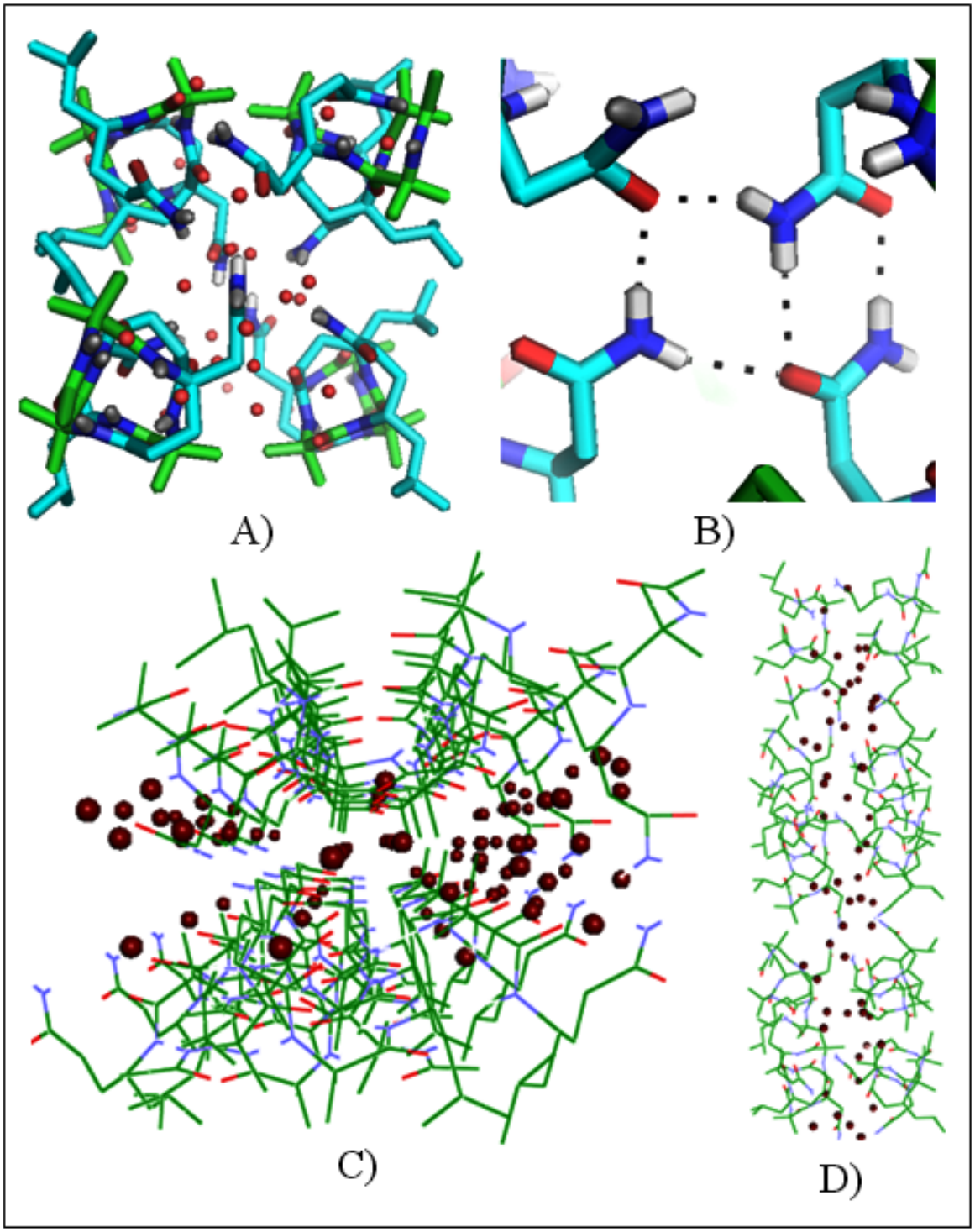

Figure 2.12 A) Crystal packing of **P4** depicting tetrameric hydrophobic pocket. B) γ^4-Asparagine side-chain amide mediated intermolecular H-bonds in the helical aggregation. C) and D) Accumulation of water along the polar side amide-chains in the crystal packing.

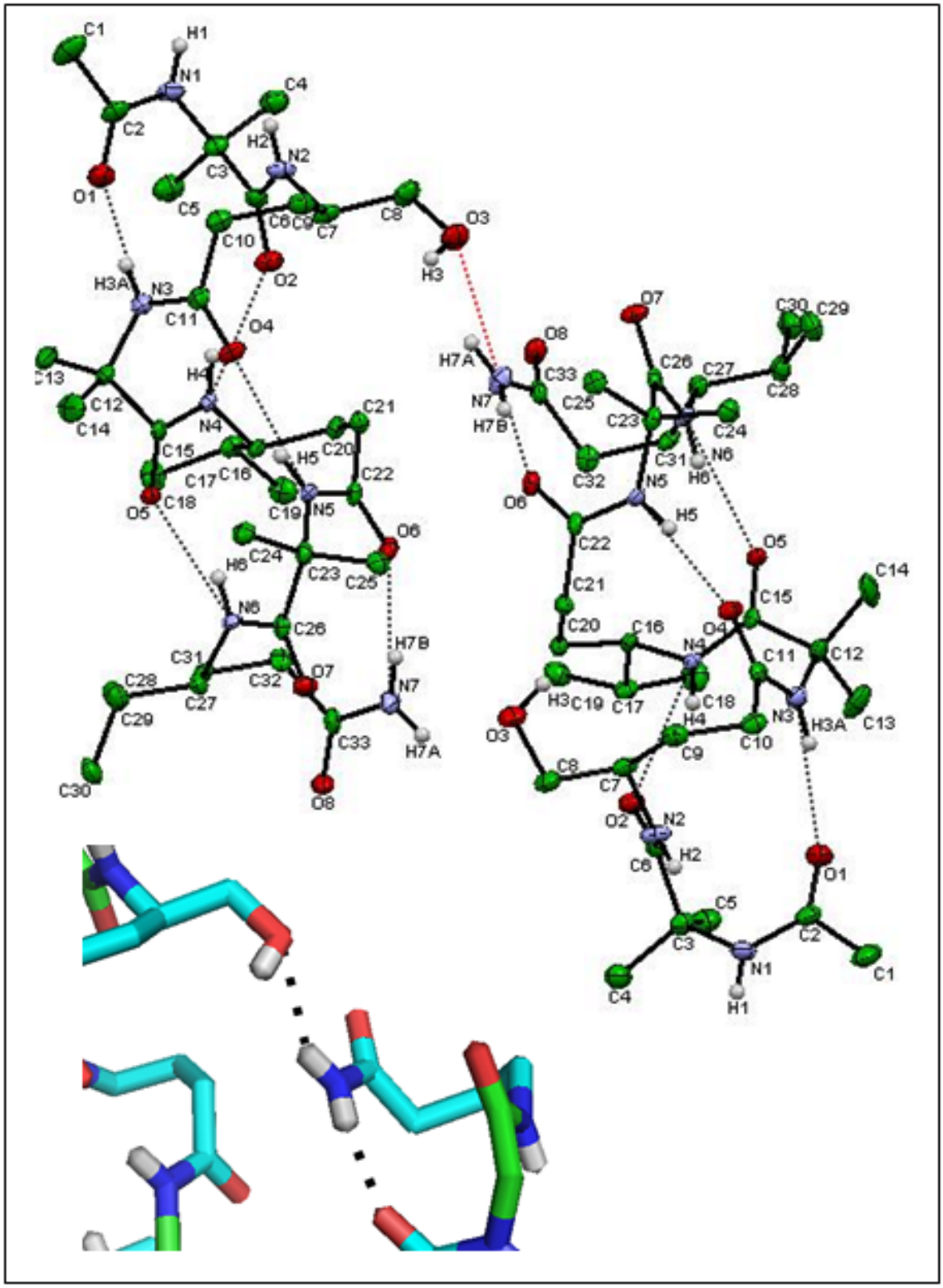

Figure 2.13 ORTEP (thermal ellipsoids are drawn to 50% probability) view of **P5** in crystals depicting interhelical H-bonding (shown in red dotted line) between γ^4-Ser side-chain with C-terminal backbone amide. High resolution picture for interhelical H-bonding in **P5** is shown in down plane.

Table 2.8 Average torsion angles (degree) for γ^4-residues in **P4** and **P5**

Pept.	**residue**	**ϕ**	**θ_1**	**θ_2**	**Ψ**
P4	γ^4-Asn	-126	52	61	-123
	γ^4-Leu	-125	52	62	-118
P5	γ^4-Ser	-136	55	58	-129
	γ^4-Val	-129	53	60	-119

In contrast to **P4**, peptide **P5** is stabilized by five consecutive intramolecular H-bonds. The average torsion angles of γ^4-residues in the both helical peptides are given in the Table 2.8. The H-bond parameters and the torsional angles of the α-residues are given in experimental section. The analysis of the torsional variables reveals that both ϕ (C'-N-C_γ-C_β) and ψ (C_β-C_α-C'-N) torsional angles of γ-residues adopted the *anticlinal* conformations with value approximately -120°, and θ_1 and θ_2 adopted the *gauche*+ (+60°) conformations in the both the peptides. Further, the α-residue, Aib, displayed the average ϕ and ψ values –60 ± 3° and –40 ±5°, respectively, in the both the hybrid peptides. These values are found to be consistent with the other α,γ-hybrid peptides containing 1:1 alternating α, and γ-amino acids. Further, we analysed the torsion variables of all γ^4-residues so far reported in the hybrid helical structures. The two dimensional Ramachandran type plot for ϕ and ψ of all γ^4- residues along with all α-residues in the peptides **P4** and **P5** is shown in Figure 2.6. In addition, the two dimensional map depicting the ϕ and ψ of all γ^4- residues reported in the literature including from our own group is shown in Figure 2.14. Analysis reveals that the γ^4-residues in C12/C14 helical structures are little scattered as compared to the hybrid peptides in the C12 and C12/C10 helices; however, γ-residues in C12 helical peptides were found to be more ordered.

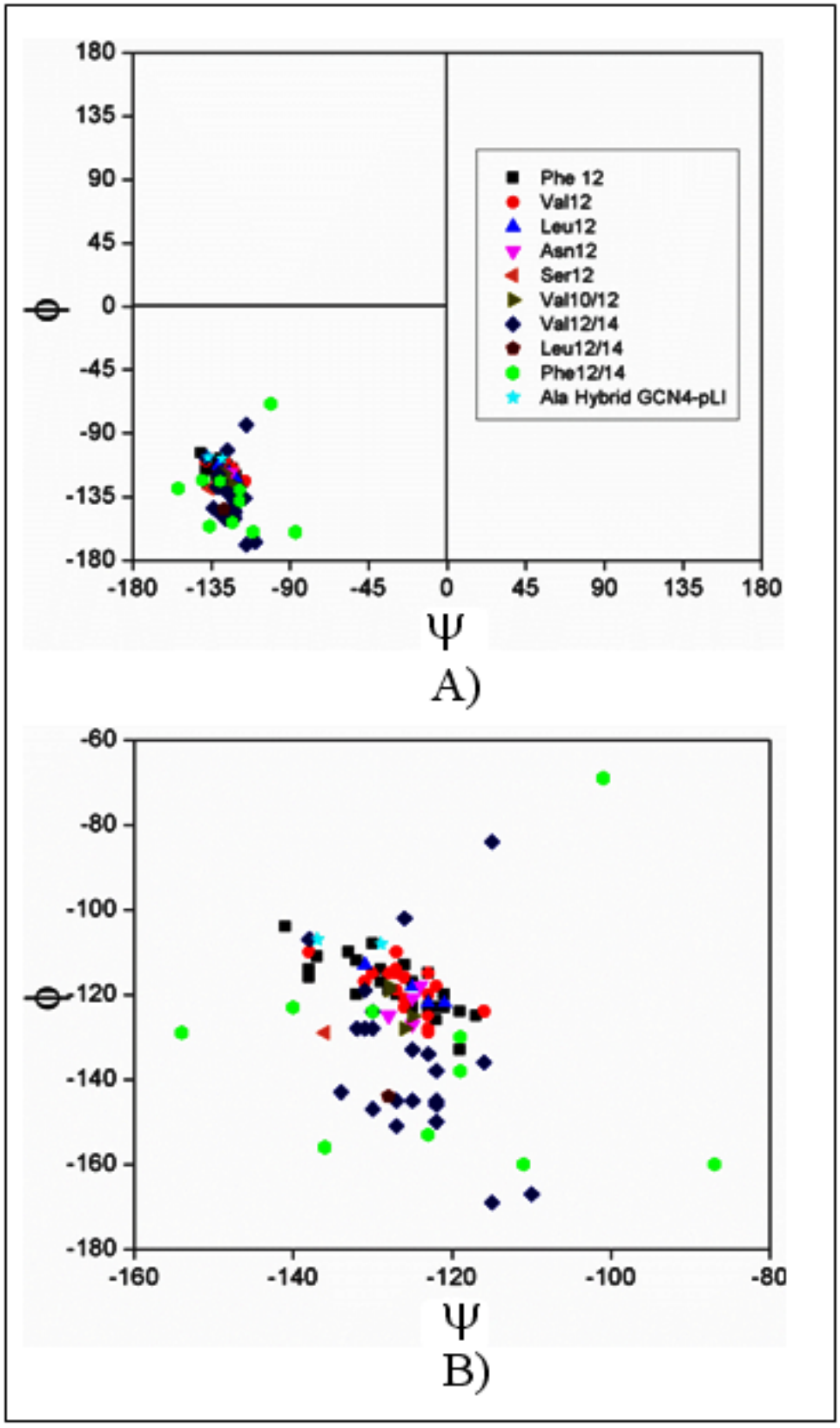

Figure 2.14 A) A two dimensional plot depicting ϕ and ψ torsion angles from the recently reported hybrid γ-peptide helices along with the γ^4-residues from **P1-P5**. Only the γ-residues which are participating in the helical conformations are considered for the analysis. The θ_1 and θ_2 torsion angles were kept constant as they adopted the *gauche* conformation. B) Expanded view of left quadrant of the plot.

2.2.6 Hydrogen bonding parameters and Torsion angles for peptides P4-P5

Table 2.9 Intramolecular and intermolecular Hydrogen bonds for **P4** [Å and deg]. Intramolecular H-bonds are 1←4 backward type.

(There are four molecules in asymmetric unit)

Molecule A

D-H...A (DHA)	d(D-H)	d(H...A)	d(D...A)	∠
N(4)-H(4)...O(1)	0.86	2.00	2.86	169.8
N(5)-H(5)...O(2)	0.86	2.07	2.89	160.7
N(6)-H(6)...O(4)	0.86	2.72	2.92	167.4
N(7)-H(7)...O(5)	0.86	2.09	2.93	167.3
N(1)-H(1)...O(8)[#]	0.86	2.08	2.90	160.9
N(2)-H(2)...O(1S)[##]	0.86	2.08	2.91	162.3
N(3)-H(3A)...O(11)*	0.86	2.20	2.98	151.4
N(3)-H(3B)...O(19) **	0.86	2.15	2.96	158.5
N(8)-H(8D)...O(5S) [$]	0.86	2.15	2.96	170.5
N(1)-H(1) [$$]...O(8)	0.86	2.08	2.90	160.9

Symmetry transformations used to generate equivalent atoms:

[#] -1+x,y,z, [##] x,y,z, * -1+x,y,z, **1-x, ½+y, 1-z, [$] x,y,z, [$$] 1+x,y,z

Molecule B

D-H...A (DHA)	d(D-H)	d(H...A)	d(D...A)	∠
N(12)-H(12)...O(9)	0.86	2.12	2.98	171.3
N(13)-H(13)...O(10)	0.86	2.08	2.90	141.6
N(14)-H(14)...O(12)	0.86	2.05	2.90	169.6
N(15)-H(15)...O(13)	0.86	2.03	2.86	162.4
N(9)-H(9)...O(16)[#]	0.86	2.12	2.96	163.3
N(10)-H(10)...O(2S)[##]	0.86	2.05	2.88	164.3
N(11)-H(11O)...O(31)*	0.86	2.24	3.04	154.7
N(11)-H(11P)...O(19S)**	0.86	1.20	2.79	152.0
N(3)-H(3A)[$]...O(11)	0.86	2.20	2.98	151.4
N(27)-H(27E) [$$]...O(11)	0.86	2.06	2.86	154.5

N(9)- H(9)[@]...O(16)	0.86	2.12	2.96	163.3

Symmetry transformations used to generate equivalent atoms:

[#] 1+x,y,z, [##] 1+x,y,z, *1-x,1/2+y,1-z, **2-x,1/2+y,1-z, [$]1+x,y,z, [$$] 2-x,1/2+y,1-z, [@] -1+x,y,z.

Molecule C

D-H...A	d(D-H)	d(H...A)	d(D...A)	∠ (DHA)
N(20)-H(20)...O(17)	0.86	2.04	2.90	175.4
N(21)-H(21)...O(18)	0.86	2.04	2.86	159.4
N(22)-H(22)...O(20)	0.86	2.09	2.93	168.0
N(23)-H(23)...O(21)	0.86	2.07	2.86	152.0
N(17)-H(17)...O(24)[#]	0.86	2.03	2.86	161.3
N(18)-H(18)...O(20S)[##]	0.86	2.17	3.01	164.5
N(19)-H(19A)...O(27)*	0.86	1.99	2.85	177.2
N(19)-H(19B)...O(8S)**	0.86	2.07	2.93	171.6
N(27)-H(27D)[$]...O(19)	0.86	2.18	3.04	178.7
N(3)-H(3B) [$$]...O(19)	0.86	2.15	2.96	158.5
N(17)- H(17)[@]...O(24)	0.86	2.03	2.86	161.3

Symmetry transformations used to generate equivalent atoms:

[#] -1+x,y,z, [##] x,y,z, *x,y,z **1-x, -½+y, 1-z, [$]x,y,z, [$$] 1-x, -½+y, 1-z, [@] 1+x,y,z.

Molecule D

D-H...A (DHA)	d(D-H)	d(H...A)	d(D...A)	∠
N(28)-H(28)...O(25)	0.86	2.05	2.90	171.7
N(29)-H(29)...O(26)	0.86	2.04	2.87	160.9
N(30)-H(30)...O(28)	0.86	2.16	3.01	171.5
N(31)-H(31)...O(29)	0.86	2.05	2.86	158.1
N(25)-H(25)...O(32)[#]	0.86	2.00	2.86	172.3
N(26)-H(26)...O(19S)[##]	0.86	2.23	3.01	150.4
N(27)-H(27D)...O(19)*	0.86	2.18	3.04	178.7
N(27)-H(27E)...O(11)**	0.86	2.06	2.86	154.5

N(19)-H(19A)$^{\$}$...O(27)	0.86	1.99	2.85	177.2
N(32)-H(32E)...O(12S)$^{\$\$}$	0.86	2.17	2.99	158.9
N(25)- H(25)$^{@}$...O(32)	0.86	2.00	2.86	172.3

Symmetry transformations used to generate equivalent atoms:

$^{\#}$ 1+x,y,z, $^{\#\#}$ x,y,z, *x,y,z **2-x,-1/2+y,1-z, $^{\$}$x,y,z, $^{\$\$}$ 1-x, -½+y, 1-z, $^{@}$-1+x,y,z.

Table 2.10 Torsion angles [deg] for **P4**

(There are four molecules of **P4** in asymmetric unit)

Molecule A

residue	ϕ	θ_1	θ_2	Ψ
Aib 1	-59.26	---	---	-38.87
γ^4Asn 2	-125.08	**50.92**	**61.19**	-121.18
Aib 3	-62.25	---	---	-43.18
γ^4Leu 4	-120.87	**52.57**	**61.34**	-122.18
Aib 5	-59.68	---	---	-42.84
γ^4Leu 6	-125.42	**59.08**	**68.90**	-169.92

Molecule B

residue	ϕ	θ_1	θ_2	Ψ
Aib 1	-59.00	---	---	-43.17
γ^4Asn 2	-125.32	**57.24**	**60.59**	-127.95
Aib 3	-63.24	---	---	-35.12
γ^4Leu 4	-125.60	**47.78**	**62.47**	-119.50
Aib 5	-56.66	---	---	-43.86
γ^4Leu 6	-126.16	**57.59**	**73.09**	-178.59

Molecule C

residue	ϕ	θ_1	θ_2	Ψ
Aib 1	-58.58	---	---	-35.80
γ^4Asn 2	-127.76	**54.26**	**57.99**	-125.30
Aib 3	-59.40	---	---	-42.85
γ^4Leu 4	-130.91	**53.22**	**57.89**	-113.92
Aib 5	-63.84	---	---	-34.59
γ^4Leu 6	-127.90	**50.12**	**62.04**	-158.99

Molecule D

residue	ϕ	θ_1	θ_2	Ψ
Aib 1	-58.09	---	---	-36.96
γ^4Asn 2	-124.33	**47.36**	**62.60**	-120.00
Aib 3	-60.57	---	---	-44.06
γ^4Leu 4	-122.88	**52.92**	**64.77**	-122.22
Aib 5	-59.95	---	---	-40.45
γ^4Leu 6	-115.31	**55.78**	**71.60**	170.99

Table 2.11 Intramolecular and intermolecular Hydrogen bonds for **P5** [Å and deg]. Intramolecular H-bonds are 1←4 backward type.

D-H...A (DHA)	d(D-H)	d(H...A)	d(D...A)	∠
N3)-H(3)...O(1)	0.86	2.07	2.92	169.2
N(4)-H(4)...O(2)	0.86	2.20	2.96	147.4
N(5)-H(5)...O(4)	0.86	2.10	2.95	168.9
N(6)-H(6)...O(5)	0.86	2.05	2.87	158.7
N(7)-H(7B)...O(6)	0.86	2.07	2.92	170.7
N(2)-H(2)...O(1S)[#]	0.86	2.26	3.05	153.9
N(7)-H(7A)*...O(3)	0.86	2.35	3.01	133.6
N(7)-H(7A)...O(3)[$]	0.86	2.35	3.01	133.6

Symmetry transformations used to generate equivalent atoms:

[#]x,y,z, *1/2+x,-1/2-y,2-z, [$]-1/2+x,-1/2-y,2-z

Table 2.12 Torsion angles [°] for **P5**

residue	ϕ	θ_1	θ_2	Ψ
Aib 1	-60.03	---	---	-36.10
γ^4Ser 2	-136.16	**54.81**	**58.47**	-128.79
Aib 3	-61.37	---	---	-37.05
γ^4Val 4	-125.82	**49.40**	**63.19**	-120.53
Aib 5	-59.77	---	---	-37.80
γ^4Val 6	-130.93	**56.20**	**56.97**	-118.22

2.3 Hierarchical Self-Assembly of hybrid peptide 12-helices in to nanotubes

Hierarchical self-assembly of biomolecules into ordered architectures is ubiquitous in nature.[29] The remarkable cellular structural integrity is mainly maintained by the self-assembly of biomolecules. Further, peptides are emerging as indispensible tools in the bionanotechnology and have been shown to adopt diverse architectures including vesicles, micelles, bilayers, fibers, ribbons, tapes and tubes.[30] The self-assembling of proteins and peptides is mainly governed by intermolecular non-covalent interactions such as hydrophobic,

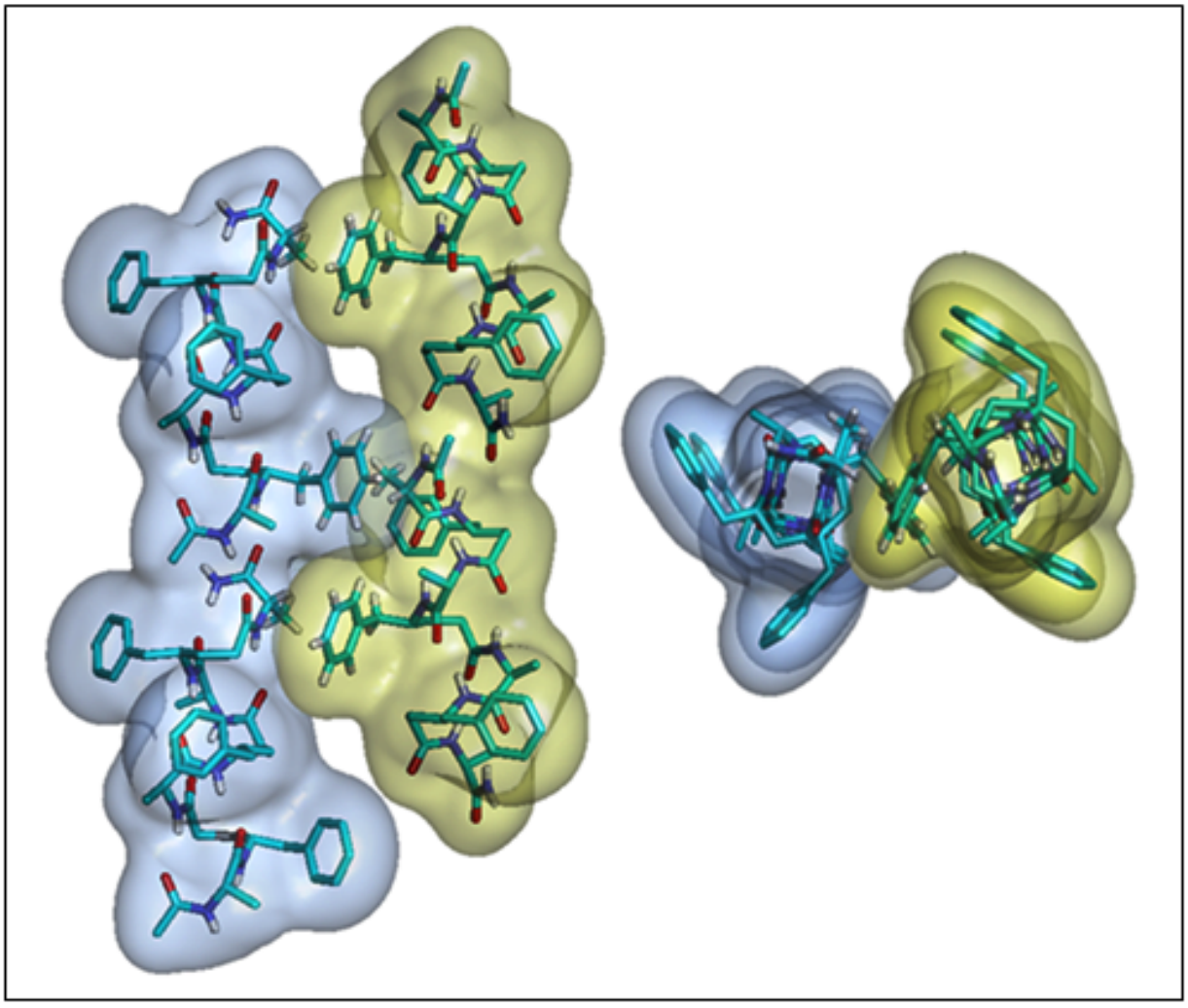

Figure 2.15 The lateral interaction of anti-parallel 12-helices of **P3** in the crystal packing and the top view of 12-helix **P3** is also shown. Top view suggest the possible lateral interactions with amino acid side-chains.

van der Waals, electrostatic, hydrogen bonds, and aromatic-π staking. The careful analysis of the crystal structures of **P1** , **P2** and **P3** containing aromatic γ-Phe residues and their crystal packing reveals the presence of interhelical weak π-π stacking interactions between the phenyl rings and CH-π interactions between the phenyl ring and benzylic protons of the γ-phe side-chains. In addition, we also observed predominant interhelical CH-π interactions between the aromatic rings and the benzylic protons as well as the backbone α-protons in **P3** (Figure 2.15). We anticipate that the fixed positions of the aromatic residues in the stable 12-helical peptides, infinite head-to-tail H-bonds between the helices and the involvement of aromatic residues in lateral non-covalent interactions may possibly lead these helical peptides into ordered supramolecular super structures in aqueous environment. Role of aromatic residues in biological system is also well known.[31]Recently, Fulop and Lee groups along with others demonstrated spectacular self-assembling properties of β-peptide helices without having any proteinogenic sidechains.[32] To understand the self-assembly properties of these hybrid peptides, 200 μL of the stock solution of respective peptide in THF (1mg/mL) was diluted to 1mL with distilled water. The aqueous solution was vortexed for 1 min, centrifuged and the filtrate was subjected to the FE-SEM analysis. Ironically, as anticipated all three hybrid peptides (**P1**-**P3)** are self-assembled into elongated discrete nanotubes. The self-assembled nanostructures of hybrid 12-helix **P3** are shown in Figure 2.16.Instructively, irrespective of the type of α-amino acids in the sequence, all three hybrid peptides are assembled into nanotubular superstructures. Microscopic images for **P1** and **P2** are shown in the Figure 2.17. The SEM images revealed the formation of both closed as well as open ended nanotubes. The lengths of tubes were found to be in range of micrometers. Bifurcated nanotubes, small piece of tubule and smaller tublet within the wider nanotubes were also observed in SEM analysis. Further, the transmission electron microscopy (TEM) suggested that peptides **P1**-**P3** formed well-ordered, elongated tubular assemblies. The TEM images of the nanotubes are shown in Figure 2.16E and F. The diameters of these nanotubes were found to be in the range of 30-90 nm. The edges of tubular structures appeared to be dark and the light at the center suggesting the hallow nature of tubes. Thickness of wall was found to be ~20 nm. These results provides the first evidence of the formation of peptide nanotubes from α,γ-hybrid helical peptides. Literature survey suggest that Ghadiri and co-workers showed formation of nanotube using cyclic peptides containing alternating D- and L-amino acids.[33]

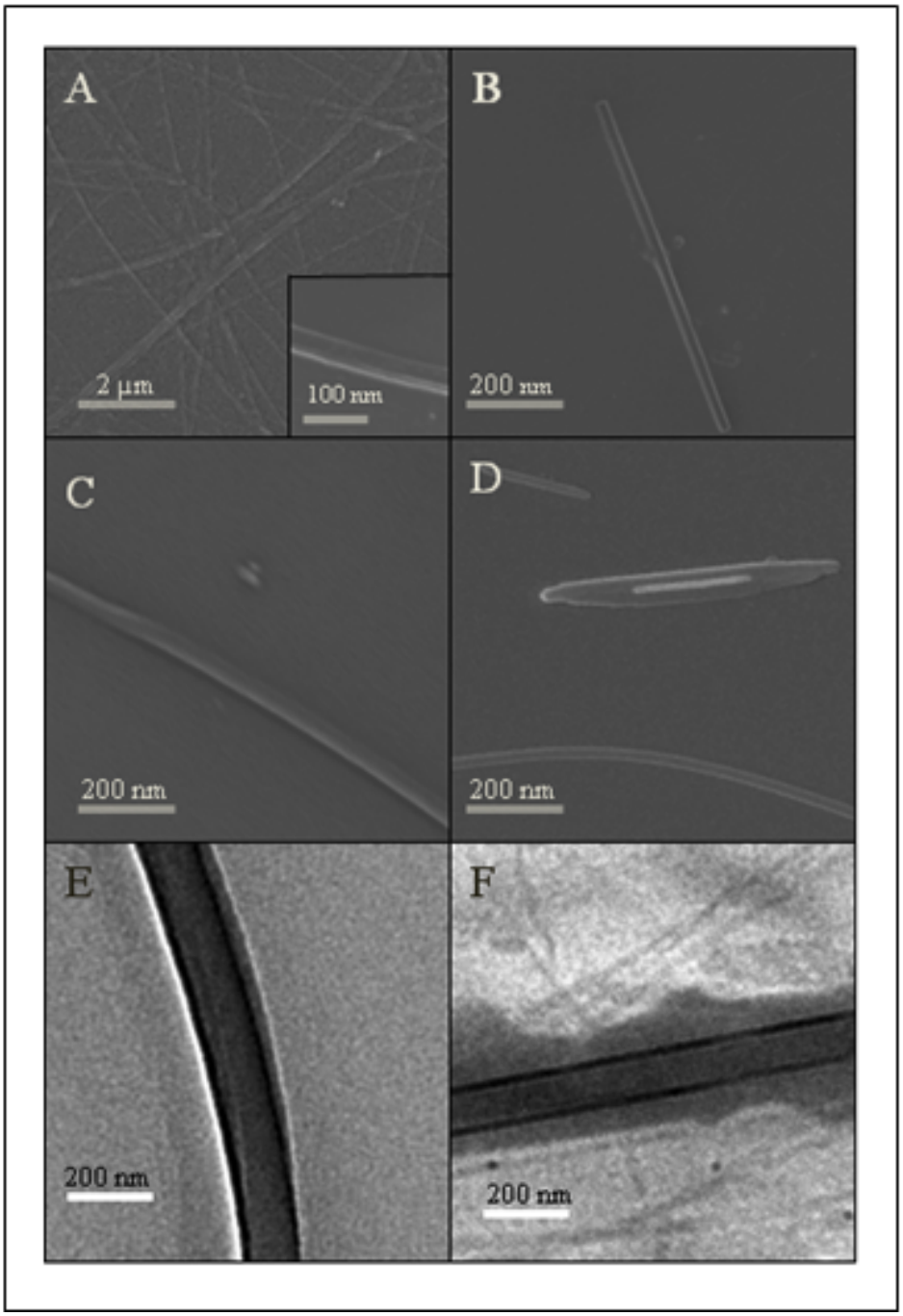

Figure 2.16 FE-SEM analysis of Peptide **P3.** A) Low resolution SEM images showing discrete nanotube formation. High resolution image of part of individual nanotube is shown in inset. B) and C) short isolated and continuous nanotube respectively. D) short tublet running through another nanotubule. E) and F) TEM analysis of hybrid peptide **P3**.

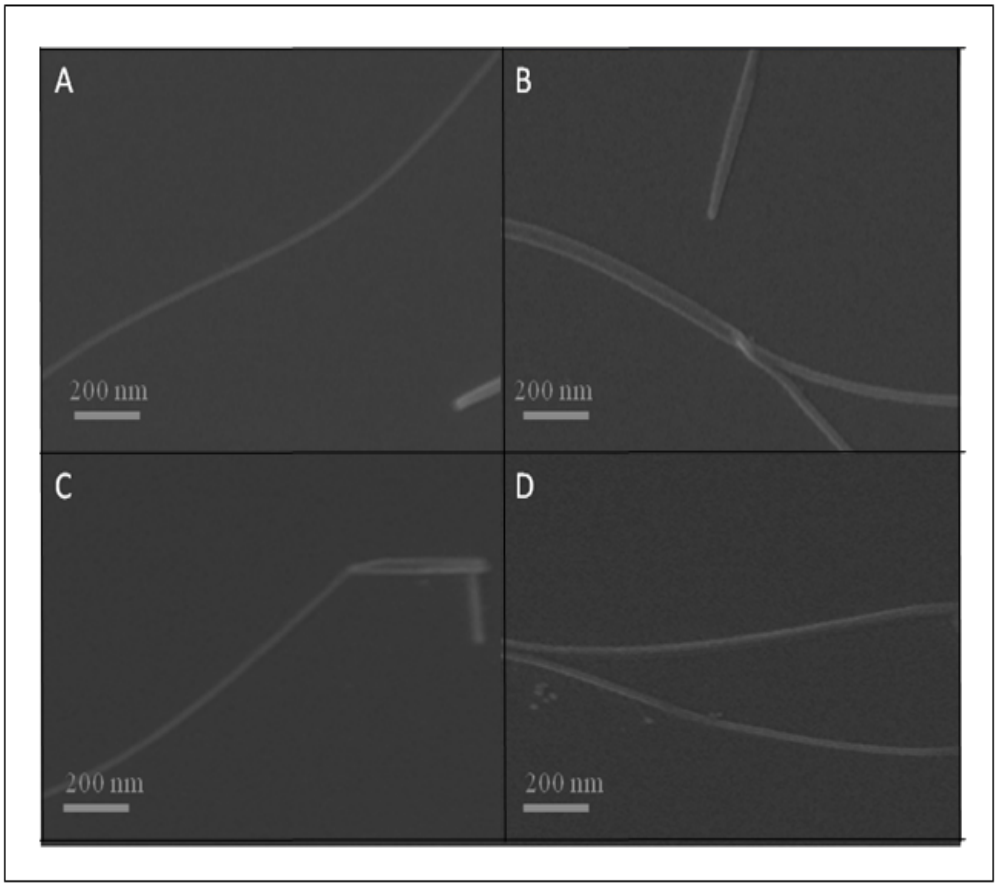

Figure 2.17 A) and B) SEM images of nanotubes formed by aqueous solution of **P1**. C) and D) SEM images of nanotubes formed by aqueous solution of **P2**.

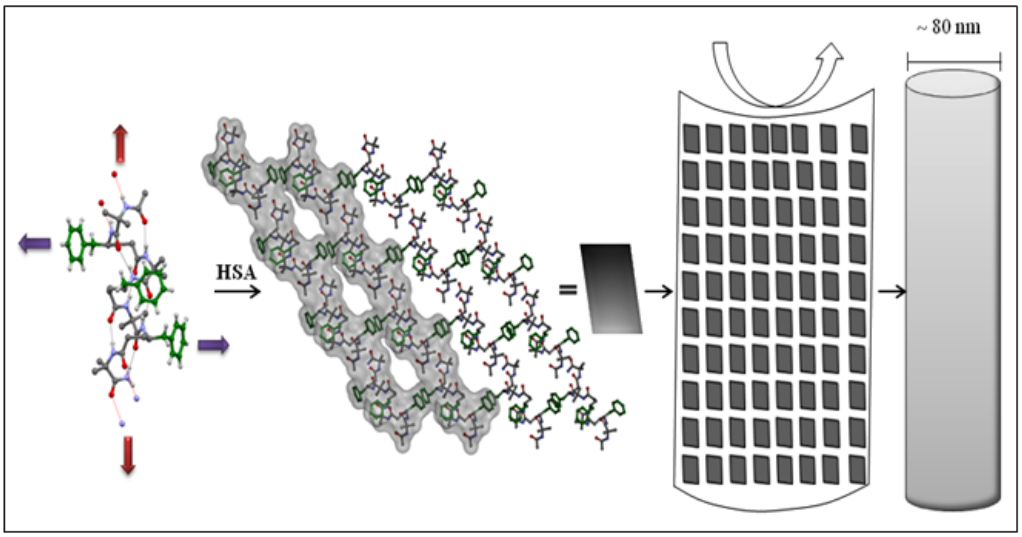

Figure 2.18 A cartoon representation of hierarchical self assembly of hybrid peptide 12-helices to nanotubes mediated by H-bonds(head-to-tail interconnection, red arrows) and non-covalent (aromatic-aromatic, CH-π and hybrophobic, purple arrows) lateral interactions. **P1** was chosen for the model representation.

In another study, Gazit et al.[34] reported the formation of PNT from the phenylalanine dipeptide motif of β-amyloid peptide. Self assembled nanotubes from cyclic α,γ-hybrid peptide composed of cyclopentane, cyclohexane and sugar based γ-residues have been recently reported.[35] Based on structural information about infinite head-to-tail H-bonds and the lateral non-covalent interactions in regular array, the formation of nanotubular assembly is elucidated in Figure 2.18

The discoveries of water filled nanotubes from the amyloidogenic sequences by Perutz and colleagues[36] and the fabrication of silver nanowires from the silver ions by Gazit et al[34] paved the way for the extensive research on the peptide nanotubes in the bionanotechnology. This inspired us to investigate whether the peptide nanotubes discovered from the α, γ-hybrid peptide 12-helices can act as templates for casting silver nanowires from silver ions. To test the hypothesis, the preformed nanotubes in solution were diluted with the aqueous silver nitrate and the reducing agent citric acid. The reaction

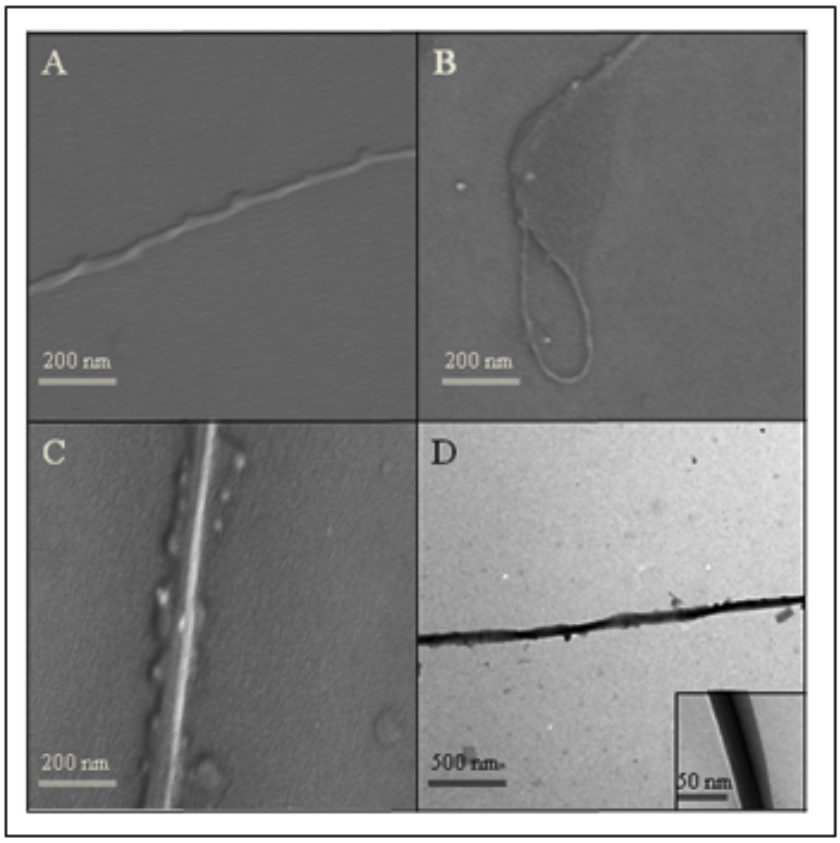

Figure 2.19 SEM image of nanotube from peptide **P3** loaded with silver nanoparticles. B) Knotted structure. C) Disruption of nanotube as Ag forms nanowire. D) TEM image of silver nanowire. TEM image of nanotube loaded with silver nanowire is shown in inset.

mixture was vortexed for 1 min and centrifuged. The filtrate was subjected to the FE-SEM and TEM analysis. The images of FE-SEM are shown in Figure 2.19. Intriguingly, diffusion of silver ions into the lumen of the nanotubes is observed. The presence of silver was confirmed by energy-dispersive X-ray analysis (EDX, see Figure 2.20). Interestingly, remarkable knotted peptide nanotubes with inclusion of silver nanoparticle have also been observed in the SEM analysis. The casting of silver nanowires may be initiated

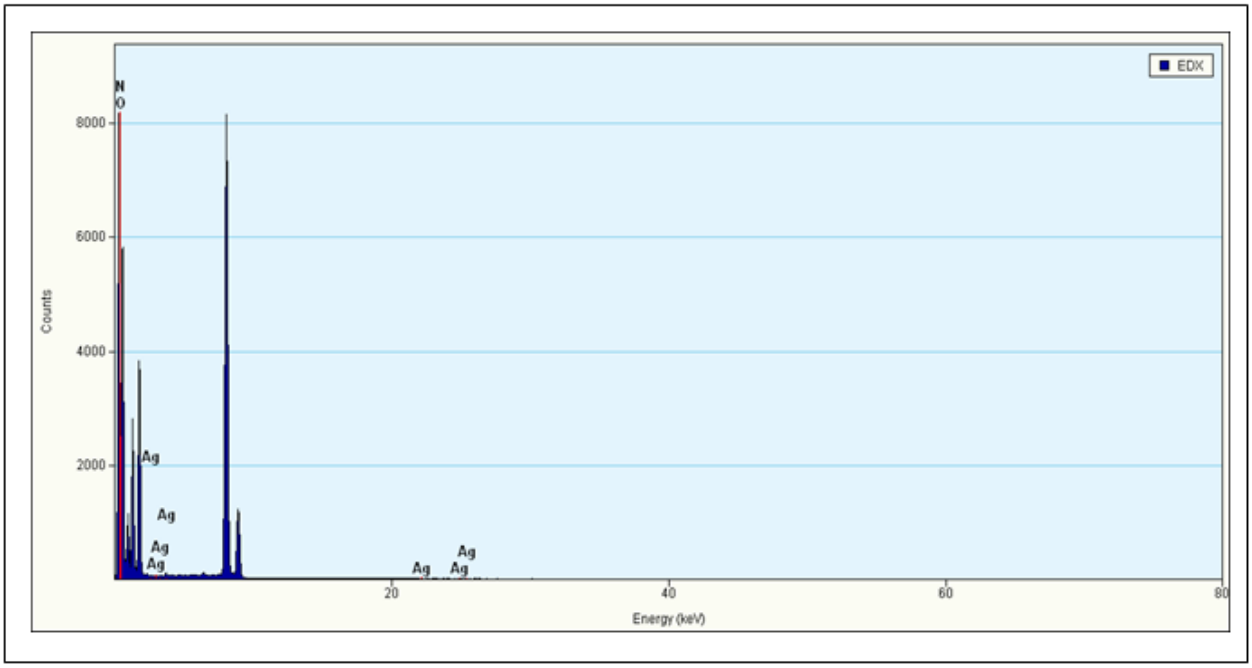

Figure 2.20 Energy-dispersive X-ray analysis (EDX) for the silver filled nanotube of **P3.**

by the silver nanoclusters formed within the lumen of the nanotubes. The bulges in the nanotubes suggest that peptide nanotube nucleates the formation of silver nanoclusters, eventually silver nanowires grow from these nucleation sites.[37]The formation of silver nanowires further lead to the collapse of the peptide nanotubes as shown in the Figure 2.19C. The TEM analysis of the silver nanowire is shown in Figure 2.19D. The diameter of the nanowire was found to be ~50 nm. The formation of silver nanowire through the hybrid peptide nanotube is illustrated in the Figure 2.21. These fascinating results demonstrate that similar to the amyloidogenic peptide nanotubes, the α,γ-hybrid peptide nanotubes can also acts as template for casting the silver nanowires.

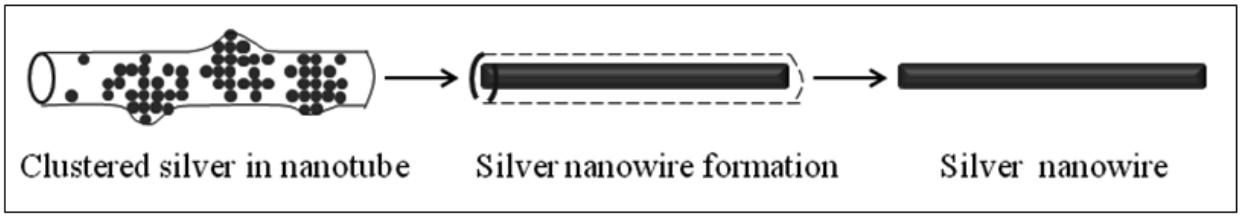

Figure 2.21 Casting of silver nanowire within the hybrid peptide nanotube.

2.4 Conclusion

We have presented the facile solid phase synthesis and single crystal conformations of various α/γ^4-hybrid peptides. The stereochemical analysis suggests that all five α/γ^4-hybrid heptapeptides adopted 12-helical conformations in single crystals. Comparison between the **P1** and **P3** reveal that 12-helical conformation can be induced in a hybrid peptide sequence solely through intramolecular H-bonding without using any stereochemical constraints. In addition, analogy with the β-peptide 12-helix suggests that α/γ^4-hybrid peptides can be used as surrogates of β-peptide 12-helices. Analysis of the helical parameters and the backbone correlation with the 3_{10}-helix suggest that the α/γ^4-hybrid peptide is comparable to α-peptide helix except the projection of the amino acid side chains. The distinct location of the amino acid residues in the helical wheel diagram presented here may be useful in the design of hybrid peptides with specific patterns. We further extended the design of α, γ-hybrid peptides incorporated with γ^4-amino acids containing side-chain functional groups, which have not been explored in the design of hybrid peptides. The hexapeptides, **P4** and **P5** displayed 12-helical conformations in single crystals. The insertion of γ^4-Asn residues in the hybrid peptide helix facilitates the helical aggregations through interhelical H-bonding between the Asn amide-side chains. Further, the hydroxyl side chain of γ^4-Ser showed the intermolecular H-bond with backbone amide of another helix in the crystal packing. Analysis of the torsional angles of γ^4-residues in all the hybrid peptide helices reveals the *anticlinal* conformations along the ϕ and ψ, *gauche* conformations along θ_1 and θ_2. We further exploited the unique projection of amino acid side-chains, their rigid geometry, and lateral interactions of the aromatic residues and head-to-tail polymerization of hybrid peptide helices in the hierarchical self-assembly. Results suggest that α,γ-hybrid peptides 12-helices composed of alternating α-amino acids and γ-Phe into nanometer scale tubular super structures. The rigid geometry of the aromatic residues and head-to-tail polymerization of hybrid peptide helices possibly dictates the tubular self-assembly. Further, these helical hybrid peptide nanotubes are

utilized for the fabrication of the silver nanowires from silver ions. Results presented here reveal that irrespective of the α-amino acid residues these hybrid helices self-assembled into nanotubes which provides unique opportunity to functionalize the nanotube surface by incorporating any functional α-amino acids. The bottom-up-approach of constructing supramolecular super structures using hybrid helical foldamers presented here is unique of its kind. As peptide nanotubes have potential applications ranging from gene delivery to nanoelectronics,[38]owing to their biocompatibility, proteolytic stability, easy synthesis by solid phase and predictable secondary structures, these α,γ-hybrid peptides can be utilized towards the synthesis of novel nanotubes for futuristic applications in nanobiotechnology and biomaterials. Overall, conformational analysis of α, γ^4-hybrid peptide 12-helices containing both hydrophobic and polar γ^4-residues, their analogy with their analogy with α- and β-peptides helices, their hierarchical self-assembly in elongated nanotubes and the utility of nanotubes in costing the silver nanowires presented here may offer the guidelines to the design α/γ^4-hybrid peptides with specific functions and biomaterials.

2.5 Experimental section

2.5.1 Solid phase synthesis of peptide

Peptide **P1-P5** were synthesized by manual solid phase peptide synthesis on Knorr Amide MBHA resin (0.3 mmol) using Fmoc-chemistry. Amino acids (2 eq.) were coupled using HBTU (2 eq.)/HOBt (2.1 eq.) and DiPEA (3 eq.) under N_2 bubbling for 40 minutes. All Fmoc deprotections were performed using 20 % piperidine in DMF by N_2 bubbling for 20 minutes. The *N*-terminal of peptide was capped with acetyl group using acetic anhydride (1 mL) and pyridine (1 mL). The final peptide was cleaved from resin by using cocktail mixture of 95 % trifluoroacetic acid, 2.5 % water and 2.5 % triisopropyl silane. The peptide was purified using reverse-phase-HPLC (detector: 254 nm and 220 nm) on C18 column with methanol/water gradients at a flow rate of 1.5 mL/min.

2.5.2 Transmission Electron Microscopy

Stock solution of all three peptides were prepared in THF by dissolving 1 mg of each peptide in 1 mL of Tetrahydrofuran (THF). 200 µL peptide stock solution was diluted to 1 mL with distilled water. The aqueous solution was vortexed for 1 min and centrifuged. 5 µL of supernatant solution was then dropcasted on 200 mesh copper grid. Samples were allowed to dry at room temperature. TECNAI G2 electron microscope operating at 300 kV

was used for viewing the samples. EDAX detector was able to yield the EDX analysis for silver filled nanotubes.

2.5.3 Scanning Electron Microscopy

200 μL peptide stock solutions were diluted to 1 mL with distilled water. The aqueous solution was vortexed for 1 min and centrifuged. 10 μL of supernatant solution was then dropcasted on silicon vapor. Samples were allowed to dry at room temperature and then coated with gold. Scanning electron microscopic imaging was performed using ZEISS ULTRA PLUS electron microscope operating at 30 kV.

2.5.4 Casting of silver nanowires

100 μL of aqueous nanotubes solution of **P3** at concentration of 0.2 mg in 1 mL was added to a 20 μL hot solution of 10 mM AgNO3.Citric acid was then added as reducing agent to make its 0.05% final concentration.The reaction mixture was sonicated for 1 min and centrifuged. After standing for 12 hrs, the filtrate was subjected to the FE-SEM and TEM analysis as described above.

2.5.5 Structural Data for peptides

a) Peptide P1

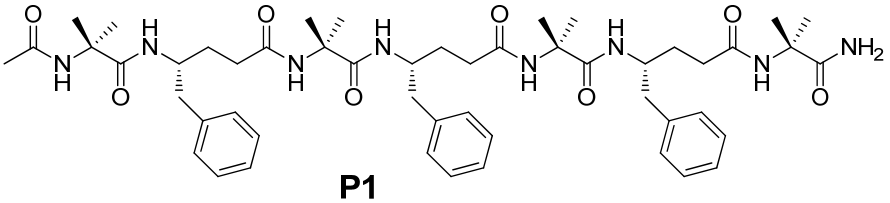

P1

^{1}H NMR (500 MHz, DMSO d_6) δ 8.29 (s, 1H), 8.08 (m, 2H), 7.97 (s, 1H), 7.72 (m, 3H), 7.40 (s, 1H), 7.07 (m, 15H, aromatic), 6.64 (s, 1H), 3.88 (m, 3H), 2.63 (m, 6H), 2.24 (m, 4H), 1.92 (m, 4H), 1.85 (s, 3H), 1.52 (m, 4H), 1.27-1.16(m, 18H, -CH_3 of Aib), 0.88 (s, 3H, -CH_3 of Aib), 0.81 (s, 3H, -CH_3 of Aib); **MALDI TOF/TOF**- *m/z* calcd. for $C_{51}H_{72}N_8O_8$ $[M+Na]^+$ 947.5371, obsrvd. 947.5378.

b) Peptide P2

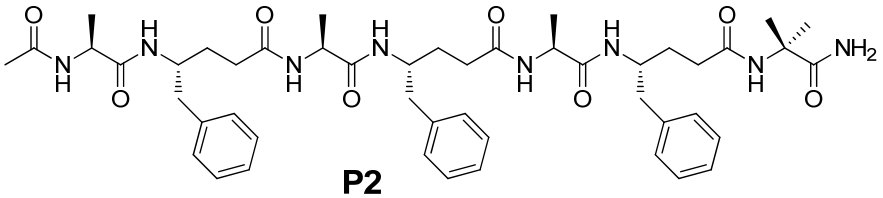

P2

^{1}H NMR (500 MHz, DMSO d_6) δ 7.93 (d, J = 7 Hz, 1H), 7.87 (d, J = 6.5 Hz, 1H), 7.77 (d, J = 6 Hz, 1H), 7.65 (m, 3H), 7.44 (s, 1H), 7.10 (m, 15H, aromatic), 6.63 (s, 1H), 4.10 (m, 1H), 3.97 (m, 1H), 3.89 (m, 1H), 3.89 (m, 3H), 2.61 (m, 6H), 2.04 (m, 4H), 1.78 (s, 3H), 1.69 (m, 4H), 1.45 (m, 4H), 1.21 (s, 3H, -CH_3 of Aib), 1.19 (s, 3H, -CH_3 of Aib), 1.09 (d, J = 7 Hz, 3H), 1.03 (d, J = 7 Hz, 3H), 0.98 (d, J = 7 Hz, 3H); **MALDI TOF/TOF**- *m/z* calcd. for $C_{48}H_{66}N_8O_8$ $[M+Na]^+$ 905.4901, obsrvd. 905.4950.

c) Peptide P3

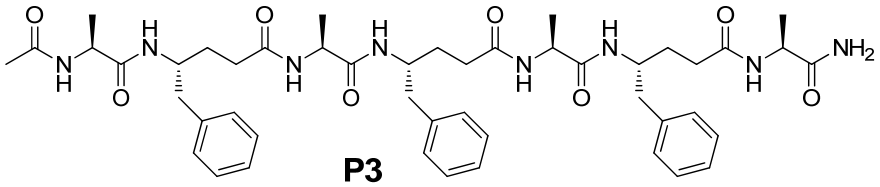

P3

^{1}H NMR (500 MHz, Methanol d_3) δ 8.21 (m, 4H), 7.97 (d, J = 6.5 Hz, 1H), 7.91 (s, 1H), 7.54 (d, J = 9.5 Hz, 1H), 7.20 (m, 15H, aromatic), 6.92 (s, 1H), 4.21 (m, 1H), 4.04 (m, 5H), 3.69 (m, 1H), 2.73 (m, 6H), 2.25 (m, 9H), 2.02 (s, 3H), 1.50 (m, 3H),1.37 (d, J = 7.5 Hz, 3H), 1.27 (d, J = 7 Hz, 3H), 1.12 (d, J = 7.5 Hz, 3H), 0.98 (d, J = 7 Hz, 3H); **MALDI TOF/TOF**- *m/z* calcd. for $C_{47}H_{64}N_8O_8$ $[M+Na]^+$ 891.4750, obsrvd. 891.5158.

2.6 Crystal data report

Table 2.13 Crystallization conditions for peptides

.

α/γ^4-peptide	crystallization condition (solvent mixture)
P1	Solvent Evaporation ($MeOH/H_2O/CF_3CH_2OH$)
P2	Solvent Evaporation ($MeOH/H_2O/CF_3CH_2OH$)
P3	Solvent Evaporation ($MeOH/H_2O$)
P4	Solvent Evaporation ($MeOH/ CHCl_3$)
P5	Solvent Evaporation ($MeOH/H_2O$)

Crystal data and structure refinement for α/γ^4-peptide P1

CCDC No.: 901428

Empirical formula: C_{51} H_{72} N_8 O_8 ; Formula weight: 925.17; Temperature: 100(2) K ; Wavelength: 0.71073 Å ; Crystal system: Monoclinic; Space group: P21; Unit cell dimensions: a = 12.866(15)Å, b = 17.403(19)Å, c = 13.962(16)Å, α = 90°, β = 107.22(3) °, γ = 90°; Volume: 2986(6) Å^3 ; Z: 2 ; Density (calculated): 1.029 Mg/m^3 ; Absorption coefficient (μ): 0.07 mm^{-1} ; F (000): 996; Crystal size: 0.40 x 0.20 x 0.12 mm^3 ; Theta range for data collection: 1.53 to 28.25° ; Index ranges: -17<=h<=11, -20<=k<=23, -18<=l<=16 ; Reflections collected: 26870; Independent reflections: 13302 [R(int) = 0.1294] ; Completeness to theta = 28.25°: 98.6 % ; Absorption correction: Empirical with SADABS ; Max. and min. Transmission: 0.992 and 0.983; Refinement method: Full-matrix least-squares on F^2 ; Data / restraints / parameters: 13302 / 1 / 596 ; Goodness-of-fit on F^2 : 0.733 ; Final R indices [I>2sigma(I)]: R1 = 0.0813, wR2 = 0.1855; R indices (all data): R1 = 0.2345, wR2 = 0.2369.

Crystal data and structure refinement for α/γ^4-peptide P2

CCDC No.: 901429

Empirical formula: C_{48} H_{66} N_8 O_8,(O) ; Formula weight: 899.09; Temperature: 100(2) K; Wavelength: 0.71073 Å; Crystal system: Triclinic; Space group: P1; Unit cell dimensions: a = 9.354(10)Å, b = 12.179(13)Å, c = 13.950(15)Å, α = 68.89(3)°, β = 85.74(3°) , γ = 71.36(3)°; Volume: 1403(3) $Å^3$; Z: 1 ; Density (calculated): 1.064Mg/m^3 ; Absorption coefficient (μ): 0.074 mm^{-1} ; F (000): 482; Crystal size : 0.40 x 0.30 x 0.20 mm^3 ; Theta range for data collection: 1.57 to 28.28° ; Index ranges: -12<=h<=12, -16<=k<=15, -18<=l<=17; Reflections collected: 24197 ; Independent reflections: 10395 [R(int) = 0.0501] ; Completeness to theta = 28.28°: 99.1 %; Absorption correction: Empirical with SADABS ; Max. and min. Transmission : 0.985 and 0.974 ; Refinement method: Full-matrix least-squares on F^2 ; Data / restraints / parameters: 110395 / 327 / 569 ; Goodness-of-fit on F^2 : 0.771 ; Final R indices [I>2sigma(I)]: R1 = 0.0833, wR2 = 0.2342; R indices (all data) : R1 = 0.1364, wR2 = 0.2723; Absolute structure parameter: 0.6(18); Largest diff. peak and hole: 0.056 and -0.257 e.$Å^{-3}$.

Crystal data and structure refinement for α/γ^4-peptide P3

CCDC No.: 901430

Empirical formula: C_{47} H_{64} N_8 O_8, 2(O); Formula weight: 901.06; Temperature: 100(2) K; Wavelength: 0.71073 Å; Crystal system: Monoclinic; Space group: P21; Unit cell dimensions: a = 11.218(17)Å, b = 14.58(2)Å, c = 15.75(2)Å, α = 90°, β = 100.06(3)°, γ = 90°; Volume: 2536(7)$Å^3$; Z: 2; Density (calculated): 1.140Mg/m^3 ; Absorption coefficient (μ): 0.079mm^{-1} ; F (000): 924; Crystal size: 0.40 x 0.29 x 0.16 mm^3 ; Theta range for data collection: 1.84 to 28.28° ; Index ranges: -14<=h<=14, -16<=k<=19, -20<=l<=20; Reflections collected: 16669; Independent reflections: 10827 [R(int) = 0.0952]; Completeness to theta = 28.28°: 98.1 % ; Absorption correction: Empirical with SADABS ; Max. and min. Transmission: 0.987 and 0.973;

Refinement method: Full-matrix least-squares on F^2; Data / restraints / parameters: 10827 / 1 / 591; Goodness-of-fit on F^2 : 0.909; Final R indices [I>2sigma(I)]: R1 = 0.0824, wR2 = 0.1713; R indices (all data): R1 = 0.2023, wR2 = 0.2352; Absolute structure parameter: -2.1(19); Largest diff. peak and hole: 0.428 and -0.366 e.$Å^{-3}$.

Crystal data and structure refinement for α/γ^4-peptide P4

CCDC No.: 955486

Crystals of **P4** were grown by slow evaporation from a solvent composition of Methanol/Chloroform (3:1). A single crystal, rectangular in shape (0.80 × 0.30 × 0.20 mm^3), was mounted on a loop. The X-ray data were collected at 100(2) K temperature on a Bruker AXS SMART APEX CCD diffractometer using Mo-Kα radiation (λ = 0.71073 Å), ω-scans (2θ = 56.56°), for a total number of 8874 independent reflections. Space group P21; a = 15.997(2), b = 34.214(4),c = 18.3336(19)Å; α = γ = 90°, β = 111.790(2)°,V = 9317.4(19)$Å^3$, monoclinic P; Z = 2 for chemical formula $C_{36}H_{66}N_8O_8$; ρ calcd. = 1.168 Mgm^{-3}; μ = 0.089 mm^{-1}; F (000) = 3536. The structure was obtained by direct methods using SHELXS-97. All non-hydrogen atoms except C9, C90, C91, C127 and C129 were refined anisotropically. The hydrogen atoms were fixed geometrically in the idealized position and refined in the final cycle of refinement as riding over the atoms to which they are bonded. Hydrogen atoms located on C128 oscillate even after higher refinement cycles which are responsible for increased shift to su ratio. The final R value was 0.0879 (wR2 = 0.2337) for 31448 observed reflections ($F_0 \geq 4\sigma$ ($|F_0|$)) and 2098 variables; S = 0.960. The largest deference peak and hole were 1.050 and -0.656 $eÅ^{-3}$, respectively.

Crystal data and structure refinement for α/$γ^4$-peptide P5

CCDC No.: 955487

Crystals of **P5** were grown by slow evaporation from a solvent composition of Methanol/water (4:1). A single crystal, rectangular in shape (0.60 × 0.40 × 0.20 mm^3), was mounted on a loop. The X-ray data were collected at 100(2) K temperature on a Bruker AXS SMART APEX CCD diffractometer using Mo-Kα radiation (λ = 0.71073 Å), ω-scans (2θ = 56.80°), for a total number of 19169 independent reflections. Space group P21 21 21; a = 9.4835(18), b = 14.598(3),c = 27.319(5)Å; α = β = γ = 90°,V = 3782.1(13)$Å^3$, orthorhombic P; Z = 4 for chemical formula $C_{33}H_{61}N_7O_8$; ρ calcd. = 1.229 Mgm^{-3}; μ = 0.085 mm^{-1}; F (000) = 1520. The structure was obtained by direct methods using SHELXS-97. All non-hydrogen atoms were refined anisotropically. The hydrogen atoms were fixed geometrically in the idealized position and refined in the final cycle of refinement as riding over the atoms to which they are bonded. The final R value was 0.0693 (wR2 = 0.1504) for 9409 observed reflections ($F_0 \geq 4\sigma$ ($|F_0|$)) and 454 variables; S = 0.885. The largest deference peak and hole were 0.304 and -0.299 $eÅ^{-3}$, respectively.

2.7 References

1. Barlow, D. J.; Thornton, J. M. *J. Mol. Biol.* **1988**, *201*, 601-619.
2. a) Ramachandran, G.N.; Sasisekharan, V. *Advan. Protein Chem*. **1968**, *23*, 283. b) Creighton, T. E. *Proteins Structures and Molecular Properties*. **1993** W.H. Freeman and Company, New York
3. a) Jones, S.; Thornton, J. M. *Proc. Natl. Acad. Sci. U.S.A.* **1996**, *93*, 13. b) Cochran, A. G.; *Curr. Opin. Chem. Biol.* **2001**, *5*, 654. c) Guharoy, M.; Chakrabarti, P. *Bioinformatics* **2007**, *23*, 1909. d) Fairlie, D. P.; West, M. W.; Wong, A. K. *Curr. Med. Chem.* **1998**, *5*, 29. e) Lavery, R. Q.; Rev. *Biophys.* **2005**, *38*, 339 f) Draper, D. E. *Ann. Rev. Biochem.* **1995**, **64**, 593.
4. a) Woolley, G. A. *Acc. Chem. Res.* **2005**, *38*, 486. b) Fujimoto, K.; Kajino, M.; Inouye, M. *Chem. Eur. J*. **2008**, *14*, 857. c) Mills, N. L.; Daugherty, M. D.; Frankel , A. D.; Guy, R. K. *J. Am. Chem. Soc*. **2006**, *128*, 3496. d) Garner, J.; Harding, M. M. *Org. Biomol. Chem*. **2007**, *5*, 3577. e) Andrews,M. J. I.; Tabor, A. B. *Tetrahedron* **1999**, *55*, 11711.
5. Patgiri, A.; Jochim, A. L.; Arora, P. S. *Acc. Chem. Res.* **2008**, *41*, 1289.
6. Cummings, C. G.; Hamilton, A. D. *Curr. Opin. Chem. Biol.* **2010**, *14*, 341.
7. a) Seebach, D.; Beck, A. K.; Bierbaum, D. J. *Chem. Biodiv.* **2004**, *1*, 1111. b) Seebach, D.; Gardiner, J. *Acc. Chem. Res.* **2008**, *41*, 1366. c) Horne, W. S.; Gellmann, S. H. *Acc. Chem. Res.* **2008**, *41*, 1399. d) Vasudev , P. G.; Chatterjee, S.; Shamala, N.; Balaram, P. *Chem. Rev.* **2011**, *111*, 657. e) Pilsl, L. K. A.; Reiser, O. *Amino acids* **2011**, *41*, 709. f) Hanessian, S.; Luo, X.; Schaum , R.; Michnick, S. *J. Am. Chem. Soc.* **1998**, *120*, 8569. g) Martinek ,T. A.; Fulop, F. *Chem. Soc. Rev.* **2012**, *41*, 687. h) Petersson, E. J.; Schepartz, A. *J. Am. Chem. Soc.* **2008**, *130*, 821. i) Giuliano, M. W.; Horne, W. S.; Gellman, S. H. *J. Am. Chem. Soc.* ***2009***, *131*, 9860. j) Sharma, G. V. M.; Jadhav, V. B.; Ramakrishna, K. V. S.; Jayaprakash, P.; Narsimulu, K.; Subash, V.; and Kunwar, A. C. *J. Am. Chem. Soc*. ***2006***, *128*, 14657. k) Goodman, J. L.; Petersson, E. J.; Daniels, D. S.; Qiu, J. X.; Schepartz, A. *J. Am. Chem. Soc*. **2007**, *129*, 14746. l) Balamurugan, D.; Muraleedharan K. M. *Chem. Eur. J.* **2012**, *18*, 9516. m) Chandrasekhar, S.; Kiranmai, N.; Kiran, M. U.; Devi, A. S.; Reddy, G. P. K.; Idris, M.; Jagadeesh, B. *Chem. Commun.* **2010**, *46*, 6962.
8. a) Karle, I; Gopi, H. N.; Balaram, P. *Proc. Natl. Acad. Sci. U.S.A.* **2001**, *98*, 3716. b) Karle, I; Gopi, H. N.; Balaram, P. *Proc. Natl. Acad. Sci. U.S.A.* **2002**, *99*, 5160. c) Vasudev, P. G.; Chatterjee, S.; Shamala, N.; Balaram, P. *Acc. Chem. Res.* **2009**, *42*,

1628. d) Karle,I. L.; Pramanik, A.; Banerjee, A.; Bhattacharjya, S.; Balaram, P. *J. Am. Chem. Soc.* **2007**, *119*, 9087.

9. De Pol, S.; Zorn, C.; Klein, C. D.; Zerbe, O.; Reiser, O. *Angew. Chem., Int. Ed.* **2004**, *43*, 511.
10. a) Hayen, A.; Schmitt, M. A.; Ngassa, F. N.; Thomasson, K. A.; Gellman, S. H. *Angew. Chem., Int. Ed.* **2004**, *43*, 505. b) Schmitt, M. A.; Choi, S. H.; Guzei, I. A.; Gellman, S. H. *J. Am. Chem. Soc.* **2005**, *127*, 13130. c) Schmitt, M. A.; Choi, S. H.; Guzei, I. A.; Gellman, S. H. *J. Am. Chem. Soc.* **2006**, *128*, 4538.
11. Seebach, D.; Jaun, B.; Sebesta, R.; Mathad, R. I.; Flogel, O.; Limbach, M.; Sellner, H.; Cottens, S. *Helv. Chim. Acta* **2006**, *89*, 1801.
12. Bouillere, F.; Laurent, S. T-.; Kouklovsky, C.; Alezra, V. *AminoAcids* **2011**, *41*, 687.
13. Horne, W. S.; Price, J. L.; Keck, J. L.; Gellman, S. H. *J. Am. Chem. Soc.* **2007**, *129*, 4178.
14. a) Daniels, D.S.; Petersson, E. J.; Qiu, J. X.; Schepartz, A. *J. Am. Chem. Soc.***2007**, *129*, 1532. b) Petersson, E. J.; Schepartz, A. *J. Am. Chem. Soc.***2008**, *130*, 821.
15. Baldauf, C.; Gunther, R.; Hofmann, H.-J. *J. Org. Chem.* **2006**, *71*, 1200.
16. Chatterjee, S.; Vasudev, P. G.; Raghothama, S.; Ramakrishnan, C.; Shamala, N.; Balaram, P. *J. Am. Chem. Soc.* **2009**, *131*, 5956.
17. Sharma, G. V. M.; Jadhav, V. B.; Ramakrishna, K. V. S.; Jayaprakash, P.; Narsimulu, K.; Subash, V.; Kunwar, A. C. *J. Am. Chem. Soc.* **2006**, *128*, 14657.
18. a) Guo, L.; Zhang, W.; Guzei, I. A.; Spencer, L. C.; Samuel H. Gellman, S. H. *Org. Lett*. **2012**, *14*, 2582. b) Guo, L.; Chi, Y.; Almeida, A. M.; Guzei, I. A.; Parker, B. K.; Gellman, S. H. *J. Am. Chem. Soc*. **2009**, *131*, 16018.
19. a) Bandyopadhya, A.; Gopi, H. N. *Org. Lett*. **2012**, *14*, 2770. b) Bandyopadhya, A.; Jadhav, S. V.; Gopi, H. N. *Chem Commun*. **2012**, *48*, 7170.
20. a) Toniolo, C.; Benedetti, E. *Trends Biochem. Sci*. **1991**, *16*, 350. b) Karle, I. L.; Balaram, P. *Biochemistry* **1990**, *29*, 6747.
21. Ramachandran, G. N.; Sasisekharan, V. *Advan. Protein Chem*. **1968**, *23*, 283.
22. a) Sugeta, H.; Miyazawa, T. *Biopolymers* **1967**, *5*, 673. b) Bansal, M.; Kumar, S.; Velavan, R. *J. Biomol. Struct. Dyn.* **2000**, *17*, 811.
23. Choi, S. H.; Guzei, I. A.; Spencer, L. C.; Gellman, S. H. *J. Am. Chem. Soc.* 2010, 132, 13879.

24. Fernandes, C.; Faure, S.; Pereira, E.; Thery, V.; Declerck, V.; Guillot, R.; Aitken, D. J. *Org. Lett*. **2010**, *12*, 3606.
25. Pelletier, H.; Sawaya, M. R. *Biochemistry* **1996**, *35,* 12778.
26. Crisma, C.; Saviano, M.; Moretto, A.; Broxterman, Q. B.; Kaptein, B.; Toniolo, C. *J. Am. Chem. Soc*. **2007**, *129,* 15471.
27. The overlayed structures of β-peptide 12-helix, α-helix and 3_{10}-helix were generated from crystal co-ordinates reported in the ref. 23, 25 and 26 respectively.
28. a) Zhou, F. X.; Cocco, M. J.; Russ, W. P.; Brunger, A. T.; Engelman, D. M.; *Nature Struct. Biol.* **2000**, *7*, 154. b) Croma, C.; Gratkowski, H.; Lear, J. D.; DeGrado, W. F. *Nature Struct. Biol.* **2000**, *7*,161.
29. a) Whitesides, G. M.; Mathias, J. P.; Seto, C. T.; *Science* **1991**, *254*, 1312. b) King, N. P.; Sheffler, W.; Sawaya, M. R.; Wollmar, B. S.; Sumida, J. P.; Andre, I.; Gonen, T.; Yeates, T. O.; Baker, D. *Science* **2012**, *336*, 1171. c) Ardejani, M. S.; Orner, B. P. *Science* **2013**, *340*, 561.
30. a) Lakshmanan, A.; Zhang, S.; Hauser, C. A. E. *Trends in Biotechnology* **2011**, *30*, 155. b) Zelzer, M.; Ulijn, R. V. *Chem. Soc. Rev.* **2010**, *39*, 3351. c) Aida, T.; Meijer, E. W.; Stupp, S. I. *Science* **2012**, *335*, 813. d) H. Tsutsumi, H. Mihara, *Mol. Biosyst.* **2013**, *9*, 609-617; d) Lakshmanan, A.; Hauser, C. A. E. *Int. J. Mol. Sci*. **2011**, *12*, 5736. e) Zhang, S.; *Nat. Biotechnol*. **2003**, *21*, 1171. f) Stephanopoulos, N.; Ortony, J. H.; Stupp, S. I. *Acta Biomater*. **2013**, *61*, 912. g) Hauser, C. A. E.; Zang, S. *Nature* **2010**, *468*, 516. h) Cherny, I.; Gazit, E. *Angew. Chem. Int. Ed*. **2008**, *47*, 4062. h) Hirst, A. R.; Escuder, B.; Miravet, J. F.; Smith, D. K. *Angew. Chem. Int. Ed.* **2008**, *47*, 8002. i) Branco, M.; Schneider, J. P. *Acta Biomater.* **2009**, *5*, 817. j) Marsden, H. R.; Kros, A. *Angew. Chem. Int. Ed*. **2010,** *49*, 2988. k) Hosseinkhani, H.; Hong, P. -D.; Yu, D. S. *Chem. Rev.* **2013**, *113*, 4837. l) Scheibel, T.; *Curr. Opinion Biotechnol*, **2005**, *16*, 427. m) Chapman, R.; Danial, M.; Koh, M. L.; Jolliffe, K. A.; Perrier, S. *Chem. Soc. Rev.,* **2012**, *41*, 6023. n) Mahmoud, Z. N.; Grundy, D. J.; Chanon, K. J.; Woolfson, D. N. *Biomaterials* **2010**, *31*, 7468. o) de la Rica, R.; Matsui, H. *Chem. Soc. Rev.* **2010**, *39*, 3499.
31. a) Meyer, E. A.; Castellano, R. K.; Diederich, F. *Angew. Chem. Int. Ed.* **2003**, *42*, 1210. b) Waters, M. L. *Biopolymers* **2004**, *76*, 435.
32. a) Martinek, T. A.; Mandity, I. M.; Fulop, L.; Toth, G. K.; Vass, E.; Hollosi, M.; Forro, E.; Fulop, F. *J. Am. Chem. Soc.* **2006**, *128*, 13539. b) Martinek, T. A.; Hetenyi, A.; Fulop, L.; Mandity, I. M.; Toth, G. K.; Dekany, I.; Fulop, F. *Angew.*

Chem., Int. Ed. **2006**, *45*, 2396. c) Kwon, S.; Jeon, A.; Yoo, S. H.; Chung, I. S.; Lee, H.-S. *Angew. Chem. Int. Ed.* **2010**, *49*, 8232. d) Kim, J.; Kwon, S.; Kim, S. H.; Lee, C. -K.; Lee, J. –H.; Cho, S. J.; Lee, H. –S.; Ilee, H. *J. Am. Chem. Soc.***2012**, *134*, 20573. e) Borgo, M. P. D.; Mechler, A. I.; Traore, D.; Forsyth, C.; Wilce, J. A.; Aguilar, M. –I.; Perlmutter, P. *Angew. Chem. Int. Ed.* **2013**, *52*, 8266.

33. Ghadiri, M. R.; Granja, J. R.; Milligan, R. A.; McRee, D. E.; Khazanovich, N. *Nature* **1993**, *366*, 324.
34. Reches, M.; Gazit, E. *Science* **2003**, *300*, 625.
35. a) Amorin, M.; Castedo, L.; Granja, J. R. *J. Am. Chem. Soc.* **2003**, *125*, 2844. b) Hourani, R.; Zhang, C.; van der Weegen, R.; Ruiz, L.; Li, C.; Keten, S.; Helms, B. A.; Xu, T. *J. Am. Chem. Soc.* **2011**, *133*, 15296. c) Reiriz, C.; Brea, R. J.; Arranz, R.; Carrascosa, J. L.; Garibotti, A.; Manning, B.; Valpuesta, J. M.; Eritja, R.; Castedo, L.; Granja, J. R. *J. Am. Chem. Soc.* **2009**, *131*, 11335.
36. Perutz, M. F.; Finch, J. T.; Berriman, J.; Lesk, A. *Proc. Natl. Acad. Sci. USA* **2002**, *99*, 5591.
37. Schuette, W. M.; Buhro, W. E. *ACSNano* **2013,** *7*, 3844.
38. a) Yan, X.; Zhu, P.; Li, J. *Chem. Soc. Rev*. **2010**, *39*, 1877. b) Scanlon, S.; Aggeli, A. *nanotoday* **2008**, *3*, 22. c) Yan, X.; He, Q.; Wang, K.; Duan, L.; Cui, Y.; Li, J. *Angew. Chem. Int. Ed*. **2007**, *46*, 2431. d) de la Rica, R.; Mendoza, E.; Lechuga, L. M.; Matsui, H.; *Angew. Chem. Int. Ed.* **2008**, *47*, 9752. e) Kim, J. H.; Ryu, J.; Park, C. B.; *Small* **2011**, *7,* 718. f) Kim, J. H.; Lee, M.; Lee, J. S.; Park, C. B. *Angew. Chem. Int. Ed.* **2012**, *51*, 517. g) Brea, R. J.; Reiriz, C.; Granja, J. R.; *Chem. Soc. Rev.* **2010**, *39*, 1448. h) Valery, C.; Artzner, F.; Paternostre, M.; *Soft Matter*, **2011**, *7*, 9583. i) Seabra, A. B.; Duran, N.; *Peptides* **2013**, *39*, 47. j) Montenegro, J.; Ghadiri, M. R.; Granja, J. R. *Acc. Chem. Res.* **2013**, **DOI:** 10.1021/ar400061d.

2.8 Appendix I: Characterization data for synthesized compounds.

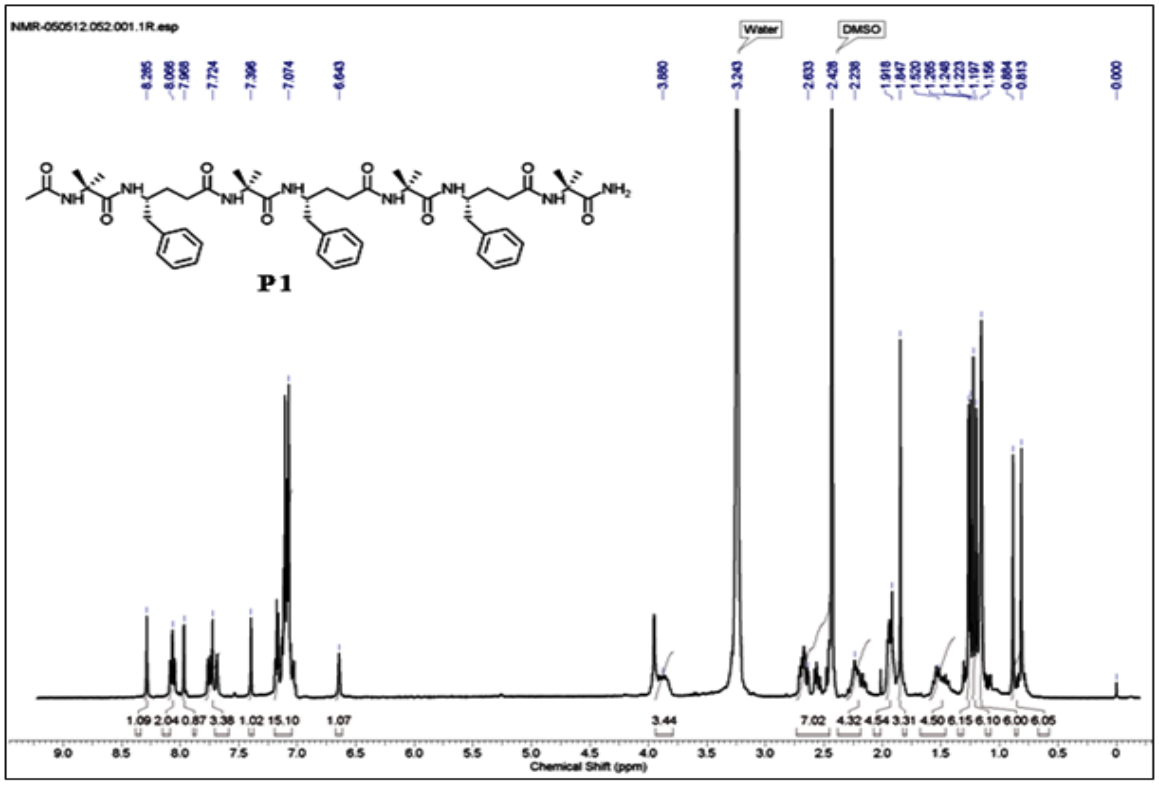
NMR-050512.052.001.1R.esp
Water
DMSO
P1
Chemical Shift (ppm)

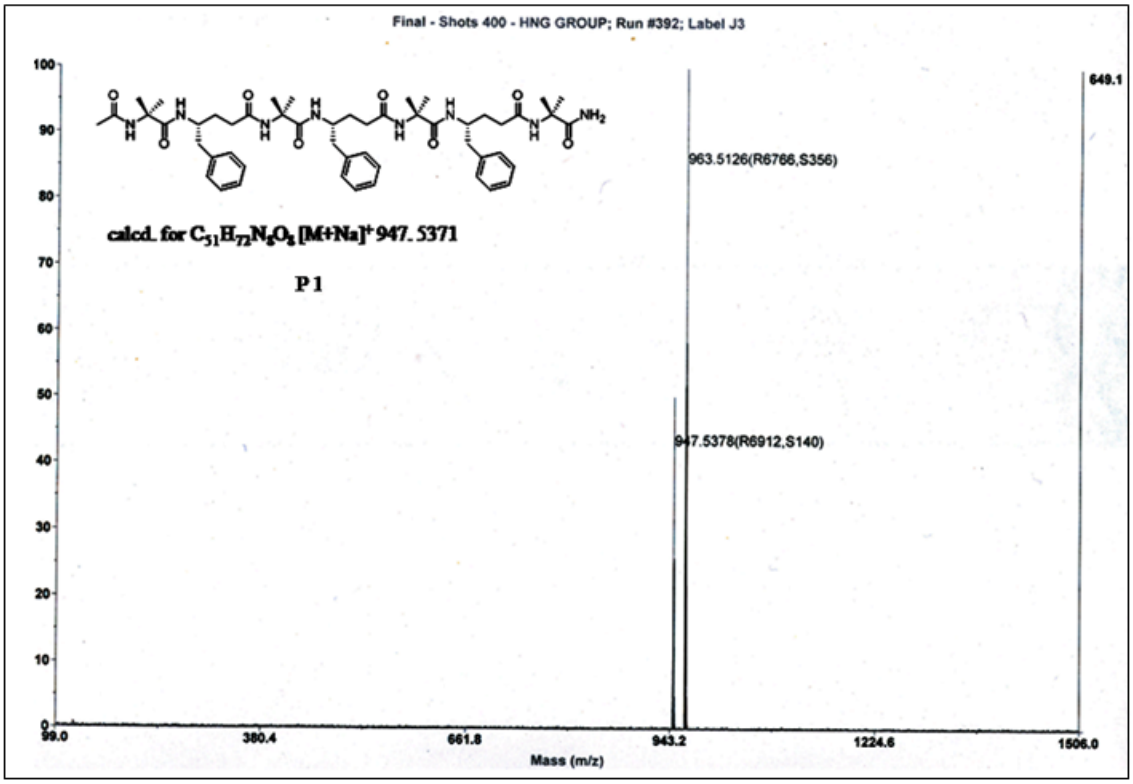
Final - Shots 400 - HNG GROUP; Run #392; Label J3
963.5126(R6766,S356)
649.1
947.5378(R6912,S140)
calcd. for C51H72N8O8 [M+Na]+ 947. 5371
P1
Mass (m/z)

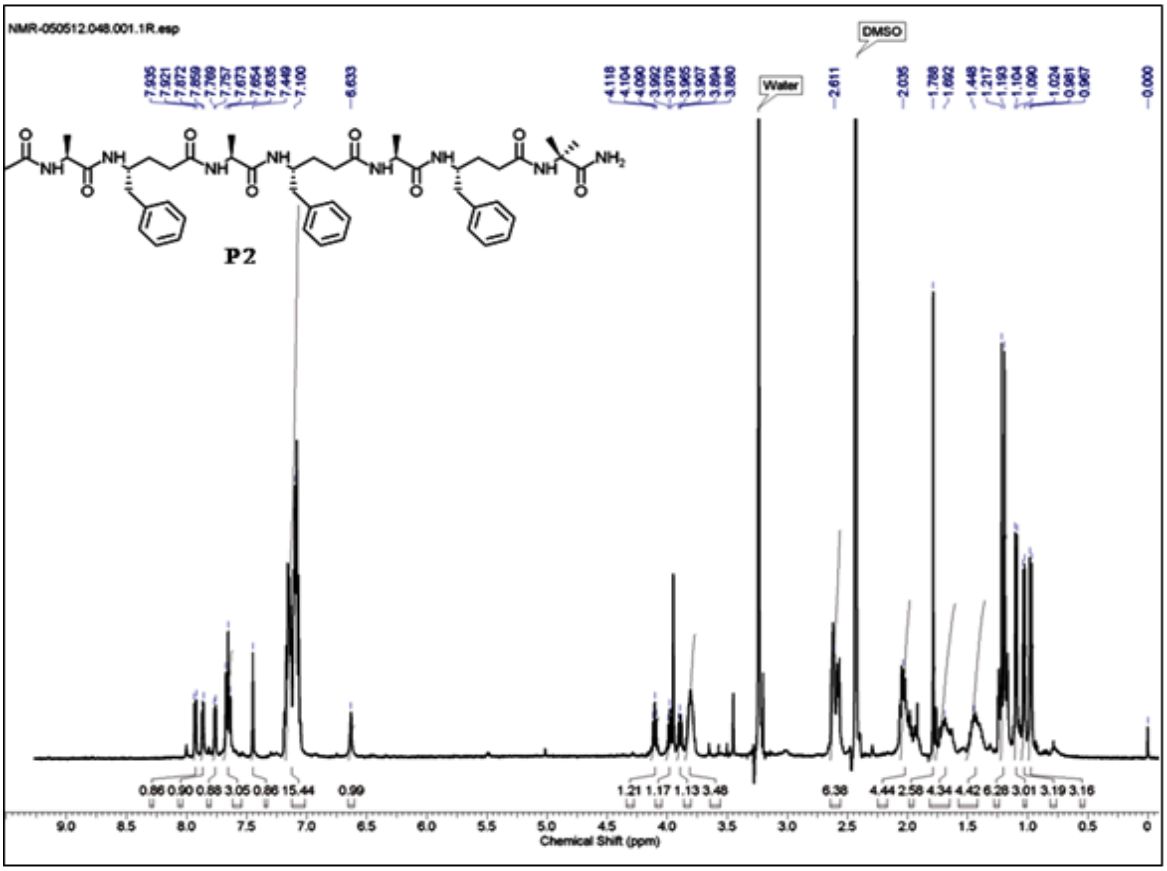
NMR-050512.048.001.1R.esp
DMSO
Water
P2
Chemical Shift (ppm)

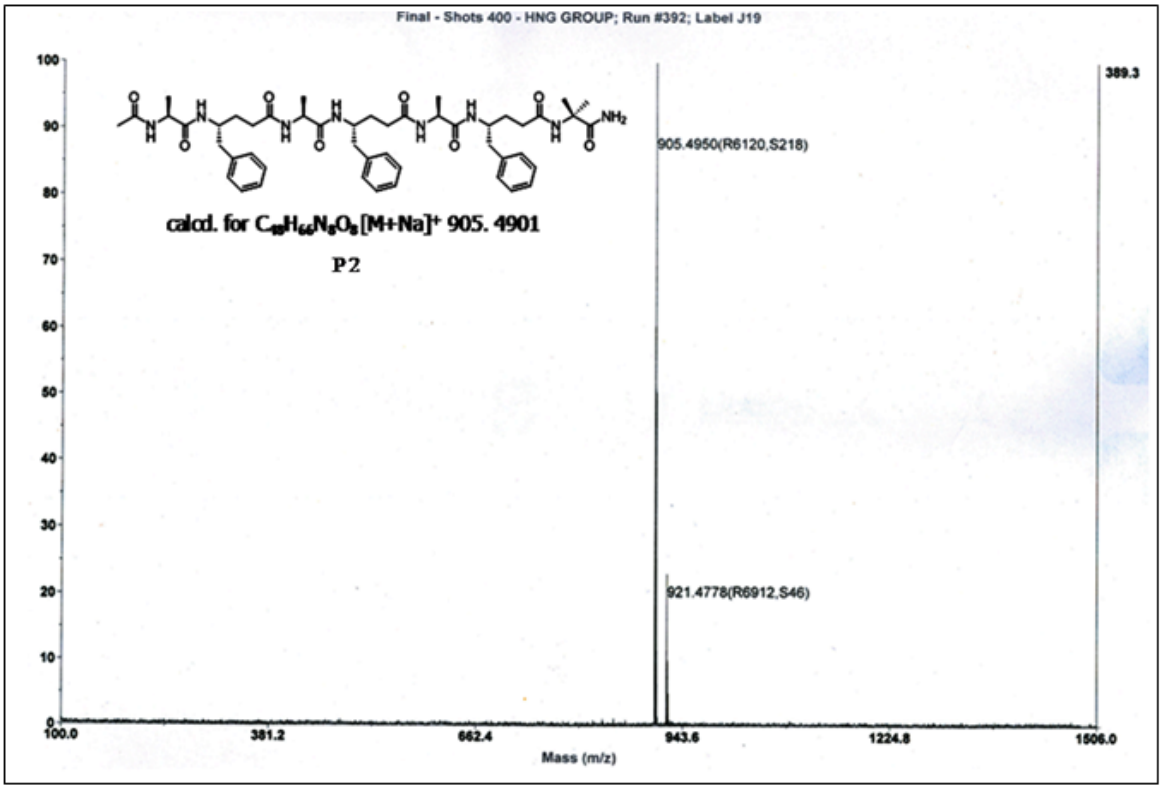
Final - Shots 400 - HNG GROUP; Run #392; Label J19
389.3
905.4950(R6120,S218)
921.4778(R6912,S46)
calcd. for C48H66N8O8[M+Na]+ 905. 4901
P2
Mass (m/z)

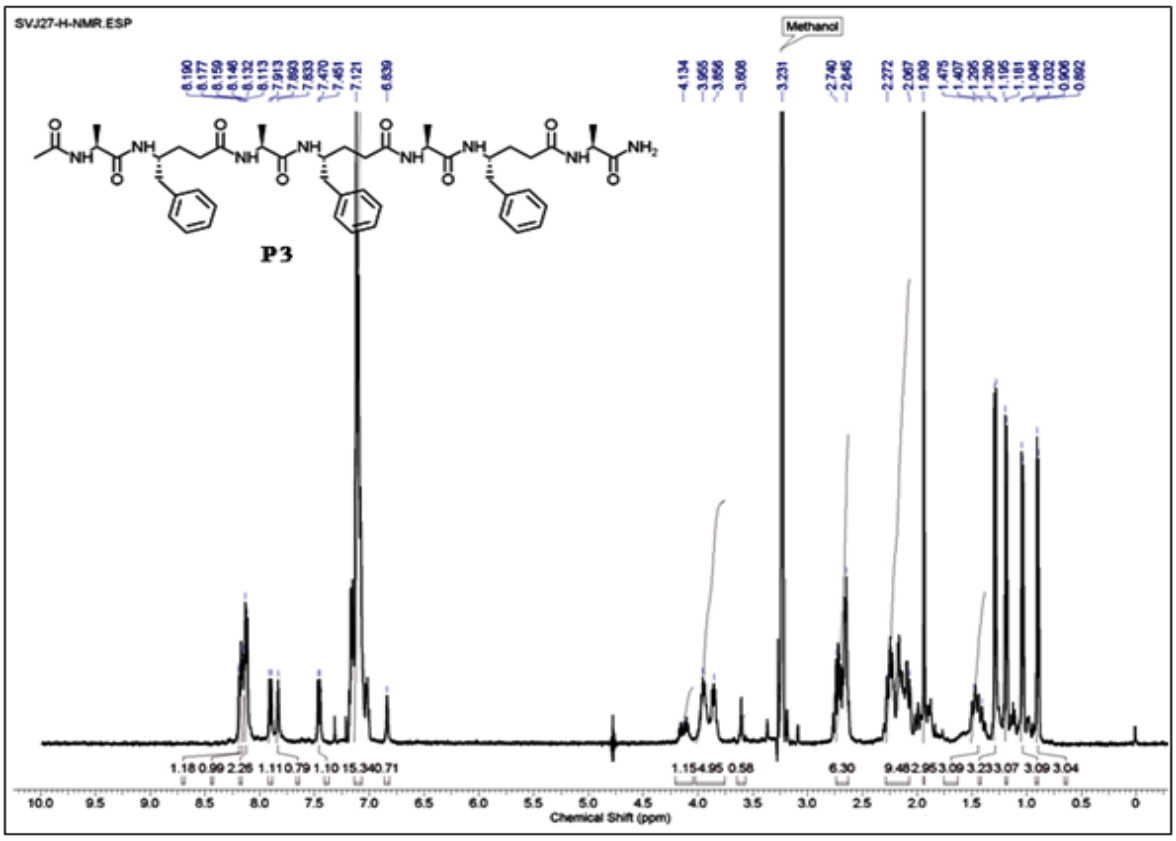
SVJ27-H-NMR.ESP
Methanol
P3
Chemical Shift (ppm)

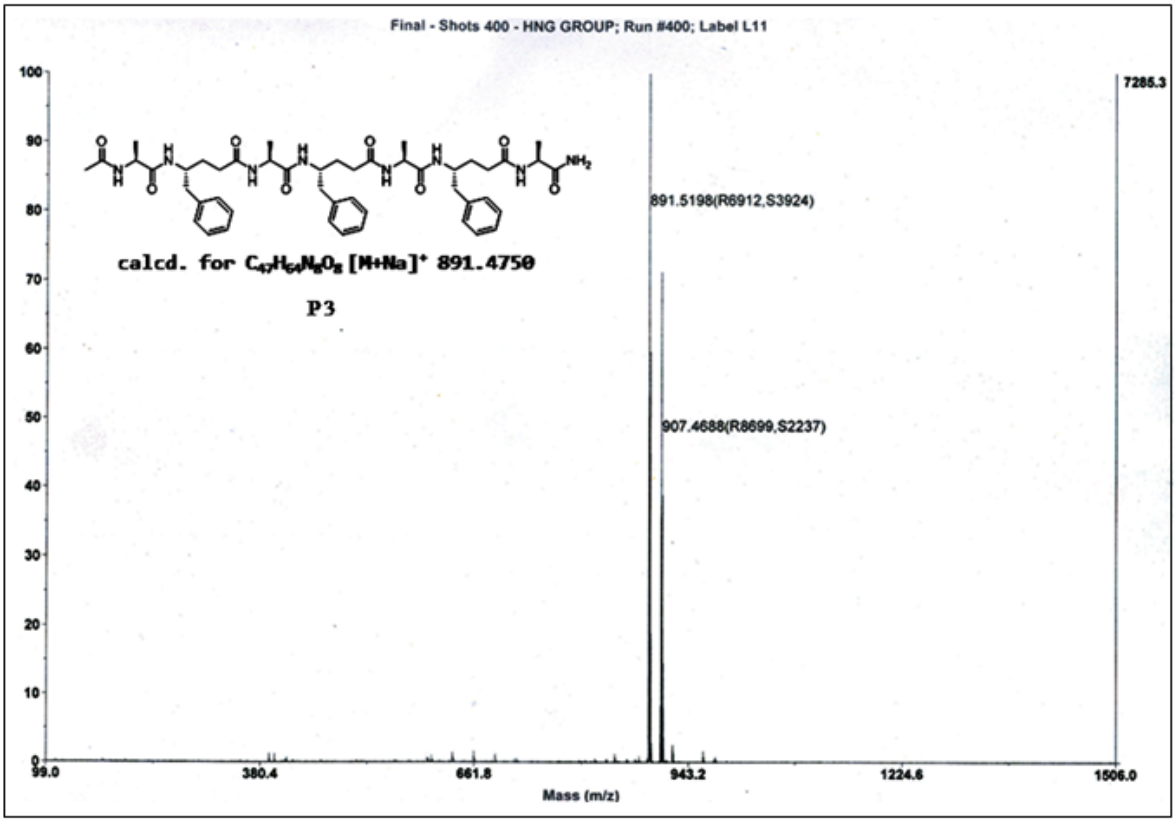
Final - Shots 400 - HNG GROUP; Run #400; Label L11
calcd. for C47H64N8O8 [M+Na]+ 891.4750
P3
891.5198(R6912,S3924)
907.4688(R8699,S2237)
7285.3
Mass (m/z)

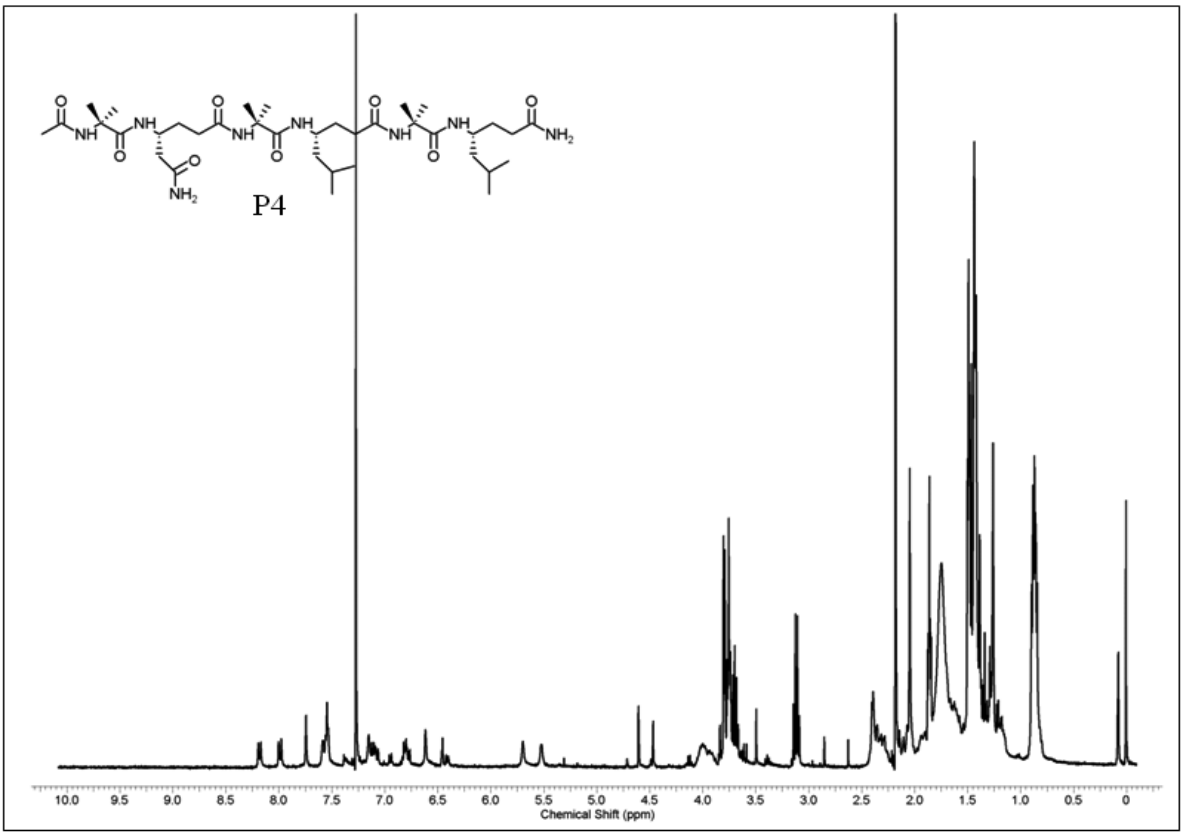
P4
10.0 9.5 9.0 8.5 8.0 7.5 7.0 6.5 6.0 5.5 5.0 4.5 4.0 3.5 3.0 2.5 2.0 1.5 1.0 0.5 0
Chemical Shift (ppm)

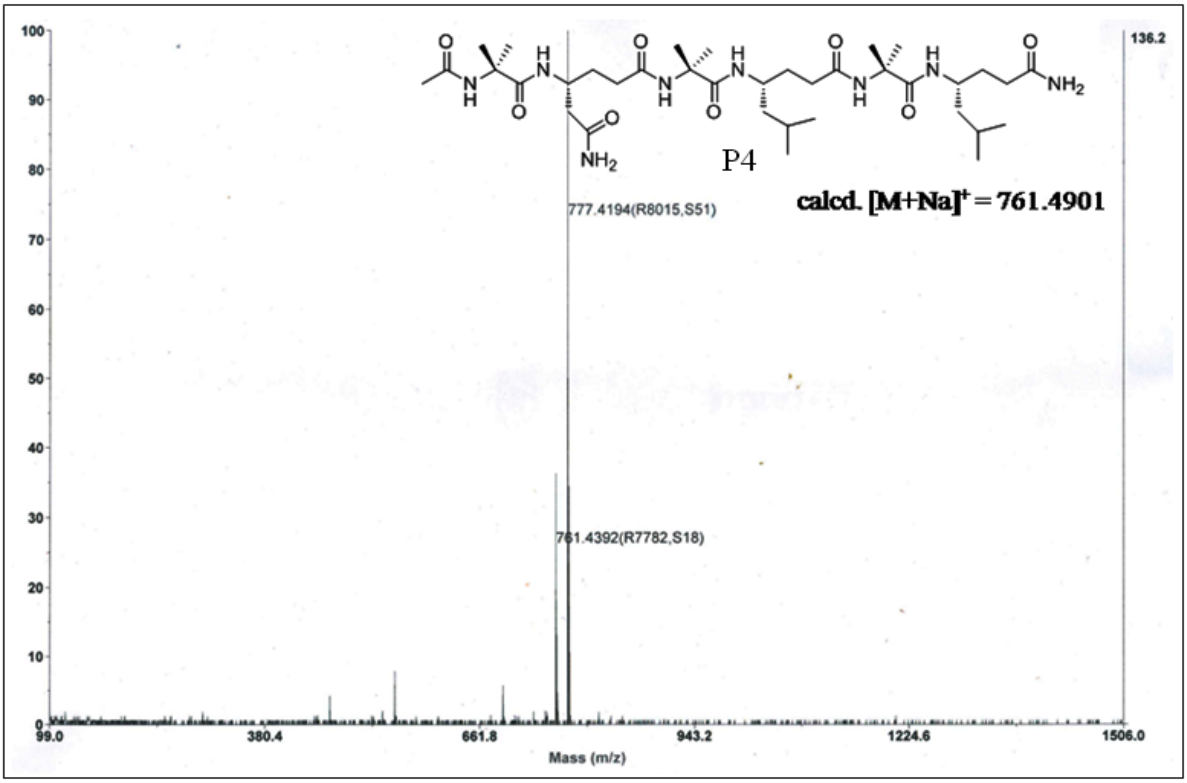
P4
777.4194(R8015,S51)
calcd. [M+Na]+ = 761.4901
761.4392(R7782,S18)
136.2
100 90 80 70 60 50 40 30 20 10 0
99.0 380.4 661.8 943.2 1224.6 1506.0
Mass (m/z)

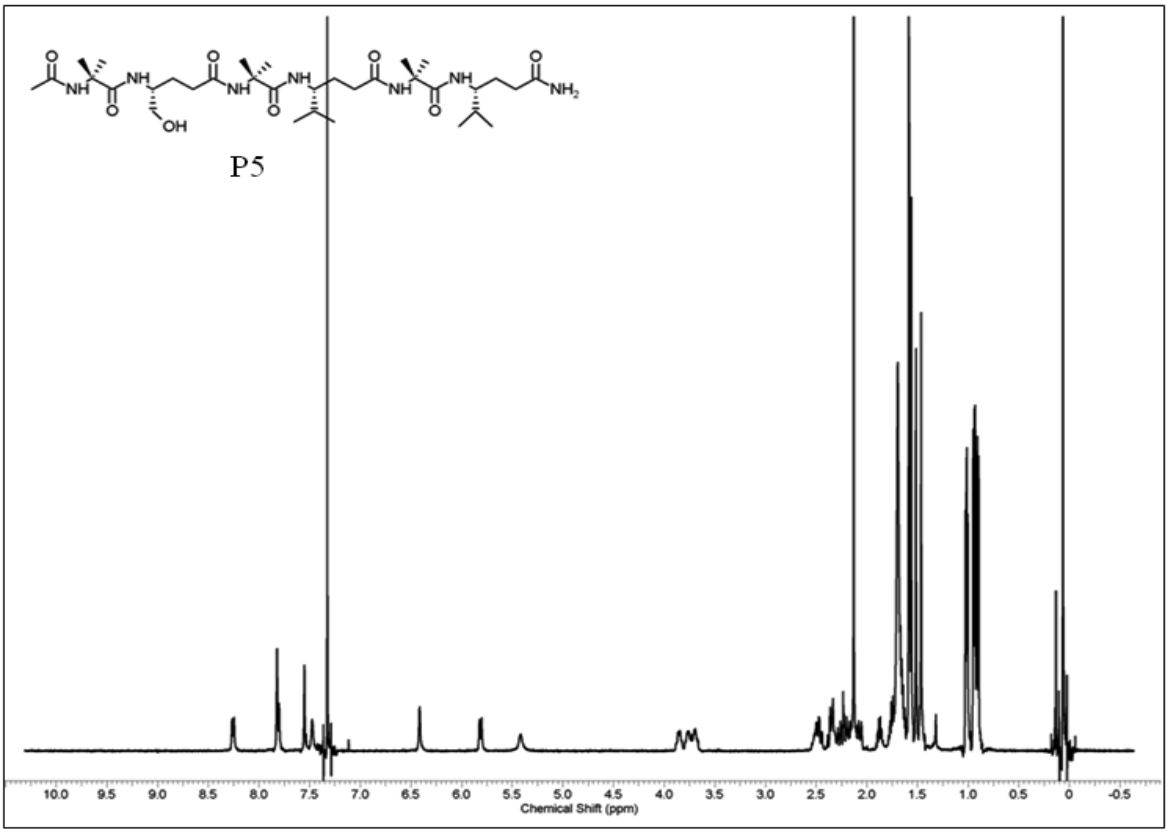
P5
10.0 9.5 9.0 8.5 8.0 7.5 7.0 6.5 6.0 5.5 5.0 4.5 4.0 3.5 3.0 2.5 2.0 1.5 1.0 0.5 0 -0.5
Chemical Shift (ppm)

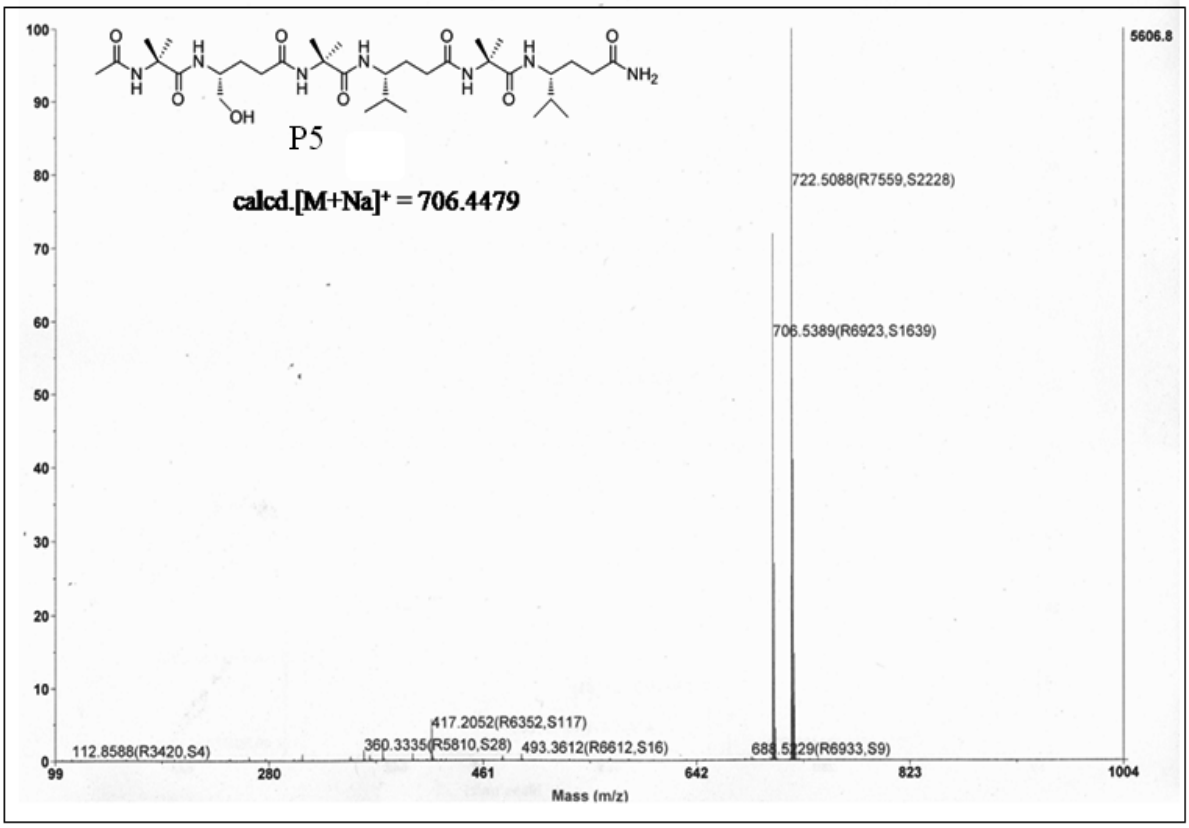
P5
calcd.[M+Na]+ = 706.4479
5606.8
722.5088(R7559,S2228)
706.5389(R6923,S1639)
417.2052(R6352,S117)
360.3335(R5810,S28)
493.3612(R6612,S16)
112.8588(R3420,S4)
99 280 461 642 823 1004
Mass (m/z)

Chapter 3

Remarkable Thermoresponsive Nanofibers from γ-Peptides

3.1 Introduction

3.1.1 Self-assembly in peptides

Supramolecular assembly of peptides and proteins has attracted considerable interest in recent years due to their utility in the design and fabrication of nano-structures with tunable physical and chemical properties. Peptide biomaterials derived from α-amino acids have been extensively studied and shown for their applications in various fields including tissue engineering, drug delivery, biomineralization, regenerative medicine, wound healing and molecular electronics.[1] Owing to their biocompatibility and easy synthesis, research in the area of peptide based gelators are gaining momentum.[1l] Ulijn laboratory have shown the remarkable hydrogelation from Fmoc-diphenylalanine based on π-π interlocked β-sheets.[1m] Banerjee et al. have investigated the gelation properties of amino acids and various short peptides.[1n-1p] Over the last two decades β-and γ-peptides have emerged as promising tools to mimic the protein secondary structures.[2] As previously discussed in Chapter 1 and Chapter 2, the β-and γ-peptides displayed a wide range of helical organizations with expanded H-bond pseudocycles. Due to their structural diversity and enhanced proteolytic stability, homologated peptides have been utilized in the design of peptidomimetics to disrupt the protein-protein interactions.[3]In addition, the self-aggregation patterns of the peptides comprised of β- and γ residues have also been recently reported. Despite of their biocompatibility, structural diversity and chemical versatility, the β- and γ-peptides have not been well explored in the design of nano-structures and biomaterials.

3.1.2 Self-assembly of peptides containing β- and γ-amino acids

Fulop and colleagues have recently described the self assembly of short β- peptide foldamers into nano scaled fibres and membrane.[2k,4] They reported the short oligomer of *cis*-ACPC (*cis*-2-aminocyclopentane carboxylic acid) forms extended strand like structures which further self-assembles into nanofibers, while short oligomer of *trans*-ACHC (*trans*-2-aminocyclohexane carboxylic acid) are shown to adopt nano scaled membrane structures. In another interesting study Ortuno et al.[5] showed the self assembling properties of β-peptides comprised of *cis*-ACBC (*cis*-2-aminocyclobutane carboxylic acid). The short four residue oligomer of *cis*-ACBC forms nanofibrillar structures. Gellman and

colleagues[6] have also showed the formation of nanofibers from β-peptide foldamers and sheet like assembly from α/β-peptide hybrid foldamers. Furthermore, Granja et al.[7]

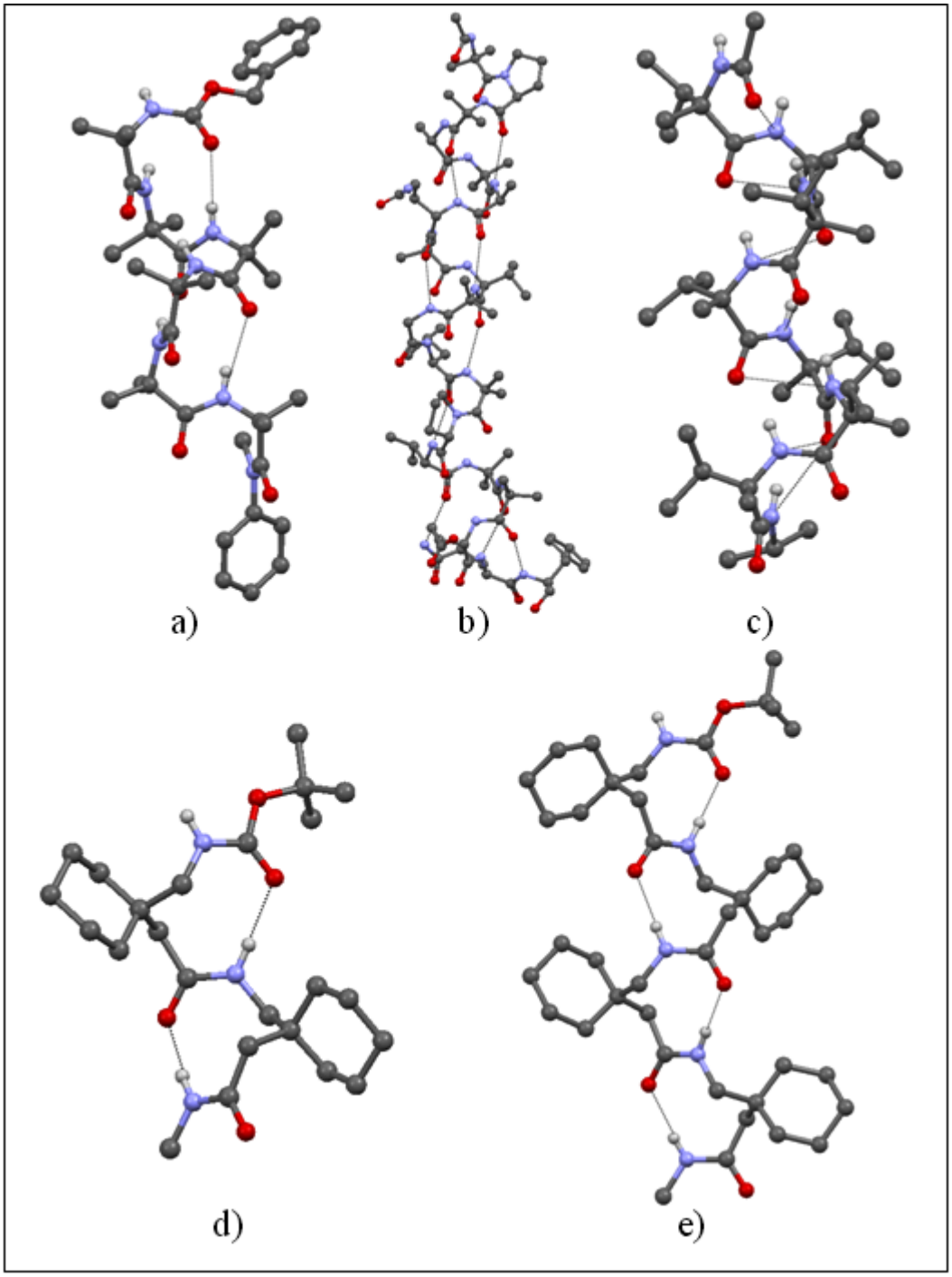

Figure 3.1 Helical conformations in crystals from geminal di-substituted amino acid containing peptides. a) Poly Aib peptide, Cbz-Aib_6-N(Me)Ph.[8g] b) Peptaibol, Alamethicin (PDB-1AMT). c) oligomer of α-methylated L-valine, Ac-[L-(RMe)Val]$_7$-NH*i*Pr.[10] d) Balaram et al.[12] reported C9-helical conformations from dipeptide (Boc-Gpn_2-NHMe) and e) tetrapeptide (Boc-Gpn_4-NHMe) oligomer of gabapentin.

have shown the remarkable nano tubular self assembly from the cyclic α/γ-hybrid peptides.

3.1.3 Geminally di-substituted amino acids in peptides

Helices are most widely studied protein secondary structures. Literature survey suggests that several efforts have been channelized for the synthesis of helical structure mimetics outside of the protein context. The α-amino isobutyric acid (Aib) has been extensively utilized in this regard to design α-peptide helical secondary structures. Balaram and Karle have extensively investigated the use of Aib in design of stable α-peptide helices.[8] Further, the helical conformations of various Aib rich peptides and homooligomers of Aib in single crystals have also been studied (Figure 3.1).[8] The structural analysis of Aib rich peptides reveal that the restriction in the backbone conformational space (ϕ and ψ) of Aib forced these peptides to adopt stable helical structures.[9] Several peptide natural products including peptaibols contains Aib in their primary sequence. Peptaibols are naturally occurring antibiotics; are rich in Aib residues which induce the helicity in their secondary structures (Figure 3.1). Besides their work regarding structural studies of Aib containing peptides, Toniolo and colleagues have showed helical conformational preference of peptides comprised of isovaline (α-methylated L-valine) (Figure 3.1).[10a] They also have investigated the conformational properties of various gem-dialkyl α-amino acid containing peptides and observed that homooligomers of gem-dialkyl α-amino acid mostly adopts helical conformations.[10] Gabapentin (neurontin) is geminally di-substituted γ-amino acid and widely used as antiepileptic drug.[2e] It is also being used in treatment of neuropathic pain.[11] Balaram laboratory[12] have extensively investigated gabapentin to design hybrid helical foldamers. The homooligomer of gabapentin adopts a stable C9 helical conformation in single crystals as shown in Figure 3.1. With this information in hand about folding propensities of peptides containing geminally di-substituted α-amino acids and γ-amino acids; we become interested to design and understand the conformational properties of γ-analogue of Aib homooligomers.

3.2 Results and discussion

3.2.1 Design and synthesis

The α-amino acid Aib (2-amino isobutyric acid) have higher propensity to induce the helicity when incorporated in peptide sequence.[9] As we have been working in the area of

hybrid peptides containing γ-amino acids to understand their conformational properties.[13] we sought to investigate the structural properties of γ-peptides containing double homologated Aib, 4, 4-gem-dimethyl substituted γ-amino acid (Aic, 4-amino isocaproic acid). Here in chapter 3 we are reporting the conformationally biased unusual extended polar sheet type of structures from Aic homooligomers (**P1**-**P4**), their unprecedented thermoreversible gels and supramolecular superstructures in various polar, apolar and protic solvents and their water resistance properties.

In order to understand conformational properties of $\gamma^{4,4}$-peptides, the $\gamma^{4,4}$-amino acid, Aic, was synthesized (as mentioned in Chapter 1) starting from N-Boc-Aib aldehyde as shown in Scheme 3.1.[14]All $\gamma^{4,4}$-peptides (**P1**-**P4**, Scheme 3.1) were synthesized in solution phase using standard DCC/HOBt coupling conditions and purified by column chromatography.

3.2.2 Synthesis of peptides

Dipeptide, tripeptide, tetrapeptide and pentapeptides were synthesized by conventional solution-phase methods using a fragment-condensation strategy. The *tert*-butyloxycarbonyl group was used for N-terminus protection, and the C-terminus was protected with ethyl ester. Deprotections were performed with trifluoroacetic acid and saponification for the N- and C-termini, respectively. Couplings were mediated by dicyclohexylcarbodiimide (DCC) and 1-hydroxybenzotriazole (HOBt). The dipeptide (**P1)** was prepared by coupling reaction between N-terminal Boc-Aic-OH and H-Aic-OEt. The tripeptide Boc-Aic-Aic-Aic-OEt (**P2**) was prepared by [2 + 1] condensation involving N-terminal dipeptide acid Boc-Aic-Aic-OH and H-Aic-OEt. The Tetrapeptide Boc-Aic-Aic-Aic-Aic-OEt (**P3**) was prepared by [2+2] condensation involving N-terminal dipeptide acid Boc-Aic-Aic-OH and H-Aic-Aic-OEt. The pentapeptide Boc-Aic-Aic-Aic-Aic-Aic-OEt (**P4**) was prepared by [3 + 2] condensation involving N-terminal tripeptide acid Boc-Aic-Aic-Aic-OH and H-Aic-Aic-OEt.

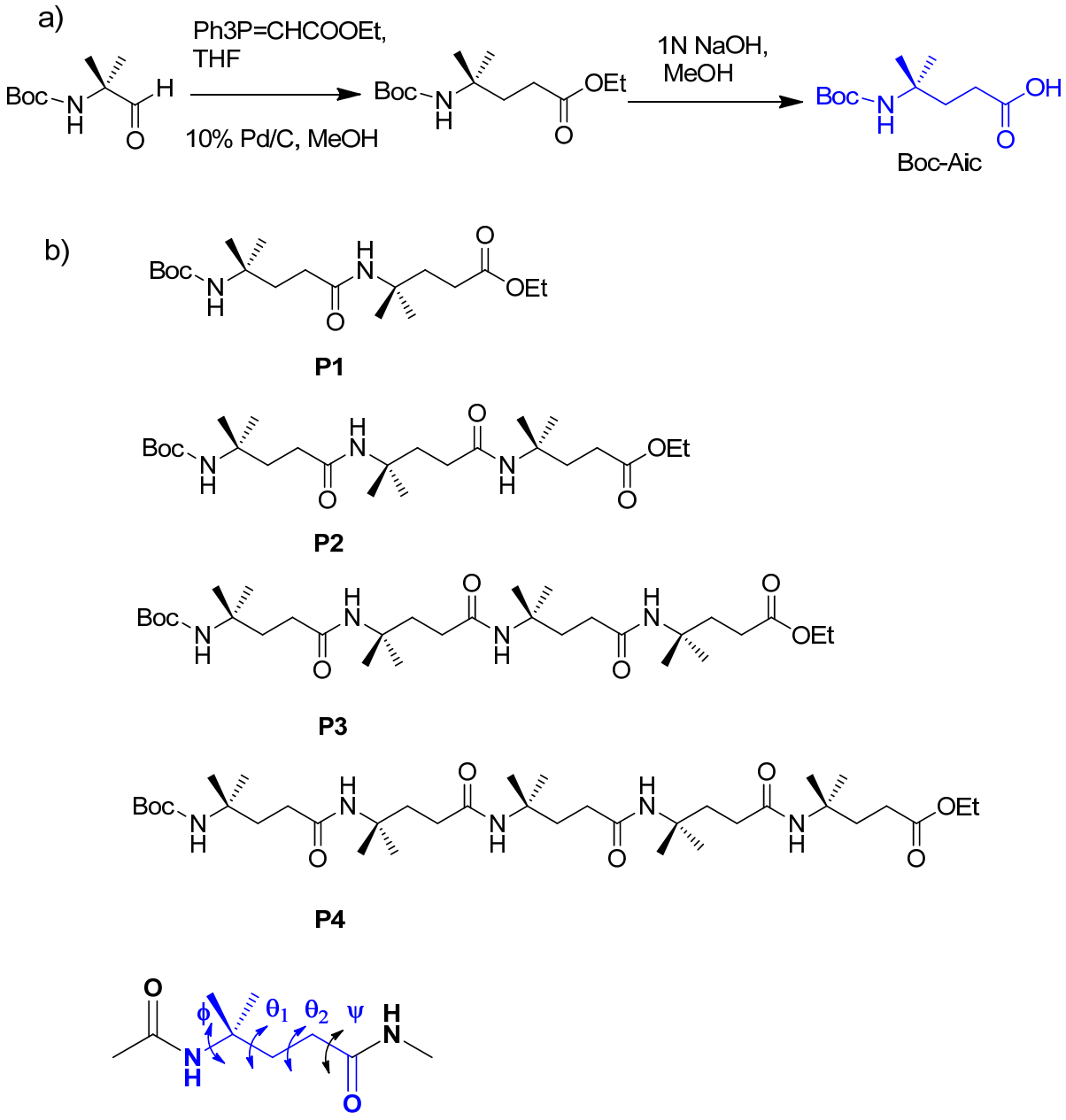

Scheme 3.1 a) Synthesis of N-Boc-Aic from N-Boc-Aib. b) Chemical structures of Aic homooligomers and local torsional variables of γ-residues.

3.3 Structural characterization of peptides

3.3.1 Single crystal X-ray analysis.

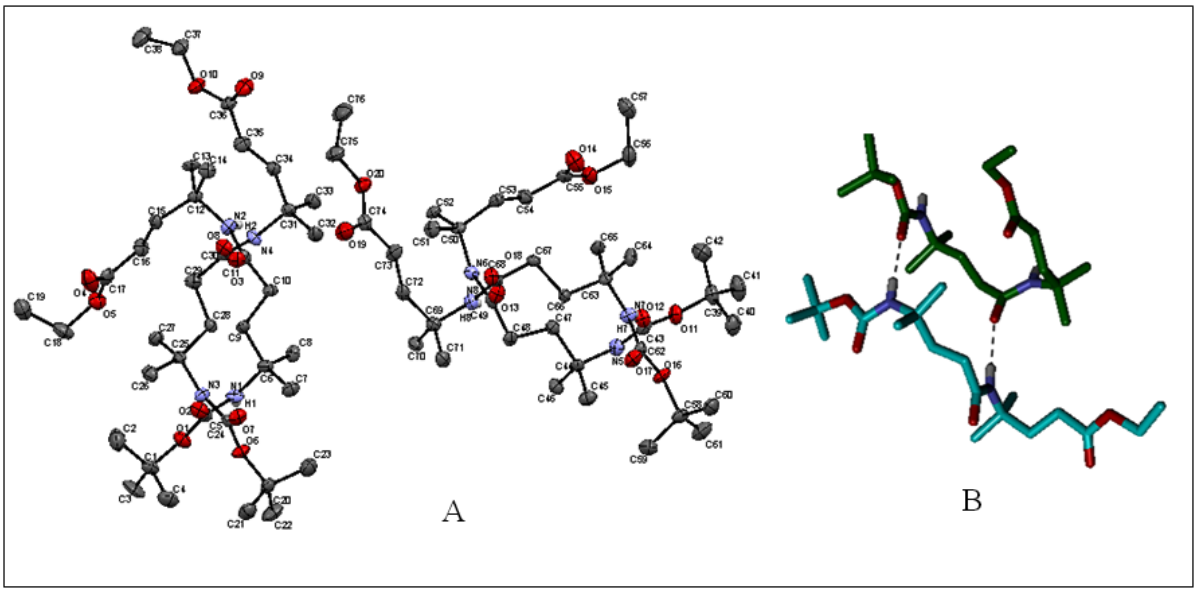

Figure 3.2 X-ray structures of Aic homooligomers **P1**. A) Packing of dipeptide **P1** in unit cell as viewed down the crystallographic a-axis. Only polar H-atoms are shown for clarity. Ellipsoids are drawn to 50% probability. B) Intermolecular hydrogen bonding in **P1** suggesting polar parallel sheet type structures.

The homooligomers of α-amino acids, Aib, is known to form stable helical structures in solution and solid state, therefore, we are interested to know the folding properties of homooligomer of Aic (4-amino isocaproic acid) both in solution and solid state. To understand the conformational properties of Aic homooligomers in solid state, we subjected pure γ-peptide for crystallization in various solvents and solvent combinations. Suitable X-ray quality single crystals of the peptides **P1** were obtained after the slow evaporation from the aqueous methanol solution and their X-ray structure is shown in the Figure 3.2. Crystal structure analysis reveals the presence of four molecules of **P1** in the asymmetric unit. Surprisingly, the peptides adopted parallel extended planar structures stabilized by two intermolecular H-bonds. In contrast, peptides with 3, 3-gem-dialkyl γ-amino acid and 3, 4–disubstituted γ-amino acid residues shows C9-helical conformations (see Figure 3.2.1) in single crystals.[12,15]Investigation reveals that one of the molecules in the asymmetric unit acts as H-bond donor and other acts as H-bond acceptor. Similar trend was also observed in the other molecular pair in the asymmetric unit suggesting the polar sheet type of character in the dipeptide. The backbone conformations were measured by introducing two

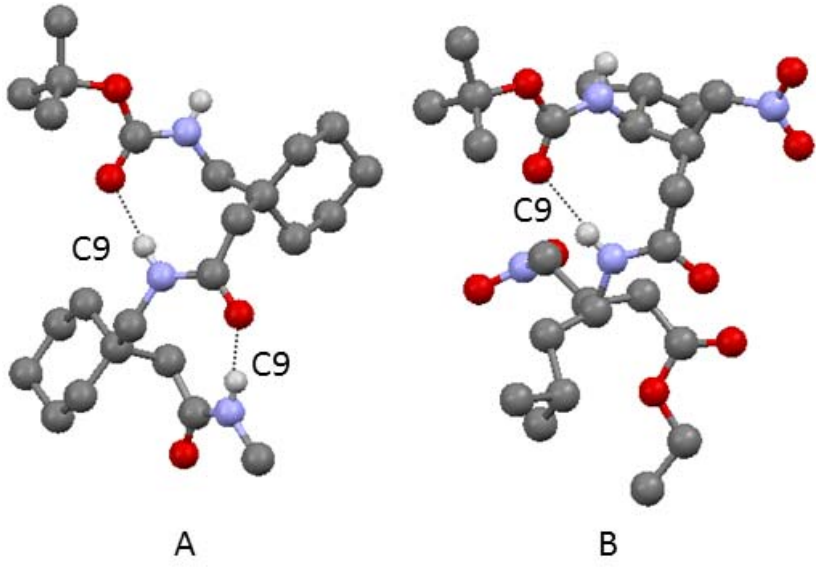

Figure 3.2.1 C9-helical conformations observed in A) Boc-Gpn-Gpn-NHMe[12] and B) Boc-NH-γV(β-CH_2NO_2)-γL-(β-CH_2NO_2)-COOEt[15]

additional torsional variables θ_1 (N-C^{γ}-C^{β}-C^{α}) and θ_2 (C^{γ}-C^{β}-C^{α}-C') along with the ϕ (C'-N-C^{γ}-C^{β}) and ψ (C^{β}-C^{α}-C'-N) (Scheme 1b).[16]

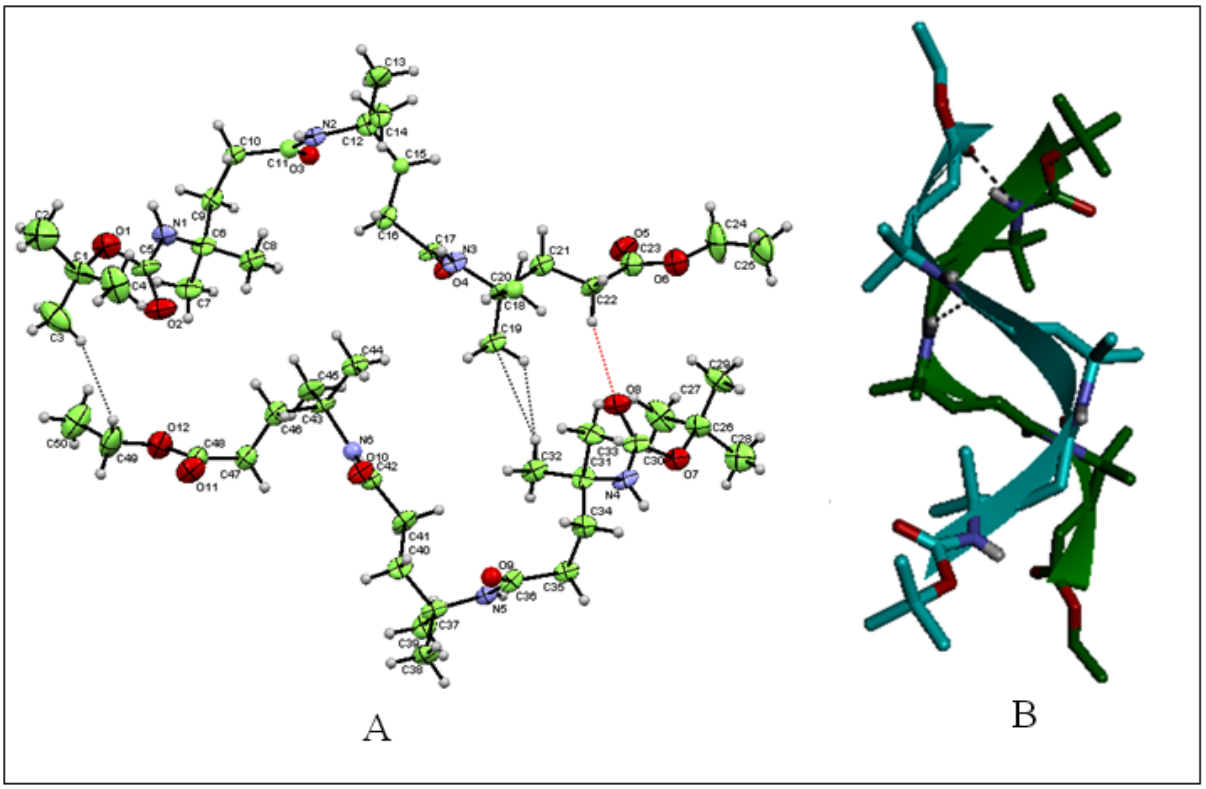

Figure 3.3 A) Arrangement of peptide **P2** in crystal packing which depicts the lateral supramolecular arrangement of molecule through intermolecular hydrophobic interactions (shown in dotted black lines) and

CH----O hydrogen bonding (shown in red dotted lines). Hydrogens are not labelled for clarity. Ellipsoids are drawn to 50% probability. B) Intermolecular Hydrogen bonding in **P2** drives double helical structure.

The torsional angle ϕ adopted *gauche* conformation with the value ± ~60°. The other torsional variables θ_1, θ_2 and ψ are adopted either *gauche* or antiperiplanar conformations.

The single crystal of **P2** suitable for X-ray diffraction was obtained after slow evaporation of methanol solution. The analysis of the single crystal structure of **P2** suggested the presence of two molecules in the asymmetric unit. Intriguingly, the molecules twisted around each other in an antiparallel fashion to give a remarkable double helix type of structure (Figure 3.3). The structure is stabilized by three intermolecular H-bonds. No intramolecular H-bonds observed in the crystal structure. In stark contrast to the stable helical conformations adopted by the other γ-peptides,[17] a marked conformational bias is observed in the Aic homooligomers. Similar to the dipeptide, all NHs of the one molecule in the asymmetric unit is involved in the H-bonding with the carbonyls of the other

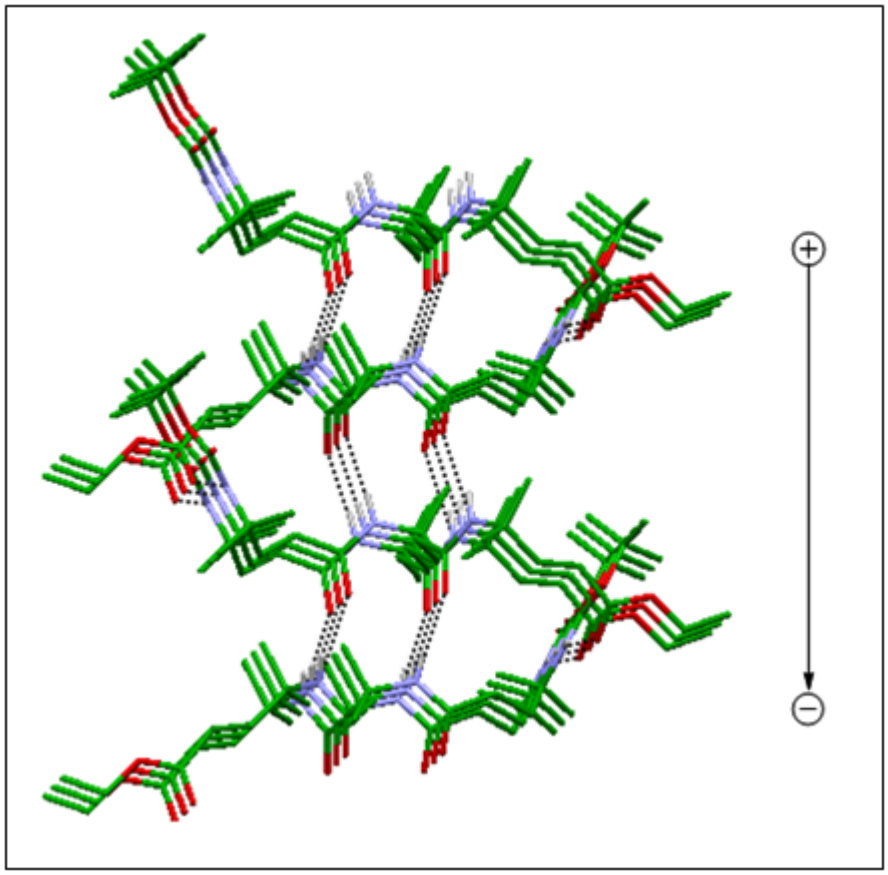

Figure 3.4 Packing of Aic homooligomer **P2** in crystals depicting polar sheet character. Arrow indicates direction of dipole in molecule

molecule, suggesting a polar sheet type of character in the tripeptide as well (Figure 3.4). This polar sheet character is generally forbidden in the α-peptide β-sheets.[18] α-Peptide β-sheets forms 12 membered H-bond pseudo-cycles when they are parallel β-sheet and 10/14-membered H-bond pseudo-cycles in antiparallel β-sheets. γ-Peptides forms expanded 16 membered H-bond pseudo-cycles both in parallel and antiparallel sheet structures. All exposed NHs and the carbonyl groups of the two strands are involved in the intermolecular H-bonding with other tripeptides. The torsional angles and the H-bond parameters of **P1** and **P2** are given in the Table 3.1 and 3.2. The survey of the crystal conformations of γ-residue containing peptides in the literature and our work presented in Chapter 2 reveals that to induce helical conformations, both torsional angles θ_1 and θ_2 must adopt *gauche* conformations (± ~ 60°), while ideal extended structures can be achieved by having the *anti* (*t*) conformations ($\theta_1 = \theta_2 = \pm 180°$).[2a, 2d, 17] It is noteworthy to mention that, torsional variables θ_1 and θ_2 in **P1** and **P2** mostly adopted *gauche* and *anti*

Table 3.1 Torsion angles [°] for **P1**

Boc-Aic-Aic-OEt

(There are four molecules in asymmetric unit of **P1**)

i) **Molecule A**

residue	ϕ	θ_1	θ_2	Ψ
Aic 1	-61.93	**-174.86**	**-172.34**	-86.89
Aic 2	-65.15	**-59.23**	**171.00**	-176.68

ii) **Molecule B**

residue	ϕ	θ_1	θ_2	Ψ
Aic 1	58.75	**169.29**	**174.46**	73.26
Aic 2	60.57	**-51.05**	**179.55**	-169.81

iii) **Molecule C**

Residue	ϕ	θ_1	θ_2	Ψ
Aic 1	61.23	**174.90**	**172.28**	86.54
Aic 2	65.36	**59.57**	**-170.91**	177.09

iv) **Molecule D**

Residue	ϕ	θ_1	θ_2	Ψ
Aic 1	-59.54	**-169.19**	**-174.82**	-72.44
Aic 2	59.29	**51.93**	**-179.58**	169.48

Table 3.2 Torsion angles [deg] for **P2**

Boc-Aic-Aic-Aic-OEt

(There are two molecules in asymmetric unit of **P2**)

i) **Molecule A**

Residue	ϕ	θ_1	θ_2	Ψ
Aic 1	176.79	**65.75**	**97.86**	-138.81
Aic 2	-57.63	**-45.08**	**-157.71**	104.29
Aic 3	59.32	**170.41**	**173.51**	149.54

ii) **Molecule B**

Residue	ϕ	θ_1	θ_2	Ψ
Aic 1	-179.42	**-75.85**	**-89.34**	137.57
Aic 2	62.34	**57.88**	**-179.46**	-144.01
Aic 3	-58.13	**-47.67**	**-172.77**	103.96

conformations along N-C^{γ}-C^{β}-C^{α} and C^{γ}-C^{β}-C^{α}-C' probably leading to the formation of polar extended structures. In order to understand the solution state conformation, we subjected **P2** for 2D NMR analysis in $CDCl_3$ (6 mM). The analysis reveals the absence of

long distance NH↔NH and NH↔CH NOEs and the strong inter- residue (i to i+1) $C^{\alpha}H\leftrightarrow$ NH and intra-residue $C^{\beta}H\leftrightarrow$NH NOEs suggesting the extended sheet type of conformation similar to the γ-peptides containing conformationally restricted peptides containing *E*-vinylogous amino acids and cyclic γ-residues.[19]

3.3.2 Remarkable thermoreversible self-assembly from γ-peptides.

The unusual extended polar sheet type of conformation observed in the tripeptide **P2** encouraged us to grow the single crystals of peptides **P3** and **P4** in various solvents and solvent combinations. Surprisingly, both the peptides formed gel on standing in methanol, isopropanol, toluene and benzene. Astonished by the solvent gelation of these peptides, we investigated the minimum concentration that required for the gelation and found that 2 mg/mL is sufficient to get stable gels in various solvents such as toluene, benzene,

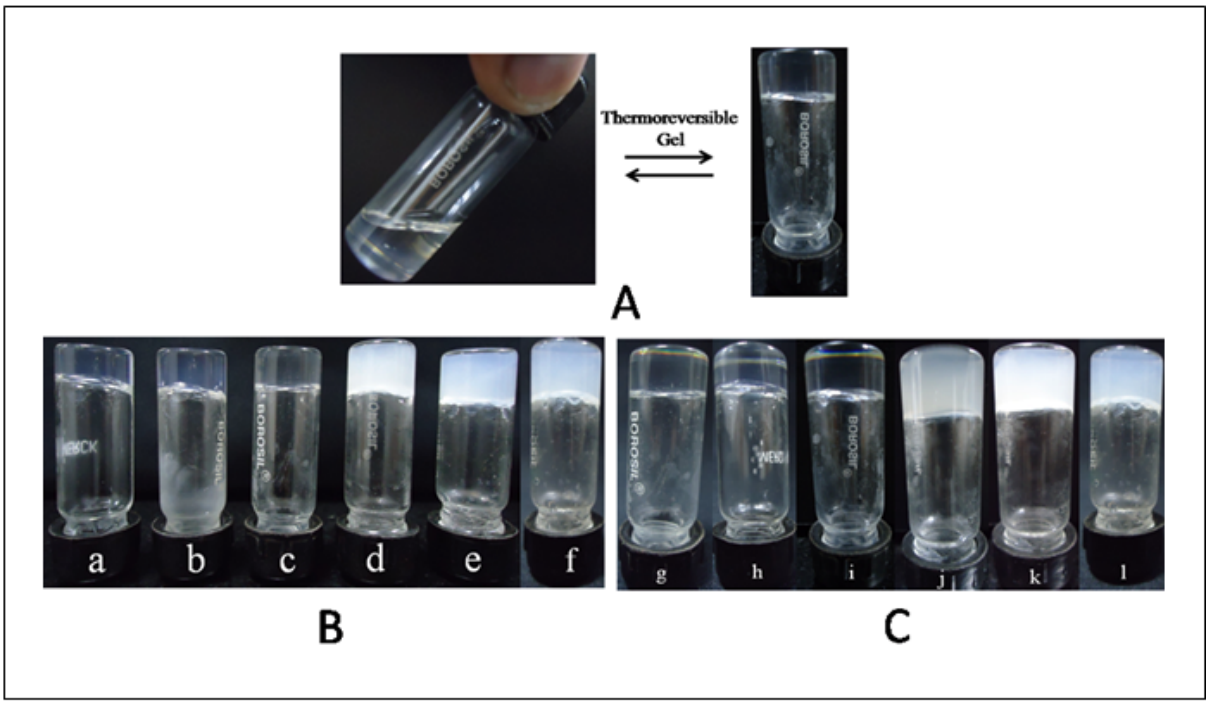

Figure 3.6 A) Thermoreversible gel formation is shown for Peptide **P3** in Toluene. Also, all other solvents are able to form thermoreversible gels. **P4** also forms thermoreversible gel in all above solvents. B) Inverted sample vial test to confirm the gel formation for the peptide **P3** in a) Benzene, b) Toluene, c) Isopropanol, d) DMF/Water (95:5), e) DMSO/Water (95:5) and f) Diglyme/Water (95:5). C) Inverted sample vial test to confirm the gel formation for the peptide **P4** in g) Benzene, h) Toluene, i) Isopropanol, j) DMF/Water (95:5), k) DMSO/Water (95:5) and l) Diglyme/Water (95:5).

isopropanol, 95% DMSO in H_2O, 95% DMF in H_2O and 95% diglyme in H_2O. Interestingly, transparent gels were obtained in the toluene, benzene and isopropanol and

opaque gels were obtained in the 95% DMSO, 95% DMF and 95% diglyme. The inverted vial experiments depicting the gel formation of peptide **P3** in various solvents is shown in Figure 3.6. Similar results were also observed for **P4** (Figure 3.6). Spontaneous gelation of the peptides in various organic solvents was also observed after the sonication; however, it is not required. All gels are found to be thermoreversible, on heating all gels transformed into solution state and reconstituted to gel on cooling. The detailed gelation properties of peptide **P3** and **P4** are tabulated in Table 3.3. The self assembling properties of α-peptides based biomaterials and other low molecular weight gelators has extensively studied and

Table 3.3. Gelation attempts for peptide **P3** and **P4** in various solvents

Solvent	P3	P4
Benzene	TG	TG
Toluene	TG	TG
o-Xylene	TG	TG
p-Xylene	TG	TG
n-Hexane	I	I
Kerosine	I	I
Petrolium	I	I
Methanol*	TG	TG
Isopropanol*	TG	TG
Chloroform	S	S
Dichloromethane	S	S
DMF	S	S
DMSO	S	S
Diglyme	S	S
DMF:H_2O(95:5)	OG	OG
DMSO:H_2O(95:5)	OG	OG
Diglyme:H_2O(95:5)	OG	OG

TG = Transparent Gel, I = Insoluble, S= Soluble, OG = Opaque Gel.
* forms transparent gel on standing for 2-3 days in partially open sample vial.

shown for their applications in various fields ranging from tissue engineering to molecular electronics.[20] The unprecedented gelation properties of short γ-peptides presented here may open possibilities of the wide range applications of these new generation biomaterials.

3.3.3 Two Dimensional-Nuclear Magnetic Resonance (2D-NMR) derived structures of γ-peptides

γ-Peptides **P3** and **P4** have formed stable gel in various organic solvent except chloroform even after standing for several days. As no gelation is observed in chloroform, we subjected these peptides to the 2D NMR analysis in $CDCl_3$ to understand their solution conformations. Unambiguous peak assignments were performed using TOCSY, COSY and ROESY spectra (Figure 3.7-3.12). No NH↔NH and long range NH↔CH NOEs were observed in both the peptides, however, the strong $C^{\alpha}H$↔NH NOEs were observed between i to i+1 residues suggesting the extended type of planar structures similar to the tripeptide **P2**. The NOEs observed in the ROESY spectrum of **P3** and **P4** is shown in Figure 3.13. Further, to know the inter-or intramolecular nature of H-bonding in **P3**, the temperature dependent ^1H NMR experiment was undertaken. In the experiment, the solution of **P3** in $CDCl_3$ was gradually heated from -40 °C to +40 °C and chemical shifts for all NHs were acquired after each 10 °C interval. Results of the experiments are shown in Figure 3.14. It has been observed a clear upfield shift of all NHs with increasing temperature suggesting the involvement of amide NHs in intermolecular H-bonding. However, urethane amide NH1 was found to show less upfield shift as compared to other amide NHs with increasing temperature.

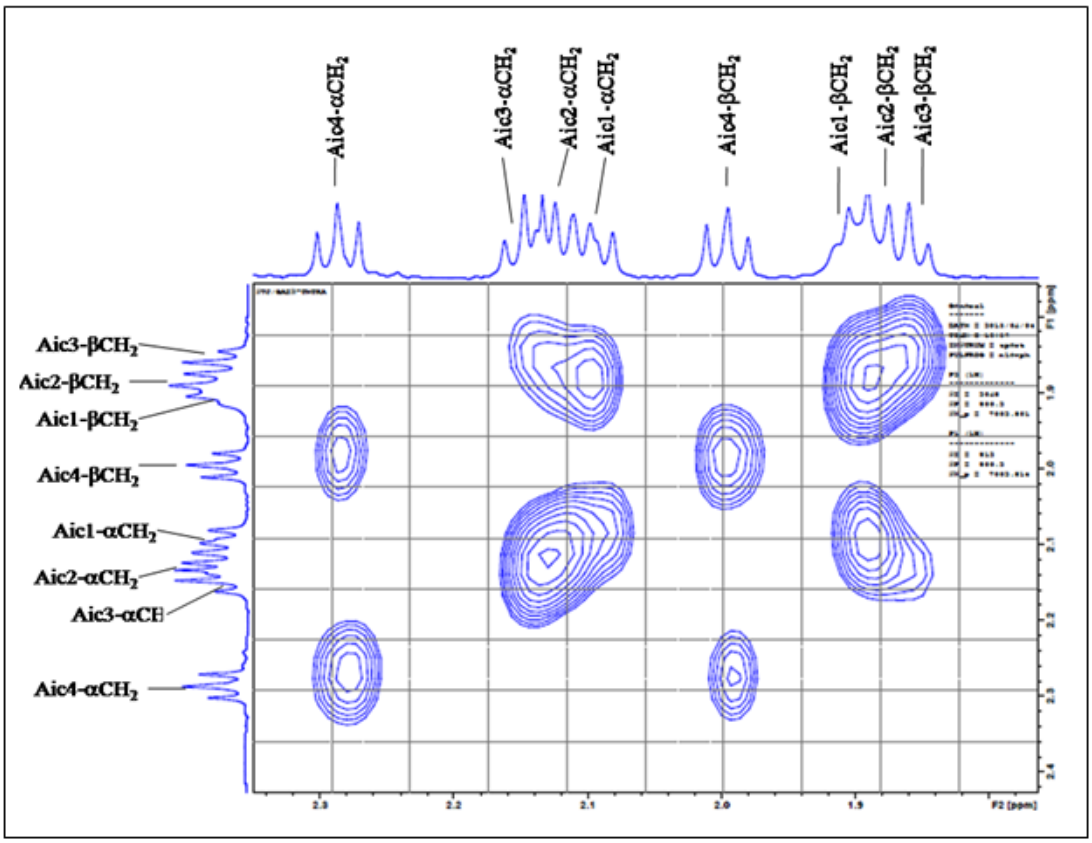

Figure 3.7 Partial TOCSY NMR spectrum of **P3** (3 mM) in $CDCl_3$.The sequential assignment of -CH_2 protons were performed using ROESY.

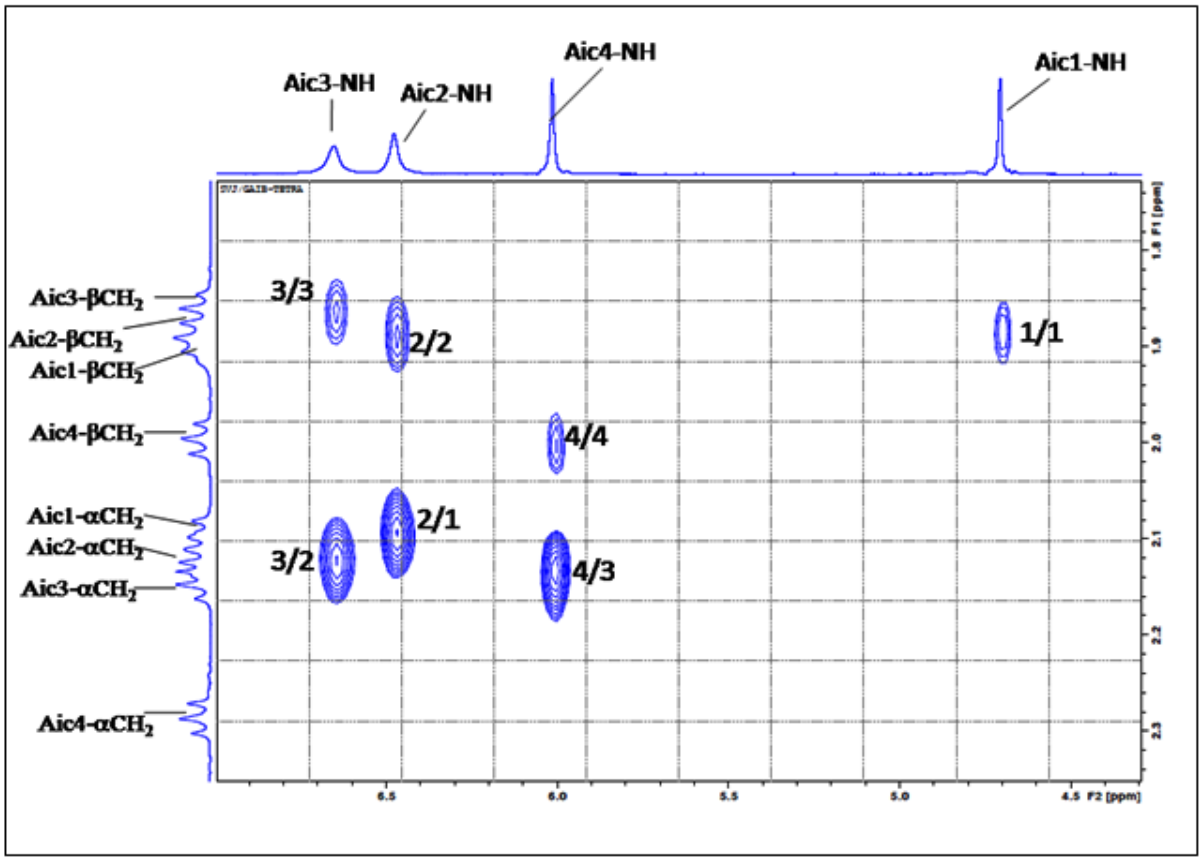

Figure 3.8 Partial ROESY spectrum of **P3** (3 mM) in $CDCl_3$ showing peaks for amide and methylene proton interactions depicting extended sheet structure.

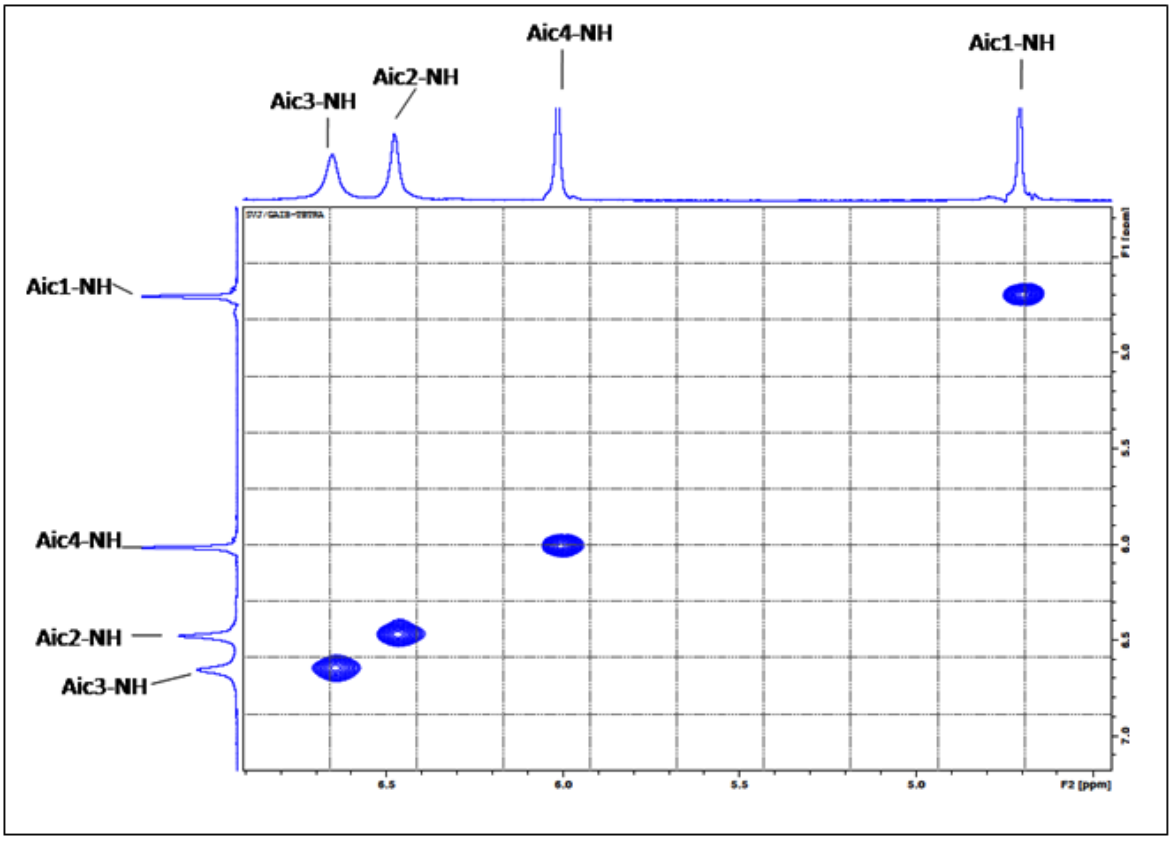

Figure 3.9 Partial ROESY spectrum of **P3** (3 mM) in $CDCl_3$ showing no interaction between amide protons through space.

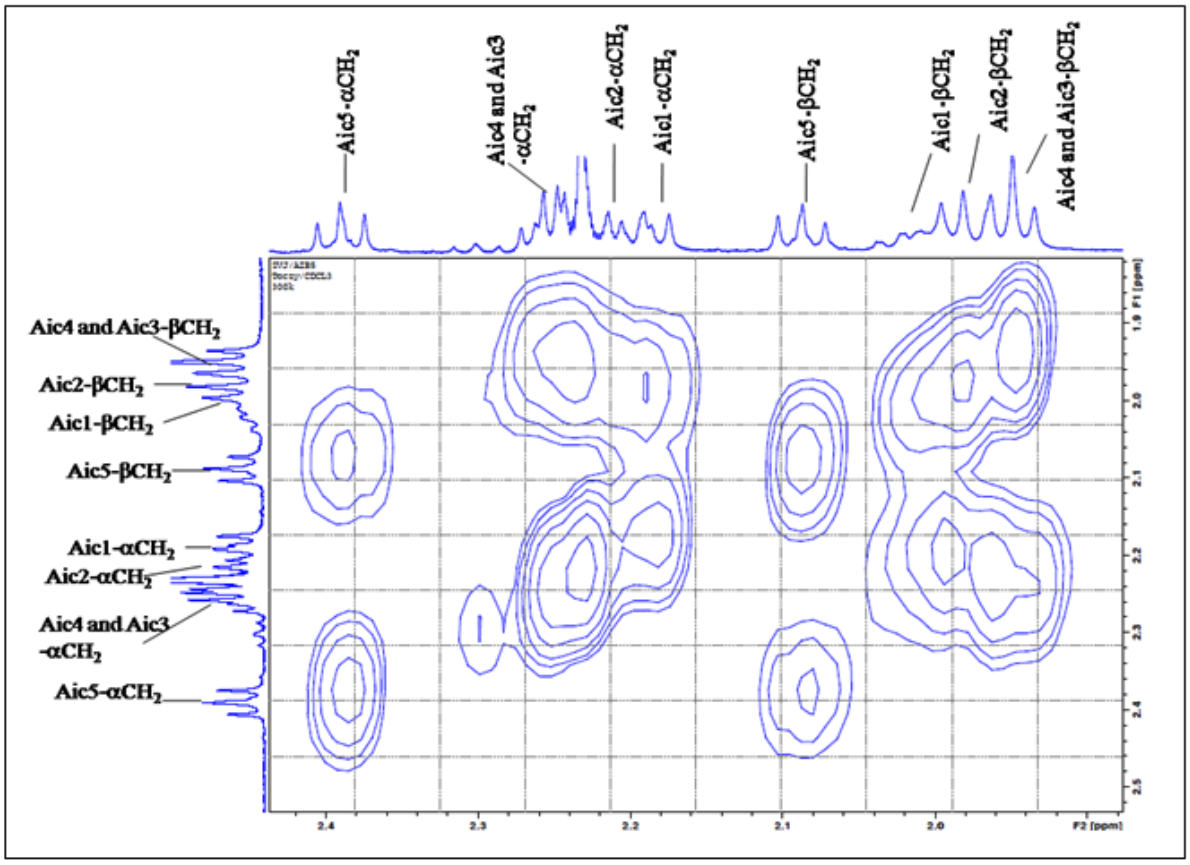

Figure 3.10 Partial TOCSY NMR spectrum of **P4** (2.0 mM) in $CDCl_3$.The sequential assignment of -CH_2 protons were performed using ROESY.

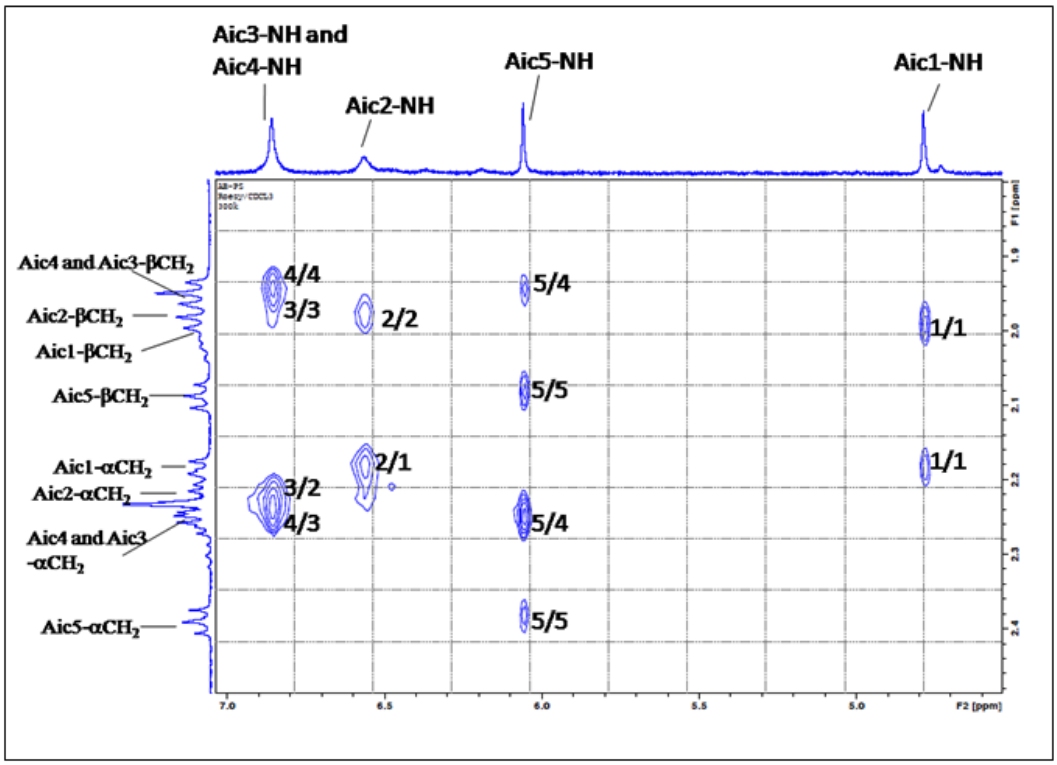

Figure 3.11 Partial ROESY spectrum of **P4** (2.0 mM) in $CDCl_3$ showing peaks for amide and methylene proton interactions depicting extended sheet structure.

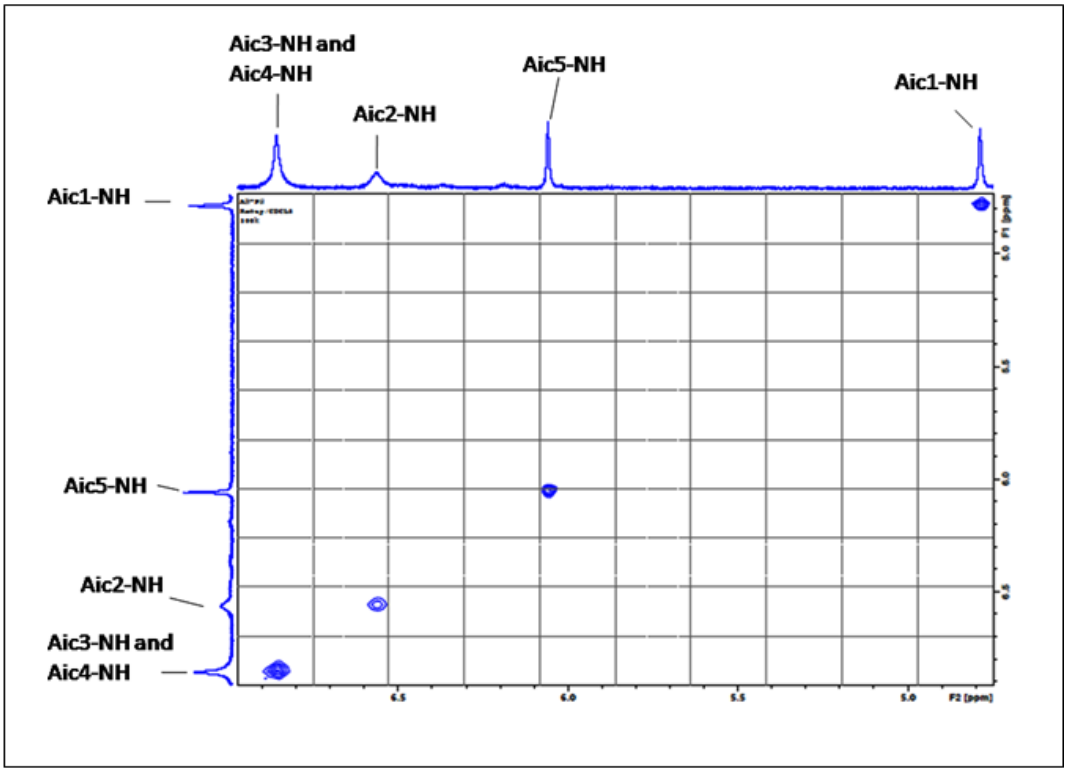

Figure 3.12 Partial ROESY spectrum of **P4** (2.0 mM) in $CDCl_3$ showing no interaction between amide protons through space.

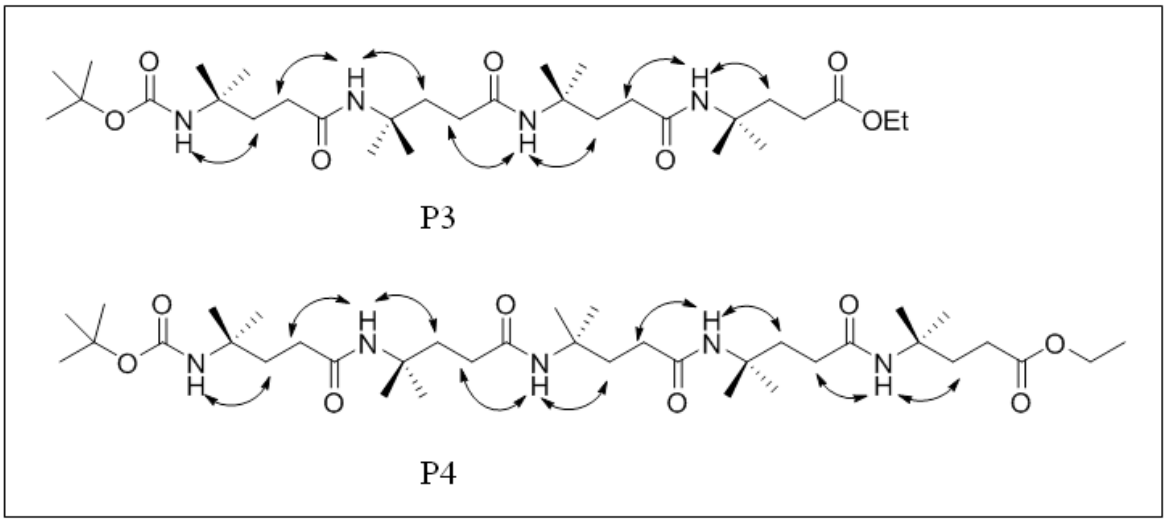

Figure 3.13 NOEs observed in the 2D NMR are highlighted with double headed arrows in both the peptides **P3** and **P4**. No long distance NOEs were observed suggesting extended structures of peptide.

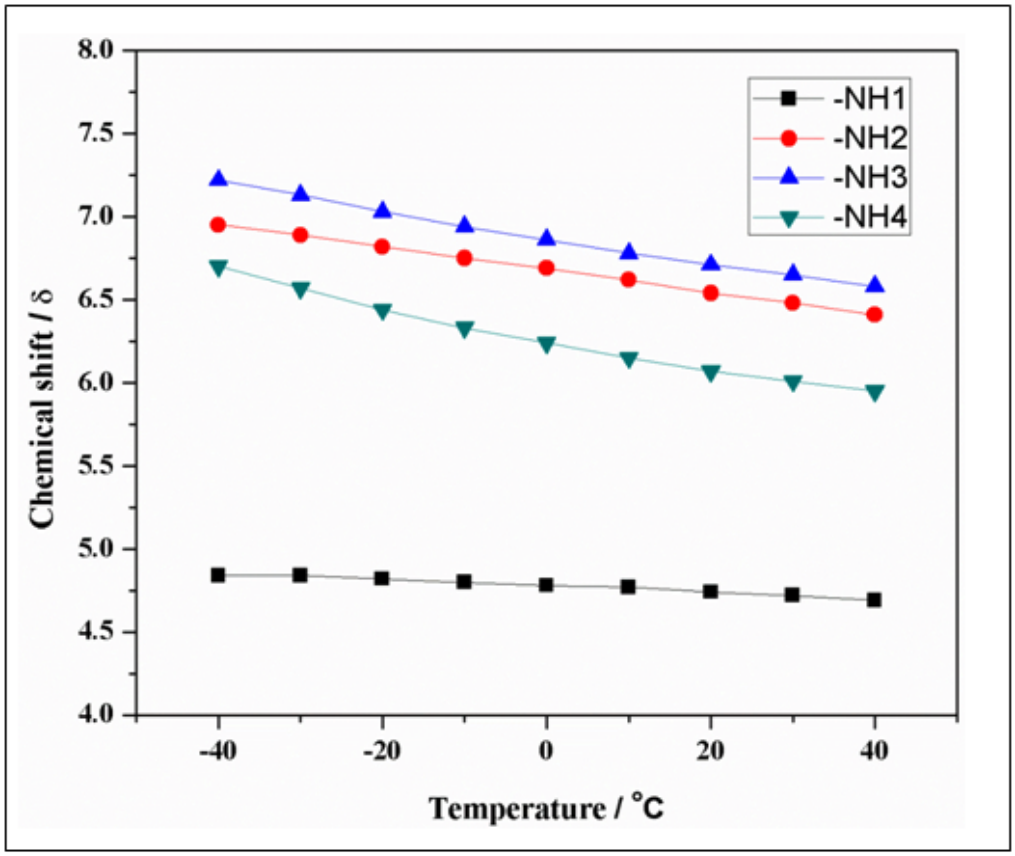

Figure 3.14 Upfield chemical shift for all amide protons is observed in ^{1}H NMR for peptide **P3** when temperature was varied from -40 to +40 ^{o}C. Spectra were recorded on 500 MHz spectrometer in $CDCl_3$ as solvent.

3.3.4 FT-IR studies support extended structures of P3 and P4

We further probed the characteristic signature of NH---O=C of Aic homooligomers to understand the H-bond mediated aggregation using FT-IR. The IR spectra of xerogels of **P3** and **P4** are shown in experimental section. Peptides **P3** and **P4** displayed a sharp NH stretching vibration (ν_{NH}) at 3270 cm^{-1} and 3273 cm^{-1}, respectively. These results support the involvement of amide NHs in the intermolecular H-bonding. Further, the amide I and amide II bands, which are directly related to the backbone conformations, were found to be 1637 cm^{-1} and 1555 cm^{-1}, respectively in **P3**. Similarly, **P4** also displayed amide I and amide II bands at 1640 cm^{-1} and 1553 cm^{-1}, respectively (See experimental section). The FT-IR values observed for Aic homooligomers are in close agreement with the values observed in the poly(Ala) infinite β-sheets.[21] All these experimental evidences support the extended conformations of the Aic homooligomers.

3.4 Morphology study of self-assembled γ-peptides

Morphologies of the organogels of **P3** and **P4** along with **P2** were studied using AFM (atomic force microscopy) and FE-SEM (field-emission scanning electron microscopy). The AFM images of **P2** in methanol and xerogels of **P3** and **P4** in toluene are shown in Figure 3.15. A network of entangled nanofibrillar aggregates of **P3** and **P4** were observed in the AFM on a mica surface. The formation of ribbon-like one-dimensional fibrils in both the peptides **P3** and **P4** suggests the similar type of self-aggregation in both the peptides. FE-SEM micrographs of **P2** in methanol are shown in Figure 3.16 which suggest the tentacle like structures. FE-SEM micrographs of **P3** xerogels in 95% DMSO and toluene and xerogels of **P4** in toluene and diglyme are shown in Figure 3.17A, 3.17B, 3.17C and 3.17D, respectively. SEM images show that the fibrils form a network with branches and entangle with each other. The diameter of fibers was found to be ranging from 120-150 nm. In toluene, more compact fibrillar network was observed compared to the 95% DMSO. In case of **P4** wider flat ribbon-type aggregations were observed from xerogels obtained in MeOH (Figure 3.18). The morphological experiments of organogels suggested that both the peptides **P3** and **P4** self-aggregate in a hierarchical fashion to form supramolecular nanostructures. These supramolecular nanostructures are further cross-linked through smaller fibrillar structures to form a larger network of superstructures. The hierarchical aggregation of peptides is promoted by the intermolecular back-bone amide H-bonds as well as van der Waals interactions of side-chains.

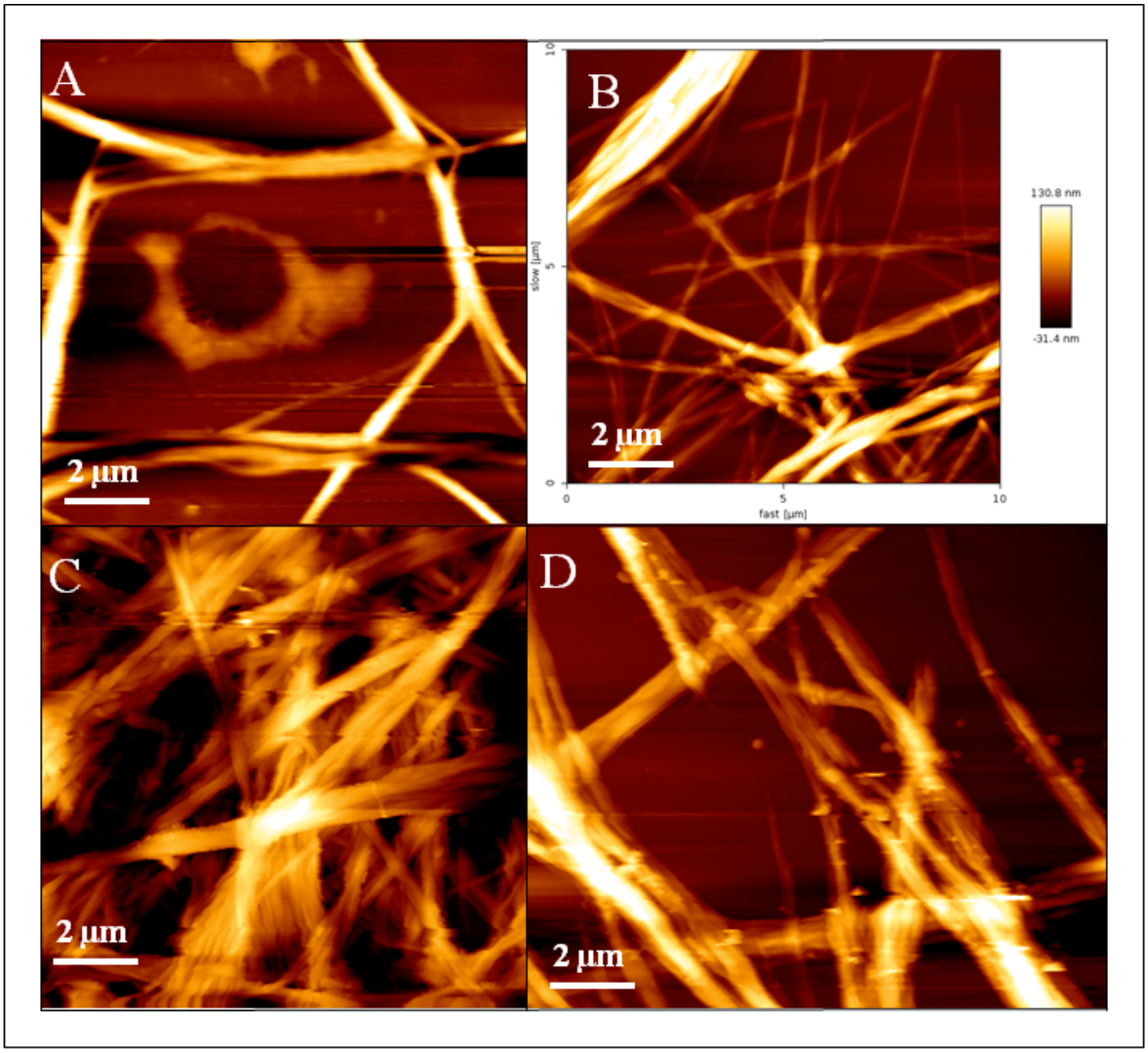

Figure 3.15 AFM images of A) **P2** in MeOH. B) and C) Xerogel of **P3** in Toluene. Height bar of xerogel morphologies is also shown. D) Xerogel of **P4** in Toluene.

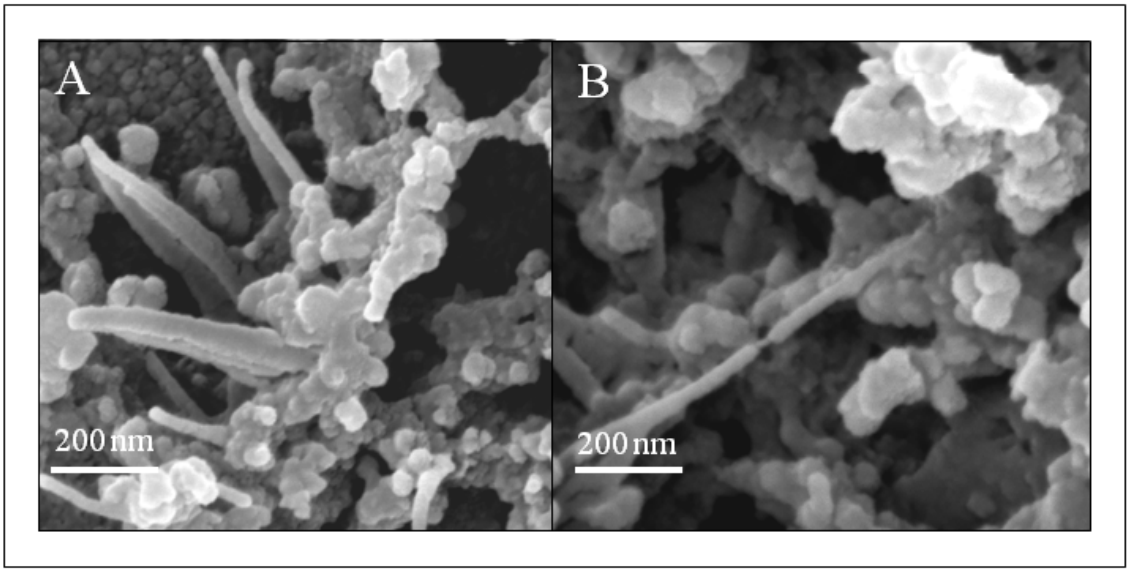

Figure 3.16 SEM microscopic images for **P2** in MeOH.

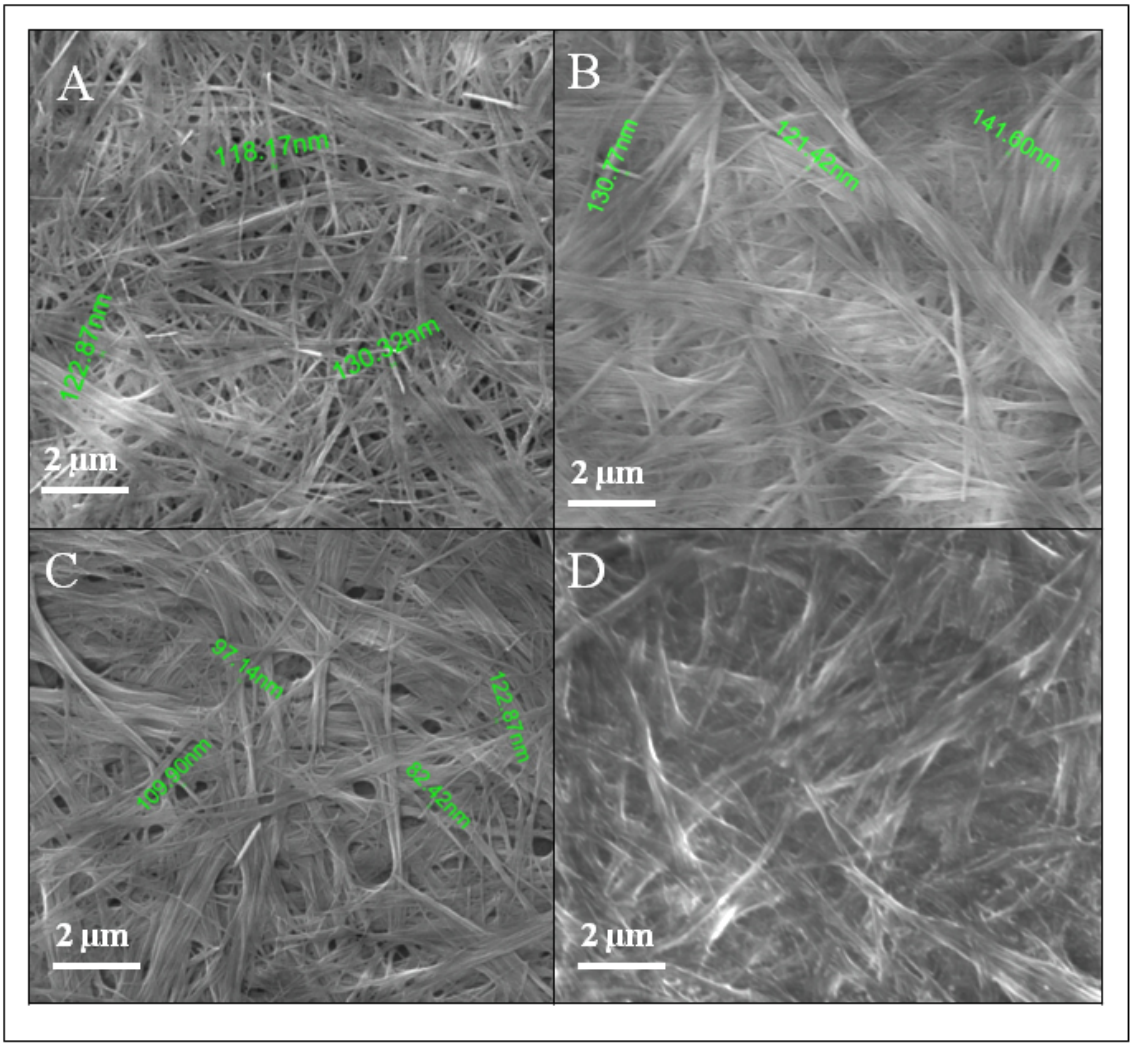

Figure 3.17 SEM images for xerogel of **P3** in A) 95% DMSO in water and B) in Toluene. SEM images for xerogel of **P4** in C) Toluene and D) 95% Diglyme in water.

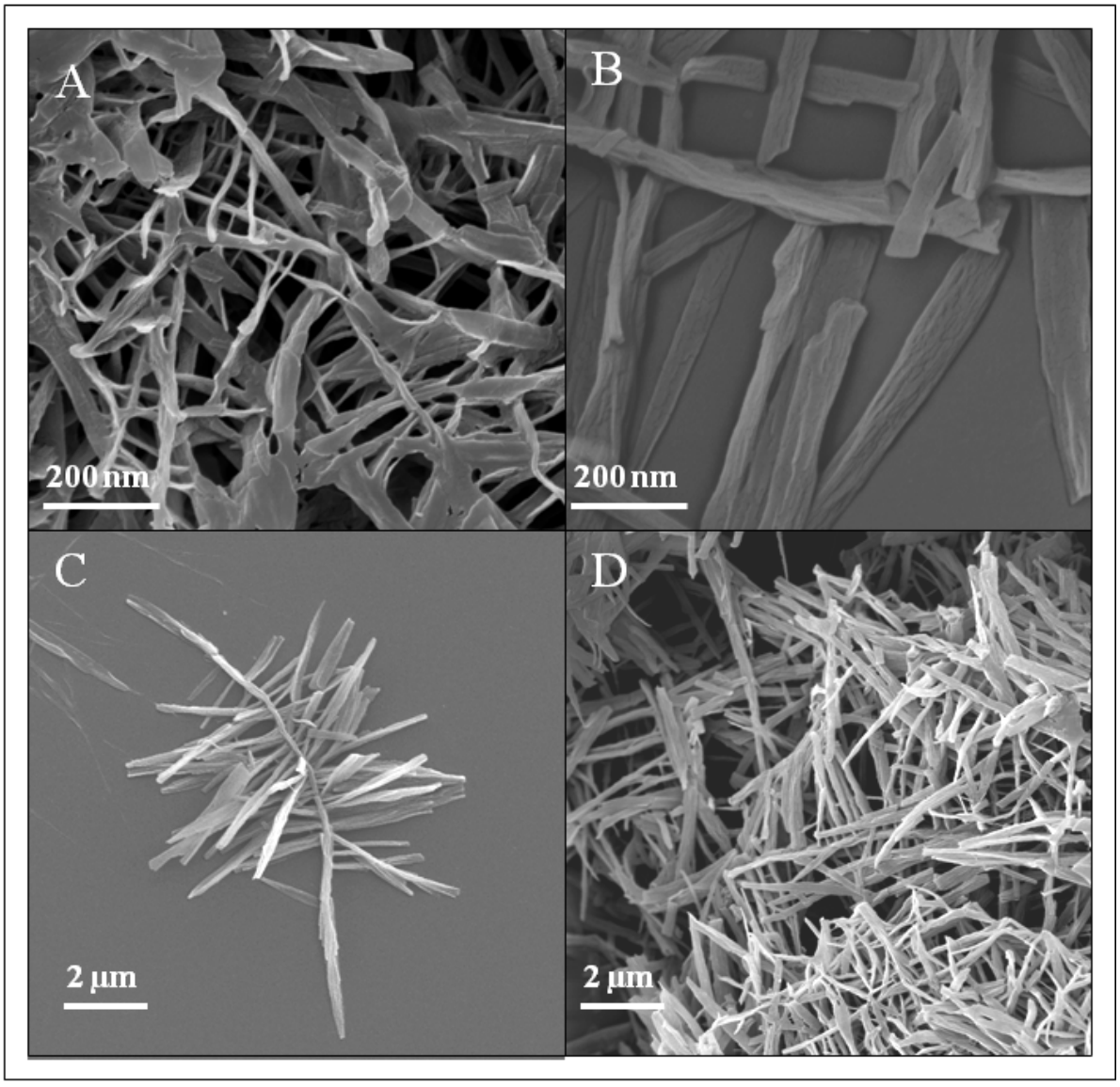

Figure 3.18 A)-D) Flat ribbon kind of morphologies observed for xerogel of **P4** in Methanol.

3.5 Rheology: Visco-elastic properties of γ-peptide gel.

In order to understand the viscoelasticity and self-healing properties of the γ-peptide organogels, rheological studies were undertaken. The experiments were performed on 0.2 % w/v concentrations of **P3** in toluene. The strain-sweep experiment at constant oscillating frequency showed that the storage modulus (G′) is substantially larger than the loss modulus (G″), which suggests the dominant elastic behavior of the γ-peptide organogel (Figure 3.19A). This measurement provides the information regarding the plateau region over which the gel state is retained. The crossover of G′ and G″ was observed at 49.39% strain. Further, the temperature-ramp rheological experiments were performed to understand the self-healing behavior of P3 organogel. Experiment was carried out using 0.2 % w/v concentrations of **P3** in toluene from 0 to 90 °C with a ramp of 2 °C/min at 0.05% strain amplitude and frequency of 10 rad/s (Figure 3.19B). During the heating cycle, both G′ and G″ values were slightly decreased up to 50 °C and more pronounced decrease was observed between 55-62 °C. To determine the change in G′ and G″ upon reconstitution, the system was subjected for cooling from 90 to 0°C, and the function of G′ and G″ was monitored. As shown in Figure 19B, on cooling the storage modulus (G′) which was initially less than the loss modulus surpasses G″ value at 37.1 °C. Similar results were also observed in the other organogels of **P3** and **P4**. Rheology experiments demonstrate the remarkable thermoreversible and self-healing behavior of these γ-peptide organogels.

3.6 Waterproofing: Water resistant properties of γ-peptide gel.

Owing to their biocompatibility, functional group versatility and easy synthesis, peptide biomaterials are gaining momentum for their use in regenerative medicines to nano devices. γ-Peptides have shown enhanced proteolytic stability as compared to their α-analogues. We have shown the formation of remarkable gel structures from newly designed γ-peptides. As these Aic γ-peptides are fully hydrophobic in nature, we anticipate that these kinds of soft materials can be used as water resistant proofs on the functional and hydrophilic surfaces. To test our hypothesis, a water drop was casted on a dry tissue paper coated with xerogel of **P3** in toluene. The tissue paper coated with peptide xerogel indeed showed resistance to the water absorption. This property of the peptide may open wide applications in biomedicine and water resistant biomaterials.

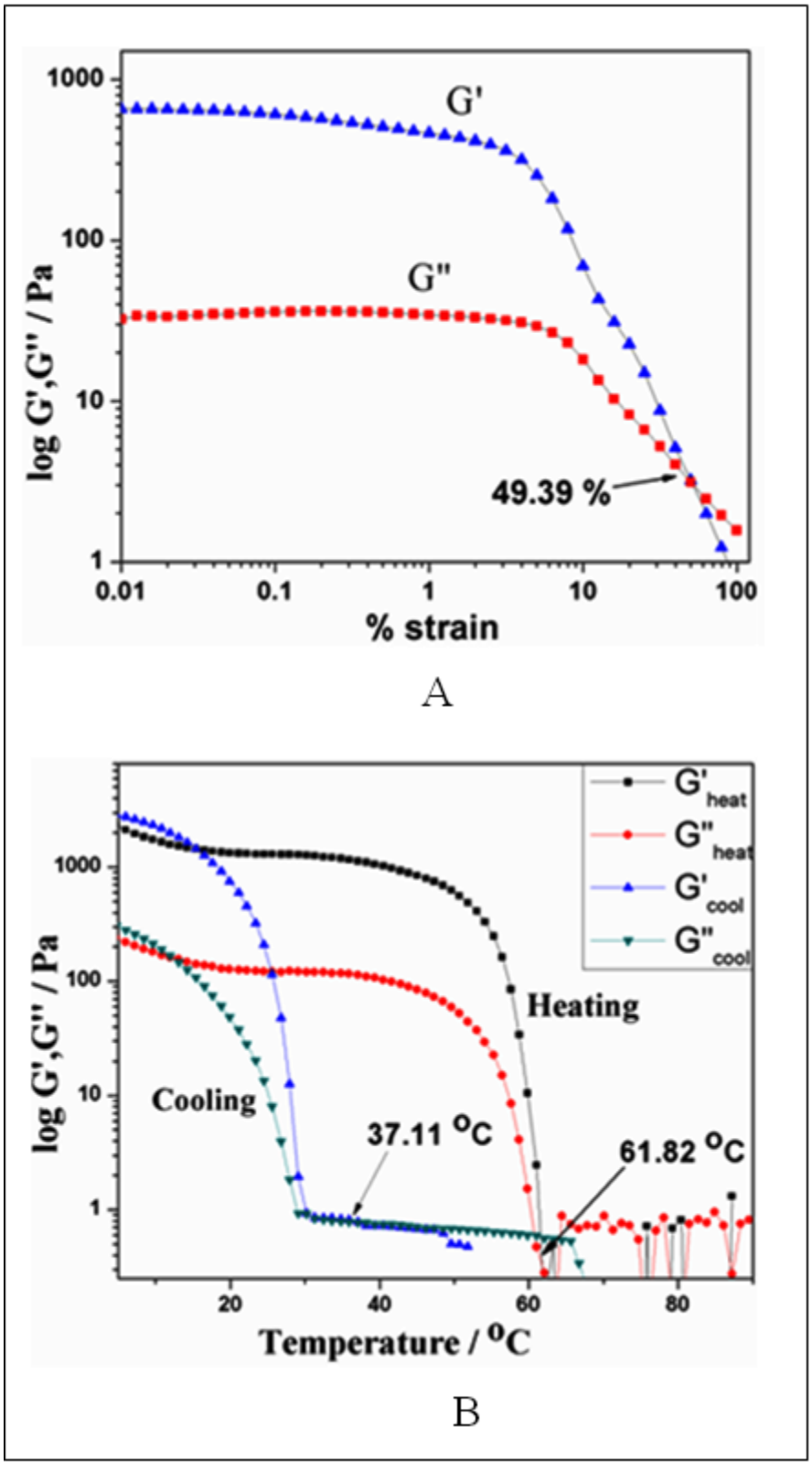

Figure 3.19 Viscoelastic study: A) Strain sweep rheological study for 0.2 % w/v of **P3** in toluene at 20 °C and a frequency of 10 rad/s B) Self healing: Temperature-ramp rheological study cycle for 0.2 % w/v of **P3** in toluene with a ramp of 2 °C/min at 0.05 % strain and 10 rad/s frequency.

Depending on all experimental results, the mechanism of gel formation in Aic γ-peptides is predicted in Figure 3.21.

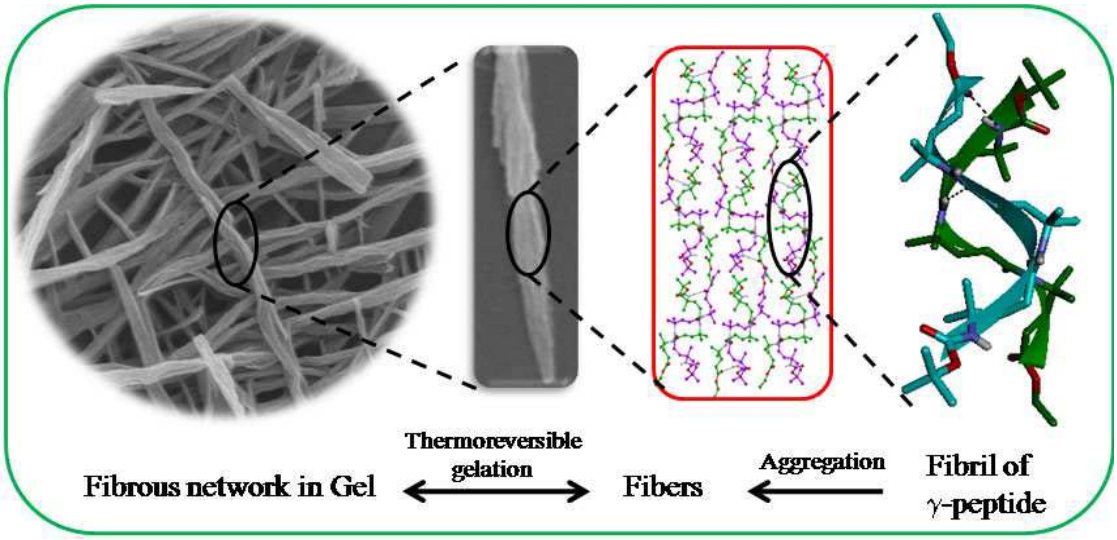

Figure 3.21 Schematic representation of gel formation in Aic homooligomers

3.7 Conclusions

In conclusion, we have studied the solution and solid state conformations of γ-peptides containing 4, 4-gem-dimethyl γ-amino acids (Aic). The conformationally biased Aic oligomers adopted extended polar sheet type structures in contrast to the helical conformations displayed by the other γ-peptides. The extended structures are stabilized by the intermolecular H-bonds between facing anti-parallel strands. Further, the extended sheet structures of tetra and penta γ- peptides displayed unprecedented thermoreversible gelation in various solvents and promoted formation of nano-fibers through self-aggregation. The rheological studies revealed that the gels were stable even at higher temperatures and reconstitute from sol to gel at ambient temperature. In addition, these γ-peptide soft materials showed the waterproofing ability on hydrophilic surfaces. As α-peptide based biomaterials have been found to have applications in various fields ranging from tissue engineering to molecular electronics, the self-assembling and gelation properties of short 4, 4-gem-dimethyl γ-peptides may offer new generation of potential templates to design soft biomaterials.

3.8 Experimental section

3.8.1 General procedures

a) Synthesis of ethyl esters of N-Boc-protected 4-Aic (4-Amino isocaproic acid)

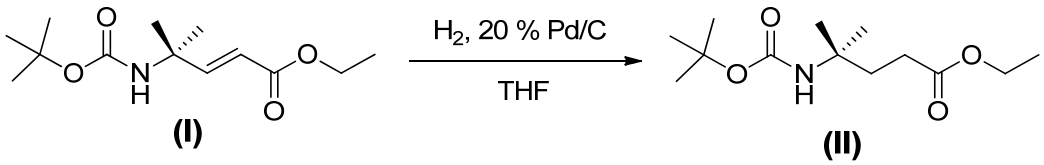

Scheme 3.2 Synthesis of 4-Aic

The suspension of activated Pd/C (20 % by weight) and (E)-ethyl 4-((tert butoxycarbonyl)amino)-4-methylpent-2-enoate(**I**) (1.028 g, 4 mmol) which was synthesized using reported method [14], in MeOH (20 mL) was stirred at room temperature in the presence of hydrogen. After completion of the reaction (TLC, ~5 Hrs), Pd/C was filtered through the bed of celite and the filtrate was evaporated to dryness under vacuum to get gummy N-Boc protected 4-Aic. The pure product was obtained after silica gel column chromatography 5% ethyl acetate in hexane in good yield (0.907 g, 90%).

b) Preparation of gel from various solvents for P3 and P4

2 mg of peptide was dissolved in 1mL of respective solvent. Solution was warmed to 50 ^{o}C. Gel in respective solvents was obtained on standing for 10-15 min. Sonication of warm solution accelerated the gelation process within 1-2 min. Gels were obtained from Methanol and Isopropanol after standing the warm solution for 2-3 days.

3.8.2 Characterization of synthesized peptides

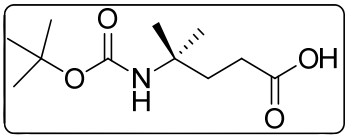

4-((tert-butoxycarbonyl)amino)-4-methylpentanoic acid:

^{1}H NMR (400 MHz, Chloroform d) δ 4.5 (bs, 1H), 2.36 (m, 2H), 2.01 (m, 2H), 1.44 (s, 9H), 1.27 (s, 6H).

^{13}C NMR (100 MHz, Chloroform d) δ 179.12, 154.23, 78.82, 51.94, 34.66, 30.92, 29.41, 28.38, 27.19.

MALDI TOF/TOF- *m/z* calcd. for $C_{11}H_{21}N_1O_4$ $[M+Na]^+$ 254.1368, obsrvd. 254.1085.

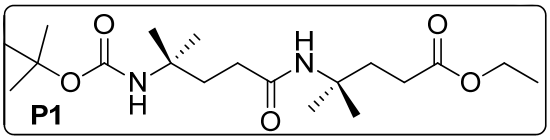

ethyl4-(4-((tert-butoxycarbonyl)amino)-4-methylpentanamido)-4-methylpentanoate (**P1**):

^{1}H NMR (400 MHz, Chloroform d) δ 5.72 (bs, 1H), 4.62 (bs, 1H), 4.12 (q, J = 8 Hz, 2H), 2.32 (t, J = 8 Hz, 2H), 2.12 (t, J = 8 Hz, 2H), 2.03 (t, J = 8 Hz, 2H), 1.96 (t, J = 8 Hz, 2H), 1.43 (s, 9H), 1.32 (s, 6H), 1.25 (m, 9H).

^{13}C NMR (100 MHz, Chloroform d) δ 174.02, 172.79, 154.71, 78.84, 60.53, 53.03, 52.23, 36.30, 34.89, 32.71, 29.55, 28.42, 27.30, 26.70, 14.18.

MALDI TOF/TOF- *m/z* calcd. for $C_{19}H_{36}N_2O_5$ $[M+Na]^+$ 395.2522, obsrvd. 395.2507.

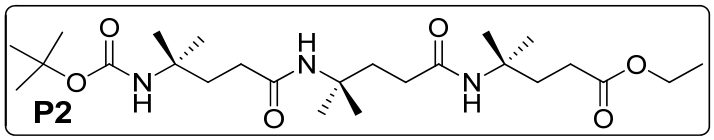

ethyl2,2,6,6,11,11,16,16-octamethyl-4,9,14-trioxo-3-oxa-5,10,15-triazanonadecan-19-oate (P2):

^{1}H NMR (400 MHz, Chloroform d) δ 6.32, (bs, 1H), 5.89 (bs, 1H), 4.70 (bs, 1H), 4.13 (q, J = 8 Hz, 2H), 2.31 (t, J = 8 Hz, 2H), 2.14 (m, 4H), 2.02 (t, J = 8 Hz, 2H), 1.93 (m, 4H), 1.42 (s, 9H), 1.31 (m, 13H), 1.25 (m, 8H).

^{13}C NMR (100 MHz, Chloroform d) δ 174.06, 173.05, 172.96, 155.41, 78.70, 60.56, 53.13, 52.19, 36.33, 34.88, 32.31, 28.42, 27.13, 26.65, 14.16.

MALDI TOF/TOF- *m/z* calcd. for $C_{25}H_{47}N_3O_6$ $[M+Na]^+$ 508.3363, obsrvd. 508.3342.

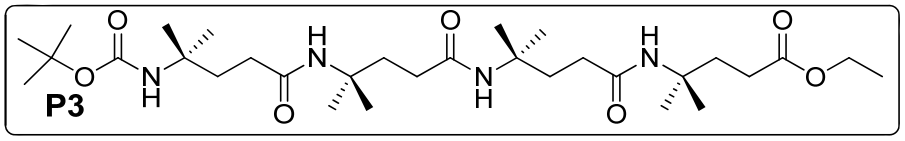

ethyl 2,2,6,6,11,11,16,16,21,21-decamethyl-4,9,14,19-tetraoxo-3-oxa-5,10,15,20-tetraazatetracosan-24-oate (P3) :

^{1}H NMR (400 MHz, Chloroform d) δ 6.72 (bs, 1H), 6.55, (bs, 1H), 6.07 (bs, 1H), 4.75 (bs, 1H), 4.13 (q, J = 8 Hz, 2H), 2.03 (m, 16H), 1.42 (s, 9H), 1.30 (m, 27H).

^{13}C NMR (100 MHz, Chloroform d) δ 174.06, 173.27, 173.11, 172.96, 154.65, 78.73, 53.11, 52.16, 36.56, 36.42, 34.87, 32.50, 32.15, 32.04, 29.49, 28.40, 27.04, 26.61, 26.53, 26.40, 20.95, 20.59, 14.14.

MALDI TOF/TOF- *m/z* calcd. for $C_{31}H_{58}N_4O_7$ $[M+Na]^+$ 621.4203, obsrvd. 621.4250.

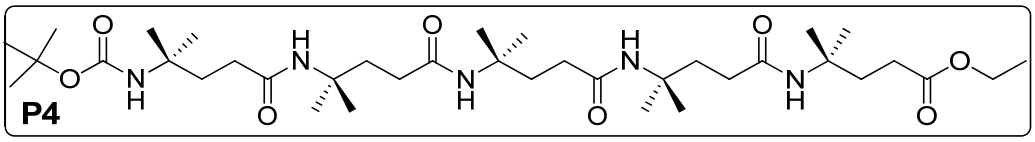

ethyl 2,2,6,6,11,11,16,16,21,21,26,26-dodecamethyl-4,9,14,19,24-pentaoxo-3-oxa-5,10,15,20,25-pentaazanonacosan-29-oate (P4):

^{1}H NMR (400 MHz, Chloroform d) δ 6.85 (bs, 2H), 6.55, (bs, 1H), 6.05 (bs, 1H), 4.75 (bs, 1H), 4.12 (q, J = 8 Hz, 2H), 2.33 (m, 2H), 2.10 (m, 8H), 1.80 (m, 10H), 1.43 (s, 9H), 1.33 (m, 24H), 1.26 (m, 9H).

^{13}C NMR (100 MHz, Chloroform d) δ 173.45, 173.38, 173.27, 173.20, 172.93, 158.11, 79.44, 60.64, 53.14, 52.24, 36.64, 36.44, 34.97, 32.08, 30.94, 29.53, 28.46, 26.62, 26.40, 14.19.

MALDI TOF/TOF- *m/z* calcd. for $C_{37}H_{69}N_5O_8$ $[M+Na]^+$ 734.5044, obsrvd. 734.5131

3.9 Crystal structure information

3.9.1 Packing of P1 and P2 molecules in crystal

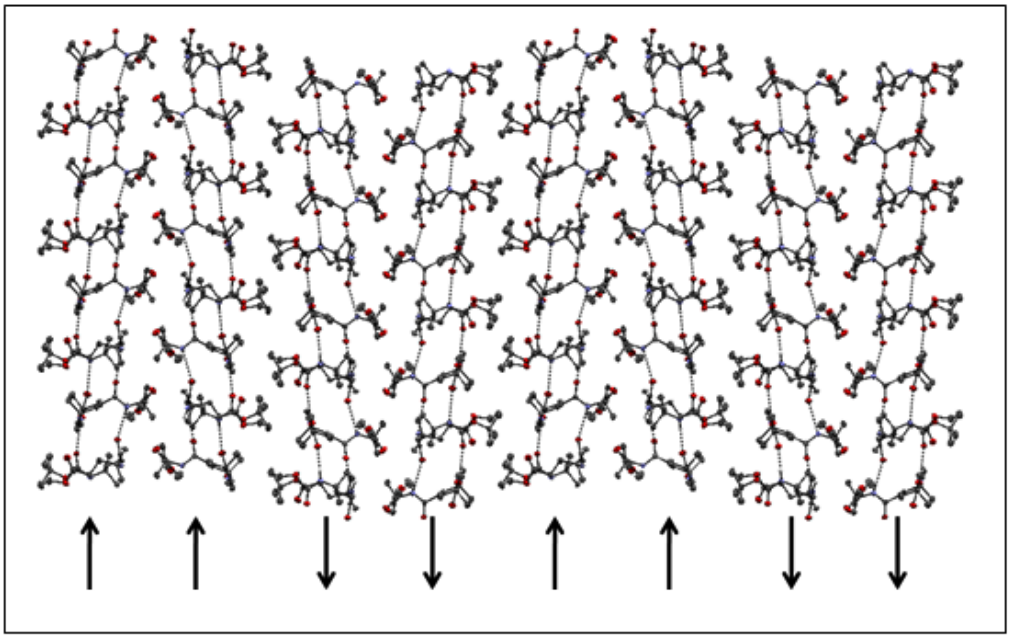

Figure 3.16 Arrangement of molecules of peptide **P1** is shown in unit cell depicting the intermolecular hydrogen bonding (shown in dotted black lines). Arrows indicates the direction of H-bond dipole in the packing as viewed down crystallographic **b**-axis.

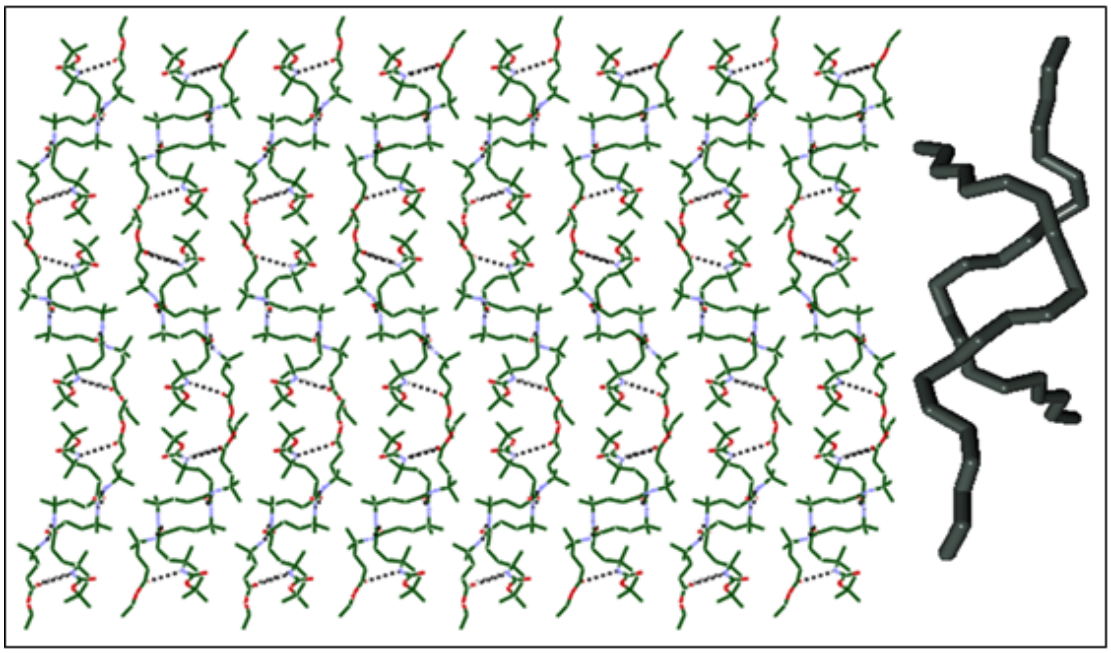

Figure 3.17 Arrangement of **P2** depicting antiparallel double helical structure as viewed down crystallographic **a**-axis. Right panel gives insight into orientation of γ-peptide (**P2**) backbone in double helical form.

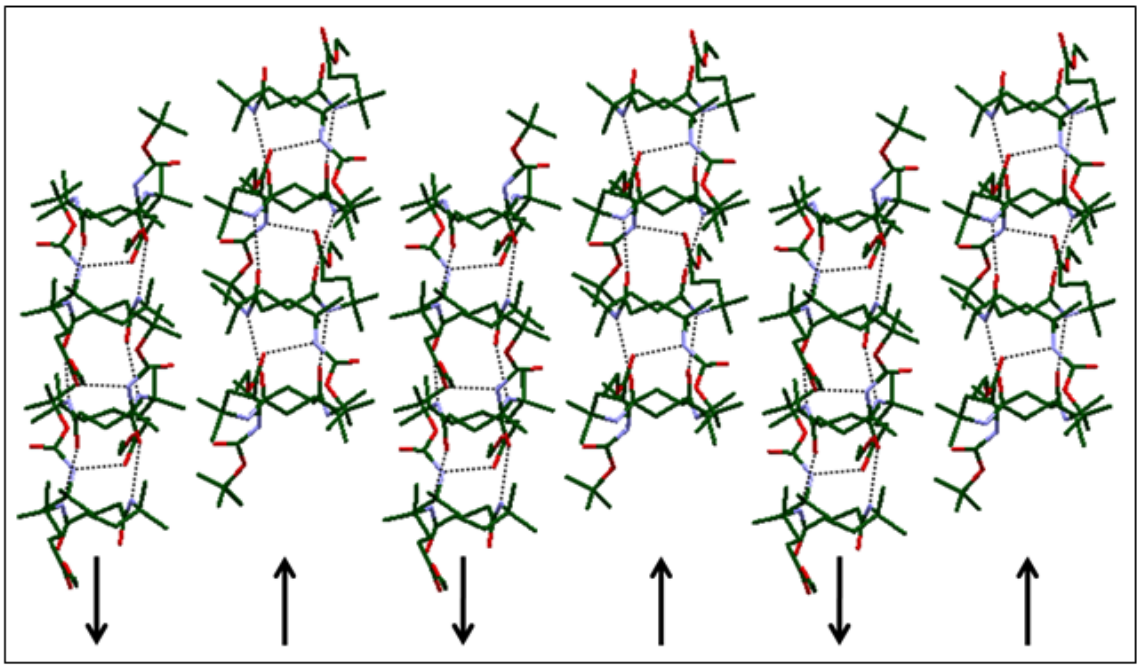

Figure 3.18 Arrangement of molecules of peptide **P2** is shown in unit cell depicting the intermolecular hydrogen bonding (shown in dotted black lines). Arrows indicates the direction of H-bond dipole in adjacent layers as viewed down crystallographic **c**-axis.

3.9.2 General procedure for crystallization of peptides

All crystallization attempts were conducted at room temperature. All oligomers of 4-Aic were purified carefully before keeping for crystallization. Glass sample vials (2 mL) were washed with acetone and dried under a nitrogen gas stream before use. PARAFILM "M" was used to close the vials. HPLC-grade solvents were used for crystallization.

Slow evaporation of a methanol/water mixture (P1)

Peptide Boc-Aic-Aic-OEt (**P1)** (8-10 mg) was dissolved in methanol (1 mL). The solution was transferred through a syringe filter into a glass vial. A few drops of water were added. The vial was closed with a PARAFILM and then pricked gently with clean and sharp needle to introduce 4 to 5 pores on PARAFILM so as to let the solvent mixture evaporate slowly. Reasonably good quality crystals were obtained after few days.

Slow evaporation of a methanol (P2)

Peptide Boc-Aic-Aic-Aic-OEt (**P2)** (2-5 mg) was dissolved in methanol (1 mL). The solution was transferred through a syringe filter into a glass vial. A few drops of water were added. The vial was closed with a PARAFILM and then pricked gently with clean and sharp needle to introduce 4 to 5 pores on PARAFILM so as to let the solvent mixture evaporate slowly. Peptide is prone to form gel during the process of crystallization. After

several attempts, we could identify reasonably good quality crystal suitable for X-ray diffraction, after few days.

3.9.3 Crystal Structure refinement report of peptide P1 and P2

i) Boc-Aic-Aic-OEt (P1)

Data Collection

A colorless crystal with approximate dimensions 0.3 x 0.1 x 0.05 mm^3 was selected under oil under ambient conditions and attached on nylon CryoLoops with Paraton-N (Hampton Research). The crystal was mounted in a stream of cold nitrogen at 100(2) K and centred in the X-ray beam by using a video camera.

The crystal evaluation and data collection were performed on a Bruker KAPPA APEX II CCD Duo diffractometer (operated at 1500 W power: 50 kV, 30 mA) with Mo Kα (λ = 0.71073 Å) radiation and the diffractometer to crystal distance of 4.0 cm. The initial cell constants were obtained from three series of ω scans at different starting angles. Each series consisted of 12 frames collected ω with the exposure time of 20 seconds per frame. Obtained reflections were successfully indexed by an automated indexing routine built in the SMART program. The final cell constants were calculated from a set of 55478 strong reflections from the actual data collection.

The data were collected to a resolution of 0.75 Å, with an exposure time 20 sec per frame. The data integration and reduction were processed with SAINT [22] software. A multi-scan absorption correction was applied to the collected reflections.

Structure Solution and Refinement

The systematic absences in the diffraction data were uniquely consistent for the space group P -1 that yielded chemically reasonable and computationally stable results of refinement.[23]

A successful solution by the direct methods provided most non-hydrogen atoms from the *E*-map. The remaining non-hydrogen atoms were located in an alternating series of least-squares cycles and difference Fourier maps. All non-hydrogen atoms were refined with anisotropic displacement coefficients. All hydrogen atoms were included in the structure factor calculation at idealized positions and were allowed to ride on the neighbouring atoms with relative isotropic displacement coefficients. No molecule participates in any intramolecular hydrogen bond.

The final least-squares refinement of 970 parameters against 21030 data resulted in residuals *R* (based on F^2 for $I \geq 2\sigma$) and *wR* (based on F^2 for all data) of 0.0914 and 0.2195, respectively.

Crystal data and structure refinement for Boc-Aic-Aic-OEt (P1)

CCDC No.: 943867

Empirical formula: C_{19} H_{36} N_2 O_5; Formula weight: 395.25; Temperature : 100(2) K ; Wavelength: 0.71073 Å ; Crystal system: Triclinic; Space group: P -1; Unit cell dimensions: a = 9.633(4)Å , b = 11.242(5)Å, c = 40.783(18)Å, α = 89.932(8)°, β = 89.996(10)°, γ = 82.953(10)°; Volume: 4383(3)$Å^3$; Z : 8; Density (calculated): 1.129Mg/m^3 ; Absorption coefficient (μ): 0.081mm^{-1} ; F (000): 1632; Crystal size: 0.30 x 0.10 x 0.5mm^3 ; Theta range for data collection: 1.00 to 28.44° ; Index ranges: -12<=h<=7, -14<=k<=15, -53<=l<=54; Reflections collected: 55478; Independent reflections: 21030 [R(int) = 0.2147] ; Completeness to theta = 28.44°: 95.2 % ; Absorption correction: Empirical with SADABS; Max. and min. Transmission: 0.996 and 0.990 ; Refinement method: Full-matrix least-squares on F^2 ; Data / restraints / parameters: 21030 / 0 / 970 ; Goodness-of-fit on F^2 : 0.798 ; Final R indices [I>2sigma(I)]; R1 = 0.0914, wR2 = 0.2195; R indices (all data): R1 = 0.2952, wR2 = 0.3591; Largest diff. peak and hole: 0.361 and -0.368 e.$Å^{-3}$.

ii) Boc-Aic-Aic-Aic-OEt (P2)

Data Collection

A colorless crystal with approximate dimensions 0.45 x 0.4 x 0.2 mm^3 was selected under oil under ambient conditions and attached on nylon CryoLoops with Paraton-N (Hampton Research). The crystal was mounted in a stream of cold nitrogen at 100(2) K and centered in the X-ray beam by using a video camera.

The crystal evaluation and data collection were performed on a Bruker KAPPA APEX II CCD Duo diffractometer (operated at 1500 W power: 50 kV, 30 mA) with Mo Kα (λ = 0.71073 Å) radiation and the diffractometer to crystal distance of 4.0 cm. The initial cell constants were obtained from three series of ω scans at different starting angles. Each series consisted of 12 frames collected ω with the exposure time of 25 seconds per frame. Obtained reflections were successfully indexed by an automated indexing routine

built in the SMART program. The final cell constants were calculated from a set of 55478 strong reflections from the actual data collection.

The data were collected to a resolution of 0.75 Å, with an exposure time 25 sec per frame. The data integration and reduction were processed with SAINT [22]software. A multi-scan absorption correction was applied to the collected reflections.

Structure Solution and Refinement

The systematic absences in the diffraction data were uniquely consistent for the space group P21 21 21 that yielded chemically reasonable and computationally stable results of refinement.[23]

A successful solution by the direct methods provided most non-hydrogen atoms from the *E*-map. The remaining non-hydrogen atoms were located in an alternating series of least-squares cycles and difference Fourier maps. All non-hydrogen atoms were refined with anisotropic displacement coefficients. All hydrogen atoms were included in the structure factor calculation at idealized positions and were allowed to ride on the neighbouring atoms with relative isotropic displacement coefficients. No molecule participates in any intramolecular hydrogen bond.

The final least-squares refinement of 604 parameters against 10226 data resulted in residuals *R* (based on F^2 for $I \geq 2\sigma$) and *wR* (based on F^2 for all data) of 0.1057and 0.2218, respectively.

Crystal data and structure refinement for Boc-Aic-Aic-Aic-OEt (P2)

CCDC No.: 943868

Empirical formula: C_{25} $H_{47}N_3$ O_6 ; Formula weight: 485.66; Temperature : 100(2) K; Wavelength: 0.71073 Å ; Crystal system: Orthorhombic; Space group: P 21 21 21; Unit cell dimensions: a = 9.633(5)Å , b = 18.305(8)Å, c = 33.028(15)Å, α = 90°, β = 90°, γ = 90°; Volume: 5824(5)$Å^3$; Z: 8; Density (calculated) : 1.108Mg/m^3; Absorption coefficient (μ): 0.078mm^{-1} ; F (000): 2128; Crystal size: 0.45 x 0.4 x 0.2mm^3 ; Theta range for data collection: 1.27 to 25.0° ; Index ranges: -10<=h<=11, -21<=k<=21, -39<=l<=39 ; Reflections collected: 80005; Independent reflections: 10226 [R(int) = 0.2720]; Completeness to theta = 25.0°; 99.4 % ; Absorption correction ; Empirical with SADABS; Max. and min. Transmission : 0.985 and 0.966 ; Refinement method ; Full-matrix least squares on F^2 ; Data / restraints / parameters: 10226/ 0 / 604; Goodness-of-fit on F^2 : 1.033

; Final R indices [I>2sigma(I)]: R1 = 0.1057, wR2 = 0.2218; R indices (all data): R1 = 0.196, wR2 = 0.2667; Absolute structure parameter: 1(2); Largest diff. peak and hole: 0.470 and -0.357 e.Å^{-3}.

3.10 References

1. a) Hosseinkhani, H.; Hong, P. -D.; Yu, D. S.; *Chem. Rev.* **2013**, DOI: 10.1021/cr300131h. b) Koutsopoulos, S.; Zhang, S. *Acta Biomater.* **2013**, *9*, 5162. c) Stephanopoulos, N.; Ortony, J. H.; Stupp, S. I. *Acta Biomater*. **2013**, *61*, 912. d) Hartgerink, J. D.; Beniash, E.; Stupp, S. I. *Science* **2001**, *294*, 1684. e) Hirst, A. R.; Escuder, B.; Miravet, J. F.; Smith, D. K. *Angew. Chem. Int. Ed.* **2008**, *47*, 8002. f) Kuang, Y.; Xu, B. *Angew. Chem. Int. Ed.* **2013**, *52*, 1. g) Zhao, F.; Ma, M. L.; Xu, B. *Chem. Soc. Rev*. **2009,** *38*, 883.h) Cavalli, S.; Albericio, F.; Kros, A. *Chem. Soc. Re*v. **2010**, *39*, 241. i) Gazit, E. *Chem. Soc. Rev*. **2007**, *36*, 1263. j) Branco, M.; Schneider, J. P. *Acta Biomater.* **2009**, *5*, 817. k) Tovar, J. D. *Acc. Chem. Res.* **2013**, 10.1021/ar3002969. l) Dasgupta, A.; Mondal, J. H.; Das, D. *RSC Adv.* **2013**, DOI: 10.1039/c3ra40234g. m) Smith, A. M.; Williams, R. J.; Tang, C.; Coppo, P.; Collins, R. F.; Turner, M. L.; Saiani, A.; Ulijn, R. V. *Adv. Mater.* **2008**, *20*, 37. n) Roy, S.; Baral, A.; Banerjee, A. *Chem. Eur. J.* **2013**, doi: 10.1002/chem.201301655, o) Nanda, J.; Biswas, A.; Adhikari, B.; Banerjee, A. *Angew. Chem. Int. Ed.* **2013**, *52*, 5041. p) Adhikari, B. Banerjee, A. *Chem. Eur. J.* **2010**, *16*, 13698.
2. a) Seebach, D.; Beck, A. K.; Bierbaum, D. J.; *Chem. Biodiv*. **2004***, 1*, 1111. b) Cheng, R. P.; Gellman, S. H.; DeGrado, W. F.; *Chem. Rev.* **2001**, *101*, 3219. c) Horne, W. S.; Gellmann, S. H. *Acc. Chem. Res.* **2008**, *41*, 1399. d) Vasudev, P. G.; Chatterjee, S.; Shamala, N.; Balaram, P. *Chem. Rev*. **2011***, 111*, 657. e) Vasudev, P. G.; Chatterjee, S.; Shamala, N. Balaram, P. *Acc. Chem. Res*. **2009**, *42***,** 1628. f) Balaram, P. *Biopolymers* **2010**, *94*, 733. g) Chatterjee, Vasudev, S. P. G.; Raghothama, S.; Ramakrishnan, C.; Shamala, N.; Balaram, P. *J. Am. Chem. Soc.* **2009**, *131*, 5956. h) Guo, L.; Zhang, W.; Reidenbach, A. G.; Giuliano, M. W.; Guzei, I. A.; Spencer, L. C.; Gellman, S. H. *Angew. Chem. Int. Ed.* **2011**, *50*, 5843. i) Pilsl, L. K. A.; Reiser, O. *Amino Acids* **2011**, *41*, 709. j) Berlicki, L.; Pilsl, L.; Wéber, E.; Mándity, I. M.; Cabrele, C.; Martinek, T. A.; Fülöp, F.; Reiser, O. *Angew. Chem., Int. Ed*. **2012**, *51*, 2208. k) Martinek, T. A.; Mandity, I. M.; Fulop, L.; Toth, G. K.; Vass, E.; Hollosi, M.; Forro, E.; Fülöp, F. *J. Am. Chem. Soc.* **2006**, *128*, 13539. l) Bouillere, F.; Laurent, S. T-.; Kouklovsky, C.; Alezra, V. *Amino*

Acids **2011**, *41*, 687. m) Pendem, N.; Nelli, Y. R.; Douat, C.; Fischer, L.; Laguerre, M.; Ennifar, E.; Kauffman, B.; Guichard, G. *Angew. Chem. Int. Ed.* **2013**, *52*, 4147. n) Basuroy, K.; Dinesh, B.; Shamala, N.; Balaram, P. *Angew. Chem. Int. Ed.* **2013**, *52*, 3136.

3. a) Horne, W. S.; Price, J. L.; Gellman, S. H. *Proc. Natl. Acad. Sci. USA* **2008***, 105,* 9151. b) English, E. P.; Chumanov, R. S.; Gellman, S. H.; Compton, T. *J. Biol. Chem.* **2006**, *281*, 2661. c) Imamura, Y.; Watanabe, N.; Umezawa, N.; Iwatsubo, T.; Kato, N.; Tomita, T.; Higuchi, T. *J. Am. Chem. Soc.* **2009**, *131*, 7353. d) Lee, E. F.; Smith, B. J.; Horne, W. S.; Mayer, K. N.; Evangelista, M.; Colman, P. M.; Gellman, S. H.; Fairlie, W. D. *ChemBioChem* **2011**, *12*, 2025. e) Lee, E. F.; Sadowsky, J. D.; Smith, B. J.; Czabotar, P. E.; Peterson-Kaufman, K. J.; Colman, P. M.; Gellman, S. H.; Fairlie, W. D. *Angew. Chem., Int. Ed.* **2009**, *48*, 4318.
4. Martinek, T. A.; Hetenyi, A.; Fülöp, L.; Mandity, I. M.; Toth, G. K.; Dekany, I.; Fülöp, F. *Angew. Chem., Int. Ed.* **2006**, *45*, 2396.
5. a) Rua, F.; Boussert, S.; Parella, T.; Diez-Perez, I.; Branchadell, V.; Giralt, E.; Ortuno, R. M.; *Org. Lett.* **2007**, *9*, 3643. b) Gorrea, E.; Nolis, P.; Torres, E.; Silva, E. D.; Amabilino, D. B.; Branchadell, V.; Ortuno, R. M. *Chem. Eur. J.* **2011**, *17*, 4588. c) Torres, E.; Gorrea, E.; Burusco, K. K.; Silva, E. D. Nolis, P.; Rua, F.; Boussert, S.; Diez-Perez, I.; Dannenberg, S.; Izquierdo, S.; Giralt, E.; Jaime, C.; Branchadell, V.; Ortuno, R. M. *Org. Biomol. Chem.* **2010**, *8*, 564. d) Celis, S.; Nolis, P.; Illa, O.; Branchadell, V.; Ortuno, R. M. *Org. Biomol. Chem.* **2013**, *11*, 2839.
6. a) Pomerantz, W. C.; Yuwono, V. M.; Pizzey, C. L.; Hartgerink, J. D.; Abbott, N. L.; Gellman, S. H. *Angew. Chem., Int. Ed.* **2008**, *47*, 1241. b) Segman-Magidovich, S.; Lee, M.; Vaiser, V.; Struth, B.; Gellman, S. H.; Rapaport, H. *Chem. Eur. J.* **2011**, *17*, 14857.
7. a) Fandino, R. G.; Amorin, M.; Castedo, L.; Granja, J. R. *Chem. Sci.* **2012**, *3*, 3280. b) Brea, R. J.; Reiriz, C.; Granja, J. R. *Chem. Soc. Rev.* **2010**, *39*, 1448.
8. a) Karle, I. L.; Balaram, P. *Biochemistry* **1990**, *29*, 6747. b) Toniolo, C.; Benedetti, E. *Trends Biochem. Sci*. **1991**, *16*, 350.c) Karle, I. L. *Biopolymers (Peptide Science)* **1996**, *40*, 157. d) Kumita, J. R.; Weston, C. J.; Choo-Smith, L. –P.; Wooley, G. A.; Smart, O. S. *Biochemistry* **2003**, *42*, 4492. e) Kaul, R.; Balaram, P. *Bioorg. Med. Chem*. **1999**, *7*, 105.f) Marshall, G. R.; Hodgkin, E. E.; Langs, D. A.; Smith, D. G.; Zabrocki, J.; Leplawy, M. T. *Proc. Natl. Acad. Sci. USA* **1990**, *87*,

487. g) Dannecker-Doring, I.; Linden, A.; Heimgartner, H. *Helv. Chim. Acta.* **2011**, *94*, 993. h) Venkataram, B. V.; Balaram, P. *CRC Crit. Rev. Biochem.* **1984**, *16*, 307. i) Karle, I. L. *Biopolymers* **2001**, *60*, 351.

9. a) Venkatraman, J.; Shankaramma, S. C.; Balaram, P. *Chem. Rev.* **2001**, *101*, 3131. b) Toniolo, C.; Crisma, M.; Formaggio, F.; Peggion, C. *Biopolymers (Peptide Science)* **2001**, *60*, 396.
10. a) Crisma, M.; Saviano, M.; Moretto, A.; Broxterman, Q. B.; Kaptein, B.; Toniolo, C. *J. Am. Chem. Soc.* **2007**, *129*, 15471. b) Crisma, M.; Peggion, C.; Moretto, A.; Banerjee, R.; Supakar, S.; Formaggio, F.; Toniolo, C. *Biopolymers* **2013**, DOI: 10.1002/bip.22450. c) Casanovas, J.; Revilla-Lopez, G.; Crisma, M.; Toniolo, C.; Aleman, C. *J. Phys. Chem. B* **2012**, *116*, 13297. d) Formaggio, F.; Crisma, M.; Ballano, G.; Peggion, C.; Venanzi, M.; Toniolo C. *Org. Biomol. Chem.* **2012**, *10*, 2413.
11. Sills, G. J. *Curr. Opin. Pharmacol.* **2006**, *6*, 108.
12. Vasudev, P. G.; Shamala, N.; Ananda, K.; Balaram, P. *Angew. Chem. Int. Ed.* **2005**, *44*, 4972.
13. a) Jadhav, S. V.; Bandyopadhyay, A.; Gopi, H. N. *Org. Biomol. Chem.* **2013,** *11*, 509. b) Bandyopadhyay, A.; Jadhav, S. V.; Gopi, H. N. *Chem. Commun.* **2012**, *48*, 7170. c) Bandyopadhyay, A.; Gopi, H. N. *Org. Lett*. **2012**, *11*, 2770.
14. Mali, S. M.; Bandyopadhyay, A.; Jadhav, S. V.; Ganesh Kumar, M.; Gopi, H. N. *Org. Biomol. Chem*. **2011**, *9*, 6566.
15. Ganesh Kumar, M.; Mali, S. M.; Gopi, H. N. *Org. Biomol. Chem*. **2013**, *11*, 803.
16. a) Baldauf, C.; Gunther, R.; Hofmann, H. –J.; *Helv. Chim. Acta*. **2003**, *86*, 2573. b) Baldauf, C.; Gunther, R.; Hofmann, H. –J. *J. Org. Chem*. **2005**, *70*, 5351.
17. a) Hanessian, S.; Luo, X.; Schaum, R.; Michnick, S. *J. Am. Chem. Soc.* **1998**, *120*, 8569. b) Hintermann, T.; Gademann, K.; Jaun, B.; Seebach, D. *Helv. Chim. Acta* **1998**, *81*, 893. c) Seebach, D.; Brenner, M.; Rueping, M.; Schweizer, B.; Jaun, B. *Chem. Commun.* **2001**, 207. d) Seebach, D.; Brenner, M.; Rueping, M.; Jaun, B. *Chem. Eur. J.* **2002**, *8*, 573. e) Seebach, D.; Hook, D. F.; Glattli, A. *Biopolymers (peptide Science)* **2006**, *84*, 23. f) Sharma, G. V. M.; Jayaprakash, P.; Narsimulu, K.; Sankar, A. R.; Reddy, K. R.; Kunwar, A. C. *Angew. Chem. Int. Ed.* **2006**, *45*, 2944. g) Byun, B. J.; Kang, Y. K. *Biopolymers* **2013**, DOI: 10.1002/bip.22287. h) Guo, L.; Zhang, W.; Guzei, I. A.; Spencer, L. C.; Gellman, S. H. *Org. Lett.* **2012**, *14*, 2582.

18. a) Pauling, L.; Corey, R. B. *Proc. Natl. Acad. Sci. USA* **1951**, *37*, 729. b) Krauthauser, S.; Christianson, L. A.; Powell, D. R.; S. H. Gellman, *J. Am. Chem. Soc.* **1997**, *119*, 11719.
19. a) Hagihara, M.; Anthony, N. J.; Stout, T. J.; Clardy, J.; Schreiber, S. L. *J. Am. Chem. Soc.* **1992**, *114*, 6568. b) Khurram, M.; Qureshi, N.; Smith, M. D. *Chem. Commun*. **2006**, 5006. c) Bouillere, F.; Feytens, D.; Gori, D.; Guillot, R.; Kouklovsky, C.; Miclet, E.; Alezra, V. *Chem. Commun*. **2012**, *48*, 1982.
20. a) Steed, J. W. *Chem. Commun*. **2011**, *47*, 1379. b) Terech, P.; Weiss, R. G. *Chem. Rev*. **1997**, *97*, 3133.
21. a) Chirgadze, Y. N.; Nevskaya,N. A. *Biopolymers* **1976**, *15*, 627. b) Qian,W.; Bandekar, J.; Krimm, S. *Biopolymers* **1991**, *31*, 193.
22. *SAINT Plus*, (Version 7.03); Bruker AXS Inc.: Madison, WI, 2004.
23. Sheldrick, G. M. *Acta. Cryst*. **2008** SHELXL. *A64*, 112.

3.11 Appendix I: Characterization data for synthesized compounds.

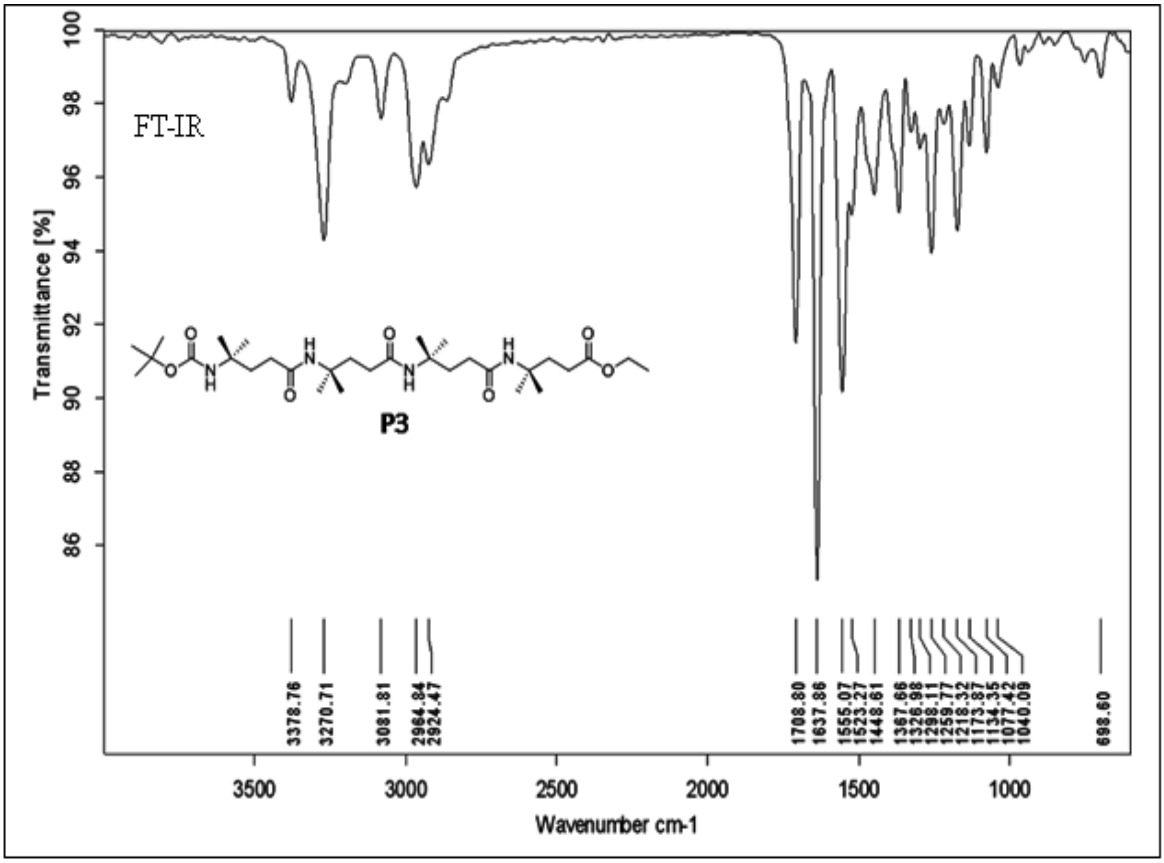
FT-IR
Transmittance [%]
100
98
96
94
92
90
88
86
P3
3378.76
3270.71
3081.81
2984.84
2924.47
1708.80
1637.86
1555.07
1523.27
1448.61
1367.66
1326.98
1259.77
1218.32
1173.87
1134.35
1077.42
1040.09
698.60
3500
3000
2500
2000
1500
1000
Wavenumber cm-1

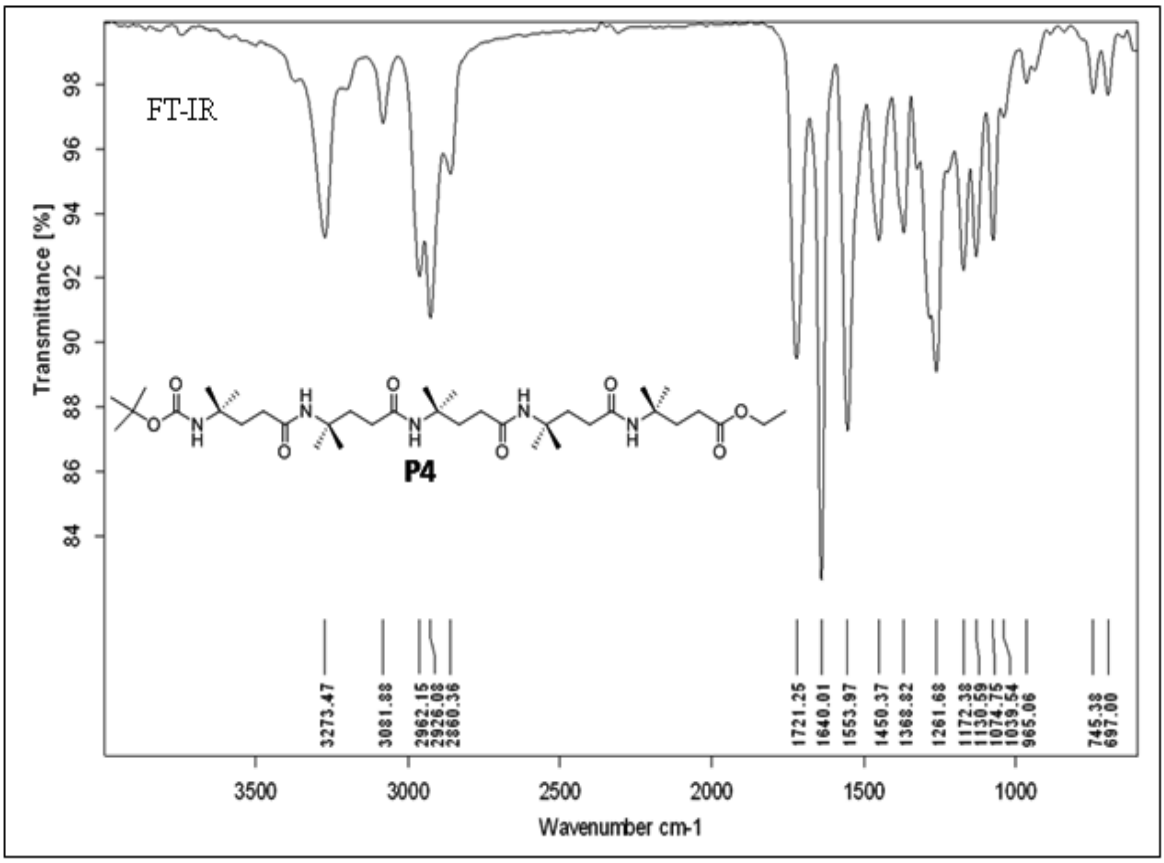
FT-IR
Transmittance [%]
98
96
94
92
90
88
86
84
P4
3273.47
3081.88
2962.15
2926.08
2860.36
1721.25
1640.01
1553.97
1450.37
1368.82
1261.68
1172.38
1130.59
1074.75
1039.54
965.06
745.38
697.00
3500
3000
2500
2000
1500
1000
Wavenumber cm-1

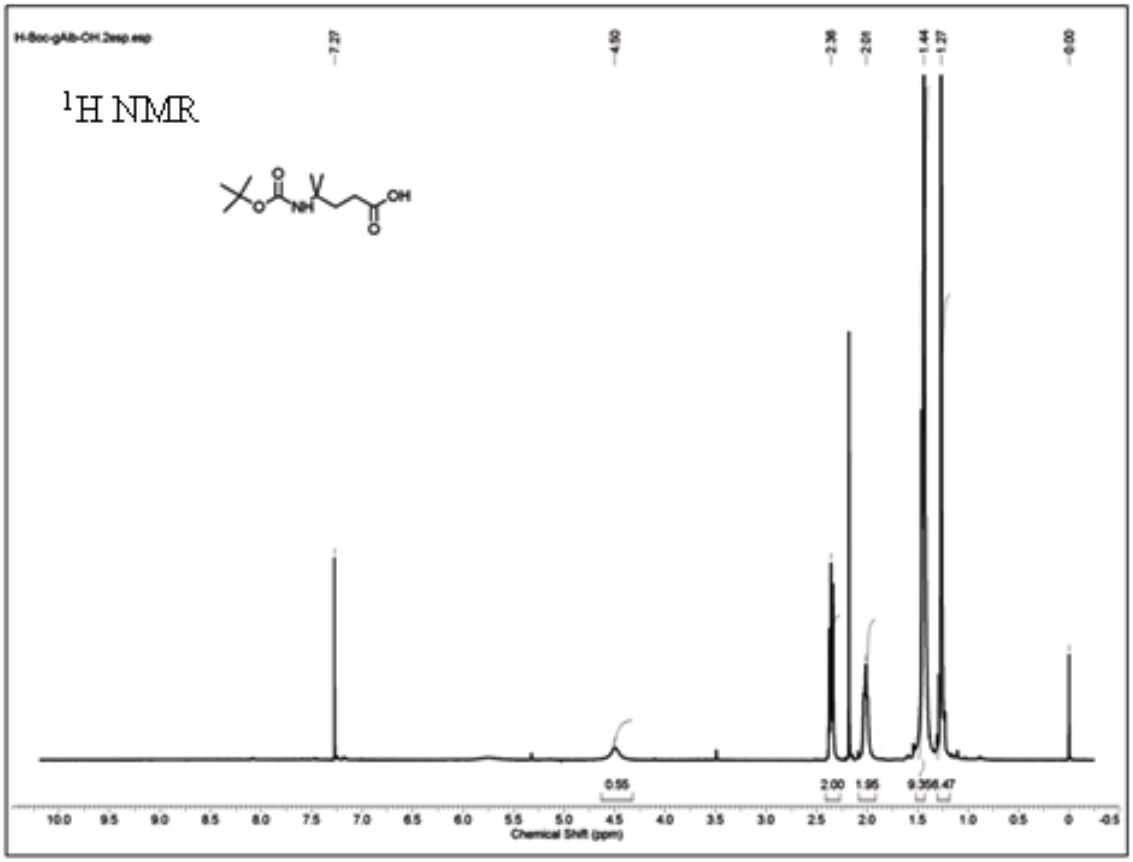
H-Boc-gAib-OH 2esp.esp
7.27
4.50
2.36
2.01
1.44
1.27
0.00
^{1}H NMR
OH
NH
0.55
2.00
1.95
9.35
6.47
Chemical Shift (ppm)

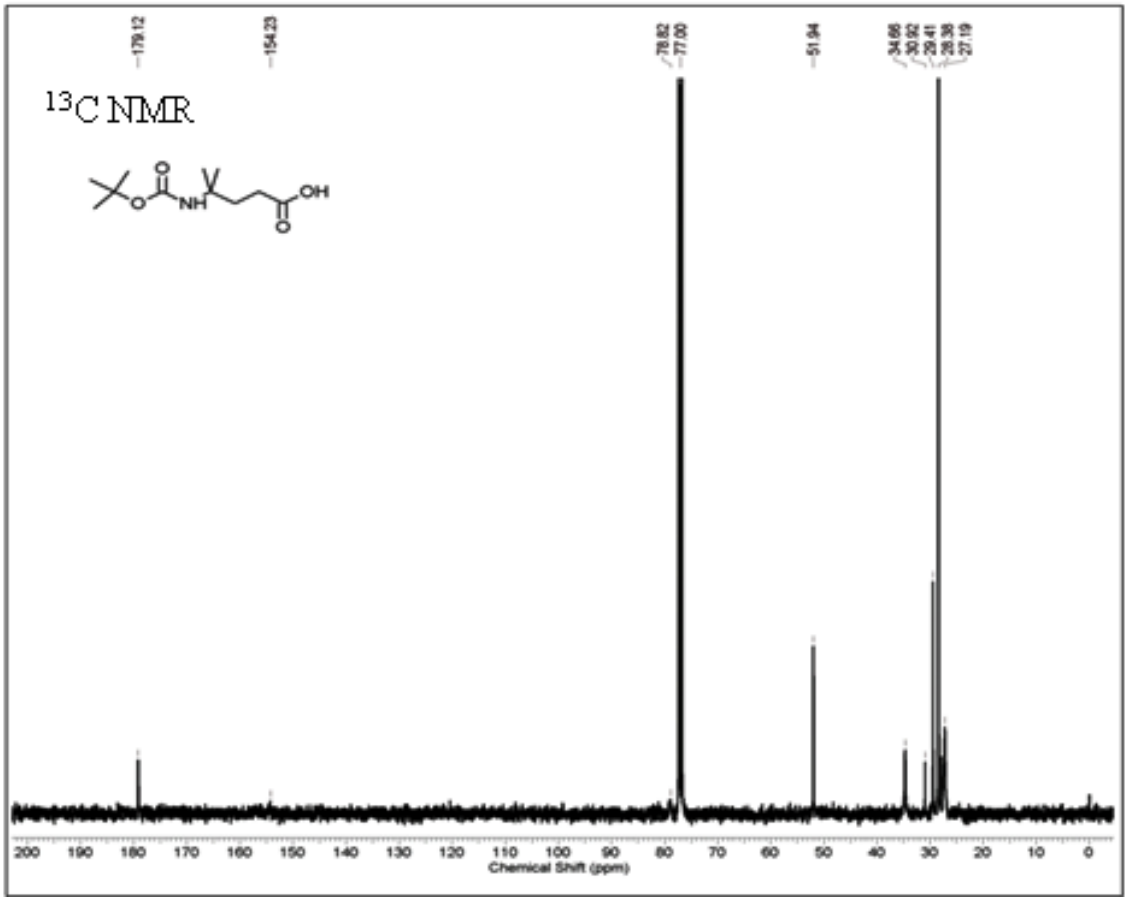
179.12
154.23
78.82
77.00
51.94
34.66
30.92
29.41
28.38
27.19
^{13}C NMR
OH
NH
Chemical Shift (ppm)

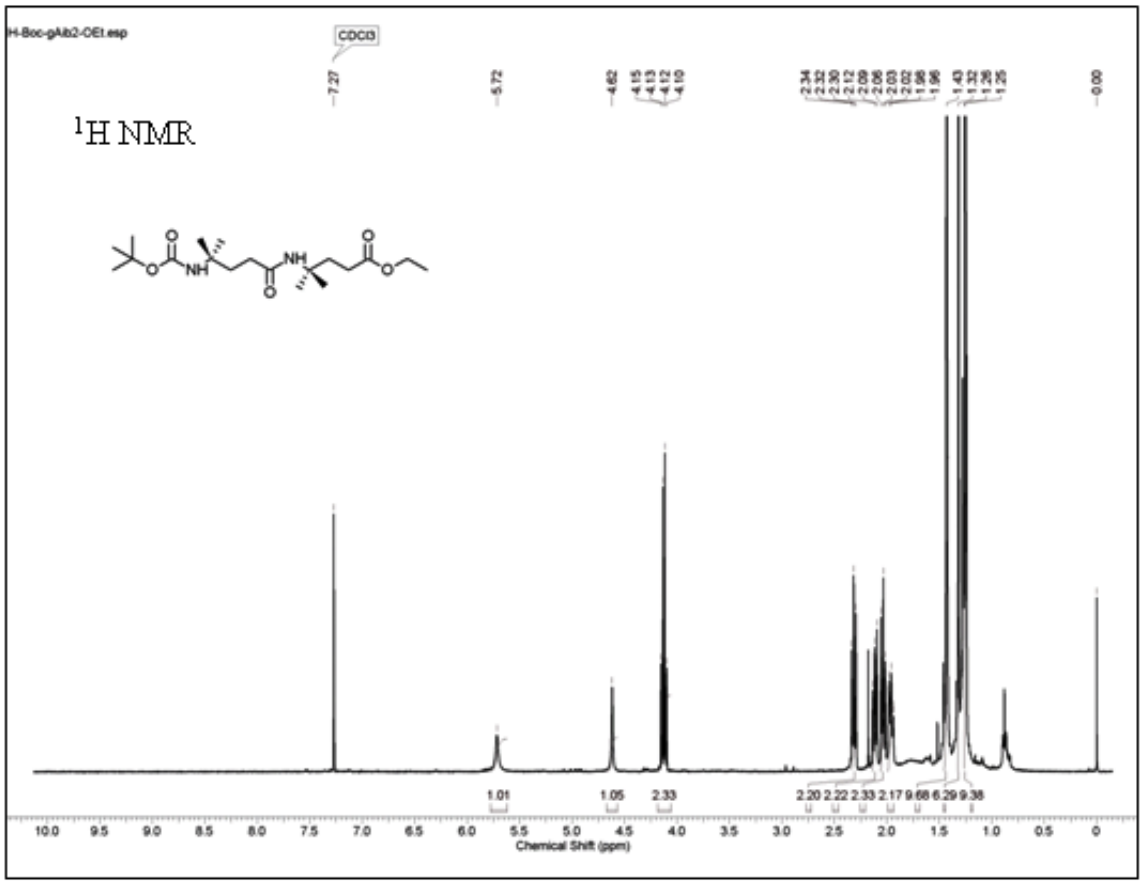
H-Boc-gAib2-OEt.esp
CDCl3
7.27
5.72
4.62
4.15
4.13
4.12
4.10
2.34
2.32
2.30
2.12
2.08
2.06
2.03
2.02
1.98
1.96
1.43
1.32
1.26
1.25
0.00
^{1}H NMR
1.01
1.05
2.33
2.20 2.22 2.33 2.17 9.68 6.29 9.38
Chemical Shift (ppm)

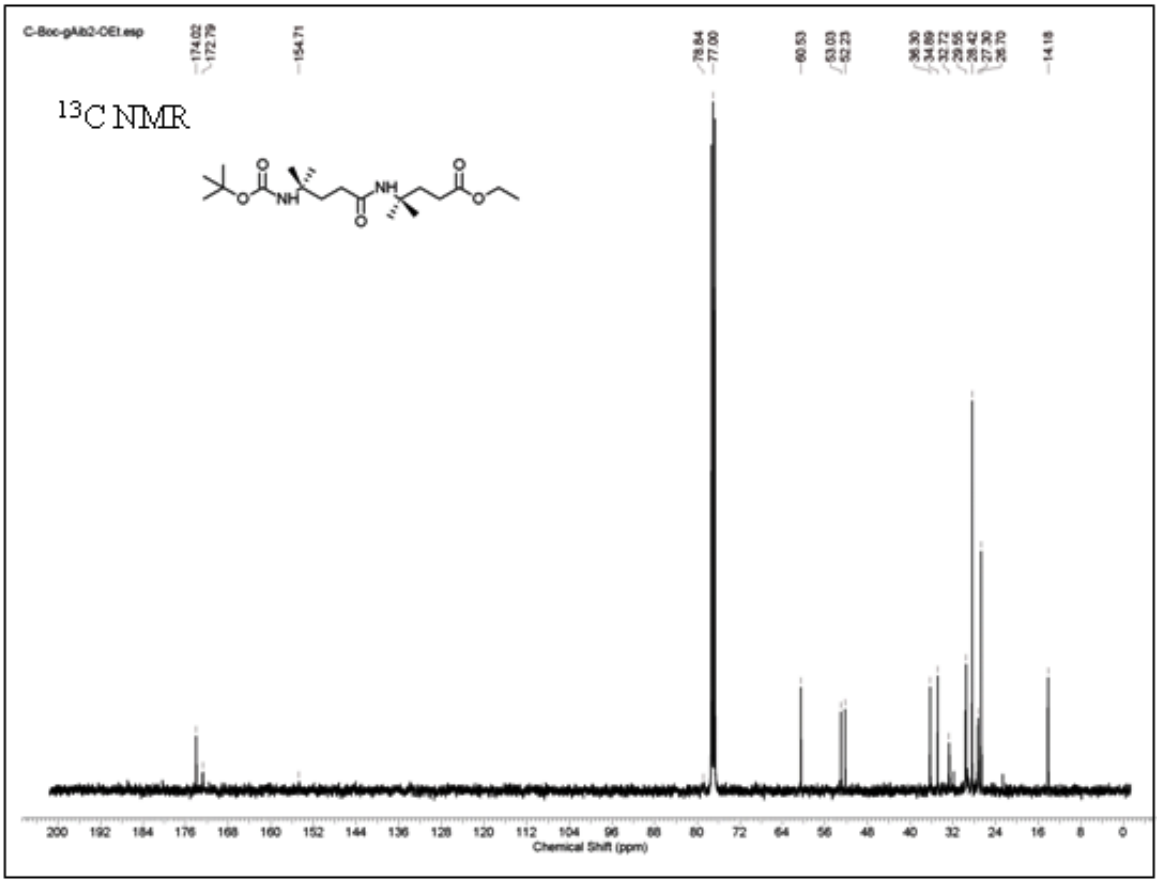
C-Boc-gAib2-OEt.esp
174.02
172.79
154.71
78.84
77.00
60.53
53.03
52.23
36.30
34.89
32.72
29.95
28.42
27.30
26.70
14.18
^{13}C NMR
Chemical Shift (ppm)

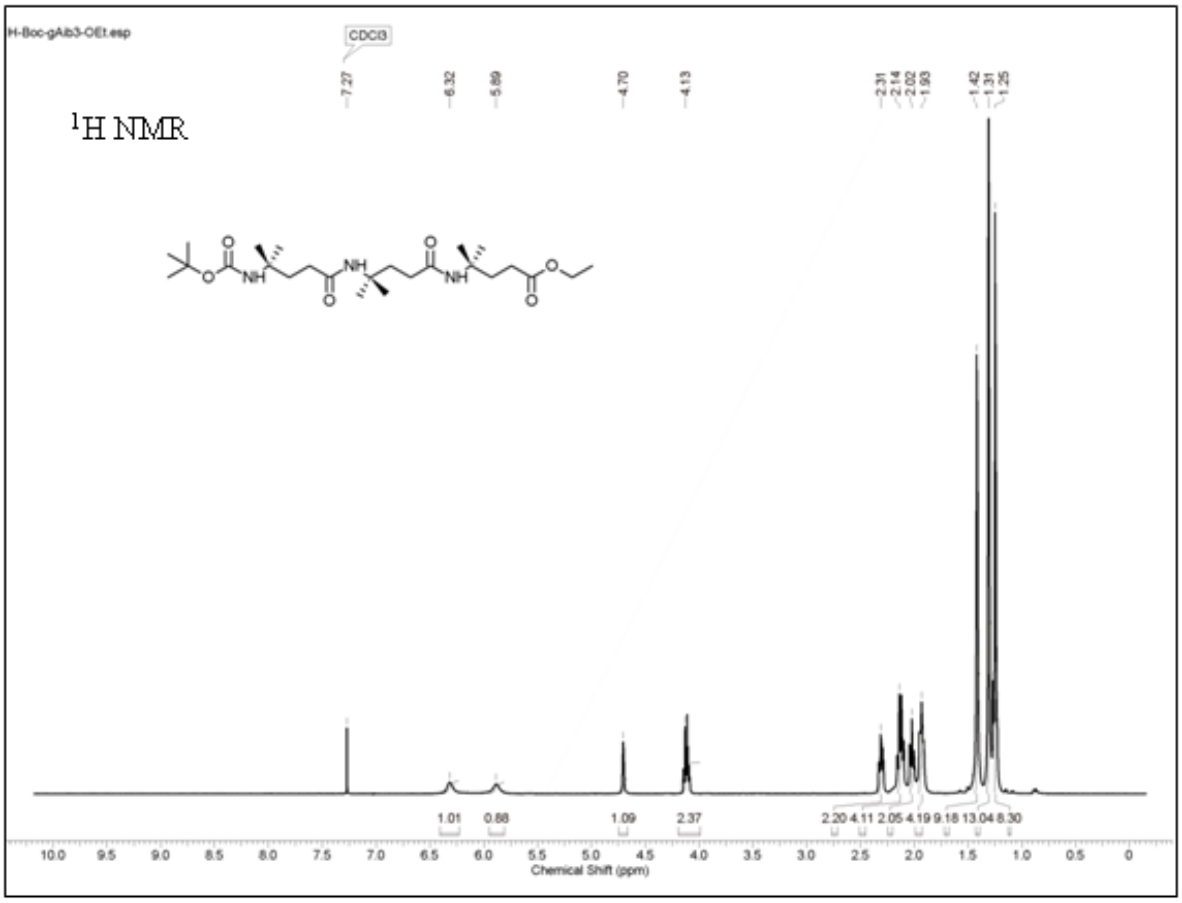
H-Boc-gAib3-OEt.esp
CDCl3
7.27
6.32
5.89
4.70
4.13
2.31
2.14
2.02
1.93
1.42
1.31
1.25
^{1}H NMR
1.01
0.88
1.09
2.37
2.20
4.11
2.05
4.19
9.18
13.04
8.30
Chemical Shift (ppm)

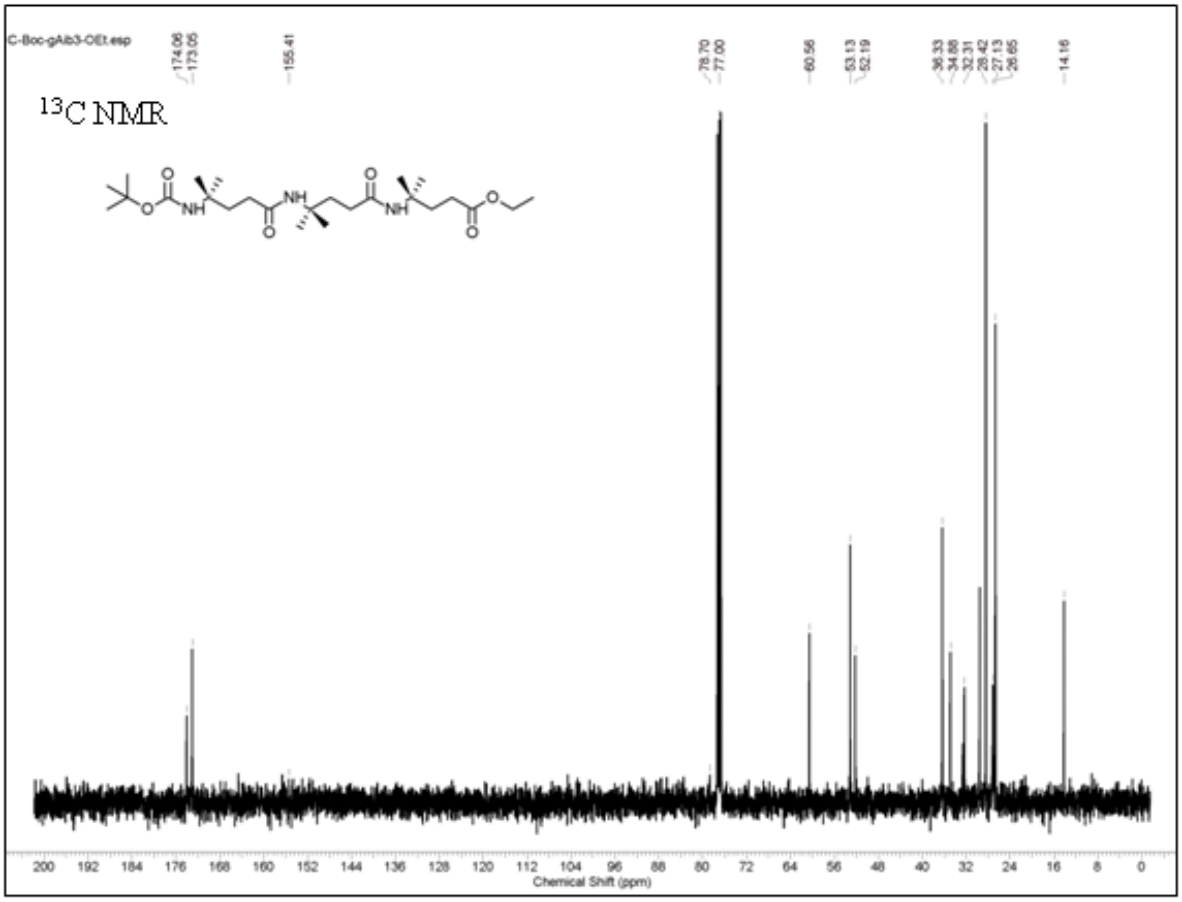
C-Boc-gAib3-OEt.esp
174.06
173.05
155.41
78.70
77.00
60.56
53.13
52.19
36.33
34.88
32.31
28.42
27.13
26.65
14.16
^{13}C NMR
Chemical Shift (ppm)

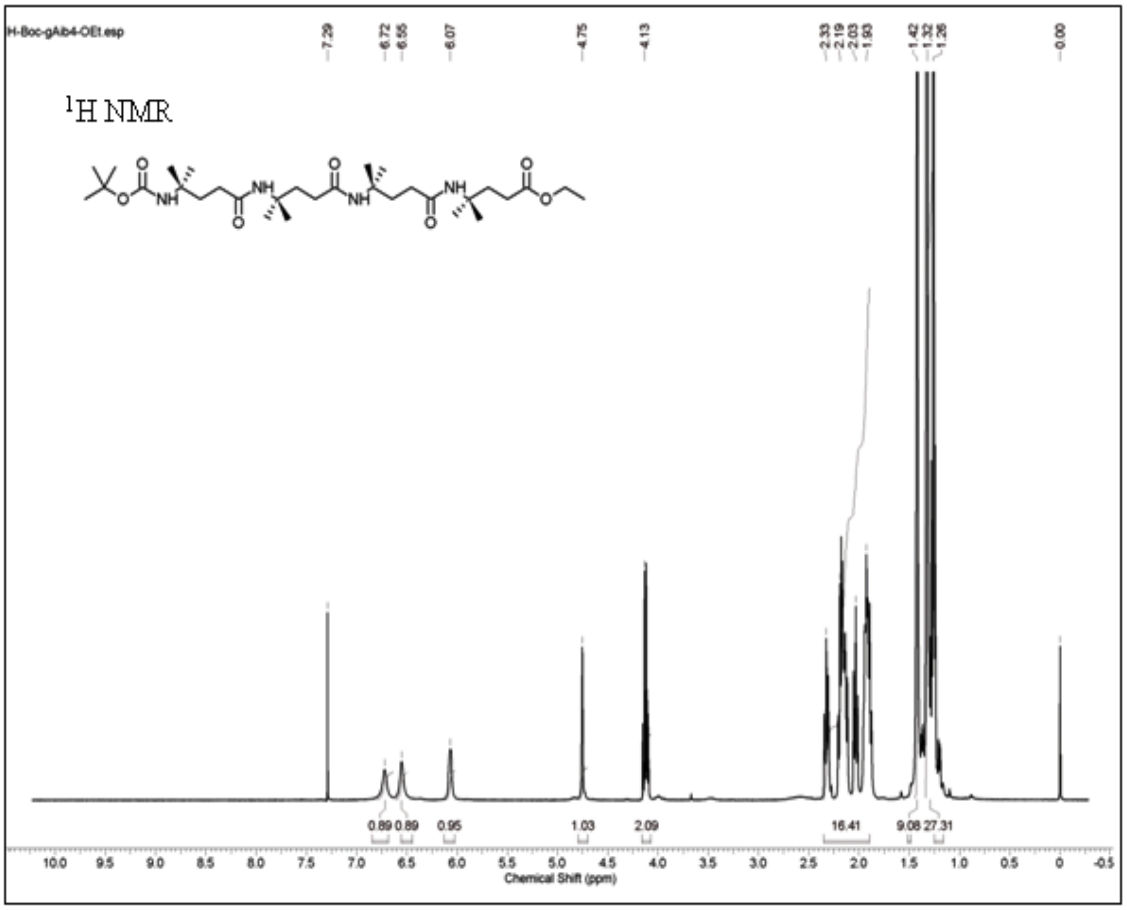
H-Boc-gAib4-OEt.esp
7.29
6.72
6.55
6.07
4.75
4.13
2.33
2.19
2.03
1.93
1.42
1.32
1.26
0.00
^{1}H NMR
0.89 0.89 0.95 1.03 2.09 16.41 9.08 27.31
Chemical Shift (ppm)

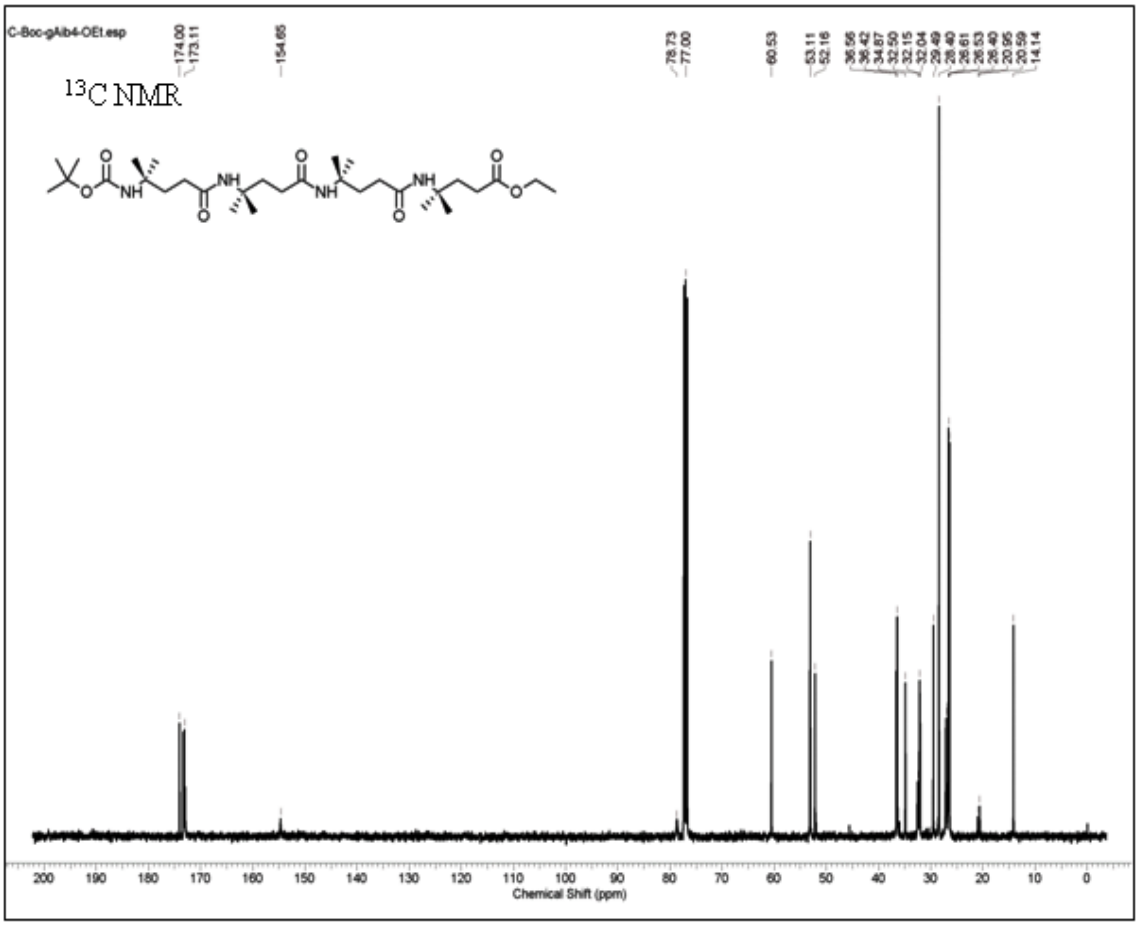
C-Boc-gAib4-OEt.esp
174.00
173.11
154.65
78.73
77.00
60.53
53.11
52.16
36.56
36.42
34.87
32.50
32.15
32.04
29.49
28.40
28.61
28.53
28.40
20.95
20.59
14.14
^{13}C NMR
Chemical Shift (ppm)

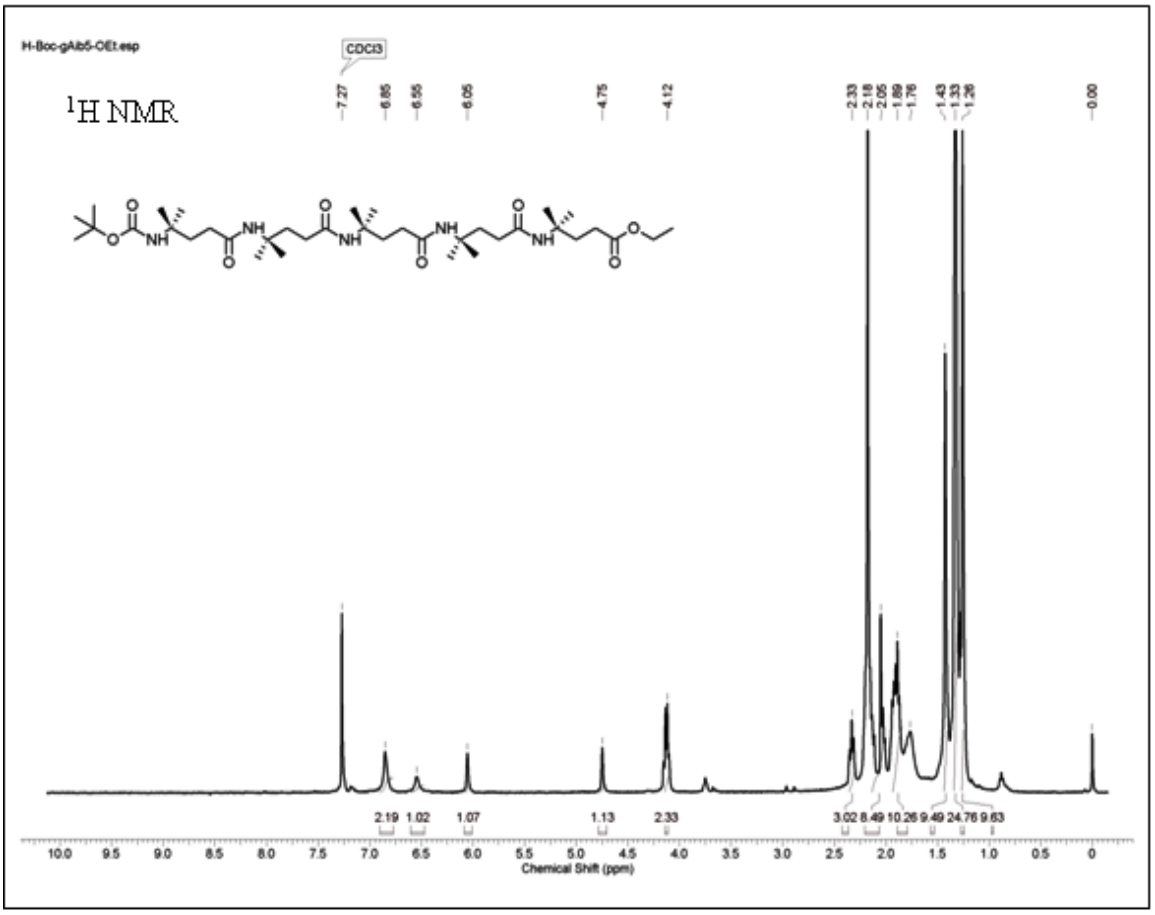
H-Boc-gAib5-OEt.esp
CDCl3
^{1}H NMR
7.27
6.85
6.55
6.05
4.75
4.12
2.33
2.18
2.05
1.89
1.76
1.43
1.33
1.26
0.00
2.19 1.02 1.07 1.13 2.33 3.02 8.49 10.26 9.49 24.76 9.63
Chemical Shift (ppm)

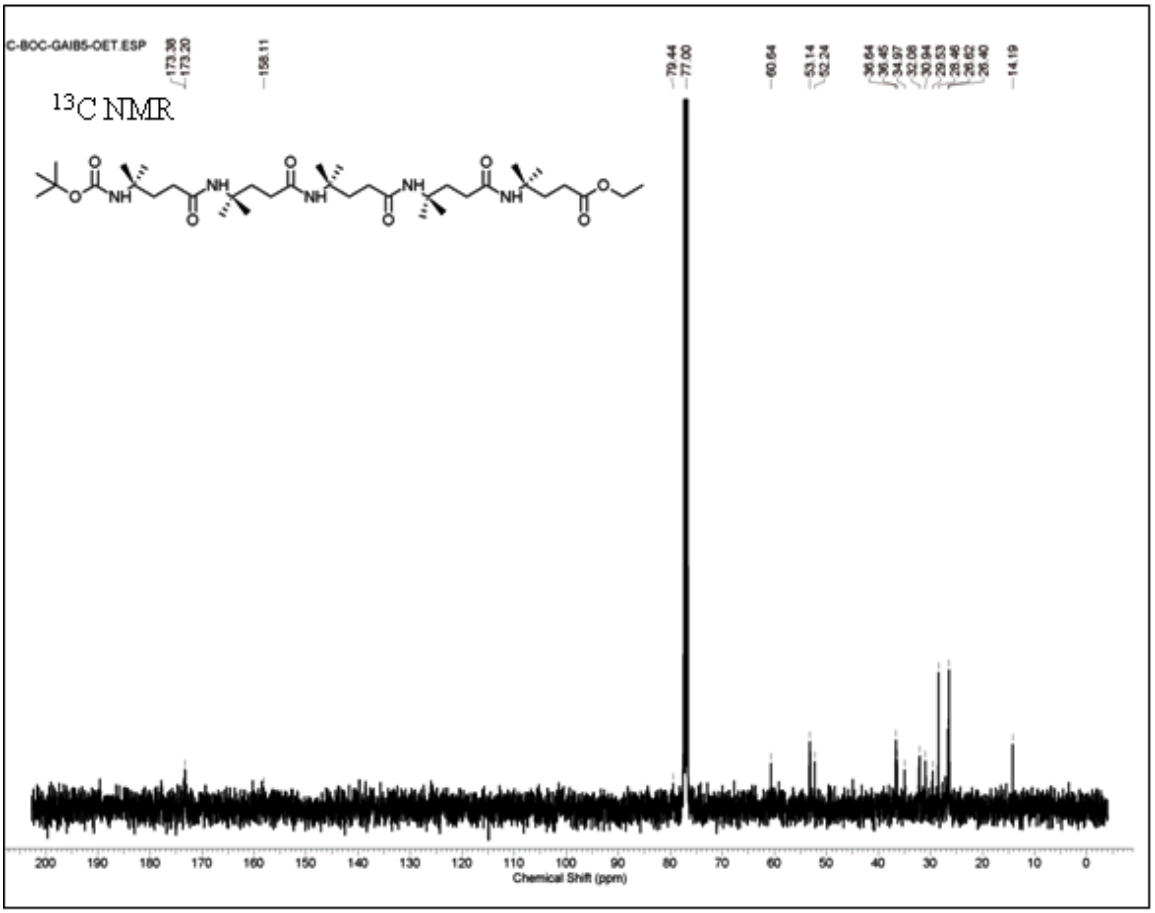
C-BOC-GAIB5-OET.ESP
^{13}C NMR
173.36
173.20
158.11
79.44
77.00
60.64
53.14
52.24
36.64
36.45
34.97
32.08
30.84
29.53
28.46
26.62
26.40
14.19
Chemical Shift (ppm)

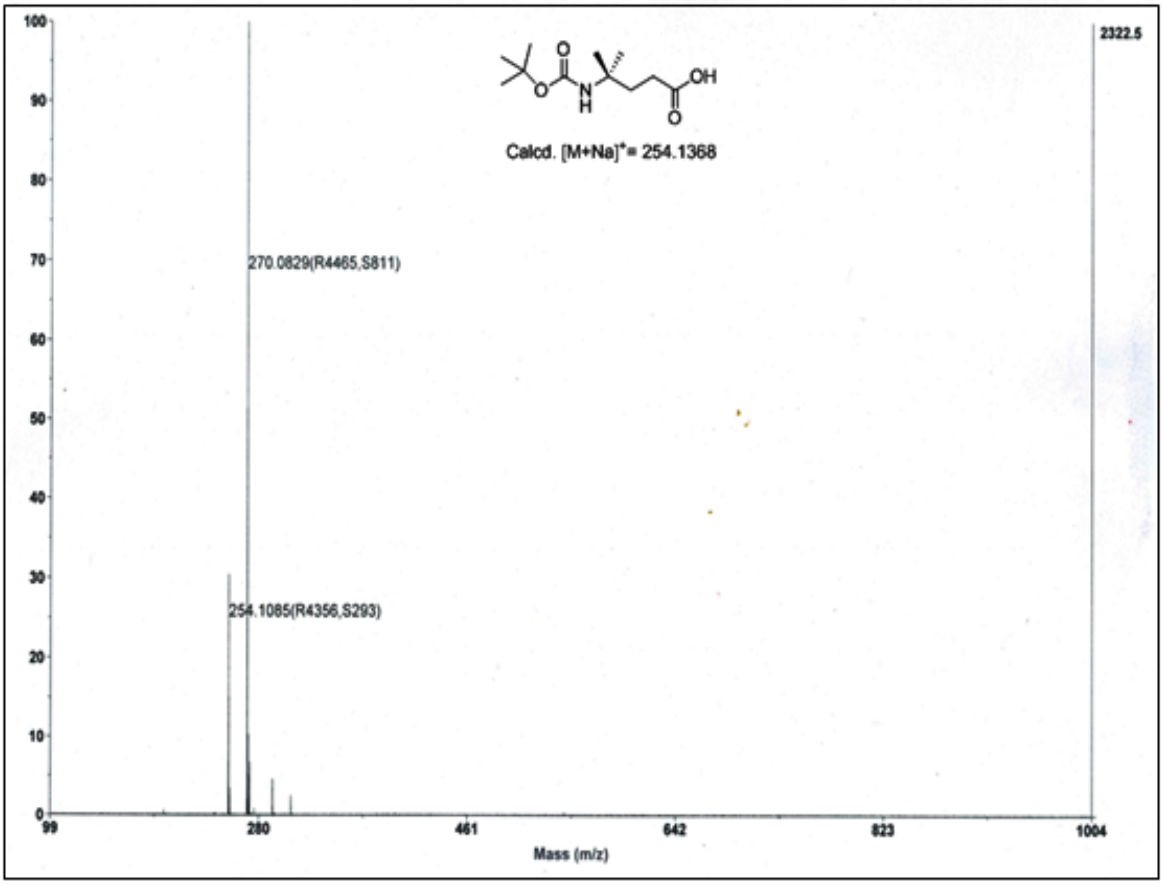
Calcd. [M+Na]+= 254.1368
270.0829(R4465,S811)
254.1085(R4356,S293)
2322.5
Mass (m/z)

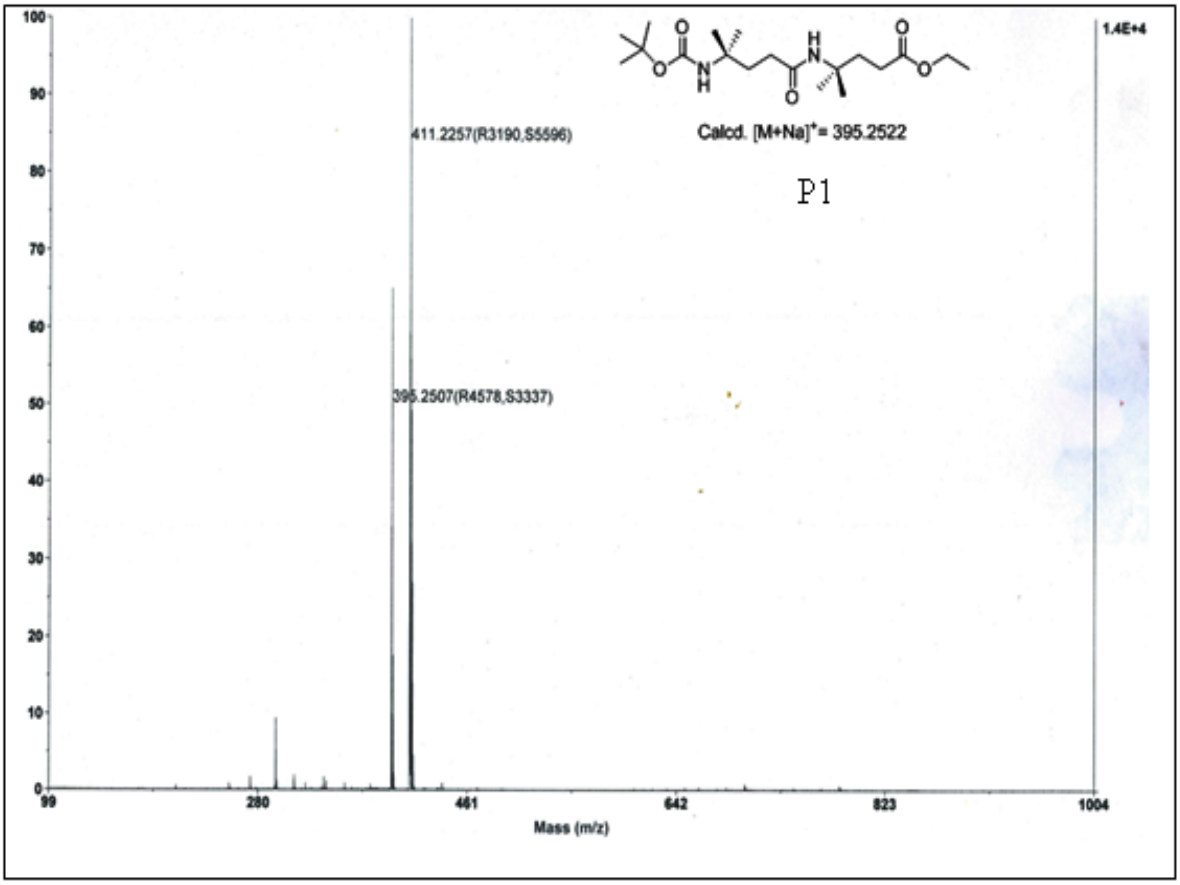
Calcd. [M+Na]+= 395.2522
411.2257(R3190,S5596)
395.2507(R4578,S3337)
P1
1.4E+4
Mass (m/z)

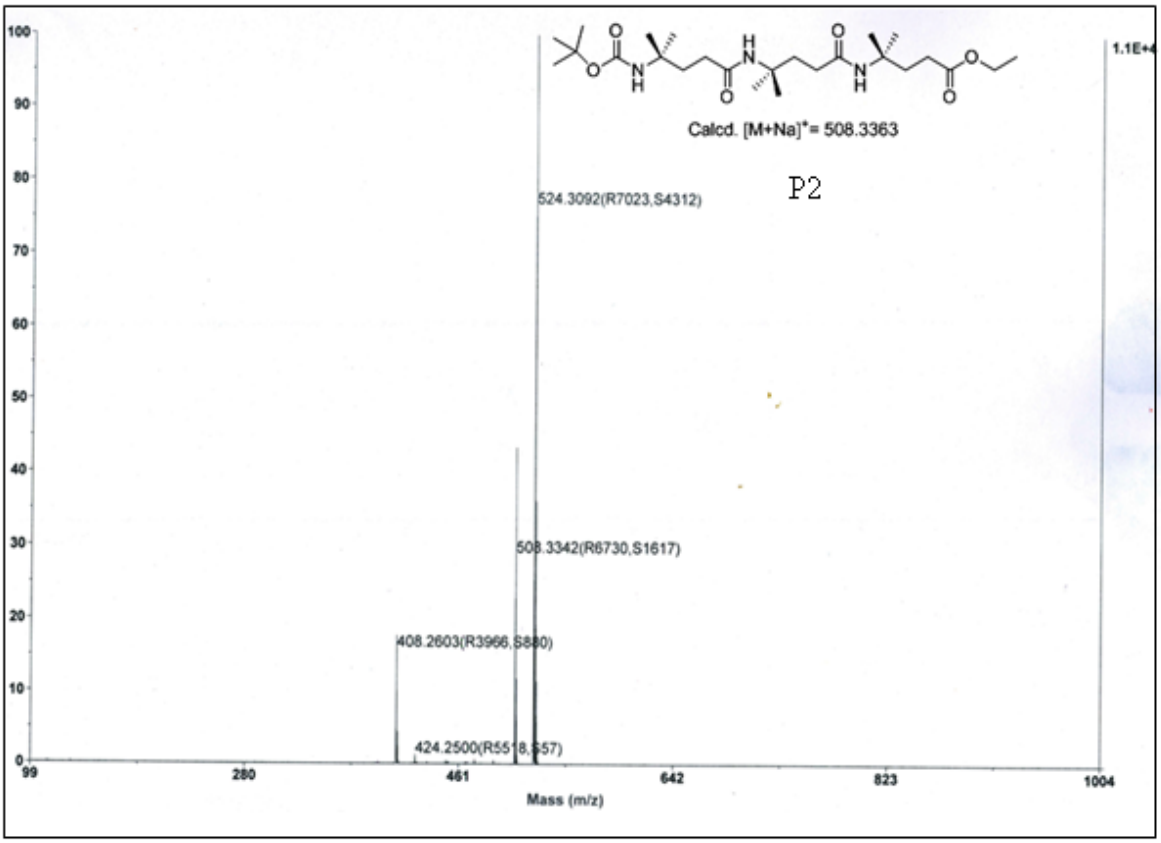
Calcd. [M+Na]+= 508.3363
P2
524.3092(R7023,S4312)
508.3342(R6730,S1617)
408.2603(R3966,S880)
424.2500(R5518,S57)
1.1E+4
Mass (m/z)

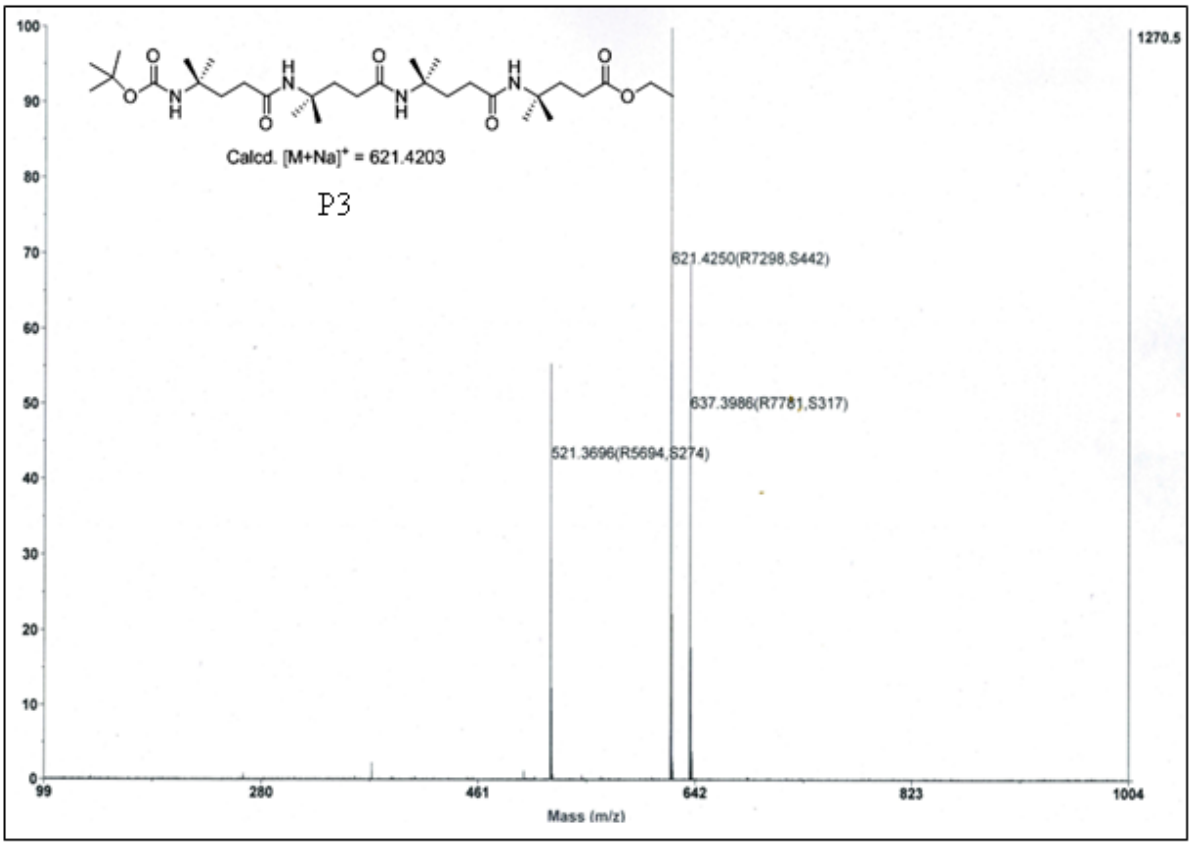
Calcd. [M+Na]+ = 621.4203
P3
621.4250(R7298,S442)
637.3986(R7781,S317)
521.3696(R5694,S274)
1270.5
Mass (m/z)

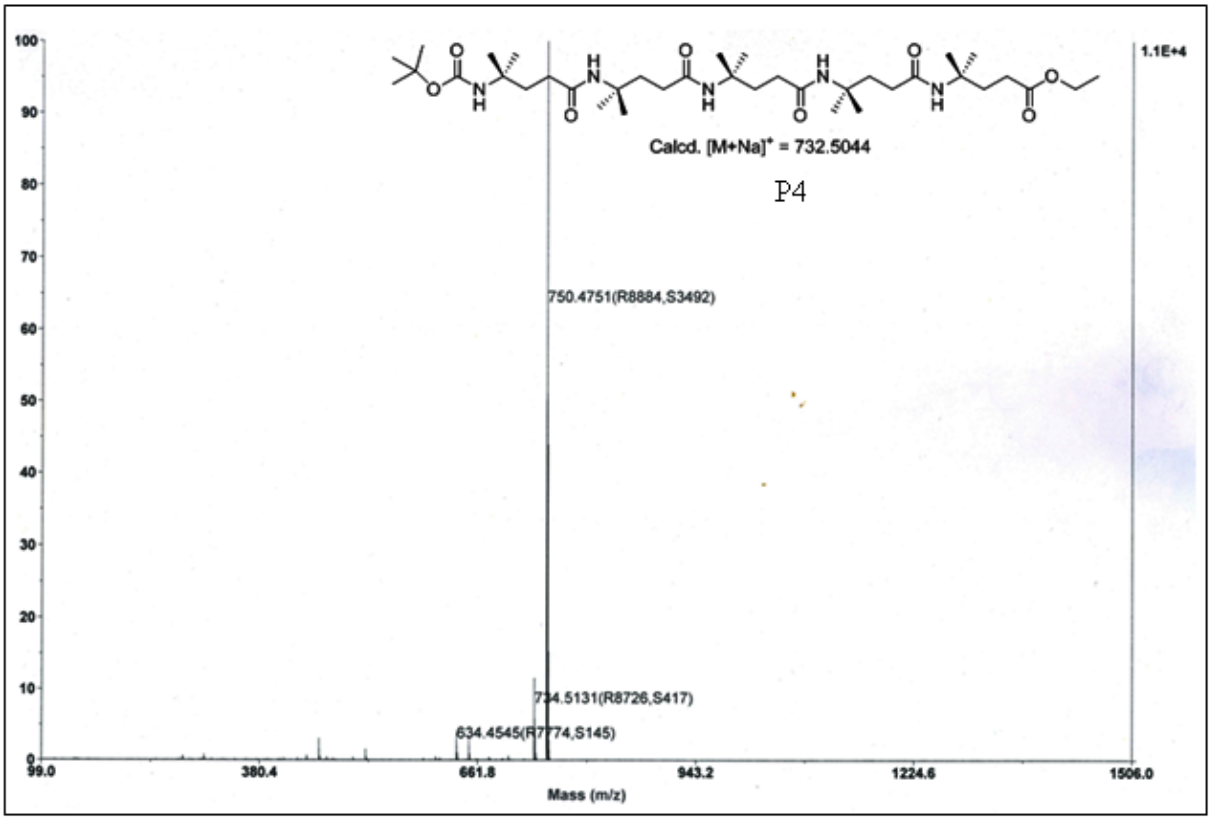
Calcd. [M+Na]+ = 732.5044
P4
750.4751(R8884,S3492)
734.5131(R8726,S417)
634.4545(R7774,S145)
1.1E+4
100
90
80
70
60
50
40
30
20
10
0
99.0
380.4
661.8
943.2
1224.6
1506.0
Mass (m/z)

Chapter 4

γ-Amino Acid Mutated α-Coiled Coils as Mild Thermal Triggers for Liposome Delivery

4.1 Introduction

Majority of the cancer drugs in current use are broadly cytotoxic and their delivery to the specific target cells is rather challenging. Due to their biocompatibility, biodegradability, low toxicity, control on size and a capacity to modify the pharmacokinetic profiles, phospholipid vesicle nanocarriers have been gaining momentum for the site-specific delivery of the drug molecules.[1]Since their first discovery in 1961, liposomal drug delivery is gaining momentum in the treatment of cancer. Liposomes are nano-vesicles composed of lipid bilayer as shown in Figure 4.1. The shortcoming of liposome based drug release is

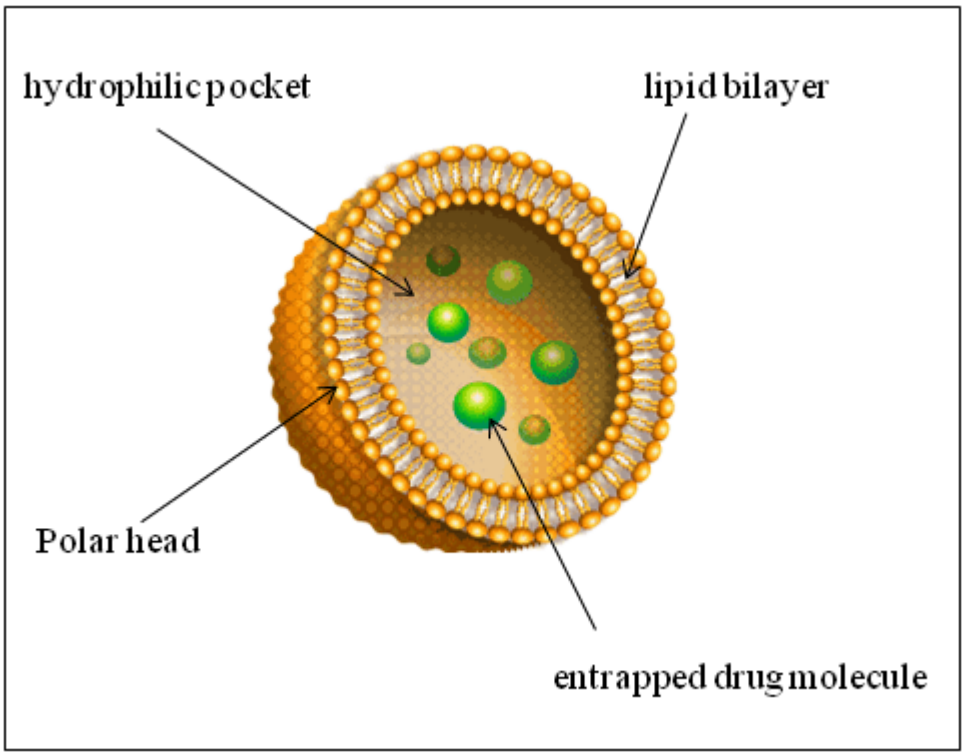

Figure 4.1 Schematic representation of liposome.

that it depends on the passive leakage of content and is a very slow process. Several efforts are since identified to enhance the rate of leakage from the liposomes. Various external stimuli-regulated release approaches have been developed for pH, ultrasound, temperature, light, enzymes, redox, magnetic field, etc. to overcome these limitations.[2] Among these, temperature-sensitive liposomes are widely studied because it is easy to vary local body temperature in response to surrounding conditions. In recent years, peptide based thermosensitive liposomes (TSL) have attracted much attention as their transition temperature can be controlled efficiently depending upon sequence and length of peptides.[3] The change in conformations of the peptides within the bilayers of liposome

when exposed to mild heating enables the release of encapsulated drug molecules. Such thermoresponsive peptides have shown promising results in the cancer therapy. Here in chapter 4, we demonstrate the utility of thermoresponsive coiled coil peptides with heterogeneous backbone as a trigger for controlled release of fluorescent marker from liposome.

4.1.1 Coiled coil peptides

Coiled coils are the best understood super secondary structural motifs widely present in protein structures[4] (Figure 4.2). The conformations of coiled-coils are prescribed primarily by a seven-residue ('heptad') sequence repeat, denoted as *a-b-c-d-e-f-g*. Positions '*a*' and '*d*' are predominantly occupied by the hydrophobic residues; often by valine, leucine and

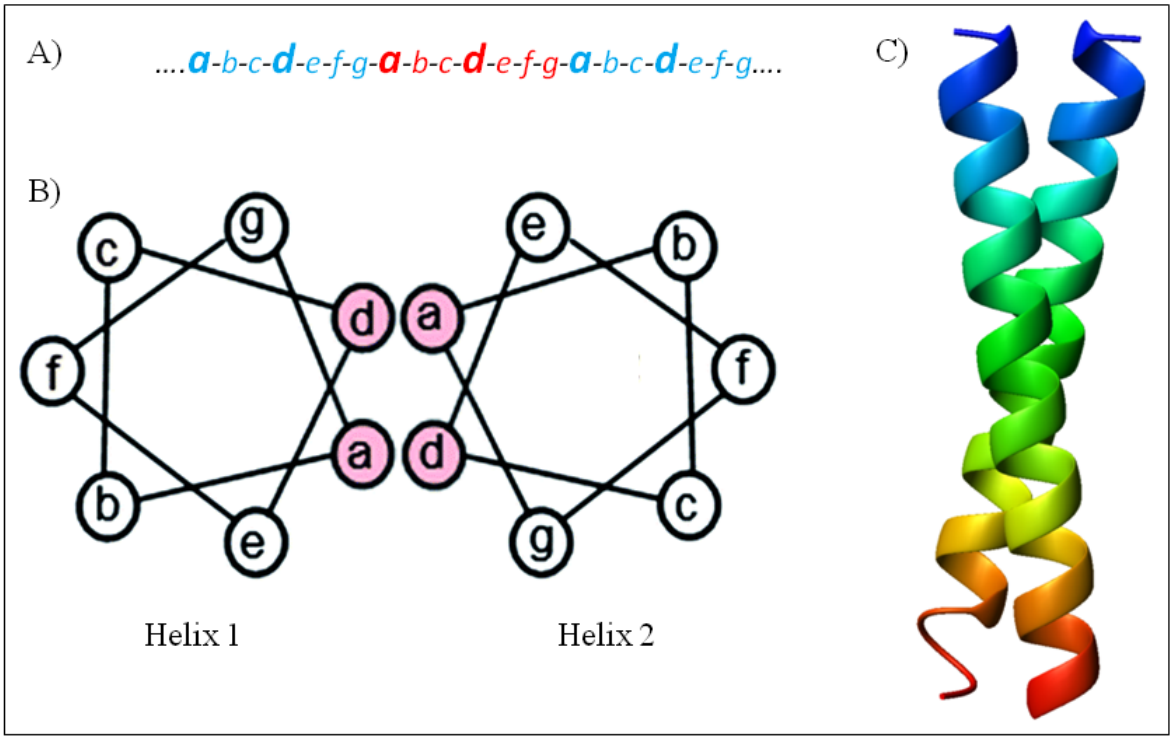

Figure 4.2 A) Heptad repeats in linear sequence of coiled coil peptides. Hydrophobic positions in each heptad are highlighted in bigger size. B) Schematic representation of dimeric coiled coil formation. Hydrophobic stripe is shown in pink color. C) Pictorial representation of left handed coiled coil.

isoleucine. The hydrophobic residues play crucial role in deciding stoichiometry of coiled-coils as when linear sequence of 'heptad' repeat folds in helical fashion, all hydrophobic residues at '*a*' and '*d*' positions align at one face of helix to form hydrophobic 'stripe'

(Figure 4.2). This hydrophobic 'stripe' further coils around another helix which drives the helical oligomerization. Left handed coiled coils are predominant in nature. The oligomerized helices in coiled coil domain are further stabilised by the polar/ionic interactions between side-chains of amino acids at '*e*' and '*g*' positions. All hydrophobic amino acids get buried in 'hydrophobic Pocket' of coiled coil. Overall, coiled coil packing is dictated by both van der Waals interactions between the side-chains of amino acids at '*a*' and '*d*' positions as well as ionic and polar interactions between sidechains of amino acids at '*e*' and '*g*' positions. Due to their active participation in various biological processes, the design of coiled coil domain has attracted much attention from various investigators for past several decades.[5,6]

4.1.2 Mutated coiled coils with unnatural β- and γ- amino acids

Helix bundle quaternary structures by selective replacement with β and γ residues are studied recently.[7-10]This literature report clearly indicates that backbone homologated amino acids such as β- and γ- amino acids can be incorporated in α-helical coiled coils to produce the artificial motif. Such kind of artificial motifs would be useful models to understand important biological events such as protein-protein interactions. Importance of coiled coil domains in protein-protein interactions which regulates various biological functions such as replication, transcriptional control, viral infection, etc. motivated us to build the artificial coiled coil model comprised of γ^4-amino acids synthesized in our laboratory as described in Chapter 1. In this regard, we sought to investigate stability, compatibility and tolerance to accommodation of γ-amino acids into the coiled-coil structures. As all above efforts reported in literature were identified mostly to incorporate backbone homologated amino acids in coiled coil peptides at the position other than hydrophobic stripe, we took the challenge to mutate coiled coil domain with γ^4-residues at hydrophobic pocket.

4.2 Results and Discussion

4.2.1 Design and Synthesis of γ-amino acid mutated coiled coils

Two additional methylene units (CH_2-CH_2) in α-amino acids yield the corresponding γ^4-amino acids. We have previously investigated the conformational preferences of heterogeneous α- and γ^4-amino acids containing peptides.[11] In order to understand the

P1 Ac-LKEIEDK LEEIESK LYEIENE LAEIEKL-NH_2

P2 Ac-LKKIKDK LEKIKSK LYKIKNE LAKIKKL-NH_2

P3 Ac-LKEIKDK LEEIESK LYEIENE LAEIEKL-NH_2

P4 Ac-LKKIKDK LEKIKSK LYKIKNE LAKIKKL-NH_2

P5 Ac-LKEIKDK LEEIESK LYEIENE LAEIEKL-NH_2

P6 Ac-LKEIKDK LEEIESK LYEIENE LAEIEKL-NH_2

P7 Ac-LKEIKDK LEEIESK LYEIENE LAEIEKL-NH_2

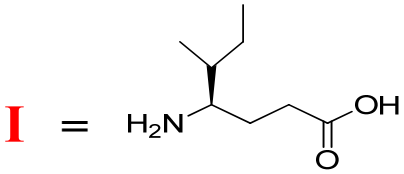

Scheme 4.1 Amino acid sequence for peptides synthesized on solid phase. Positions of γ^4-isoleucine are shown in red color.

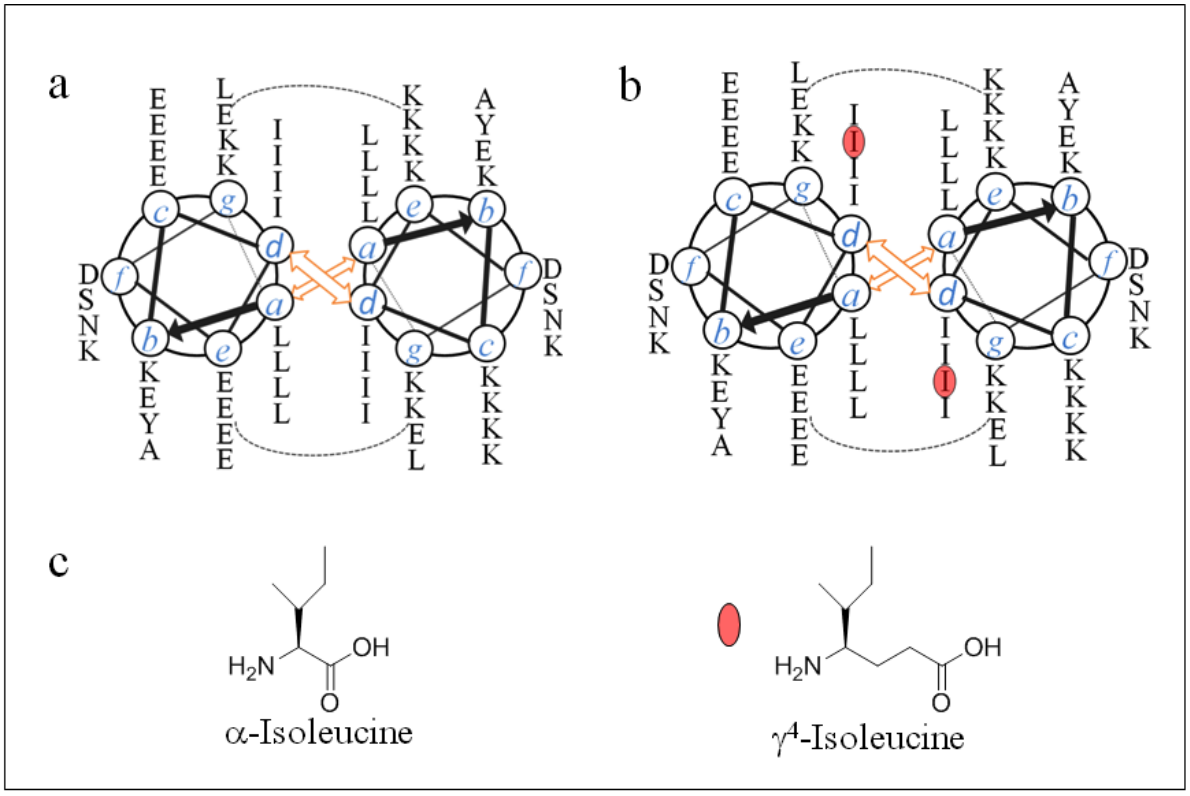

Figure 4.3 Arrangement of amino acids in coiled coil heterodimer of a) wild type **P1**/**P2** and b) mutated **P3**/**P4** is shown in wheel diagram. Mutations in hydrophobic stripe are shown in red circles. c) Structures of α- and γ^4-isoleucine.

stability and stoichiometry of coiled coil α-peptide sequence on selective α→γ replacement in hydrophobic stripe, we chose to adopt engineered heteromeric variant of GCN4 pLI sequence **P1** and **P2** earlier characterized by Fairman and co-workers.[12] The amino acid sequence for heteromeric coiled coils are shown in Scheme 4.1. In the mutated peptides **P3** and **P4**, we selectively replaced eighteenth α-isoleucine residue in third heptad of **P1** and **P2** with γ^4-isoleucine, respectively (Figure 4.3). All peptides were synthesized using MBHA Knorr amide resin by standard Fmoc-chemistry and HBTU/HOBt coupling conditions. The γ^4-Ile was synthesized starting from α-isoleucine as described earlier in Chapter 1 and protected with solid phase compatible Fmoc-group. In **P3** and **P4**, original side-chains are retained at modification sites while two additional methylene units are introduced in the backbone which makes it heterogeneous.

4.2.2 Conformational studies of synthesized peptides using Circular Dichroism (CD)

Further, to understand the folding properties of synthesized peptides, CD analysis was undertaken. Investigations revealed that similar to the **P1** and **P2**, individual peptide **P3** and **P4** displays random coil conformations in solution while their equimolar (15μM each) mixture displayed the coiled-coil conformation in solution (Figure 4.4A and B). This observation suggests that single modification at hydrophobic stripe of complementary peptides is tolerated in coiled coil formation. Instructively, CD analysis also reveals the coiled-coil conformation in equimolar complex between complementary **P1** and **P4** as well as **P2** and **P3** giving indication that tolerance of single mutation in the complementary sequences. We subjected all four sets of coiled-coils (**P1**/**P2**, **P1**/**P4**, **P2**/**P3** and **P3**/**P4**) for the temperature dependent unfolding CD experiments. Results are shown in Figure 4.5. We found that all peptides displayed coiled coil conformation at 20 °C and dissociate slowly with increasing temperature. These peptides further regain the coiled coil conformation upon cooling which suggests the thermoreversible nature of coiled coils. The thermal unfolding of the coiled coils was measured using the molar ellipticity values at 222 nm. The sigmoidal plot in Figure 4.6 was fitted to the two-state transition model as described by Marky and Breslauer.[13]Interestingly, peptide conformation melting temperature (T_m) for **P1**/**P2** was found to be 67 °C while that of for **P3**/**P4** was observed as ~ 40 °C. Peptide **P1**/**P4** and **P2**/**P3** displayed the melting temperature 66 and 56 ^oC respectively. The peptide conformation melting temperature (T_m) and free energy of the

process (ΔG) was determined using MATLAB program and the results are given in Table 4.1.

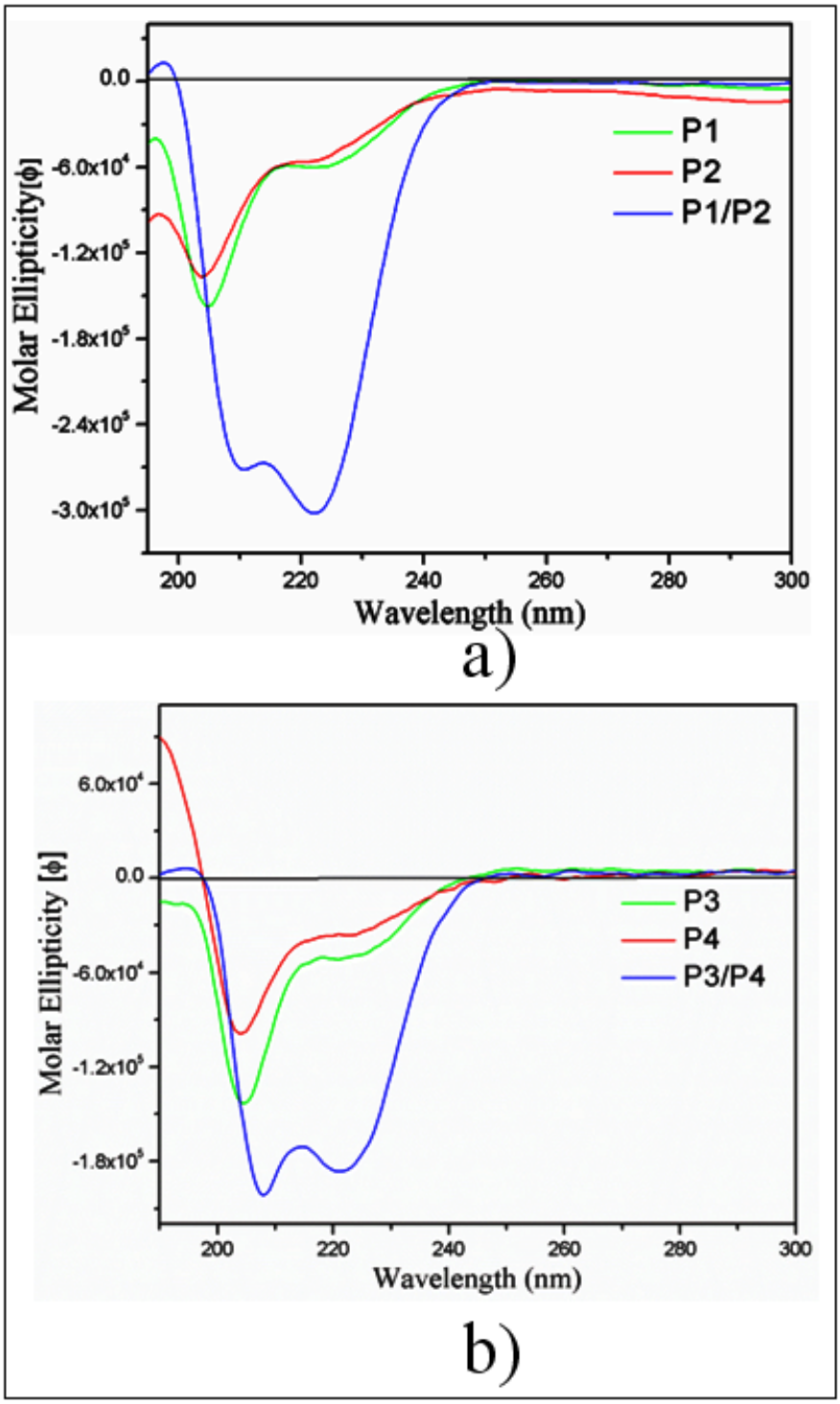

Figure 4.4 CD plot depicting the conformations of a) **P1**/**P2** and b) **P3**/**P4**.

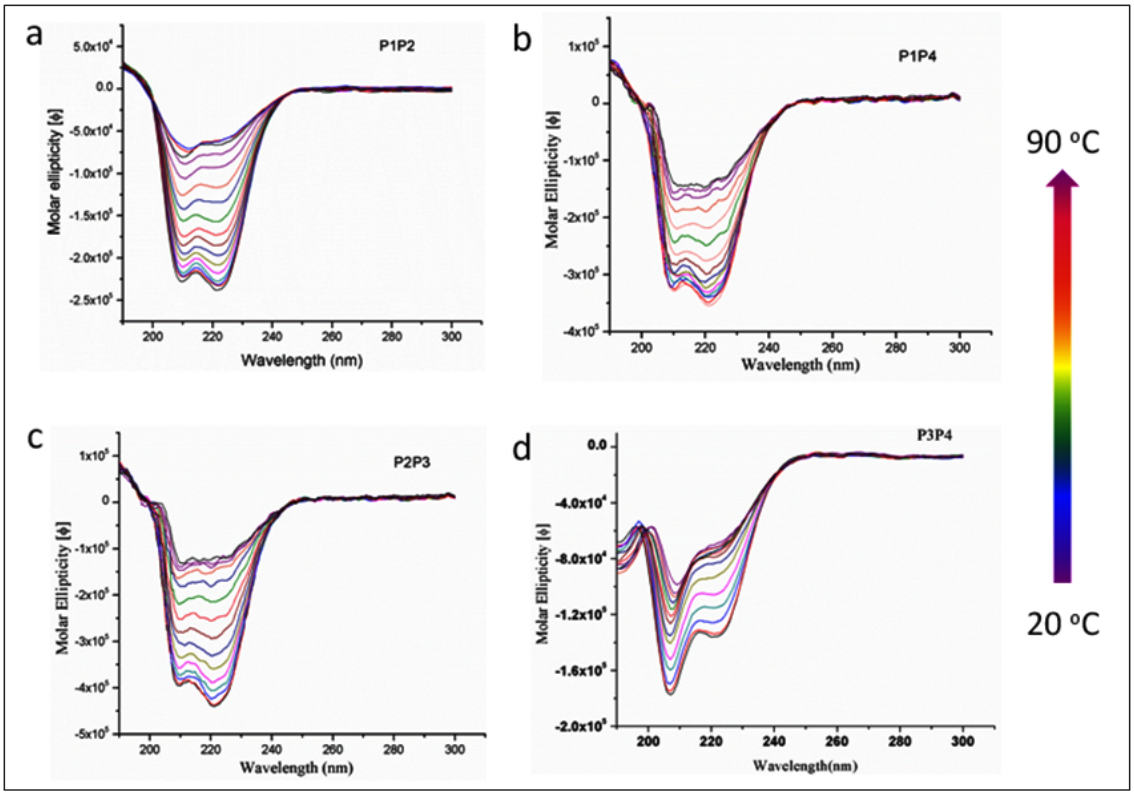

Figure 4.5 CD analysis depicting temperature-dependent conformational changes of coiled coil peptide hybrids. Concentration of each peptide is 15 µM (10 mM PBS, 150 m M NaCl) at 7.4 pH

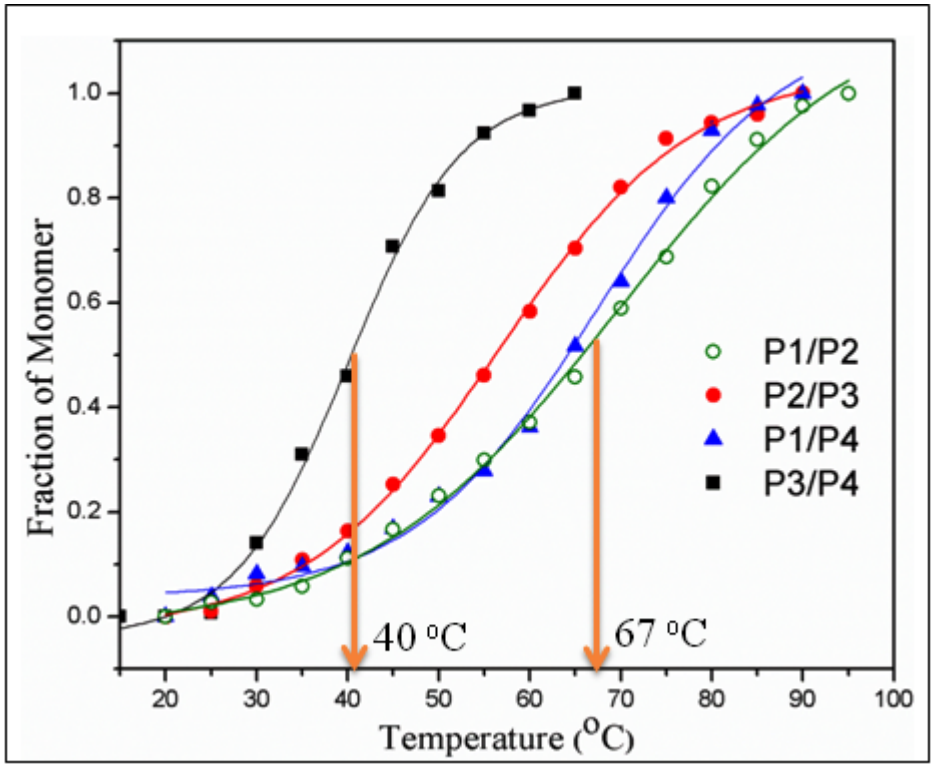

Figure 4.6 Two-state transition plot for equimolar peptide complex of complementary peptides.

Table 4.1 Thermodynamic parameters obtained from CD-thermal denaturation analysis of heterodimers.

peptide	ΔH(T_m) (Kcal/mole)	T_m (K)	ΔG_o (37°C) (Kcal/mole)
P1P2	-28.4426)	340.00	-9.617441
P1P4	-30.5341	339.38	-9.603605
P2P3	-33.37805	329.00	-8.701894
P3P4	-39. 8574	312.99	-6.812802

We anticipate that selective insertion of γ-amino acids and thereby adding two extra methylene groups in the backbone at modification site of complementary coiled-coils may lead to the partial perturbation in both hydrophobic and ionic interactions and eventually dissociates to individual peptides when exposed to mild thermal energy. As lowered T_m

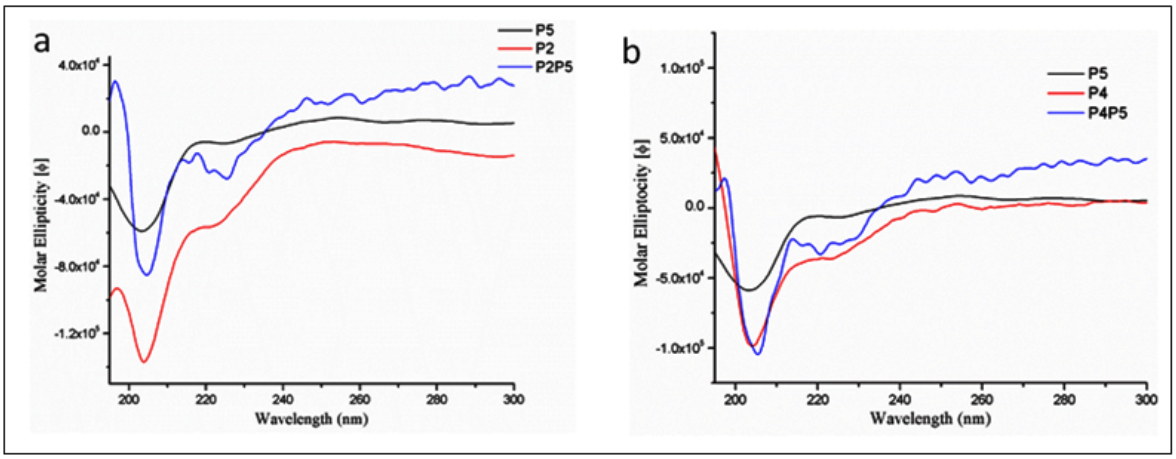

Figure 4.7 CD analysis suggests that **P5** with two mutation sites at hydrophobic stripe is reluctant to form coiled coil structures with a) **P2** and b) **P4.** Concentration of each peptide is 15 μM (10 mM PBS, 150 mM NaCl) at 7.4 pH and 20 °C.

values are obtained from the single site mutated peptides, we anticipate that another mutation in the hydrophobic pocket of the heptad repeat may not be tolerated for coiled coil folding. To confirm the anticipation, we synthesized **P5**, **P6** and **P7** respectively with two, three and four mutations in hydrophobic stripe of heptad repeats (Scheme 4.1). Indeed, CD analysis

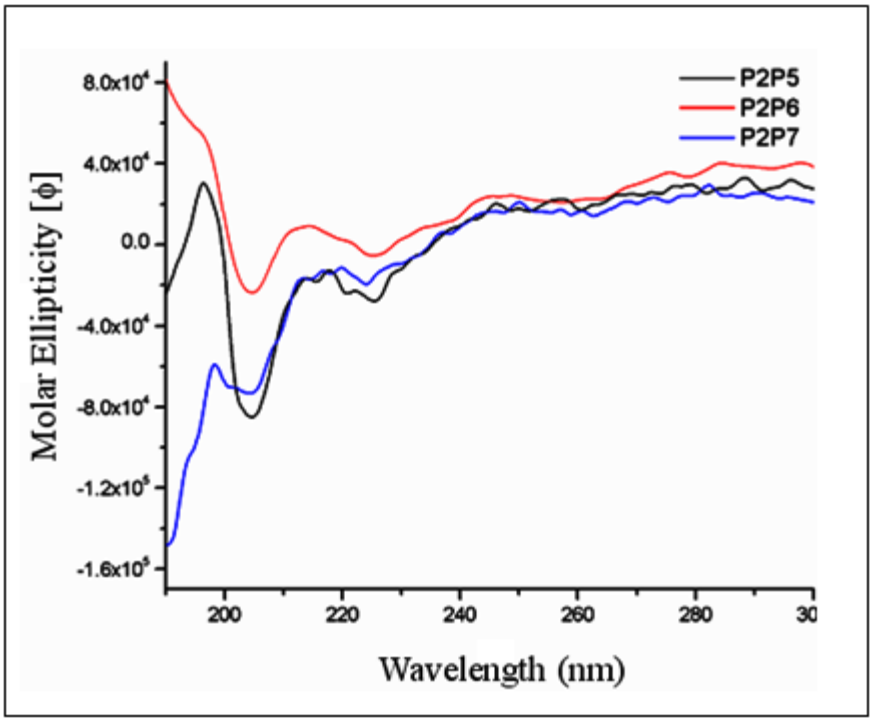

Figure 4.8 CD analysis depicting that peptides **P5**, **P6** and **P7** are unable to form coiled coil structures with complementary peptide **P2**. Concentration of each peptide is 100 µM (10 mM PBS, 150 m M NaCl) at 7.4 pH and 20 ^{o}C.

revealed that (Figure 4.7) double mutated peptide **P5** was found to be reluctant towards formation of coiled coil with complementary peptides **P2** and **P4**. Further, CD analysis of equimolar mixtures of **P5**, **P6** and **P7** with control peptide **P2** is also reluctant to undergo coiled-coil formation even at higher concentrations (100 µM each) as shown in Figure 4.8.

4.2.3 Isothermal Titration Calorimetry: Binding stoichiometry for complementary peptides

Isothermal titration calorimetry (ITC) is a versatile technique to understand the thermodynamic parameters and stoichiometry for various biological interactions such as protein-protein interactions, ligand-protein interactions and peptide-protein interactions.[14] We subjected the mutated coiled-coil **P3**/**P4** for isothermal titration calorimetry (ITC) experiments to understand binding thermodynamics and complex stoichiometry. The result of ITC binding isotherm after subtraction of background heat of dilution is shown in Figure 4.9A. In an exothermic event of binding between **P3** with **P4**, dissociation constant (K_d) was found to be 1.4 µM and surprisingly complex stoichiometry was found to be ~ 1, which clearly indicates that mutated peptides are coiled coils heterodimers in solution.

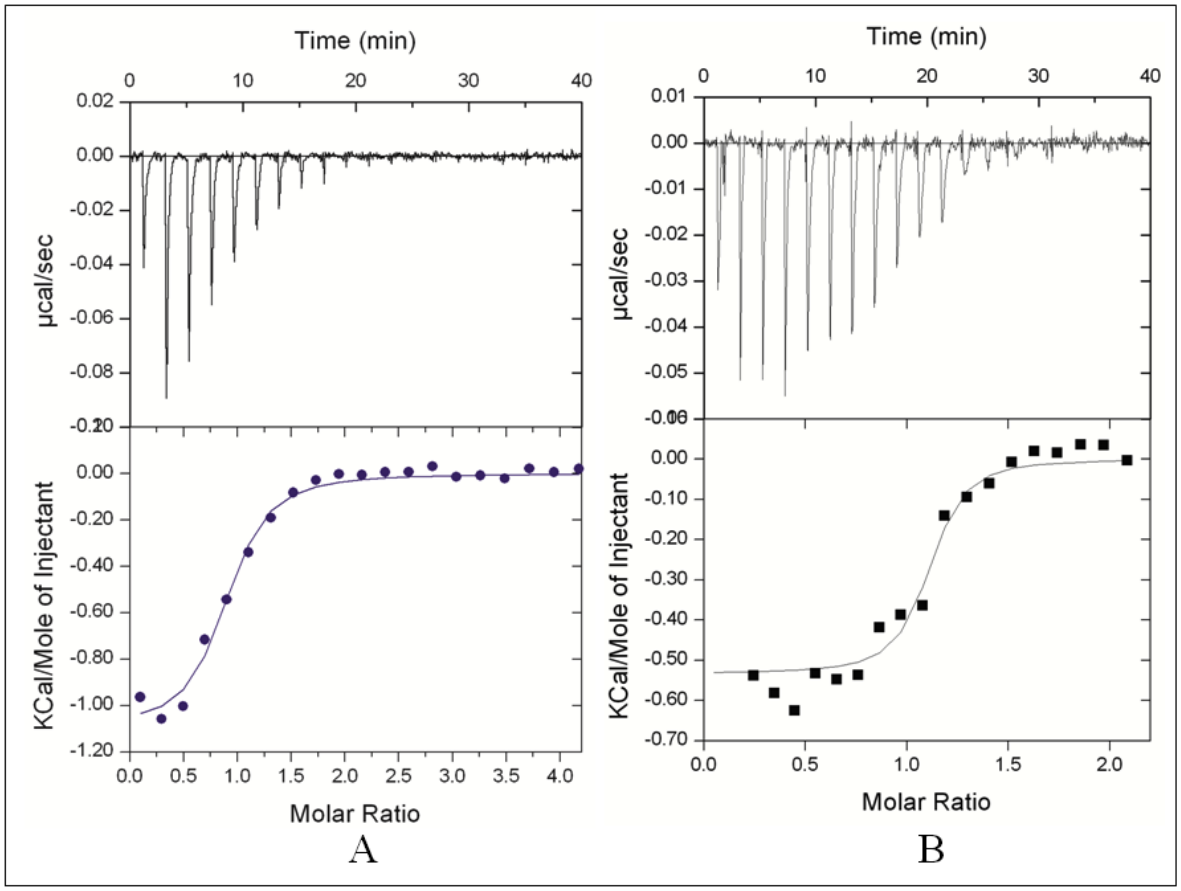

Figure 4.9 Isothermal titration calorimetry studies: isotherm showing exothermic binding in heterodimer formation between A) **P3** and **P4** and B) **P2** and **P3**

Similarly, isothermal titration between **P2** and mutated **P3** also displayed dimeric coiled coil folding. (Figure 4.9B). Although, α-peptide coiled coils **P1** and **P2** displayed tetrameric organization, the mutated coiled-coils showed heterodimeric coiled-coil conformation.[12] There are several evidences in literature which elucidates the effect of guest residues on complex stoichiometry of α-amino acid sequence of coiled coil peptides.[6]

4.3 Liposomes in drug delivery

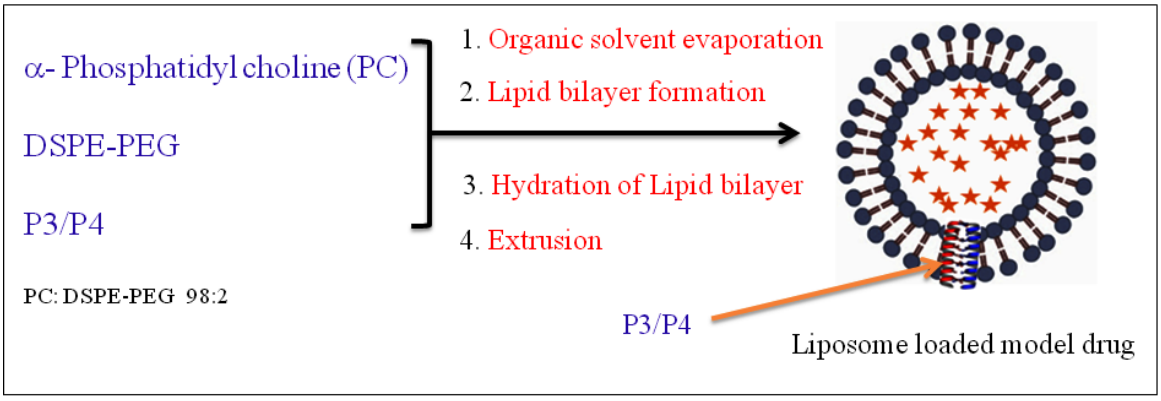

Figure 4.10 Synthesis of coiled coil peptide (**P3**/**P4**) decorated liposomes encapsulated with carboxyfluorescein as model drug.

As an evident from CD and ITC analysis, selective introduction of γ^4-isoleucine in α -coiled coil peptide can be used as a tool to tune their conformational properties. The control of γ-residues on T_m values of coiled coil peptides motivated us to understand whether these hybrid complementary heterodimers can be used as external thermal trigger for the controlled release of encapsulated drug molecules from liposomes on mild heating. Kostarelos and colleagues recently demonstrated the use of forty three residue homodimer of leucine zipper peptides for

release of doxorubicin from the liposomes by mild hyperthermia.[15] Coiled coil heterodimers are also gaining much attention due to their diverse utility in ranging from signal transduction to self-assembling biomaterials.[16] Diederichsen[17] and Kros[18]laboratories have recently demonstrated the use of coiled coil heterodimers in mimicry of SNARE-proteins in membrane fusion. Motivated with T_m values little above the physiological temperature (~ 40 °C), we anticipate that these **P3**/**P4** heterodimers can be utilized as a trigger to release entrapped drug molecules or genes from liposomes on thermal stimuli.

4.3.1 Liposomes integrated with γ-amino acid mutated coiled coil

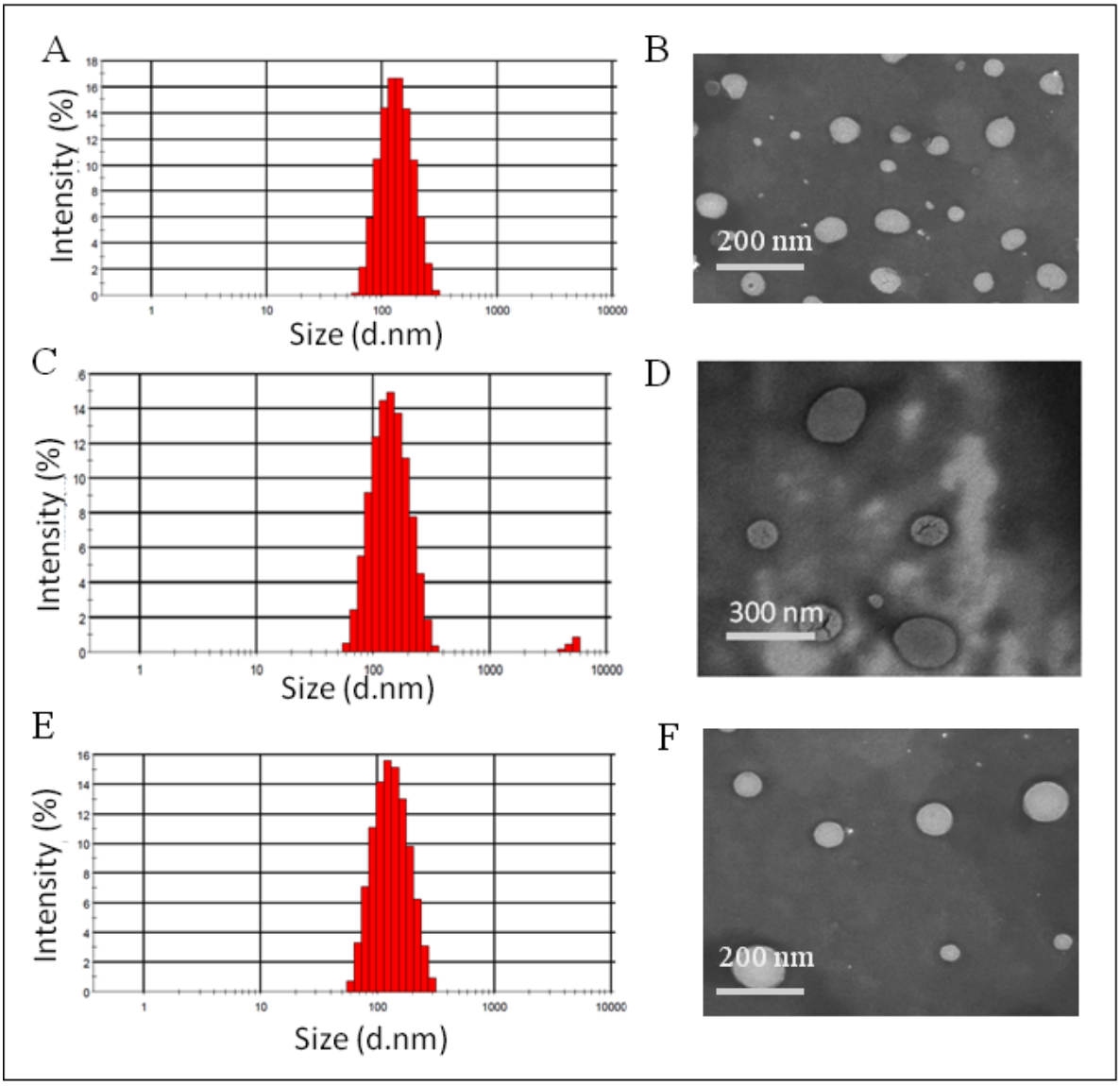

Figure 4.11 DLS and SEM analysis for **P3**/**P4** liposome composite (A and B), **P1**/**P2** liposome composites (C and D) and for plain liposome (E and F).

To test our hypothesis, we synthesized lipid-peptide hybrid vesicles encapsulated with carboxyfluorescein as fluorescent marker via extrusion as shown in Figure 4.10.[2a] Coiled coil heterodimer **P3**/**P4** was mixed with PC/DSPE-PEG_{2000} (98:2) lipid combination before bilayer formation at the molar ratio of 10:1 (lipid: peptide). Similarly, Liposome composite of **P1**/**P2** and plain liposome without any coiled coil decoration were also synthesized as a control. Mean diameter of synthesised hybrid liposomes were found to be ~ 126 nm as evident from dynamic light scattering (DLS) and scanning electron microscopy (SEM)

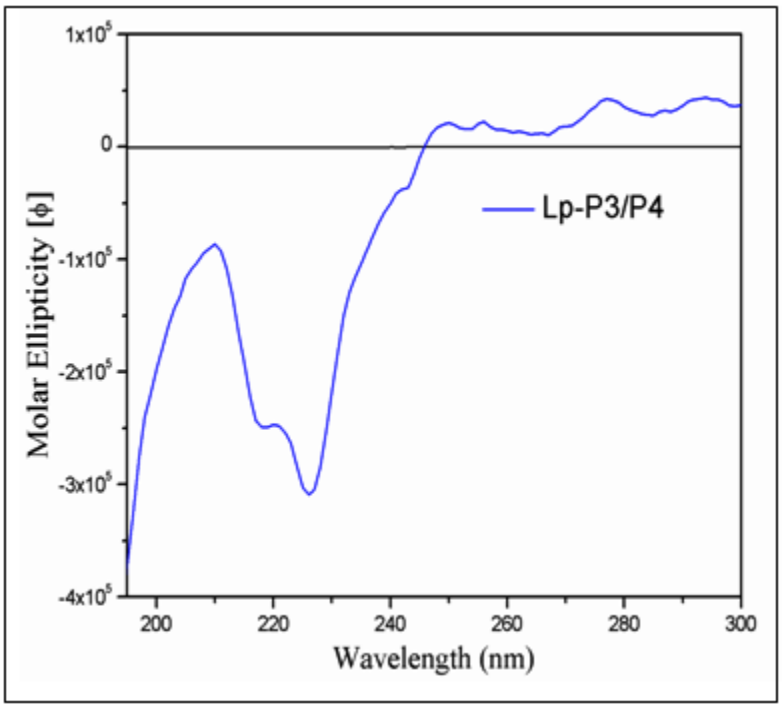

Figure 4.12 CD Spectrum of carboxyfluorescein loaded **P3**/**P4** liposome composite at 20 ^{o}C.

analysis as shown in Figure 4.11. The incorporation of the coiled-coils in the liposome bilayers was confirmed by CD analysis (Figure 4.12). Further, hybrid coiled coils (**P3**/**P4**) exhibited the unaltered thermoreversible folding (T_m ~ 40 °C) in lipid environment.

4.3.2 Release kinetics for thermoresponsive leakage from liposomes

The release of entrapped fluorescent molecules from liposome composites of **P1**/**P2** and **P3**/**P4** were monitored at room temperature (25 °C). No leakage of fluorescent molecule was observed from either of hybrid liposomes even after two days. Then we subjected both the hybrid liposome composites for mild hyperthermia at 40 °C. Course of reaction was monitored by fluorescence measurement of released carboxyfluorescein. The release profile is shown in Figure 4.13A. Intriguingly, the hybrid liposome comprised of mutated coiled coils **P3**/**P4** slowly released entrapped carboxyfluorescein and the leakage was continued up to 26 hrs. While no significant fluorescence leakage has been observed from **P1**/**P2** liposome composite at 40 ^{o}C. These results clearly indicates that when incorporated into bilayers of liposomes, the hybrid peptide **P3**/**P4** coiled coil can be used as thermal trigger for controlled release of content on mild hyperthermia which may further offers the unprecedented opportunities for controlled delivery of drugs, genes and other biomolecules at little above the body temperature. Depending on experimental results we have shown

the schematic representation for utilisation of heterogeneous backbone containing coiled coil as thermoresponsive trigger for model drug release from liposome (Figure 4.14).

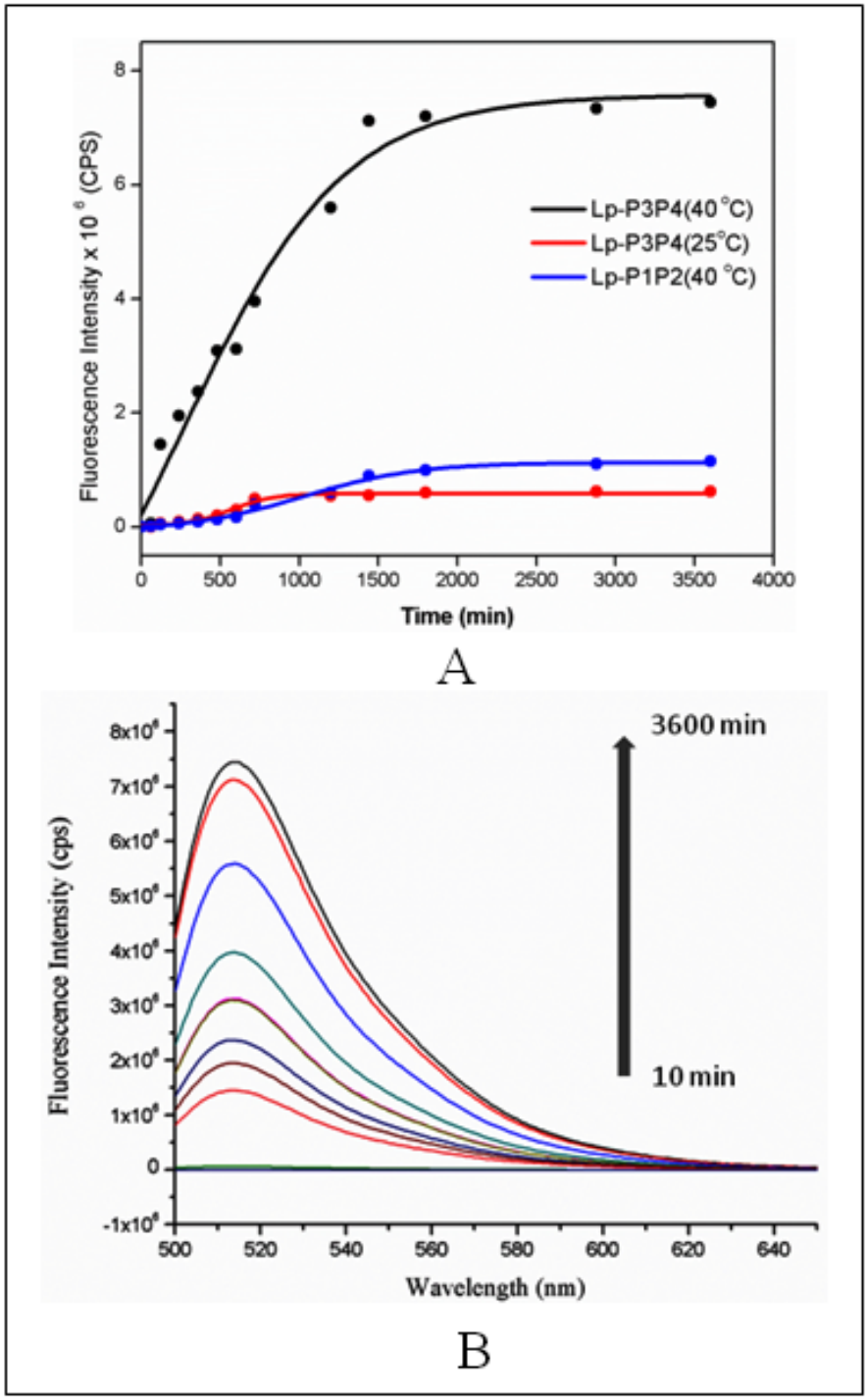

Figure 4.13 A) Release profile (emission at 514 nm) for leakage of carboxyfluorescein marker from liposomes decorated with coiled coil peptides. B) Fluorescence emission spectra at 514 nm indicate controlled release of carboxyfluorescein from **P3**/**P4** liposome composite at 40 °C.

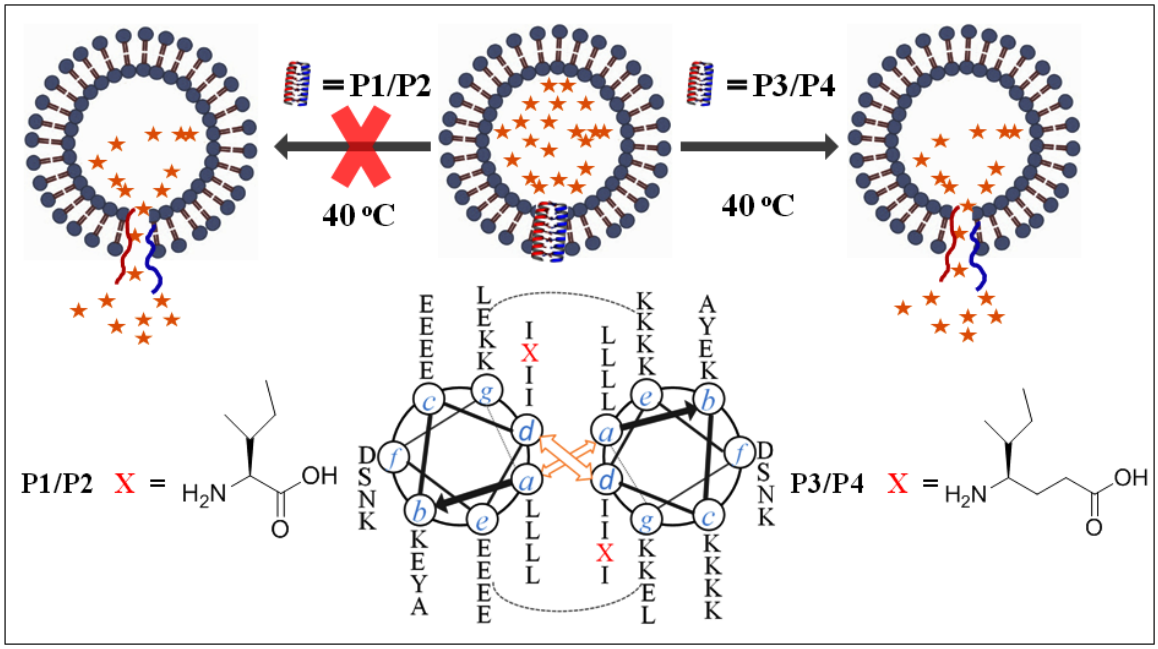

Figure 4.14 Schematic presentation depicting response of **P3**/**P4** to thermal stimuli for release of carboxyfluorescein from liposome.

4.4 Conclusion

In conclusion, we have demonstrated tolerance of α-coiled coils with single mutation with γ-residues at the hydrophobic positions of the heptad repeat without deviating the overall folding of the molecules. Mutations at more than one position at the hydrophobic sites lead to the loss of coiled coil conformations. The mismatched hydrophobic interactions due to two additional methylene units upon insertion of the γ-residues may lead to the decrease in their thermal denaturation temperature. The thermoreversible nature and the low T_m value observed for hybrid coiled coil peptides offer a unique opportunity to use them as external stimuli in liposomes upon mild hyperthermia to release the entrapped molecules.

4.5 Experimental section

4.5.1 Instrumentation

High Performance Liquid Chromatography (HPLC) was performed on a Waters 600 system. C18 reverse phase column (5 µm, 10 X 250 mm) from Waters was used for purification of peptides. The gradient applied was from 95% A to 95% B in 60 min, where A was water (0.1% TFA) and B was acetonitrile (0.1% TFA). Pure fractions of peptide were collected monitoring UV-Vis trace at 220 nm. Mass of pure peptides was confirmed

by Matrix Assisted LASER Desorption Ionisation (MALDI) TOF/TOF (4800 *Plus* from Applied Biosystems). Fluorescent measurement experiments were carried out in triplicate using FluoroMax-4 HORIBA fluorimeter, with 490 nm excitation and 500-650 nm emission range using 1/3 slit and 1 nm data interval. JASCO J-815 spectropolarimeter was used for circular dichroism (CD) analysis. Isothermal titration calorimetry (ITC) experiments were performed on iTC_{200} calorimeter from MicroCal at 25 ^{o}C. Liposomes were extruded using mini-extruder from Avanti Polar Lipids (USA). Dynamic light scattering (DLS) analysis of liposomes was carried out using *NanoZS90* Zetasizer (Malvern from UK). Scanning electron microscopic (SEM) imaging was performed using ZEISS ULTRA PLUS electron microscope operating at 30 kV.

4.5.2 Materials

All N-Fmoc protected amino acids were purchased at their synthesis purity grade from Sven Genetech. MBHA knorr amide resin (substitution value 0.2 mmol/g) was purchased from Novabiochem. Following compounds bought from Sigma-Aldrich: O-(benzotriazol-1-yl)-N, N, N', N'-tetramethyluronium hexafluorophosphate (HBTU), dimethyl formamide (DMF), N-methyl-2-pyrrrolidone (NMP), diisopropylethylamine (DIPEA), piperidine, trifluoroacetic acid (TFA), triisopropyl silane (TIPS), α-phosphatidylcholine (PC), monobasic potassium and dibasic sodium phosphate, sodium chloride, sephadex G-50 and carboxyfluorescein. HPLC grade acetonitrile was purchased from Merck. Water was obtained from Milli-Q water purification system (Millipore). 1,2-Distearoyl-***sn***-glycero-3-phosphoethanolamine-N-[amino(polyethylene glycol)-2000] (ammonium salt) i.e. DSPE-PEG(2000)Amine was purchased from Avanti Polar Lipids Inc. A stock solution of 0.1 M phosphate buffer was adjusted to pH 7.4. 10 mM phosphate buffer was prepared as needed by diluting the 0.1 M stock and adjusting to pH 7.4. All biophysical characterizations were performed in phosphate-buffered saline (PBS: 10 mM phosphate, 150 mM NaCl, pH 7.4). Final concentrations of all peptides were prepared from their respective stock solution as needed.

4.6 Methods

4.6.1 Peptide Synthesis:

The *N*-acetylated peptides were synthesized on a MBHA Knorr amide resin on a 0.1 mmol scale on a CEM microwave-assisted synthesizer. The synthesis was carried out in NMP by a standard Fmoc protocol using HBTU as coupling reagent. Fmoc deprotection was

accomplished by a solution of 20% piperidine in DMF. N-Acetylation of the peptides was carried out using acetic acid anhydride/pyridine (1:9). Acidic cleavage from the resin was achieved by treatment of the resin with a mixture of trifluoroacetic acid (TFA)/ triisopropylsilane/water (90:5:5, 2 h). The resin was extracted with additional TFA (5 mL), and the combined extracts were concentrated under vacuum. The crude peptide was then precipitated in cold diethyl ether (30 mL) and isolated by centrifugation and decantation of the ether. The precipitate was redissolved in 5 mL of a 1:1 mixture of acetonitrile/water and then lyophilized to give a fine white solid.

4.6.2 Peptide purification:

Peptides were purified by reversed-phase HPLC using a Waters C18 column (5 μm, 10 X 250 mm). The gradient applied was from 95% A to 95% B in 60 min; where A was water (0.1% TFA) and B was acetonitrile (0.1% TFA) at a flow rate of 2 mL/min. Pure fractions of peptide were collected monitoring UV-Vis trace at 220 nm.

4.6.3 Peptide characterization:

The peptides were characterized by mass spectrometry on an Applied Biosystems 4800 *Plus* MALDI-TOF/TOF instrument (matrix: α-cyano-4 hydroxycinnamic acid (CHCA), external calibration). Purity of peptides was also tested by HPLC trace.

4.6.4 Circular Dichroism (CD) Spectroscopy:

CD spectra and thermal-denaturation curves were recorded using a JASCO J-815 spectropolarimeter fitted with a Peltier temperature controller. CD spectra were measured at 30 μM total peptide concentration (15 μM each) in PBS (10 mM phosphate, 150 mM NaCl, pH 7.4) at 20 °C in 2 mm quartz cuvettes at 50 nm/min scanning speed. Thermal-denaturation experiments were performed by heating from 20 to 90 °C at a rate of 1 °C/min. The CD signal at 222 nm was recorded at 5 °C intervals. Each experiment was performed in triplicate.

4.6.5 Isothermal titration calorimetry (ITC):

ITC experiments were performed on iTC200 calorimeter from MicroCal. Following conditions are applied for experiment: auto baseline equilibration at 25 ^{o}C temperature, 1000 rpm stirring speed, 60 s initial delay, 18 injections of 2 μL spaced by 120 s, 5 s filter period. Both the cell and syringe were washed and dried thoroughly at the beginning of

experiment. All peptides solutions were prepared in PBS (10 mM phosphate, 150 mM NaCl, pH 7.4) buffer. Concentration of peptide in cell (P3) and syringe (P2 or P4) were fixed at 30 μM and 600 μM, respectively. Final concentration of peptides was prepared by dilution of their respective stock solutions. The centrifugated peptide solutions stored at 20 ^{o}C and degassed for 5 min prior to the experiments. Results were reproduced thrice for each experiment. MicroCal Origin software was used to analyse the data. Sigmoidal curve fitting was performed with "one binding site" model.

4.7 Thermodynamic parameter measurements from CD-thermal denaturation analysis:

Thermodynamic parameters were determined by nonlinear least square fitting of the normalized CD melting curves to five parameters (a, $[\theta]_M$ (0), $[\theta]_D(0)$, ΔH_m , and T_m). Ellipticity was normalized to fraction monomer using the equation (1).

$$\theta = (\theta_M - \theta_D)f_M + \theta_D \quad (1)$$

where θ_M and θ_D represent the ellipticity values for the fully unfolded monomer and fully folded dimer species respectively at each temperature. θ_M was found to be constant at the temperatures higher than the melting region for all the pepetides studied. θ_D was approximated by a linear function of temperature $\theta_D = \theta_D[0] + aT$. The fraction monomer ($f_M$) was expressed in terms of the equilibrium constant after solving the equation for a bimolecular reaction 2M → D:

$$P_M = [(8KC + 1)^{1/2}-1]/4KC \quad (2)$$

where K is the equilibrium constant and C is the total peptide concentration. K was assumed to be temperature dependent according to the equation (3):

$$K = e^{-\Delta G/RT} \quad (3)$$

The Gibbs–Helmholtz equation can be used to express the temperature dependence of ΔG in terms of ΔH_m and T_m as given by Equation (4):

$$\Delta G = \Delta H_m \,.\, (1 - T/T_m) + \Delta C_p \,.\, (T - T_m - T \,.\, ln(T/T_m)) \quad (4)$$

where ΔH_m is the enthalpy change at the melting temperature T_m , that is defined as the temperature at which P_m = 0.5. ΔC_p is the change in heat capacity that was initially assumed to be zero for the purpose of fitting because due to the high interdependence of ΔH_m and ΔC_p these parameters cannot be fitted simultaneously. Equations (1) through (4) were combined and the data fitted directly. ΔC_p was calculated afterwards from the dependence of ΔH_m from T_m and the standard free energy of unfolding ΔG_o (1 M standard state) was then calculated at T_o= 37 ^{o}C according to Equation (5):

$$\Delta G_o = \Delta H_m \,.\, (1 - T_o/T_m) + \Delta C_p \,.\, \{T_o - T_m - T_o \,.\, ln\,(T_o/T_m)\} - RT_o ln(C) \quad (5)$$

4.8 Coiled coil peptide decorated liposomes

4.8.1 Peptide-liposome hybrid vesicle preparation:

Egg yolk L-α-phosphatidylcholine (EYPC, 22.6 mg, 29.4 μmol) and 1,2-Distearoyl-sn-Glycero-3-Phosphoethanolamine-N-[Amino(Polythylene Glycol)2000](DSPE-PEG2000, 0.17 mg, 0.6 μmol) were dissolved in 1 mL DCM. The 200 μL solution of P3/P4 (1:1, 3 μmol) was prepared by diluting their stock solution in MeOH. Both the organic solutions (DCM and MeOH) were mixed together in small round bottom flask. Thin and uniform lipid-peptide bilayer was formed by evaporation of organic solvent on rota-evaporator at 30 ^{o}C with 50 rpm rotations. Last traces of organic solvent were completely removed by applying high vacuum to the bilayer for 2 hrs. Bilayer film was hydrated with 1 mL solution of 0.1 mM carboxyfluorescein in PBS buffer (10 mM phosphate, 150 mM NaCl, and pH 7.4). Hydration process was carried out for 1 hour with continuous agitation at room temperature and occasional sonication (total time 120 s). Size exclusion chromatographic separation was carried out using Sephadex G-50 column to remove extra-vesicular carboxyfluorescein (Eluent: 10 mM PBS, 150 mM NaCl at pH 7.4). Liposome containing aliquots were collected and small unilamellar liposomes were obtained after 20 times extrusion through 100 nm polycarbonate membrane using mini-extruder (Avanti Polar Lipids, Alabaster, AL). Size and morphology of liposomes were confirmed by using Zetasizer *NanoZS90* and FE-SEM respectively. Liposomes were stored at 8 ^{o}C for further use.

4.8.2 Size distribution analysis of hybrid nanoparticles by DLS:

Mean diameter of liposomes was measured by dynamic light scattering (DLS) experiment using 90^{o} scattering angle. Samples were prepared by diluting 50 μL liposome solution to 1mL with PBS buffer at pH 7.4.

4.8.3 Field Emission-Scanning Electron Microscopy (FE-SEM): Morphology analysis of liposomes:

10 μL of liposome solution was dropcasted on silicon vapor. Samples were allowed to dry at room temperature and then coated with gold. Scanning electron microscopic imagings were performed using ZEISS ULTRA PLUS electron microscope operating at 30 kV.

4.8.4 Procedure for fluorescent leakage study:

Lipid-peptide hybrid liposome (500 µL) loaded with carboxyfluorescein was sealed in dialysis membrane having molecular weight cut off 500 Daltons. This dialysis bag was suspended in agitating PBS buffer (3 mL, 10 mM phosphate, 150 mM NaCl, and pH 7.4) at the 25 ^{o}C and 40 ^{o}C, separately. 100 µL aliquot of suspension medium was timely collected and quantification of released carboxyfluorescein was carried out by fluorimeter. All experiments were repeated in triplicates.

4.8.5 Fluorescence measurement:

Fluorescent measurement experiments were carried out using FluoroMax-4 HORIBA fluorimeter, with 490 nm excitation and 500-650 nm emission range using 1/3 slit and 1 nm data interval. 100 µL aliquots obtained from leakage assay were diluted to 500 µL with PBS buffer (pH 7.4). 10 mm quartz cuvette (from Hellma) was used for fluorescence measurement. Emission at 514 nm was monitored.

4.9 References

1. a) Drummond, D. C.; Zignani, M.; Leroux, J. *Prog. Lipid Res.* **2000**, *39*, 409. b) Zhang, J. X.; Zalipsky, S.; Mullah, N.; Pechar, M.; Allen, T. M. *Pharmacol. Res*. **2004**, *49*, 185. c) Needham, D. M.; Dewhirst, W. *Adv. Drug Delivery Rev.* **2001**, *53*, 285. d) Zurbriggen, R.; Novak-Hofer, I.; Seeling ,A.; Gluck, R. *Prog. Lipid Res.* **2000**, *39*, 3. e) Soussan, E.; Cassel, S.; Blanzat, M.; -Lattes, I. R. *Angew. Chem. Int. Ed.* **2009**, *48*, 274. f) A. Sorrenti, O. Illa and R. M. Ortuno, *Chem. Soc. Rev*. **2013**, *42*, 8200.

2. a) Sevimly, S.; Inci, F.; Zareie, H. M.; Bulmus, V. *Biomacromolecumes* **2012**, *13*, 3064. b) Oerlemans, C.; Deckers, R.; Storm, G.; Hennink,W. E.; Nijsen, J. F. W. *J. controlled release* **2013**, *168*, 327. c) Hossann, M.; Wiggenhorn, M.; Schwerdt, A.; Wachholz, K.; Teichert, N.; Eibl, Issels, H. R. D.; Lindner, L.H. *Biochim. Biophys. Acta.* **2007**, *1768*, 2491. d) Fomina, N.; Sankaranarayanan, J.; Almutairi, A. *Adv. Drug Delivery Rev.* **2012**, *64*, 1005. e) de la Rica, R.; Aili, D.; and Stevens, M. M. *Adv. Drug Delivery Rev.* **2012**, *64*, 967. f) Ong, W.; Yang, Y.; Cruciano, A. C.; McCarley, R. L. *J. Am. Chem. Soc.* **2008**,*130*,14739. g) Bibi, S.; Lattamann, E.; Mohammed, A. R. Perrie, Y. *J. Microencapsul*. **2012**, *29*, 262. h) Lindner, L. H.; Hossann, M. *Curr. Opin. Drug. Discov. Devel.* **2010**, *13*, 111.
3. a) Mackay, J. A.; Chilkoti, A. *Int. J. Hyperthermia* **2008**, *24*, 483. b) Zhang, Q.; Tang,J.; Fu, L.; Ran, R.; Liu, Y.; Yuan, M.; He, Q. *Biomaterials* **2013**, *34*, 7980. c) McFarlane, A. A.; Orriss, G. L.; Stetefeld, J. *Eur. J. Pharmacol.* **2009**, *625*, 101.

4. a) Lupas, A. N.; Gruber, M. *Adv. Protein. Chem.* **2005**, *70*, 37. b) Woolfson, D. N. *Adv. Protein. Chem.* **2005**, *70*, 79. c) Scholtz, J. M.; Baldwin, R. L. *Annu. Rev. Biophys. Biornol. Struct.* **1992**, *21*, 95. d) Rackham, O. J. L.; Madera, M.; Armstrong, C. T.; Vincent, T. L.; Woolfson, D. N.; Gough, J. *J. Mol. Biol.* 2**010**, *403*, 480.
5. a) Root, M. J.; Kay, M. S.; Kim, P. S. *Science* **2001**, *291*,884. b) Wild, C. T.; Shugars, D. C.; Greenwell, T. K.; McDanal, C. B.; Matthews, T. J. *Proc. Natl. Acad. Sci. U. S. A.***1994**, *91*, 9770.

6. a) Harbury, P. B.; Zhang, T.; Kim, P. S.; Alber, T. *Science* **1993**, *262*, 1401. b) Ciani, B.; Bjelic, S.; Honnappa, S.; Jawhari, H.; Jaussi, R.; Payapilly, Jowitt, A.; T.; Steinmetz, M. O.; Kammerer, R. A. *Proc.Natl. Acad. Sci. U. S. A.* **2010**, *107*, 19850. c) O'Neil, K. T.; DeGrado, W. F. *Science* **1990**, *250*, 646. d) Litowski, J. R.;

Hodges, R. S. *J. Mol. Biol.* **2002**, *277*, 37272. e) Tsang, B. P.; Bretscher, H. S.; Kokona, B.; Manning, R. S.; Fairman, R. *Biochemistry* **2011**, *50*, 8548. f) Hicks, M. R.; Walshaw, J.; Woolfson, D. N. *J. Struct. Biol.* **2002**, *137*, 73.

7. a) Horne, W. S.; Price, J. L.; Keck, J. L.; Gellman, S. H. *J. Am. Chem. Soc.* **2007**, *129*, 4178. b) Giuliano, M. W.; Horne, W. S.; Gellman, S. H. *J. Am. Chem. Soc.* **2007**, *131*, 9860.
8. a) Goodman, J. L.; Petersson, E. J.; Daniels, D. S.; Qiu, J. X.; Scheprtz, A. *J. Am. Chem. Soc.***2007**, *129*, 14749. b) Daniels, D. S.; Petersson, E. J.; Qiu, J. X.; Scheprtz, A. *J. Am. Chem. Soc.***2007**, *129*, 1532.
9. a) Araghi, R. R.; Jackel, C.; Colfen, H.; Salwiczek, Volkel, M.; A.; Wagner, S. C.; Wieczorek, S.; Baldauf, C.; Koksch, B. *ChemBioChem* **2010**, *11*, 335. b) Araghi, R. R.; Koksch, B. *Chem. Commun.* **2011**, *47*, 3544.
10. Shin, Y. -H.; Mortenson, D. E.; Satyshur, K. A.; Forest, K. T.; Gellman, S. H. *J. Am. Chem. Soc.* **2013**, *135*, 8149.
11. a) Bandyopadhyay, A.; Gopi, H. N.; *Org. Lett*. **2012**, *11*, 2770. b) Bandyopadhyay, A.; Jadhav, S. V.; Gopi, H. N. *Chem. Commun.* **2012**, *48*, 7170. c) Jadhav, S. V.; Bandyopadhyay, A.; Gopi, H. N. *Org. Biomol. Chem.* **2013,** *11*, 509.
12. Root, B. C.; Pellegrino, L. D.; Crawford, E. D.; Kokona, B.; Fairman, R. *Protein Sci.* **2008**, *18*, 329.
13. a) Marky, L. A.; Breslauer, K. J. *Biopolymers* **1987**, *26*, 1601. b) Krylov, D.; Mikhailenko, I.; Vinson, C. *EMBO J.* **1994**, *13*, 2849. c) Greenfield, N. J. *Nat. Protoc*. **2006**, *1*, 2527.
14. a) Ward, W. H.; Holdgate. G. A. *Prog. Med. Chem.* **2001**, *38*, 309. b) Leavitt, S.; Freire, E. *Curr. Opin. Struct. Biol.* **2001**, *11*, 560. c) Ladbury, J. E. *Biotechniques* **2004**, *37*, 885. d) Falconer, R. J.; Collins, B. M. *J. Mol. Recognit.* **2011**, *24*, 1.
15. Al-Ahmady, Z. S.; Al-Jamal, W. T.; Bossche, J. V.; Bui, T. T.; Drake, A. F.; Mason, A. J.; Kostarelos, K. *ACSNano* **2012**, *6*, 9335.
16. a) Nakase, I.; Okumura, S.; Tanaka, G.; Osaki, K.; Imanishi, M.; Futaki, S. *Angew. Chem. Int. Ed.* **2012**, *51*, 7464. b) Bashor, C. J.; Helman, N. C.; Yan, S.; Lim, W. A. *Science* **2008**, *329*, 1539. c) Boyle, A. L.; Bromley, E. H. C.; Bartlett, G. J.; Sessions, R. B.; Sharp, T. H.; Williams, C. L.; Curmi, P. M. G.; Forde, N. R.; Linke, H.; Woolfson, D. N. *J. Am. Chem. Soc.* **2012**, *134*, 15457.
17. Meyenberg, K.; Lygina, A. S.; van den Bogaart, G.; Jahnb, R.; Diederichsen, U. *Chem. Commun*. **2011**, *47*, 9405.

18. a) Marsden, H. R.; Elbers, N. A.; Bomans, P. H. H.; Sommerdijk, N. A. J. M.; Kros, A. *Angew. Chem. Int. Ed.* **2009**, *48*, 2330.

4.10 Appendix I: Structural characterization for synthesized compounds

HPLC profiles for Peptide **P1**-**P7**

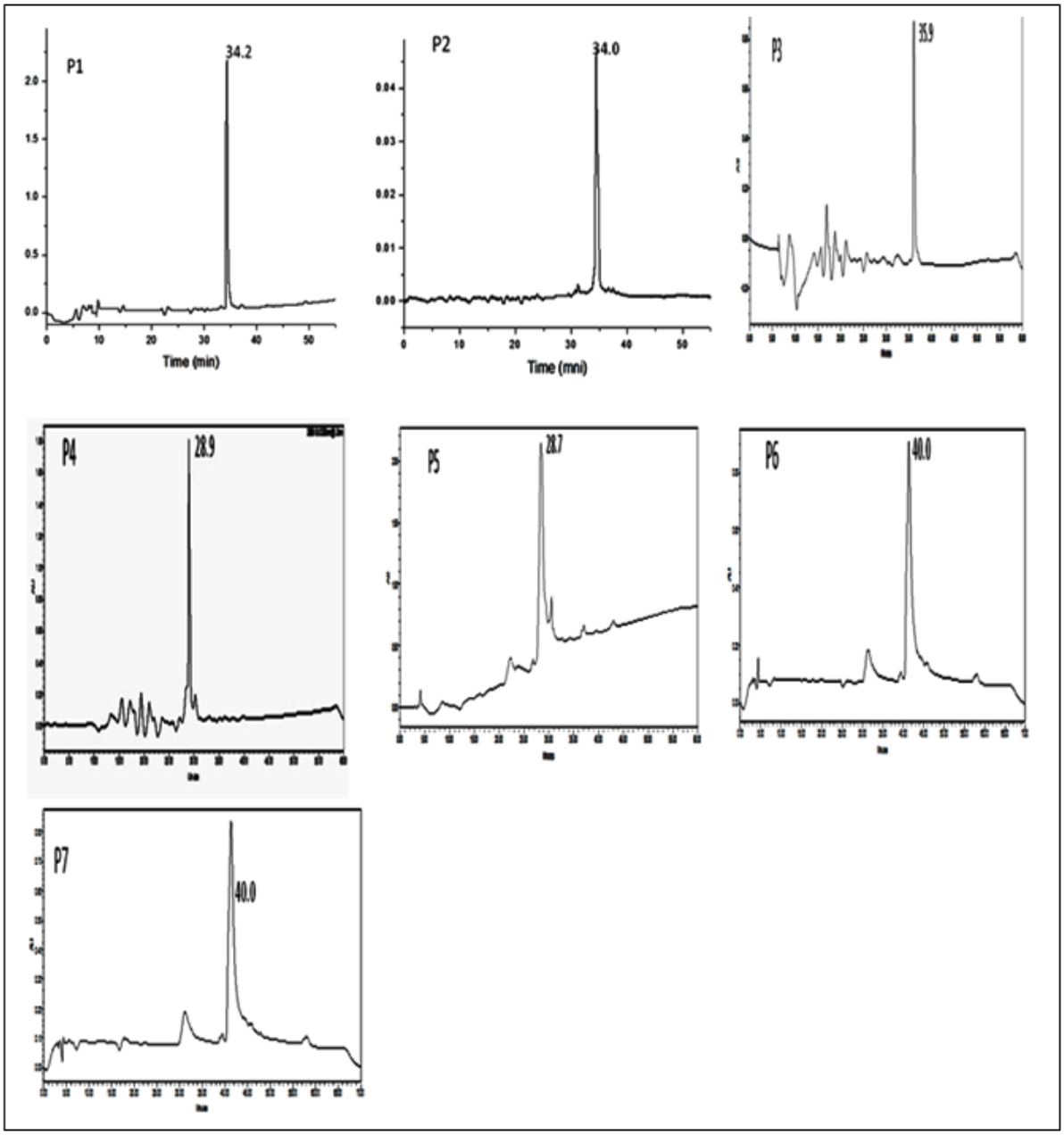

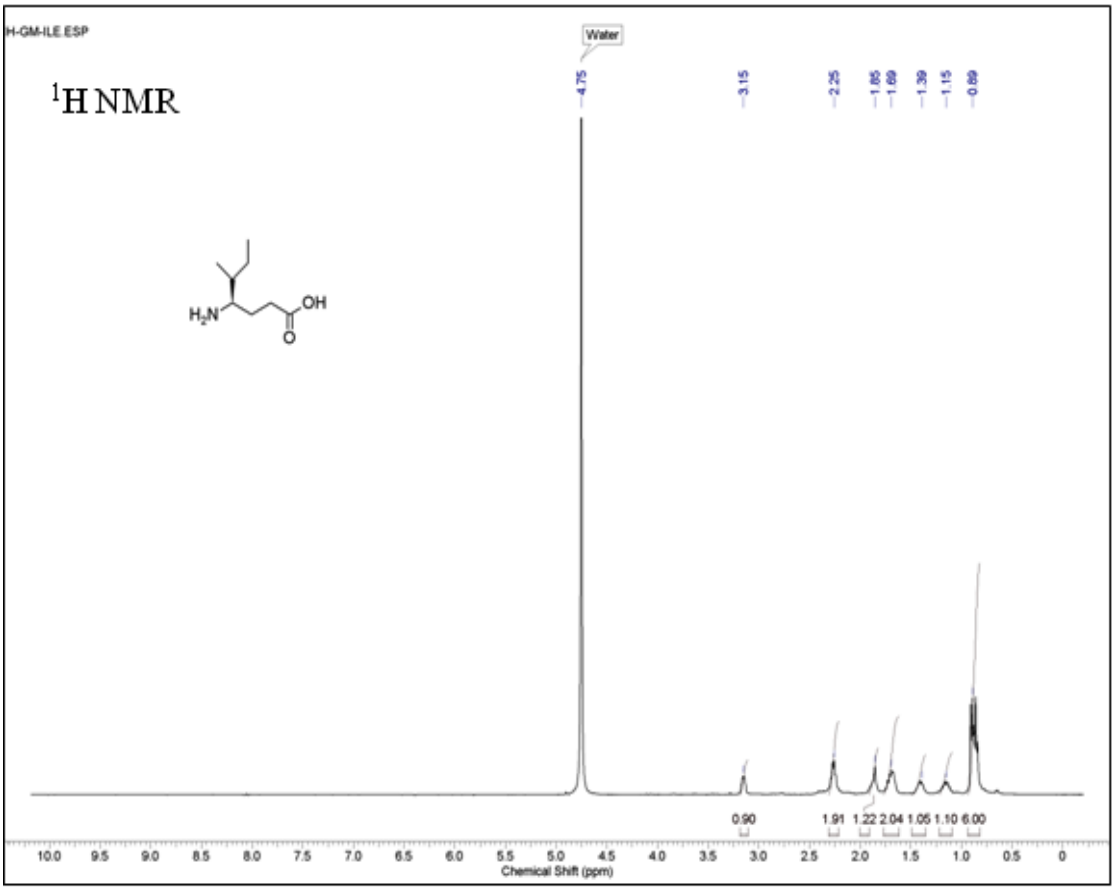
H-GM-ILE ESP
^{1}H NMR
Water
4.75
3.15
2.25
1.85
1.69
1.39
1.15
0.89
OH
H_2N
O
0.90
1.91
1.22
2.04
1.05
1.10
6.00
Chemical Shift (ppm)

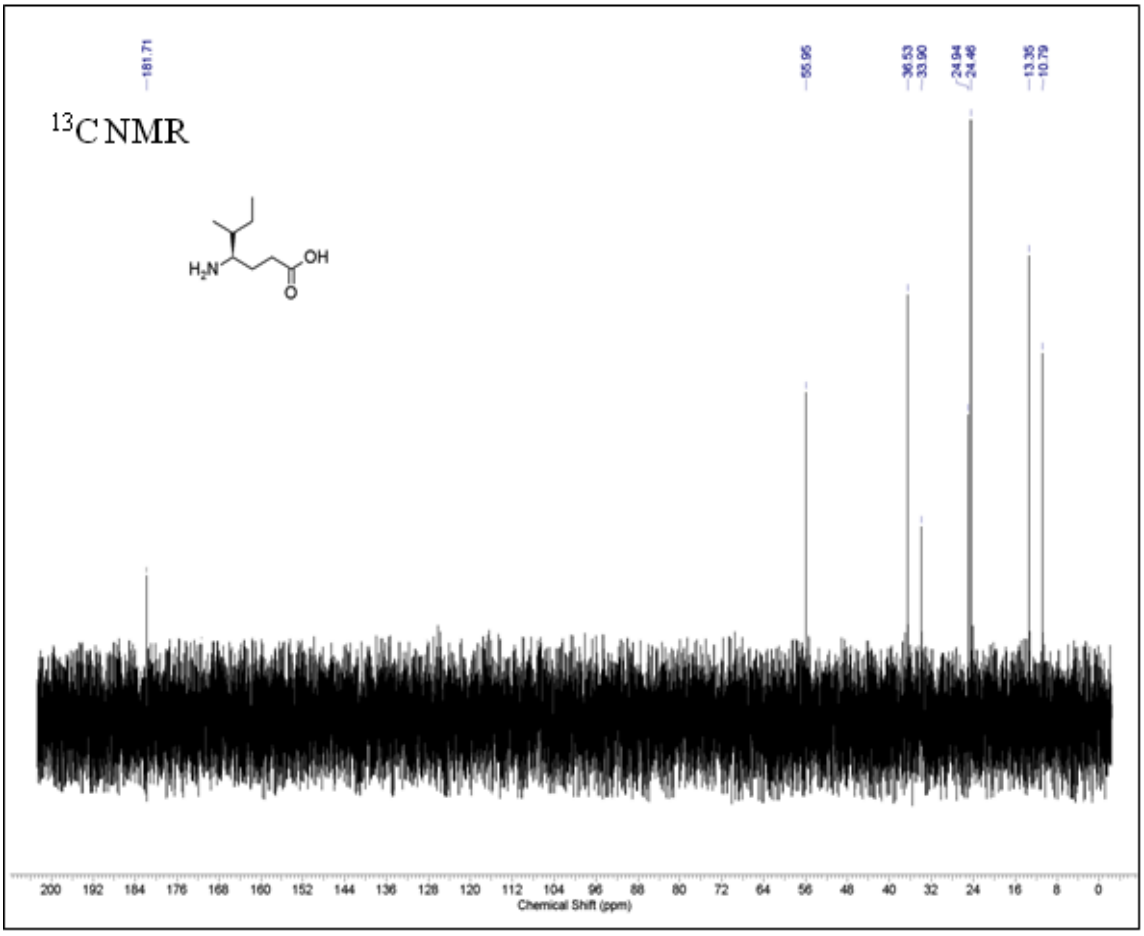
181.71
55.96
36.53
33.90
24.94
24.46
13.35
10.79
^{13}C NMR
OH
H_2N
O
Chemical Shift (ppm)

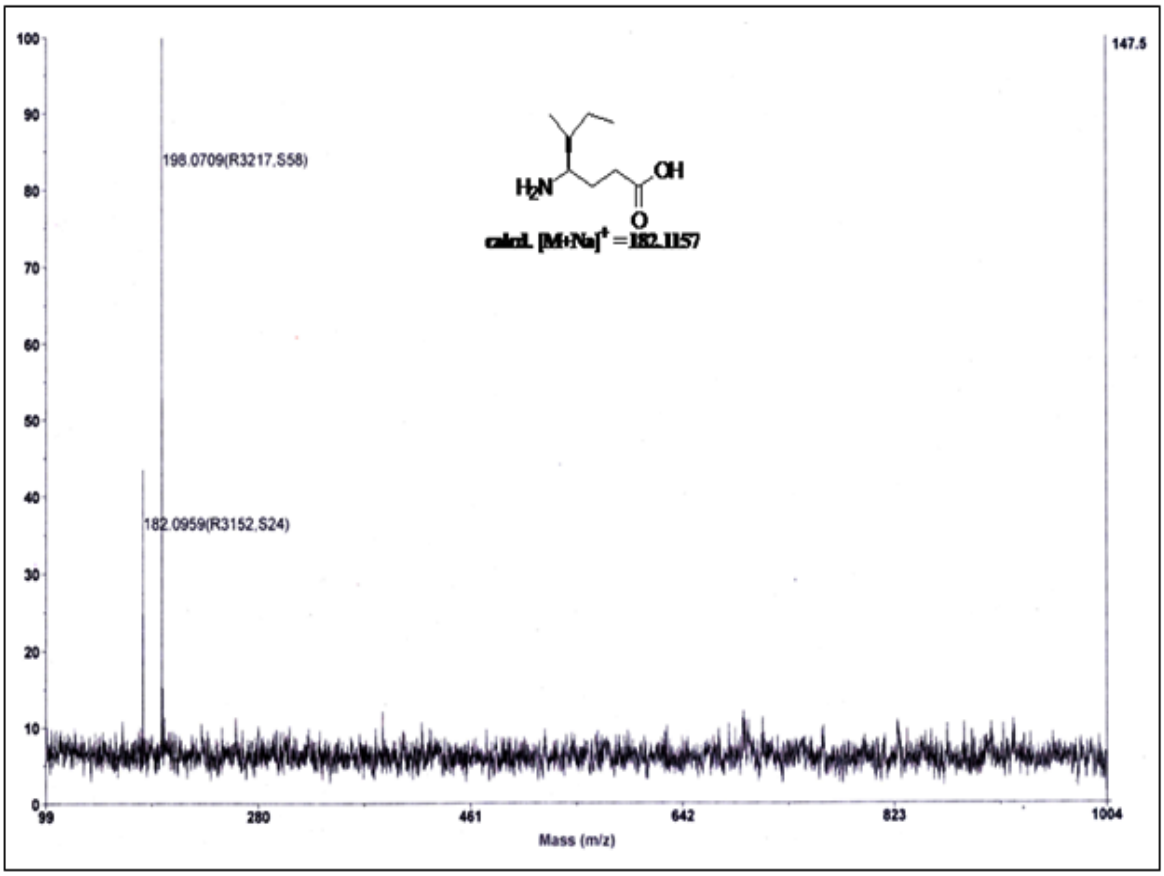
198.0709(R3217,S58)
182.0959(R3152,S24)
147.5
H2N
OH
O
calcd. [M+Na]+ = 182.1157
Mass (m/z)

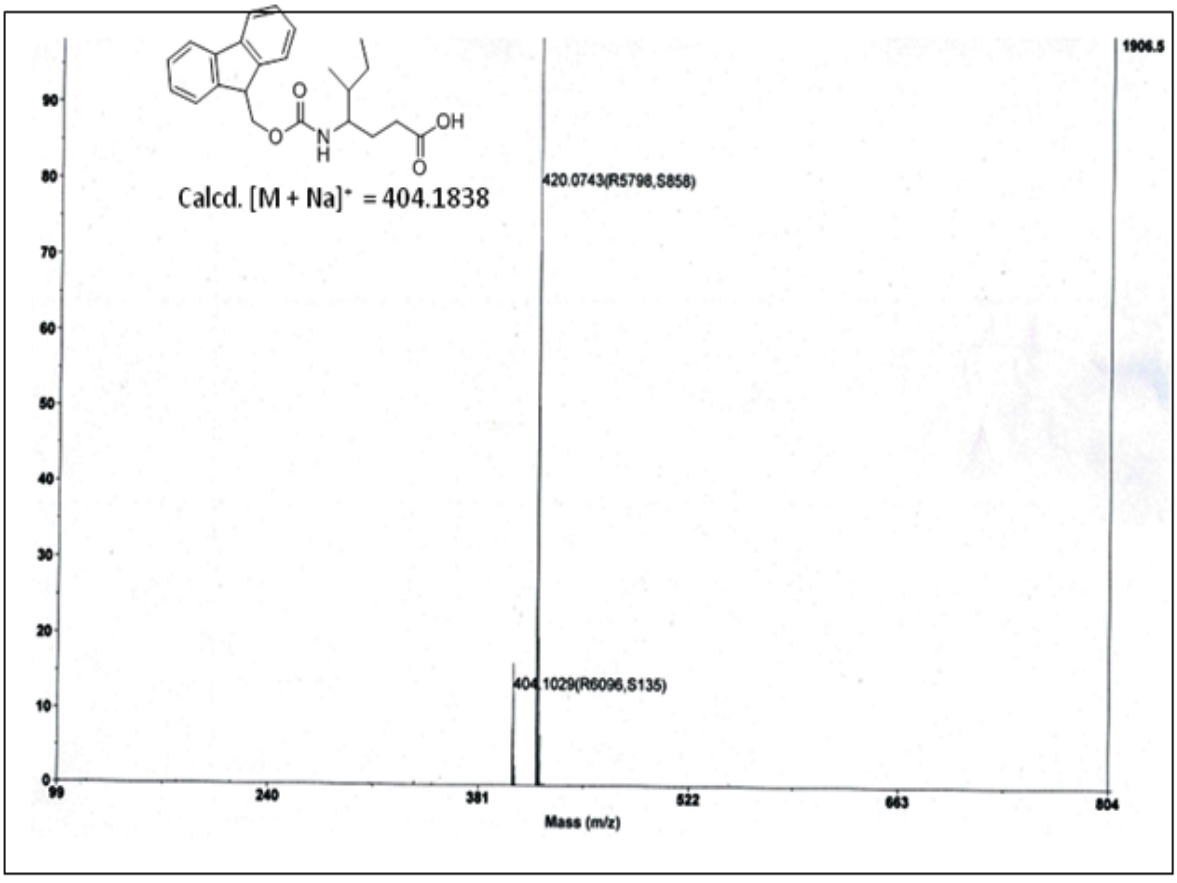
Calcd. [M + Na]+ = 404.1838
420.0743(R5798,S858)
404.1029(R6096,S135)
1906.5
Mass (m/z)

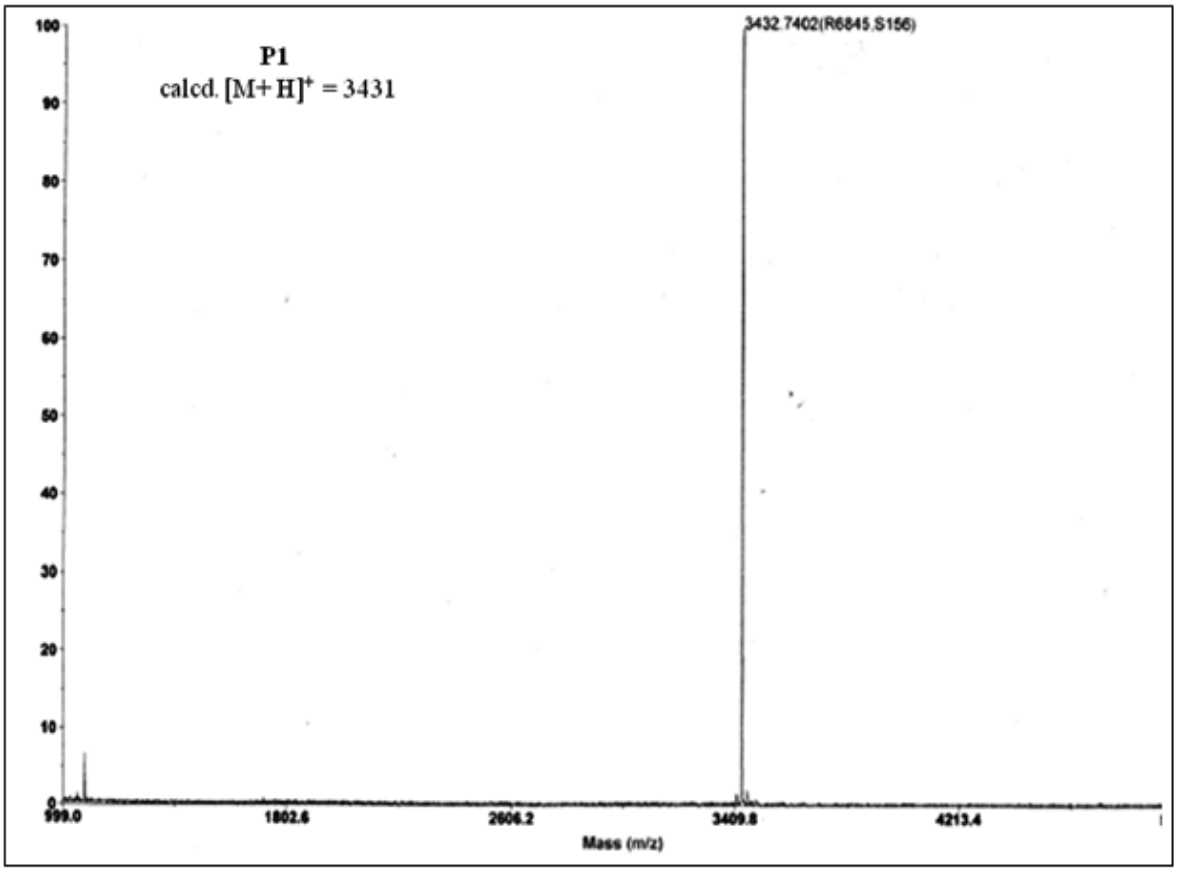
P1
calcd. [M+H]+ = 3431
3432.7402(R6845,S156)
100
90
80
70
60
50
40
30
20
10
0
999.0
1802.6
2606.2
3409.8
4213.4
Mass (m/z)

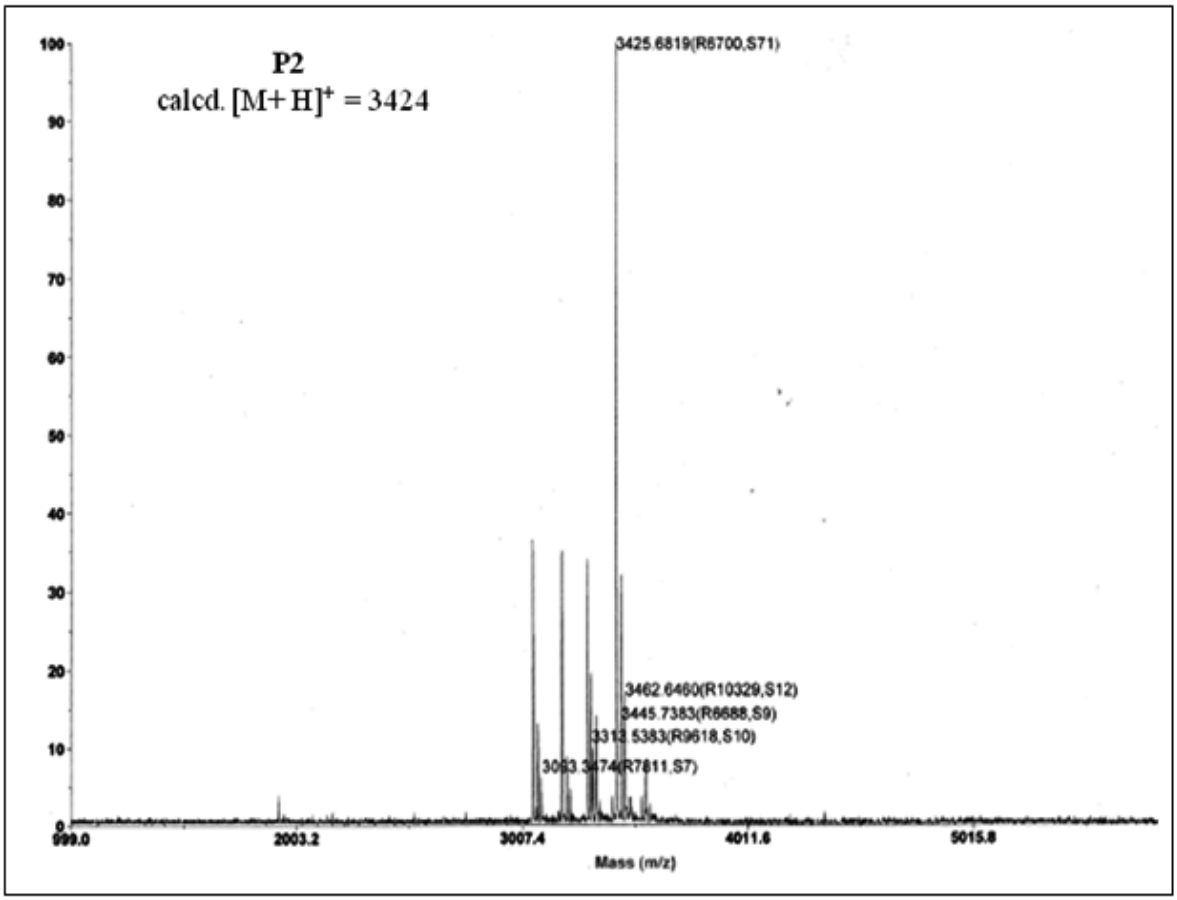
P2
calcd. [M+H]+ = 3424
3425.6819(R6700,S71)
3462.6460(R10329,S12)
3445.7383(R6688,S9)
3313.5383(R9618,S10)
3083.3474(R7811,S7)
100
90
80
70
60
50
40
30
20
10
0
999.0
2003.2
3007.4
4011.6
5015.8
Mass (m/z)

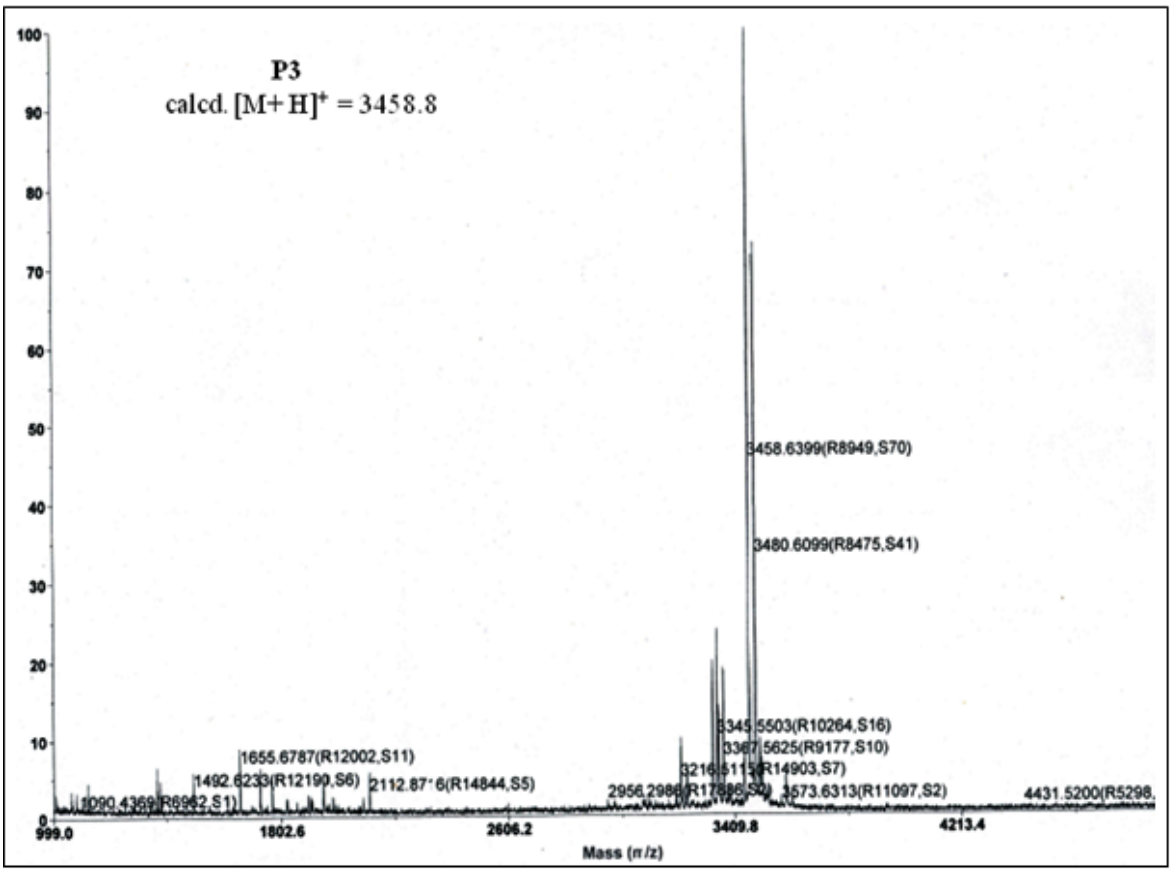
P3
calcd. [M+H]+ = 3458.8
3458.6399(R8949,S70)
3480.6099(R8475,S41)
1655.6787(R12002,S11)
1492.6233(R12190,S6)
2112.87*6(R14844,S5)
1573.6313(R11097,S2)
4431.5200(R5298,
999.0
1802.6
2606.2
3409.8
4213.4
Mass (m/z)

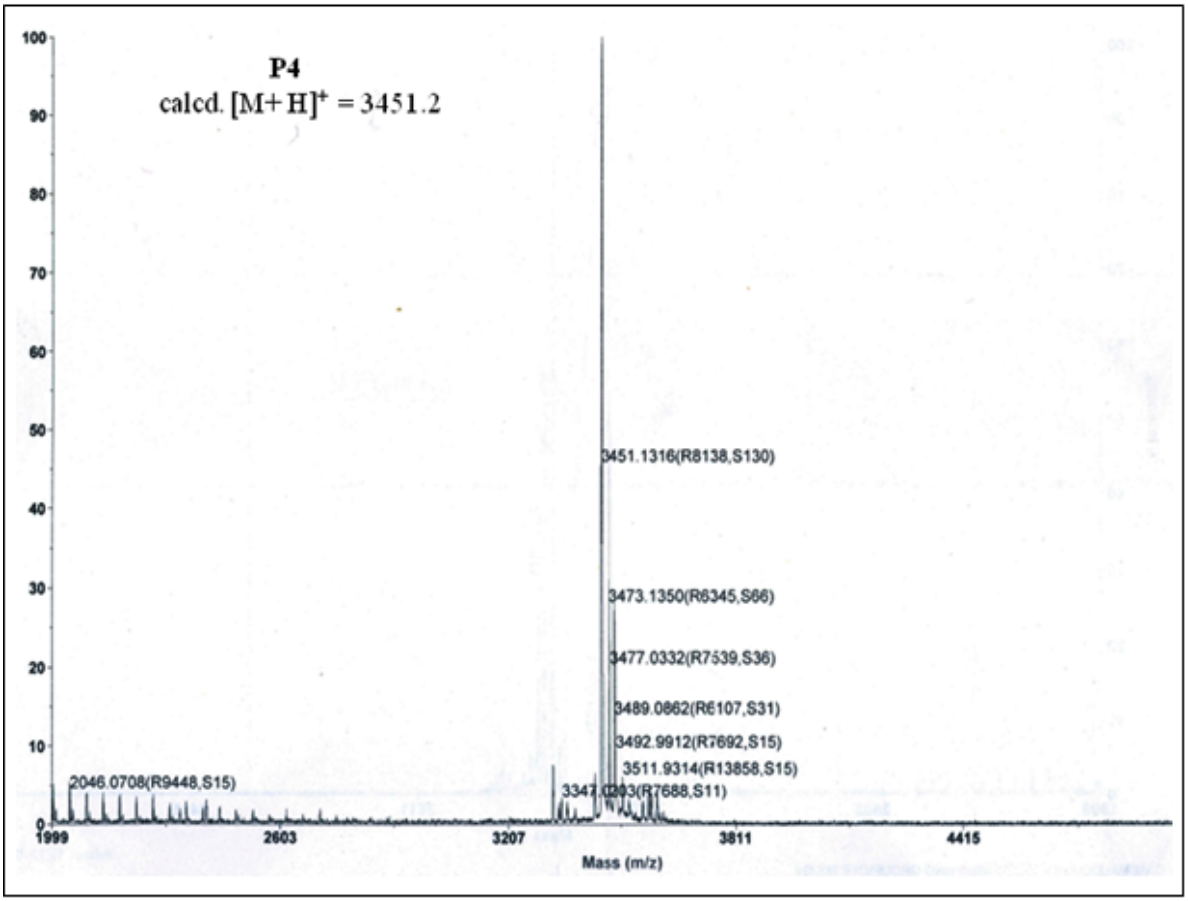
P4
calcd. [M+H]+ = 3451.2
3451.1316(R8138,S130)
3473.1350(R6345,S66)
3477.0332(R7539,S36)
3489.0862(R6107,S31)
3492.9912(R7692,S15)
3511.9314(R13858,S15)
2046.0708(R9448,S15)
1999
2603
3207
3811
4415
Mass (m/z)

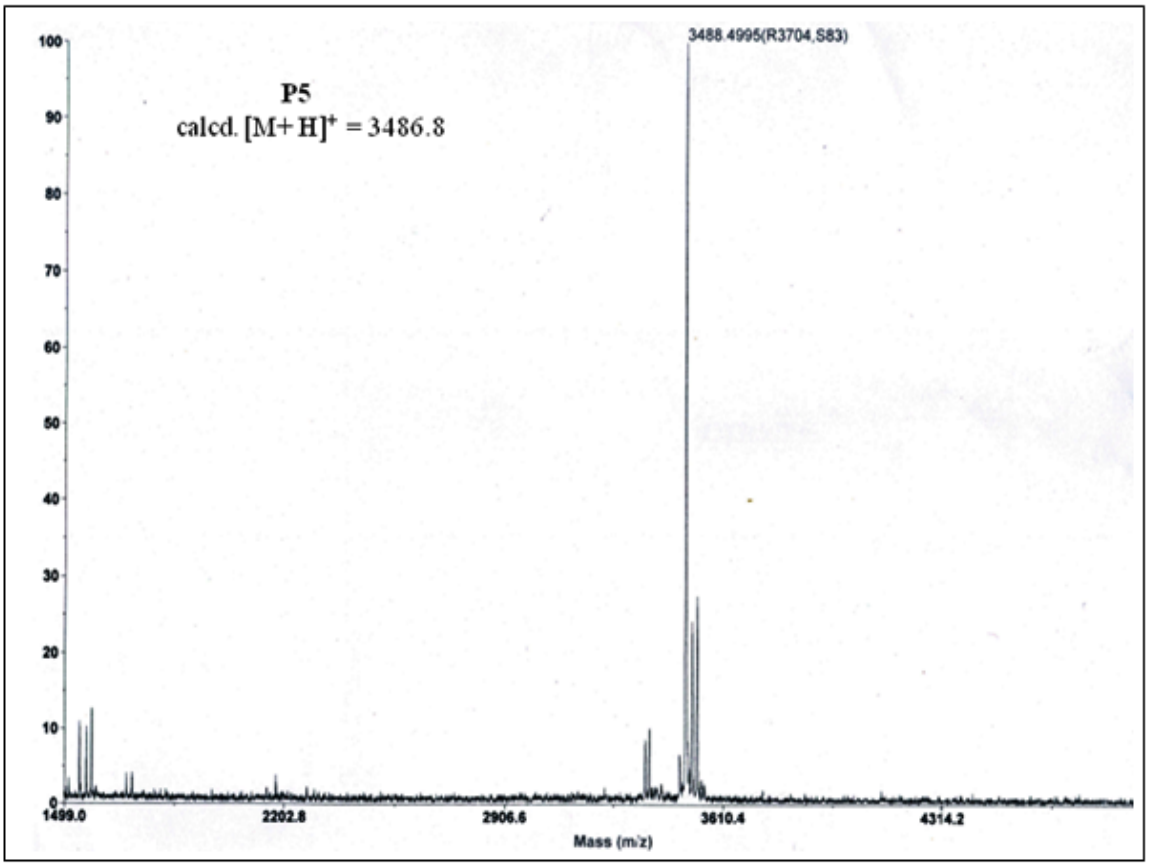
P5
calcd. [M+H]+ = 3486.8
3488.4995(R3704,S83)
100
90
80
70
60
50
40
30
20
10
0
1499.0
2202.8
2906.6
3610.4
4314.2
Mass (m/z)

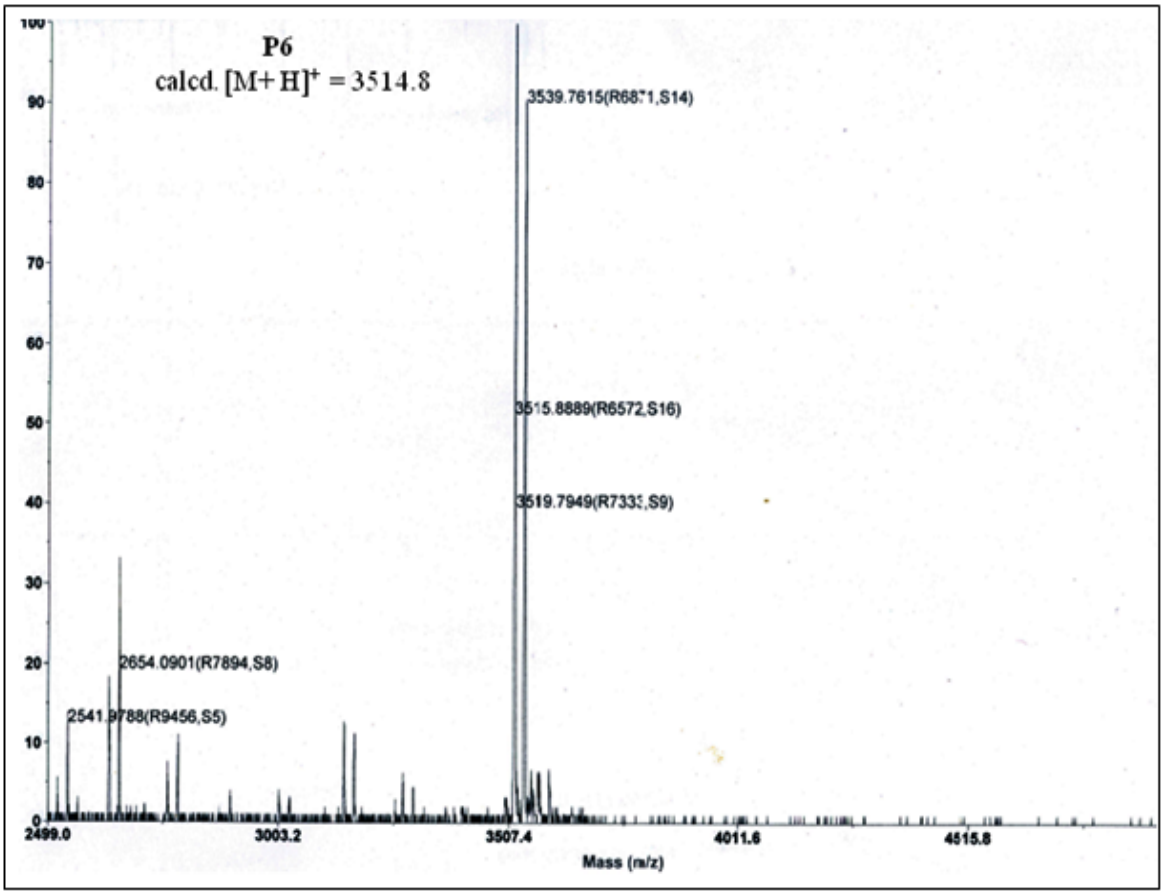
P6
calcd. [M+H]+ = 3514.8
3539.7615(R6871,S14)
3515.8889(R6572,S16)
3519.7949(R7333,S9)
2654.0901(R7894,S8)
2541.9788(R9456,S5)
100
90
80
70
60
50
40
30
20
10
0
2499.0
3003.2
3507.4
4011.6
4515.8
Mass (m/z)

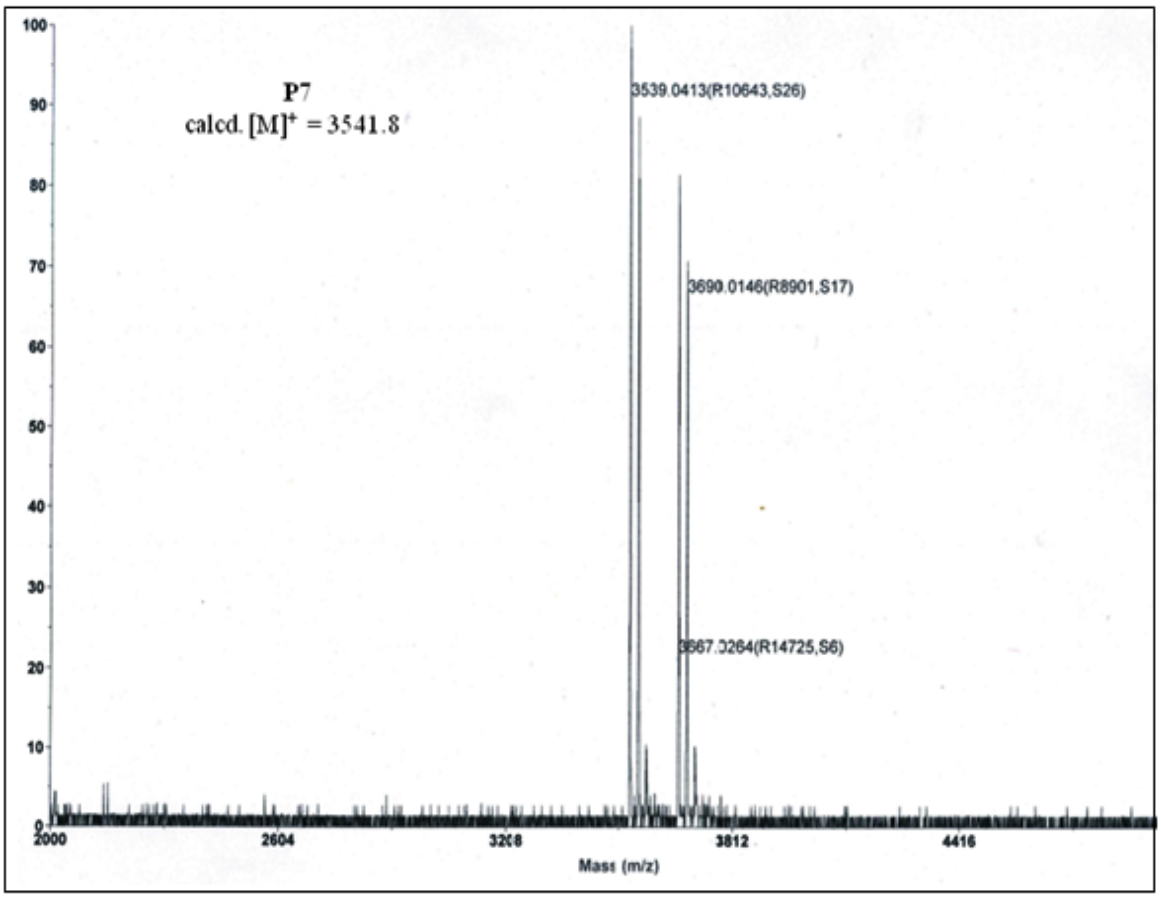
P7
calcd. [M]+ = 3541.8
3539.0413(R10643,S26)
3690.0146(R8901,S17)
3567.3264(R14725,S6)
100
90
80
70
60
50
40
30
20
10
0
2000
2604
3208
3812
4416
Mass (m/z)